

Copyright  
by  
Ronald James Travis Houk  
2007

**The Dissertation Committee for Ronald James Travis Houk Certifies that this is the  
approved version of the following dissertation:**

**Case Studies on the Aspects of Molecular Signaling: Binding Forces,  
Signal Generation, and a Mature Receptor.**

**Committee:**

---

Eric V. Anslyn, Supervisor

---

Brent L. Iverson

---

John F. Stanton

---

Philip D. Magnus

---

Charles B. Mullins

**Case Studies on the Aspects of Molecular Signaling: Binding Forces,  
Signal Generation, and a Mature Receptor.**

**by**

**Ronald James Travis Houk, B.S.**

**Dissertation**

Presented to the Faculty of the Graduate School of  
The University of Texas at Austin  
in Partial Fulfillment  
of the Requirements  
for the Degree of

**Doctor of Philosophy**

**The University of Texas at Austin**

**May, 2007**

## **Dedication**

This dissertation is dedicated to my wonderful family and  
friends for their immeasurable love and support.

Thank you so much.



## **Acknowledgements**

There are so many people without whom this penultimate milestone in my lifelong education would never have been achieved. It has been a long and bumpy road to this way point, yet I have had plenty of help.

I must begin with my mother and father. The love and support I have received over the years has been more than I could ever have hoped for. From my early days as a scientist discussing why the sky was blue with my father to my mother always making sure I was out the door on time with all the creature comforts I could take with me, I say thank you for all that you have given me.

If I was taught how to think by my parents, I was taught how to live by my sisters, Andi and Katie. Thanks for all the laughs (and fights) that have made me the person I am today.

To my wonderful friends both here and across the globe, you've always provided whatever I needed: a shoulder, a beer, a laugh, a hug. Catherine, Aaron, Heather, Joe, Steve, Sean, Natalie, Carina, Jacque, Jeff, and everyone else. Thank you so much, you are my pedestal.

Finally, Eric, how could this possibly have come to pass with you? We've had trials and tribulations, but here I am, and somehow you got me through it. I only hope that one day I will be able to lead a research team with as much dignity and grace as you have shown me. Thank you.

**Case Studies on the Aspects of Molecular Signaling: Binding Forces,  
Signal Generation, and a Mature Receptor.**

Publication No. \_\_\_\_\_

Ronald James Travis Houk, Ph.D.

The University of Texas at Austin, 2007

Supervisor: Eric V. Anslyn

The field of molecular and atomic sensing has seen a vast growth over the last few decades. Yet many advances still remain to be made. This dissertation takes an in depth look at the two major aspects in a molecular sensing or signaling scaffold—namely the binding of a target followed by the transduction of an observable signal. Chapter 1 will deal with intermolecular binding forces in the form of a case study on electrophilic coordination to carbonyl compounds. Computational studies are performed to determine the optimal geometry of an electrophile interacting with a carbon acid to affect the greatest enhancement in the acidity at the  $\alpha$ -carbon. We find that partial interaction through the  $\pi$ -system of the carbonyl and the resulting enolate affords the greatest acidity enhancement. Chapter 2 then switches to studies on the development of a novel signaling method for a molecular signaling assay. Two novel elements—transition metal catalytic signal amplification and peroxyoxalate chemiluminescence—are utilized to generate a signaling motif incorporating two new methodologies for signal generation. The first uses of catalytic signal amplification for the detection of small organic analytes and

peroxyoxalate chemiluminescence for signal generation in a molecular recognition event are described. Finally, both elements are brought together in Chapter 3, which describes a mature ionophoric chemodosimeter with both highly sensitive binding and strong signal output. The use of a squaraine dye as a signaling unit for the detection of palladium(II) salts is described in which an aliphatic thiol acts as the theoretical “host” in a covalent displacement type assay. Palladium(II) and other transition metal detection is of importance both industrially and environmentally, and the assay described is sensitive to levels desired in both arenas.

## Table of Contents

<b>LIST OF TABLES</b>	<b>XII</b>
<b>LIST OF FIGURES</b>	<b>XIII</b>
<b>LIST OF SCHEMES</b>	<b>XVIII</b>
<b>CHAPTER 1: CARBONYL COORDINATION CHEMISTRY FROM A NEW ANGLE</b>	<b>1</b>
1.0 Introduction.....	1
1.1 Background.....	2
1.1.1 Enzymatic Enolization.....	2
1.1.1.2 Triosephosphate Isomerase.....	3
1.1.1.2 Mandelate Racemase .....	7
1.1.1.3 Citrate Synthase .....	11
1.1.2 Low Barrier Hydrogen Bonds.....	14
1.1.2.1 Principle of Non-perfect Synchronization .....	18
1.1.3 Beyond LBHBs.....	22
1.2 Experimental Design.....	28
1.3 The Lithium-Acetaldehyde Model.....	31
1.4 Design and Synthesis of Scaffold 1.13 .....	37
1.5 Conclusions.....	44
1.6 Experimental section.....	45
1.6.1 Computational Specifics .....	45
1.6.2 General Synthesis.....	49

1.7	References.....	55
<b>CHAPTER 2: LUMINESCENT ASSAYS FOR KETONES AND ALDEHYDES EMPLOYING CATALYTIC SIGNAL AMPLIFICATION</b>		<b>62</b>
2.0	Introduction.....	62
2.1	Background.....	63
2.1.1	Supramolecular Chemistry and Molecular Recognition.....	63
2.1.2	Chromogenic Sensing Motifs .....	66
2.1.2.1	Organic Dyes .....	66
2.1.2.2	Metal Complexes .....	72
2.1.3	Fluorogenic Sensing Motifs.....	73
2.1.3.1	Fluorescence Phenomena.....	74
2.1.3.2	Fluorogenic Chemosensors.....	77
2.1.4	Peroxyoxalate Chemiluminescence .....	80
2.1.4.1	The Mechanism.....	81
2.1.4.2	Detection using POCL .....	85
2.1.5	Enzymatic Signal Amplification.....	87
2.1.6	Transition Metal Signal Amplification .....	89
2.2	Target Choice and Assay Design.....	95
2.3	Sonogashira Assay .....	96
2.3.1	Design .....	96
2.3.2	Choice of Fluorophores.....	98
2.3.3	Measurement.....	100
2.3.4	Derivation of Kinetics.....	102
2.3.4	Rate Studies .....	106
2.3.5	Chemiluminescence Measurements.....	108
2.4	Suzuki Based Assay .....	110
2.4.1	Design .....	111
2.4.2	Fluorescence vs. Chemiluminescence .....	115

2.5	Conclusions.....	117
2.6	Experimental Section.....	118
2.6.1	Materials and Methods.....	118
2.6.2	Kinetics Determination in the Sonogashira Assay.....	119
2.6.2.1	Dithiolane Formation.....	119
2.6.2.2	Palladium Poisoning and Sonogashira.....	120
2.6.2.3	Aliquot Work-up.....	120
2.6.2.4	Fluorescence .....	120
2.6.2.5	Chemiluminescence .....	121
2.6.3	Kinetics Determination for the Suzuki Assay.....	121
2.6.3.1	Dithiane Condensation.....	121
2.6.3.2	Suzuki Coupling.....	122
2.6.3.3	Fluorescence .....	123
2.6.3.4	Chemiluminescence .....	123
2.7	References.....	124
<b>CHAPTER 3: A DIAGNOSTIC COLORIMETRIC SENSOR FOR RESIDUAL Pd(II) IN CROSS-COUPLED REACTIONS</b>		<b>132</b>
3.0	Introduction.....	132
3.1	Chemodosimeters.....	133
3.1.1	Signal Liberating Dosimeters .....	135
3.1.2	Complex Forming Dosimeters.....	140
3.2	Squaraine Dyes .....	146
3.2.1	Photophysical Properties and Applications .....	147
3.2.1.1	Solvent Effects .....	147
3.2.1.2	Aggregation and Solid State Applications.....	153
3.3	Design of a Palladium Sensor .....	156
3.3.1	Synthesis and Characterization of 3.26.....	157
3.3.2	Understanding the Squaraine-Thiol Interaction.....	159

3.3.2.1	<sup>1</sup> H-NMR Studies .....	160
3.3.2.2	van't Hoff Analysis.....	161
3.3.3	Initial Attempts at Pd(II) Detection .....	165
3.3.3.1	UV-Vis Titrations .....	165
3.3.3.2	Fluorescence Titrations.....	167
3.3.3.3	Testing Unknowns .....	169
3.3.4	Pd(NO <sub>3</sub> ) <sub>2</sub> Characterization.....	172
3.3.3.1	The Verkade Base.....	175
3.3.3.2	Calibration Curves for DMSO-Verkade System .....	177
3.3.4	UV-Vis Studies in DMF .....	182
3.3.4.1	Calibration Curve for the DMF system .....	185
3.4	Conclusions.....	187
3.5	Experimental Section.....	189
3.5.1	UV-Vis Titrations in DMSO with DBU .....	190
3.5.2	UV-Vis Titrations in DMSO with Verkade Base .....	190
3.5.3	van't Hoff Analysis.....	191
3.5.4	UV-Vis Titrations in DMF.....	191
3.5.4	Kinetics and Calibration Curve Determination.....	192
3.6	References.....	193
	<b>BIBLIOGRAPHY</b>	<b>204</b>
	<b>VITA</b>	<b>227</b>

## List of Tables

<b>TABLE 1.1</b>	<b>OUTPUT ENERGIES FOR THE ACETALDEHYDE-Li<sup>+</sup> COMPLEX (TOP) AND THE ENOLATE-Li<sup>+</sup> COMPLEX (BOTTOM). ENERGIES ARE GIVEN IN HARTREES (H)</b>	<b>48</b>
<b>TABLE 3.1</b>	<b>SPECTRAL DATA OF SYMMETRICAL ANILINE SQUARAINES IN METHYLENE CHLORIDE.<sup>50</sup></b>	<b>149</b>
<b>TABLE 3.2</b>	<b>A) FOUR SAMPLES OF KNOWN CONCENTRATION TESTED AGAINST THE ABSORBANCE CALIBRATION CURVE (FIRST COLUMN), THE HALF-TIME CALIBRATION CURVE (SECOND COLUMN). B) DATA FOR ARBITRARY KNOWN SAMPLES TESTED AGAINST A FULLY EQUILIBRATED TITRATION ISOTHERM GENERATED FROM THE SAME STOCK SOLUTION OF 3.27.</b>	<b>181</b>
<b>TABLE 3.3</b>	<b>DATA FOR THREE SAMPLES OF KNOWN Pd(II) CONCENTRATION TESTED AGAINST THE CALIBRATION CURVE IN FIGURE 3.16B.</b>	<b>187</b>



## List of Figures

- FIGURE 1.1** CRYSTAL STRUCTURE ELUCIDATION OF THE ACTIVE SITE TIM BINDING THE TRANSITION STATE ANALOGUE PGH. A) COMPUTER GENERATED MODEL FROM THE CRYSTALLOGRAPHIC DATA REPRINTED FROM REF. 8. B) SCHEMATIC OF THE ACTIVE SITE RESIDUES WITH POTENTIAL HYDROGEN BONDS AS DOTTED LINES WITH DISTANCES IN Å REPRINTED FROM REF. 9. 4
- FIGURE 1.2** ACTIVE SITE OF MR WITH (S)-MANDELATE SHOWS FIVE KEY ELEMENTS:  $Mg^{2+}$ , Lys164, Lys166, His297, AND GLU317. REPRINTED FROM REF. 19 9
- FIGURE 1.3** ACTIVE SITE BINDING OF ACETYL-CoA FROM A TERNARY COMPLEX OF D-MALATE, ACETYL-CoA, AND CS. THE HYDROGEN BOND FROM THE  $\Delta 1N$ -H TO THE CARBONYL OXYGEN IS INDICATED. REPRINTED FROM REF. 31. 13
- FIGURE 1.4** A) NORMAL HYDROGEN BOND  $A-H-A \geq 2.8\text{\AA}$ ; B) LOW BARRIER HYDROGEN BOND  $2.55\text{\AA} \geq A-H-A \geq 2.3\text{\AA}$ ; C) SINGLE WELL HYDROGEN BOND  $A-H-A \leq 2.3\text{\AA}$ . REPRINTED FROM REF. 36 16
- FIGURE 1.5** THE PNS DEPENDENCE OF CARBON ACID DEPROTONATION LEADS TO THE SITUATION IN WHICH ELECTRON WITHDRAWING EFFECTS ( $X > Z$ ) HAVE A GREATER AFFECT ON THE TRANSITION STATE THAN THE PRODUCT. 20
- FIGURE 1.6** A) MODEL OF 4-(NITROPHENYL)ACETYL-CoA BOUND TO MCADH WITH  $\pi$ -DIRECTED HYDROGEN BONDS TO THE SUBSTRATE ANALOGUE. REPRINTED FROM REF. 60. B) CRYSTAL STRUCTURE OF THE ACTIVE SITE OF 4-CHLOROBENZOYL-CoA DEHALOGENASE WITH BACKBONE AMIDE HYDROGEN BONDS TO THE  $\pi$ -FACE OF THE THIOESTER. REPRINTED FROM REF. 61. C) ENOLIC STRUCTURE OF THE MEISENHEIMER INTERMEDIATE FROM THE MECHANISM OF 4-CHLOROBENZOYL-CoA DEHALOGENASE. 24
- FIGURE 1.7** THERMODYNAMIC CYCLE OF ENZYME-ASSISTED ACID DISSOCIATION. 30
- FIGURE 1.8** SURFACES WERE OBTAINED BY ITERATION IN 5 DEGREE INCREMENTS ALONG BOTH THE Li-O-C BOND ANGLE (LEFT) FROM  $45^\circ$ - $180^\circ$  AND THE Li-O-C-C DIHEDRAL ANGLE (RIGHT) FROM  $0^\circ$ - $180^\circ$ . 32
- FIGURE 1.9** A)  $Li^\oplus$  DIHEDRAL ANGLE VS. Li-O-C BOND ANGLE ENTHALPY (KCAL/MOL) CONTOUR PLOT FOR THE  $Li^\oplus$ -ACETALDEHYDE COMPLEX GENERATED AT THE MP2 LEVEL WITH A 6-31G\* BASIS SET, AND B) A GRAPHICAL REPRESENTATION OF THE MINIMUM ENERGY STRUCTURE. 33

- FIGURE 1.10** A)  $\text{Li}^\oplus$ -DIHEDRAL ANGLE VS.  $\text{Li-O-C}$  BOND ANGLE ENTHALPY (KCAL/MOL) CONTOUR PLOT FOR THE  $\text{Li}^\oplus$ -ETHYLENOLATE COMPLEX GENERATED AT THE MP2 LEVEL WITH A 6-31G\* BASIS SET. THE GLOBAL MINIMUM STRUCTURE (RIGHT) IS SHOWN WITH A DIHEDRAL ANGLE OF  $45^\circ$  AND A  $\text{Li-O-C}$  BOND ANGLE OF  $85^\circ$ . 33
- FIGURE 1.11** CONTOUR PLOT OF THE GAS PHASE ACIDITY (KCAL/MOL) OF THE ACETALDEHYDE- $\text{Li}^+$  COMPLEX DERIVED AS THE DIFFERENCE OF THE ABOVE ACETALDEHYDE AND ENOLATE SURFACES. 35
- FIGURE 1.12** (TOP) FRONT AND SIDE VIEWS OF THE OPTIMUM GEOMETRY FOR LITHIUM COORDINATION TO ENHANCE THE ACIDITY OF ACETALDEHYDE. (BOTTOM) ANALOGOUS VIEWS OF THE ENOLATE COMPLEX. 35
- FIGURE 1.13** Z-MATRIX INPUTS FOR A) THE ACETALDEHYDE- $\text{Li}^+$  COMPLEX AND B) THE ENOLATE- $\text{Li}^+$  COMPLEX. PARAMETER A IS THE  $\text{Li-O-C}_A$  BOND ANGLE AND PARAMETER T IS THE  $\text{Li-O-C}_A\text{-C}_B$  DIHEDRAL ANGLE ALL STARRED PARAMETERS WERE FULLY OPTIMIZED WITH EACH RUN. IN THE COMMAND LINE, BASIS SETS THE BASIS SET FOR THE CALCULATION, CALC SETS THE CALCULATION TYPE/LEVEL, CHARGE SETS THE OVERALL CHARGE OF THE SYSTEM, SCF\_MAXCYC SETS THE LIMIT ON THE NUMBER OF SELF CONSISTENT FIELD OPTIMIZATION CYCLES ALLOWED BEFORE THE JOB AUTOMATICALLY CANCELS, AND MEMORY SETS THE MAX NUMBER OF MEMORY WORDS TO BE EXPLOITED FOR THE CALCULATION. 47
- FIGURE 2.1** A) CHEMOSENSOR DESIGN IN WHICH THE BINDING UNIT AND THE SIGNALING UNIT ARE COVALENTLY LINKED. B) THE DISPLACEMENT DESIGN IN WHICH THE ANALYTE AND INDICATOR COMPETE FOR THE BINDING SITE. C) TWO TYPES OF CHEMODOSIMETER IN WHICH AN IRREVERSIBLE REACTION OCCURS UPON BINDING TO GENERATE A SIGNAL. 65
- FIGURE 2.2** THE EXTENSION OF THE CONJUGATED SYSTEM IN BPEA LOWERS THE ENERGY OF THE HOMO-LUMO GAP TO GIVE A LONGER WAVELENGTH ABSORBANCE THAN ANTHRACENE. 67
- FIGURE 2.3** ORGANIC DYES SUCH AS AZOBENZENES AND SQUARAINES EXHIBIT CT INTERACTION BETWEEN THE DONATING AND WITHDRAWING GROUPS ATTACHED TO THE CONJUGATED  $\pi$ -SYSTEM. 68
- FIGURE 2.4** A) PET QUENCHING FROM A DONOR. B) PET QUENCHING FROM AN ACCEPTOR. C) EET MECHANISM THAT CAN RESULT IN QUENCHING OR SENSITIZATION 75
- FIGURE 2.5** SCHEMATIC OF THE FÖRSTER ENERGY EXCHANGE MECHANISM 76

<b>FIGURE 2.6</b>	<b>A CARTOON OF AN ELISA ASSAY. HIV IS ROUTINELY DETECTED VIA THIS METHOD.</b>	<b>87</b>
<b>FIGURE 2.7</b>	<b>A SELECTIVE SENSOR FOR ssDNA INCORPORATING ENZYMATIC SIGNAL AMPLIFICATION.</b>	<b>88</b>
<b>FIGURE 2.8</b>	<b>EXCITATION AND EMISSION SPECTRA IN ETHYL ACETATE OF A) 9,10-DIBROMOANTHRACENE 2.10 AT <math>2 \times 10^{-6}</math> M, B) 9-BROMO-10-(PHENYLETHYNYL)ANTHRACENE 2.4 AT <math>2 \times 10^{-6}</math> M, C) 9,10-BIS(PHENYLETHYNYL)ANTHRACENE (BPEA) AT <math>8 \times 10^{-7}</math> M, AND D) 2,5-DIPHENYLOXAZOL (PPO) AT <math>8 \times 10^{-7}</math> M.</b>	<b>100</b>
<b>FIGURE 2.9</b>	<b>OVERLAID COMPARISON OF THE NORMALIZED EXCITATION SPECTRA OF THE ANTHRACENE DYES VERSUS THE INTERNAL STANDARD 2,5-DIPHENYLOXAZOLE (PPO).</b>	<b>101</b>
<b>FIGURE 2.10</b>	<b>A) PLOT OF THE RATIO OF BPEA EMISSION TO PPO EMISSION VS. TIME FOR 1-10MM 2-BUTANONE. FOR ALL: 1,3-PROPANEDITHIOL: INITIAL <math>8.60 \times 10^{-3}</math> M; AFTER DILUTION <math>7.17 \times 10^{-4}</math> M; Pd(MeCN)<sub>2</sub>Cl<sub>2</sub> <math>7.17 \times 10^{-4}</math> M; 9-BROMO-10-(PHENYLETHYNYL)ANTHRACENE <math>4.00 \times 10^{-3}</math> M; PHENYLACETYLENE <math>1.49 \times 10^{-2}</math> M; COPPER(I) IODIDE <math>8.75 \times 10^{-4}</math> M; 2,5-DIPHENYLOXAZOLE <math>6.33 \times 10^{-3}</math> M. B) PLOT OF THE RATES FROM (A) VS. %CATALYST/KETONE</b>	<b>106</b>
<b>FIGURE 2.11</b>	<b>A) FLUORESCENCE MEASUREMENT AN ASSAY WITH 70% ANALYTE LOADING. B) CHEMILUMINESCENCE MEASUREMENT FOR AN ASSAY WITH 70% ANALYTE LOADING. ALL REACTION CONDITIONS ARE AS GIVEN IN FIGURE 2.10. FOR B) 2 mL OF ALIQUOT SOLUTION, 50 MG (.074 MMOL) 2.31, 10 <math>\mu</math>L 0.1 M NaOH, 50 <math>\mu</math>L 30% H<sub>2</sub>O<sub>2</sub>.</b>	<b>110</b>
<b>FIGURE 2.12</b>	<b>A) EXITATION AND EMISSION SPECTRA FOR 9,10-DIPHENYLANTHRACENE (DPA) IN THF AT <math>3.74 \times 10^{-7}</math> M, AND B) NORMALIZED SPECTRAL OVERLAY OF 9,10-DIBROMOANTHRACENE AND DPA SHOWING VERY LITTLE SHIFT IN EMISSION.</b>	<b>112</b>
<b>FIGURE 2.13</b>	<b>RATE PROFILES OF THE SUZKI ASSAY FOR CINNAMALDEHYDE USING A) FLUORESCENCE AND B) CHEMILUMINESCENCE</b>	<b>116</b>
<b>FIGURE 3.1</b>	<b>TWO TYPES OF CHEMODOSIMTERS. A) THE ANALYTE REACTS WITH THE DOSIMETER TO GENERATE A NEW SIGNAL PRODUCING COMPLEX WHICH INTEGRATES BOTH ORIGINAL PIECES. B) THE ANALYTE REACTS WITH THE DOSIMETER TO CHANGE ITS CONSTITUTION SUCH THAT THE SIGNAL GENERATING SPECIES IS LIBERATED.</b>	<b>134</b>

- FIGURE 3.2** BEER'S LAW ANALYSIS OF SQUARINE **3.26** FROM  $9 \times 10^{-7}$  M TO  $9 \times 10^{-6}$  M. LINEARITY IS MAINTAINED AS HIGH AS 2 ABSORBANCE UNITS AND AN EXTINCTION COEFFICIENT OF  $2.3 \times 10^5$  L MOL<sup>-1</sup>CM<sup>-1</sup> WAS OBTAINED.<sup>102</sup> 159
- FIGURE 3.3** <sup>1</sup>H-NMR TITRATIONS OF **3.26** WITH ETHANETHIOL IN THE PRESENCE OF DBU IN CHCl<sub>3</sub>-D. [3.26]<sub>0</sub> = 37 mM; [DBU]<sub>0</sub> = 37 mM.<sup>101</sup> 161
- FIGURE 3.4** VAN'T HOFF ANALYSIS OF **3.27** AT  $1.2 \times 10^{-5}$  M. A) SPECTRAL DATA OF FREE **3.26** AT TEMPERATURES FROM 288.5 K TO 317.8 K SHOWING A BREAK UP OF THE SOLVENT-SOLUTE COMPLEX. B) VAN'T HOFF PLOT OF  $\ln K_{eq}$  VS. 1/T SHOWING AN OVERALL ASSOCIATION CONSTANT OF  $2.9 \times 10^6$  M<sup>-1</sup>.<sup>102</sup> 163
- FIGURE 3.5** TITRATIONS OF A) Pd(OAc)<sub>2</sub> AND B) Pd(PPh<sub>3</sub>)<sub>2</sub>Cl<sub>2</sub> INTO SOLUTIONS OF **3.27** AT  $2.35 \times 10^{-5}$  M IN DMSO. **3.27** COMPLEXATION WAS FACILITATED WITH 1 EQUIVALENT OF ETHANETHIOL AND 2 EQUIVALENTS OF DBU.<sup>101</sup> 166
- FIGURE 3.6** FLUORESCENCE TITRATIONS OF A) Pd(OAc)<sub>2</sub> AND B) Pd(PPh<sub>3</sub>)<sub>2</sub>Cl<sub>2</sub> IN DMSO. COMPLEX **3.27** WAS FORMED WITH ETHANETHIOL AND 2 EQUIVALENTS DBU. THEORETICAL [3.27] =  $2.35 \times 10^{-7}$  M.  $\lambda_{ex}$  = 650 NM;  $\lambda_{MAXF}$  = 660 NM.<sup>101</sup> 169
- FIGURE 3.7** A) COLORIMETRIC CALIBRATION CURVE FOR Pd(OAc)<sub>2</sub> IN DMSO. [3.27] =  $2.35 \times 10^{-5}$  M. B) FLUORESCENCE CALIBRATION CURVE FOR Pd(OAc)<sub>2</sub> IN DMSO. [3.27] =  $2.35 \times 10^{-7}$  M. C) UV-VIS SPECTRA OF **3.27** SOLUTION WITH ADDITION OF 25 mL ALIQUOTS FROM THE SUZUKI COUPLING IN SCHEME 3.13 AT 0, 60, AND 120 MINUTES REACTION TIME.<sup>107</sup> 171
- FIGURE 3.8** SPECTRAL DATA FOR SAMPLES FROM SUZUKI COUPLES DIGESTED WITH NITRIC ACID. THE SAMPLES WERE SUBJECTED TO DIFFERENT WORK UP CONDITIONS PRIOR TO NITRATION AS SHOWN. [3.27] =  $2.35 \times 10^{-5}$  M. 172
- FIGURE 3.9** TITRATION DATA FOR Pd(NO<sub>3</sub>)<sub>2</sub> INTO **3.27** ( $2.35 \times 10^{-5}$  M IN DMSO) FORMED WITH ETHANETHIOL AND 2 EQUIVALENTS DBU. 173
- FIGURE 3.10** PLOT OF THE CONCENTRATION OF **3.26** CALCULATED FROM THE EXTINCTION COEFFICIENT VERSUS THE CONCENTRATION OF PALLADIUM ADDED IN THE TITRATION FROM FIGURE 3.9. 174
- FIGURE 3.11** TITRATION OF Pd(NO<sub>3</sub>)<sub>2</sub> INTO  $8.8 \times 10^{-6}$  M **3.27** IN DMSO FORMULATED WITH ETHANETHIOL AND VERKADE BASE **3.31**. TITRATION WAS CONDUCTED AFTER 4 HOURS REACTION TIME BETWEEN SQUARINE **3.26** AND ETHANETHIOL. 176

**FIGURE 3.12** TITRATION OF  $\text{Pd}(\text{NO}_3)_2$  INTO  $1.2 \times 10^{-5} \text{ M}$  **3.27** IN DMSO FORMULATED WITH ETHANETHIOL AND VERKADE BASE **3.31**. TITRATIONS WERE CONDUCTED AFTER 12-15 HOURS REACTION TIME BETWEEN SQUARINE **3.26** AND ETHANETHIOL 177

**FIGURE 3.13** A) NORMALIZED KINETIC TRACES OF CALIBRATION CURVE DATA USING A SERIES OF SAMPLES OF INCREASING PALLADIUM CONCENTRATION. BELOW 1 EQUIVALENT SHOWN IN BLACK, ABOVE SHOWN IN RED. THE INSET SHOWS THE HALF-TIME.  $[\text{3.27}] = 1.2 \times 10^{-5}$ ;  $[\text{Pd}]$  RANGE =  $9.1 \times 10^{-7}$  TO  $1.5 \times 10^{-5}$  178

**FIGURE 3.14** A) MAXIMUM ABSORBANCE CALIBRATION CURVE WITH LINEAR FIT AND B) HALF-TIME CALIBRATION CURVE WITH LINEAR FIT FOR KINETICS DETERMINATION SHOWN IN **FIGURE 3.13**. 180

**FIGURE 3.15** TITRATION OF  $\text{Pd}(\text{NO}_3)_2$  INTO **3.27** ( $1.2 \times 10^{-5} \text{ M}$ ) IN DMF WITH NO EXOGENOUS BASE. 184

**FIGURE 3.16** A) NORMALIZED KINETIC TRACES FOR  $\text{Pd}(\text{NO}_3)_2$ -INDUCED COLOR TURN-ON OF THE **3.27** COMPLEX. INSET SHOWS THE TREND IN THE HALF-TIMES TO COMPLETION.  $[\text{3.27}] = 1.2 \times 10^{-5} \text{ M}$  B) ISOTHERM OF ABSOLUTE ABSORBANCE VALUES FOR KINETICS IN A SHOWING NO SATURATION. 186

## List of Schemes

<b>SCHEME 1.1</b>	<b>PROPOSED ENEDIOL ROUTE FOR TIM MECHANISM</b>	<b>7</b>
<b>SCHEME 1.2</b>		<b>8</b>
<b>SCHEME 1.3</b>	<b>PROPOSED ROUTE CONTAINING NEUTRAL INTERMEDIATES FOR BOTH GENERAL ACID CATALYZED STEPS</b>	<b>12</b>
<b>SCHEME 1.4</b>		<b>17</b>
<b>SCHEME 1.5</b>		<b>40</b>
<b>SCHEME 1.6</b>		<b>41</b>
<b>SCHEME 1.7</b>		<b>42</b>
<b>SCHEME 1.8</b>		<b>43</b>
<b>SCHEME 2.1</b>	<b>SEQUESTRATION OF A POTASSIUM CATION BY 18-CROWN-6</b>	<b>64</b>
<b>SCHEME 2.2</b>	<b>GENERALLY ACCEPTED POCL MECHANISM INVOLVING AN ELECTRON EXCHANGE STEP TO GENERATE THE FIRST SINGLET EXCITED STATE OF THE FLUOROPHORE.</b>	<b>82</b>
<b>SCHEME 2.3</b>	<b>CIEEL MECHANISM APPLIED TO TWO OF THE MAJOR INTERMEDIATES THOUGHT TO BE RESPONSIBLE FOR CHEMIEXCITATION IN POCL</b>	<b>84</b>
<b>SCHEME 2.4</b>	<b>COMPETITION ASSAY FOR DETECTION OF HEAVY TRANSITION METALS BASED ON FRET SIGNAL AMPLIFICATION FROM Cu(I) CATALYZE HUISGEN CYCLIZATION.</b>	<b>90</b>
<b>SCHEME 2.5</b>	<b>TWO ASSAYS WHICH UTILIZE THE HECK CROSS-COUPLING REACTION TO ENHANCE SIGNAL OUTPUT IN THE DETECTION OF (A) COPPER(II) AT nM CONCENTRATIONS AND (B) CADMIUM(II) AT <math>\mu</math>M CONCENTRATIONS.</b>	<b>92</b>
<b>SCHEME 2.6</b>	<b>AN ALLOSTERIC CATALYST SCAFFOLD REPORTED BY MIRKIN ET AL. USED AS A CHLORIDE ANION SENSOR AT CONCENTRATIONS AS LOW AS .8 <math>\mu</math>M BY “NAKED-EYE” DETECTION</b>	<b>93</b>
<b>SCHEME 2.7</b>	<b>SCHEMATIC OF THE ASSAY FOR KETONES BASED ON A SONOGASHIRA CROSS-COUPLING REACTION AS THE SIGNAL AMPLIFICATION PROCESS. REACTIONS WERE CONDUCTED AT MILLIMOLAR CONCENTRATIONS FOR TENABLE REACTION KINETICS.</b>	<b>98</b>

<b>SCHEME 2.8</b>	<b>THE GENERALLY ACCEPTED MECHANISM FOR THE SONOGASHIRA CROSS-COUPLED REACTION. TWO PROPOSED METHODS OF REDUCING A Pd(II) PRECATALYST TO THE ACTIVE Pd(0) SPECIES HAVE BEEN PROPOSED.</b>	<b>102</b>
<b>SCHEME 2.9</b>	<b>THE COMPLEX EQUILIBRIUM IS PROPOSED TO ACCOUNT FOR THE NONLINEAR INCREASE IN REACTION RATE AT HIGH CATALYST CONCENTRATIONS.</b>	<b>108</b>
<b>SCHEME 2.12</b>	<b>SCHEMATIC OF THE ASSAY FOR ALDEHYDES USING A SUZUKI COUPLING.</b>	<b>113</b>
<b>SCHEME 3.1</b>		<b>135</b>
<b>SCHEME 3.2</b>		<b>136</b>
<b>SCHEME 3.3</b>		<b>137</b>
<b>SCHEME 3.4</b>		<b>138</b>
<b>SCHEME 3.5</b>		<b>139</b>
<b>SCHEME 3.6</b>	<b>THE CRYSTAL STRUCTURE OF 3.13 REPRINTED FROM REF. 31</b>	<b>141</b>
<b>SCHEME 3.7</b>		<b>143</b>
<b>SCHEME 3.8</b>		<b>144</b>
<b>SCHEME 3.9</b>		<b>145</b>
<b>SCHEME 3.10</b>		<b>146</b>
<b>SCHEME 3.11</b>		<b>148</b>
<b>SCHEME 3.12</b>		<b>157</b>
<b>SCHEME 3.13</b>		<b>170</b>

# Chapter 1: Carbonyl Coordination Chemistry from a New Angle

## 1.0 INTRODUCTION

Supramolecular chemistry is defined as the study of intermolecular noncovalent interactions.<sup>1</sup> The range of science encompassed by this umbrella is undoubtedly huge; however, at its core there are truly only a small handful of building blocks that supramolecular chemists use to describe the wide array of interacting molecular systems. Van der Waals, coulombic, and hydrophobic forces account for all of the intermolecular and many of the intramolecular forces from which supramolecular chemistry is derived. From self-assembling polymers to molecular recognition to drug delivery dendrimers, they are all held together by these same basic forces. Indeed, these same guidelines constrict even biological modes of interaction, and though we describe these forces as the fundamental building blocks to all the interactions we call supramolecular, there is a very great deal left unknown about them.

Perhaps the most widely utilized yet least well understood class of noncovalent forces is the coulombic forces. This class can be broken down into a number of subsets such as ion pairing, dipole-dipole, cation- $\pi$ , hydrogen bonding, and metal-ligand interactions to name a few.<sup>2</sup> While a strict adherence to Coulomb's law results in a one dimensional dependence on distance, for the more complex subsets like dipole-dipole and ion dipole interactions, a second or third dimension is inherently added. This chapter will focus on the idea of how these extra degrees of dependence affect not only the strength of the dipole interaction but also processes affected by the interaction.



In particular, this chapter will delve into the effect that directionality plays in the process of coordinatively assisted enolate formation. The impetus for these studies arises from the study of enzymology in which enzymes are capable of facile transformation of carbon acids to their corresponding conjugate bases at pH's several orders of magnitude lower than their  $pK_a$ 's. A brief discussion of these types of transformations will be followed by discussion of computational studies involving a simple system showing the effect of directionality of electrophilic coordination on the  $pK_a$  of a carbon acid. Finally, the design of a molecular scaffold incorporating a directionally constrained hydrogen bond along with synthetic efforts towards its completion will be discussed.

## **1.1 BACKGROUND**

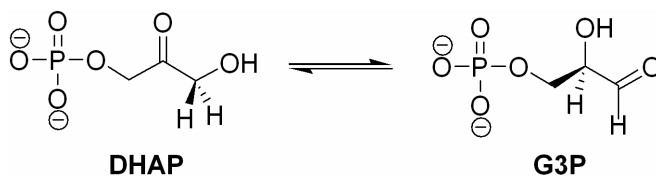
### **1.1.1 Enzymatic Enolization**

It has been known for quite some time that enzymatic transformations which involve the removal of an  $\alpha$ -proton from a carbon acid are essential to many metabolic pathways.<sup>3</sup> To enzymologists and physical organic chemists, these reactions present a singularly interesting dilemma. How does an enzyme, working with a cadre of relatively weak acids and bases, facilitate the deprotonation of a carbon acid? The  $pK_a$ 's of typical  $\alpha$ -hydrogens can range from as low as 12 to as high as 30 depending on the type of carbon acid. Yet, enolases, racemases, aldolases, and various other enzyme classes readily perform  $\alpha$ -carbon proton abstractions using acids and bases with  $pK_a$ s closer to the 6-10 range at physiological pH. Here we will discuss a couple of examples of enzymes which undergo proton transfer catalysis of carbon acids and their elucidated

mechanisms to gain a better understanding of the methods by which enzymes stabilize these transformations.

#### ***1.1.1.2 Triosephosphate Isomerase***

Triosephosphate isomerase or TIM, catalyzes the interconversion of dihydroxyacetone phosphate (DHAP) to glyceraldehyde-3-phosphate (G3P) (see below). DHAP and G3P are products of the cleavage of fructose 1,6-bisphosphate by fructose 1,6-bisphosphate aldolase. The further catabolism of G3P to pyruvate, acetyl-CoA, and/or carbon dioxide is a significant source of ATP and NADH.<sup>4</sup> The mechanism associated with TIM can be superficially labeled a 1,2-proton shift, and the question of whether the transformation is a fully concerted process or a stepwise mechanism has been thoroughly investigated.<sup>5,6</sup>



Through a series of tritium labeling experiments, it was determined that the enzyme-catalyzed transformation of DHAP to G3P is stereospecific and must occur through a semi-stable intermediate that allows for solvent-catalyst proton-triton exchange.<sup>6</sup> In other words, the mechanism of the 1,2-proton transfer is not concerted but goes through a two step process in which a transiently stable intermediate, presumably an enediolate, is formed. A nearly complete free energy reaction coordinate diagram for this mechanism was derived through a series of further labeling experiments and represents the first free energy reaction coordinate ever developed for an enzyme-catalyzed process.<sup>5</sup> It is interesting to note that the reaction coordinate shows the process to occur

under kinetic control from the two pathways available to the intermediate. Starting from the common intermediate, on the pathway towards DHAP, the limiting step was determined to be the proton transfer, whereas going towards G3P, diffusion of the product from the active site was limiting. Hence working under reversible conditions, the overall rate limiting step is diffusion of G3P in or out of the active site. This observation has led some to claim that TIM is a perfect enzyme in that it has reached its catalytic limit. This observation is sensible because the role of TIM is to ensure that both DHAP and G3P are funneled into the glycolysis pathway, and it should naturally select for DHAP over G3P.<sup>7</sup>

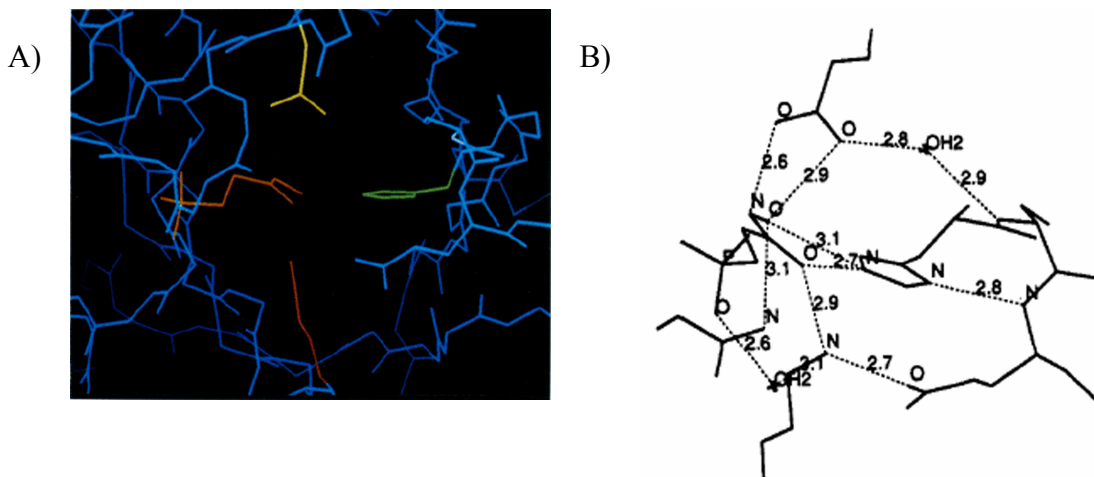


**Figure 1.1** Crystal structure elucidation of the active site TIM binding the transition state analogue PGH. A) Computer generated model from the crystallographic data reprinted from ref. 8. B) Schematic of the active site residues with potential hydrogen bonds as dotted lines with distances in Å reprinted from ref. 9.

As useful as the reaction coordinate diagram was, it was not until the active site structure of TIM bound to an intermediate analogue was resolved that actual controversy

began.<sup>8, 9</sup> It was determined by structural analysis that rather than simply general base catalysis from Glu165 (yellow in Figure 1.1A), the transformation actually proceeds *via* general base-general acid catalysis with electrophilic/acid catalytic help from the  $\epsilon^2\text{N}$  of a histidine residue, His95 (green in Figure 1.1A). Crystal structures of TIM and the intermediate analogue/inhibitor phosphoglycolo-hydroxamate (PGH) (orange in Figure 1.1A) were generated which showed distinct interactions between the oxygens of PGH and the imidazole of His95. The crystal structure of the mutant H95Q showed several perturbations of the active residue positions, most notably a large shift in the general base, Glu165. Though the mutant was still somewhat catalytically active, it was determined that by changing the imidazole to the amide of glutamine, the mechanism of the reaction completely changed.<sup>8, 10</sup>

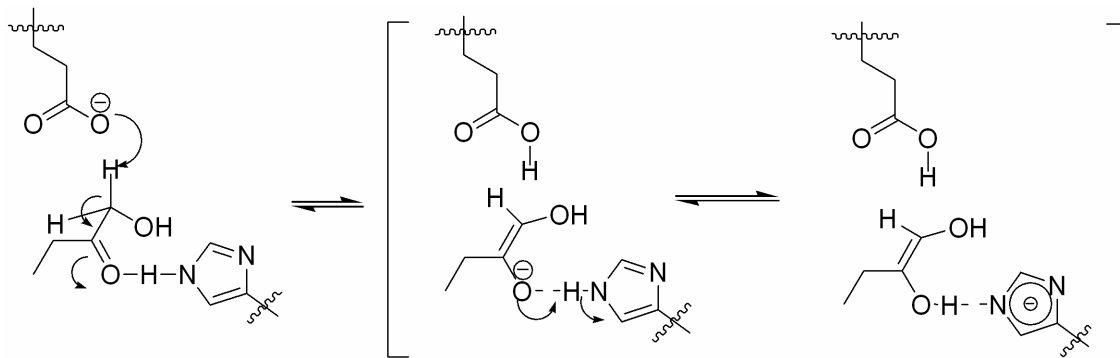
There was, and still is, uncertainty however, over how the crucial histidine goes about assisting this transformation. It was shown well before His95 was known to be involved, that DHAP becomes polarized upon active site binding in TIM.<sup>11</sup> It was postulated at the time that substrate binding was accompanied by an electrophilic coordination to the carbonyl oxygen which helped in the catalysis. This coordination was reported as a direct extension of the idea of ground-state destabilization put forth by Jencks in the mid 1970's.<sup>12</sup> This topic is discussed in greater detail below. In the case at hand, the first question to be answered was in what protonation state is the imidazole at the start of the reaction. The  $\text{pK}_a$  of the His95 imidazolium in the denatured protein has been estimated as roughly 6.5 and so it is not unreasonable to think that His95 would be fully protonated at the start of the reaction.<sup>13</sup> However, preliminary crystallographic analysis shows a hydrogen bond possibility between the non-substrate interacting  $\delta^1\text{N}$  of His95 and the backbone amide NH of Glu97 (Figure 1.1B).<sup>9</sup> This hydrogen bond would

preclude any true protonation at this site and suggest that the imidazole is a neutral catalyst.

The next possibility is that the neutral imidazole gives up its proton to the intermediate to form the neutral enediol and an imidazolate anion.<sup>9</sup> The  $pK_a$  associated with this process is usually considered to be close to 14.5, however it has been postulated that the position of His95 at the N-terminus of an  $\alpha$ -helix provides a great deal of shielding, which could significantly perturb its  $pK_a$ s.<sup>14, 15</sup> Some impressive  $^{13}\text{C}$  and  $^{15}\text{N}$ -NMR studies in the Knowles laboratory revealed that at least one  $pK_a$  of His95 is greatly decreased such that it remains *neutral* in both unliganded and ligand bound TIM over a pH range of 4.3-9.5.<sup>16</sup> Moreover, the studies showed that in the absence of substrate or intermediate analogue, both imidazole nitrogens are free of any hydrogen bonding interactions. This result contrasted sharply with the crystallographic data, which showed the possibility for a backbone- $\delta^1\text{N}$  interaction. In the presence of PGH, the  $\epsilon^2\text{N}$ —conclusively shown to bare the hydrogen—shows a strong 9 ppm downfield shift, indicating the formation of a rather strong hydrogen bond with the ligand. Perhaps the most important study with respect to this discussion, these results illustrate several key points. (1) By virtue of its surrounding environment, the  $pK_a$ s of His95 lie outside the working range of TIM, i.e. lower than 4 and higher than 10. (2) The imidazole is completely shielded against coulombic interactions until the substrate is bound. (3) The active site appears to be preferentially oriented to stabilize the enediol(ate) intermediate, not the substrate. (4) If both  $pK_a$ s shift equally, as shown with other substituted imidazoles, the 2<sup>nd</sup>  $pK_a$  of His95 could well be much more closely matched to the proposed  $pK_a$  of an enediol-type intermediate of this reaction. This matching could allow for rapid proton exchange from the imidazole to the intermediate.<sup>16-18</sup> Knowles

assessment of this data was that the predominant intermediate in the conversion of DHAP to G3P was an enediol facilitated by rapid proton exchange from His95 (Scheme 1.1).

**Scheme 1.1** Proposed enediol route for TIM mechanism



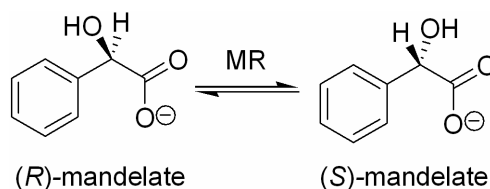
Reassessment of kinetic and thermodynamic data of the catalysis in conjunction with the structural and spectroscopic data has led to some controversy over the details of this intermediate.<sup>7, 19</sup> Discussion of this debate will continue below in the context of all three case studies.

#### 1.1.1.2 Mandelate Racemase

The enzyme mandelate racemase (MR) from *Pseudomonas putida* catalyzes the  $\text{Mg}^{2+}$ -assisted interconversion of the stereoisomers of mandelate, the sole source of carbon and energy for these organisms (Scheme 1.2). Only the *S*-enantiomer of mandelate can be converted into succinate and acetyl-CoA, which is essential in the generation of enzymatic cofactors and ATP. The ultimate goal of MR is to convert the *R*-enantiomer to the useful *S*-enantiomer. Under reversible conditions, a true or very close to racemic mixture would result due to nearly equal affinity of MR for both enantiomers of mandelate.<sup>20</sup> However, (*S*)-mandelate is normally oxidized quickly and removed from

the equilibrium. Due to the apparently simplistic nature of the reaction catalyzed by this enzyme, the structure, function, and mechanism of MR have been and are still being widely studied. MR represents the simplest example of an enzyme catalyzed carbon acid  $\alpha$ -proton abstraction.

**Scheme 1.2**



The 1,1-proton transfer mechanism has been studied in great detail, and has been shown to be the result of a two-base general base mechanism.<sup>21</sup> The active site structure was elucidated from crystal structures of inhibitor ((*S*)-atrolactone) and inactivator (alkylation of Lys166 by (*R*)- $\alpha$ -phenylglycidate) bound enzyme and was found to contain five critical elements for binding and catalysis.<sup>22</sup> Figure 1.2 shows a schematic of the active site of MR bound to (*S*)-mandelate extrapolated from the (*R*)- $\alpha$ -phenylglycidate alkylated crystal structure. Unlike TIM above and citrate synthase discussed below, MR requires the use of a doubly charged metal such as  $\text{Mg}^{2+}$ ,  $\text{Co}^{2+}$ ,  $\text{Ni}^{2+}$ , or  $\text{Mn}^{2+}$ .<sup>23, 24</sup> The native form of MR utilizes  $\text{Mg}^{2+}$ , which has been found to be essential to substrate and analogue binding. The crystal structures show interaction of the metal with one carboxylate oxygen and the  $\alpha$ -hydroxy group.

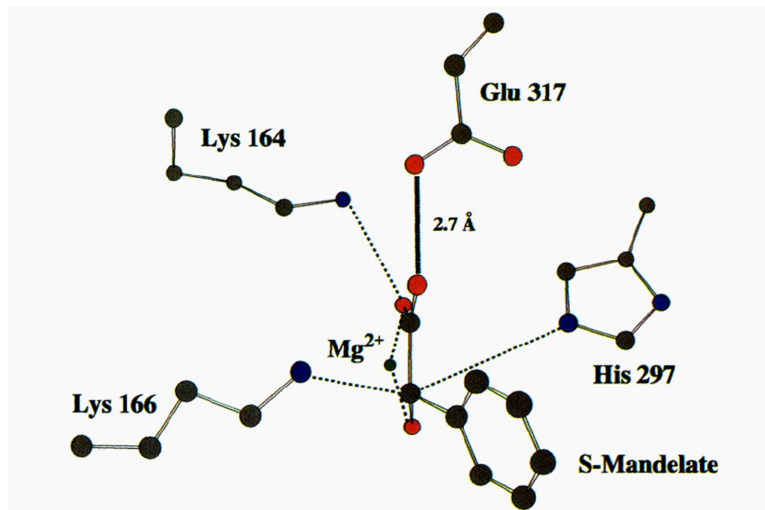


**Figure 1.2** Active site of MR with (S)-mandelate shows five key elements:  $\text{Mg}^{2+}$ , Lys164, Lys166, His297, and Glu317. Reprinted from ref. 19

A hydrogen bond from Lys164 to the same oxygen of the carboxylate bound to the metal, also appears to be present. These two elements, apart from helping the substrate to bind, have also been suggested to allow the carboxylate to exist in an environment where it more closely resembles a carboxylic acid.<sup>7, 19</sup> The  $\text{pK}_a$  of the  $\alpha$ -proton of a carboxylate anion has been proposed to be 29-32 and carboxylic acids 22-25.<sup>25</sup> The reason for an environment in which mandelate more closely resembles mandelic acid then is immediately apparent.

The two general bases mentioned above, have been determined to be Lys166 for the *S*-enantiomer and His297 for the *R*-enantiomer. Likewise, solvent protonated Lys166 acts to protonate the reaction intermediate generated from the *R*-enantiomer and vice versa for His297. These residues were assigned by site-directed mutagenesis experiments using H297N and K166R mutants as well as the previously mentioned (*R*)- $\alpha$ -phenylglycidate inactivation.<sup>21, 26</sup> Using the H297N mutant, racemase activity was



completely turned off, however Lys166 was still able to abstract the  $\alpha$ -proton as determined by conducting experiments in D<sub>2</sub>O. The *S*-enantiomer, though not racemized, showed a steady decrease in the <sup>1</sup>H-NMR resonance as H-D exchange occurred. The *R*-enantiomer showed no change. Similar experiments were conducted with the K166R mutant.<sup>26</sup> It was found that this mutant catalyzed the elimination of bromide from (*R*)-*p*-(bromomethyl)mandelate, but not *S*. These experiments demonstrated both the assignments of the general base catalysts and that the same residues act as acids to transfer a solvent proton to the intermediate. The H297N experiment also bolstered the evidence for a stepwise mechanism with a transiently stable intermediate through the incorporation of solvent deuterium into the stereochemically conserved (*S*)-mandelate. The synergistic roles of these two residues cannot be overstated, in that even though they have different apparent p*K*<sub>a</sub>s, they each catalyze the proton transfer at the same or nearly the same rate. The dependence of *k*<sub>cat</sub> on pH suggests that, in both directions, there are functionalities with p*K*<sub>a</sub>s of 6.4 and 10, which is reasonable in the R→S direction with His297 as the base, but is fairly unusual when Lys acts as the base.<sup>3,21</sup>

The final element of the active site crucial to catalysis is the Glu317 residue. The crystal structure analysis shows a likely hydrogen bond between the carbonyl oxygen of the mandelate carboxylate and a *neutral* glutamic acid carboxylic acid side chain.<sup>22</sup> As in TIM, there seems to be a significant environmental effect of the enzyme active site which perturbs the p*K*<sub>a</sub>s of several residues. In this case, however, it is unclear what structural bias is present to generate this change in the p*K*<sub>a</sub> of Glu317. It is clear however, that this coordination plays a large role in catalysis.<sup>27</sup> It has been suggested once again, that Glu317 acts as an electrophilic (general acid) catalyst in this system. This hypothesis is supported by experiments with an E317Q mutant. It was found that the rate of

racemization in both directions was reduced by roughly  $10^4$ -fold and that the enzyme could not catalyze the elimination of *p*-(bromomethyl)mandelate, which requires significant lowering of the  $pK_a$  of the  $\alpha$ -proton. Also the  $pK_a$  of the protonated intermediate ( $\sim 6.6$ ) and that of Glu317 is likely  $\sim 6$  which allows for good matching in the intermediate structure.<sup>28</sup> According the analysis by Knowles from the previous case study, this  $pK_a$  matching should allow for rapid proton exchange between the acid residue and the intermediate structure to give the geminal enediol intermediate. Again, the kinetic and thermodynamic data show some discrepancies with this neutralized intermediate, and similar solutions have been proposed, which will be discussed below.

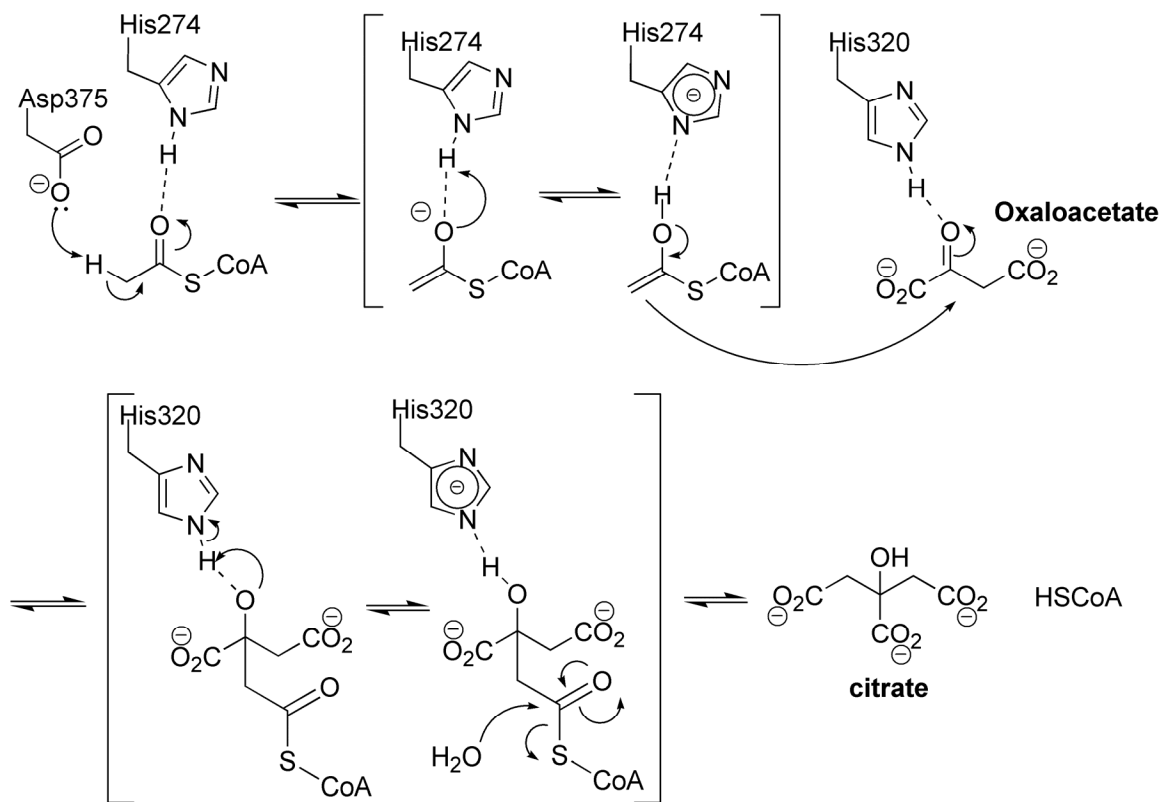
#### ***1.1.1.3 Citrate Synthase***

The tricarboxylic acid cycle, or the Krebs cycle, is chiefly responsible for converting the acetyl-CoA produced by the oxidation of pyruvate to three equivalents of the reductive cofactors NADH and one  $FADH_2$ .<sup>4</sup> These cofactors are then used to produce the energy storage molecule ATP. The first step of the TCA cycle condenses acetyl-CoA with oxaloacetate using the enzyme citrate synthase (CS).<sup>4</sup> A proposed condensation mechanism is shown in Scheme 1.3. It begins with the deprotonation of the  $\alpha$ -carbon of acetyl-CoA by Asp375 with concomitant coordination/protonation of the carbonyl oxygen by His274. Claisen condensation of the resulting enol(ate) with oxaloacetate with general base/general acid (electrophilic) catalysis provided by His274 and His320 then follows.<sup>29, 30</sup> This reaction produces the intermediate citryl-CoA which then adds water and loses HSCoA to form citrate.

The residues involved in the mechanism were elucidated by the high-resolution crystal structures of ternary complexes of chicken heart CS, D- or L-malate and acetyl-

CoA or the intermediate analogue carboxymethyl-CoA.<sup>31</sup> The structures showed interactions of both acetyl-CoA and carboxymethyl-CoA with both Asp375 and His274 and the  $\delta^1\text{N-H}$  of His274 was determined to be the general acid or electrophilic catalyst and the anionic carboxylate of Asp375 acts as the general base. Figure 1.3 shows the binding of the ternary complex of D-malate, acetyl-CoA, and CS with the hydrogen bond from the His274  $\delta^1\text{N}$  to the carbonyl of the thioester delineated. The carboxylate from Asp375 is poised on the opposite side of the substrate in close proximity to the methyl group. The specific orientation of this hydrogen bond will become more important later in this discussion.

**Scheme 1.3** Proposed route containing neutral intermediates for both general acid catalyzed steps



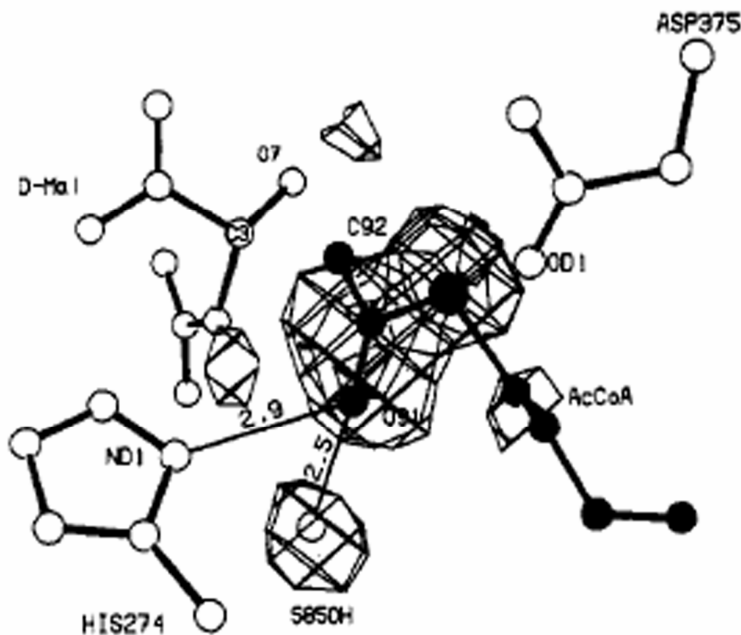


**Figure 1.3** Active site binding of acetyl-CoA from a ternary complex of D-malate, acetyl-CoA, and CS. The hydrogen bond from the  $\delta 1\text{N-H}$  to the carbonyl oxygen is indicated. Reprinted from ref. 31.

As in the case with TIM, compelling evidence that the environmental positioning of these residues causes significant altering of their  $pK_a$ s was reported through several site-directed mutagenesis studies.<sup>29, 32, 33</sup> It was found that any attempt to change the active site residues resulted in dramatically increased stability towards thermal denaturing. The implication is that the active site of the wild-type enzyme is specifically organized to electronically or sterically destabilize these residues in such a way that it generates a shift in their acid/base catalyzing properties.<sup>3</sup> In fact, crystallographic analysis shows similar environments for His274 and His320 in CS as for His95 of TIM.<sup>34</sup> Both residues are situated near the N-termini of helical portions of the protein, an observation used to argue for the decrease in histidine  $pK_a$ s in TIM. Hence it is

reasonable to assume that both His274 and His320 are more than just proton donors and help to polarize their respective carbonyls such that deprotonation of acetyl-CoA is more feasible. In fact, it was shown spectroscopically that such polarization of oxaloacetate occurs through similar imidazole hydrogen bonding from His320 prior to alkylation in the second step of Scheme 1.3.<sup>35</sup>

Following the Knowles argument, the environmental perturbation of the histidine  $pK_a$ s causes a matching of acidity between the neutral  $\delta^1\text{N-H}$  and the neutral enol intermediate.<sup>16, 18</sup> This  $pK_a$  matching should result in a rapid proton exchange from the imidazole to generate the neutral enol and the imidazolate or the neutral tetrahedral intermediate and the imidazolate. These rapid proton exchanges are indicated by the bracketed portions of Scheme 1.3. As such, in a very analogous fashion to both TIM and MR, CS appears to conduct a general acid-general base catalysis for both the formation of an enol intermediate, and the nucleophilic addition to oxaloacetate. Further electrophilic catalysis from His274 in the final hydrolytic cleavage has not been elucidated.

### 1.1.2 Low Barrier Hydrogen Bonds

A different theory for the specific role of these electrophilic general acid catalysts has been postulated by Gerlt and Gassman, as well as others.<sup>19, 36-38</sup> This theory involves the formation of very short, strong hydrogen bonds between the electrophilic catalysts and the respective substrates in the transient intermediates. These short strong hydrogen bonds have also been called low barrier hydrogen bonds or LBHBs, which stems from the idea shown in Figure 1.4. As the heteroatom distance of a hydrogen bond shrinks, the potential energy barrier for proton exchange between the heteroatoms also shrinks.<sup>39</sup> In

the gas phase, crystals, and nonaqueous solvents, LBHBs have been shown to be very strong on the order of  $\geq 20$  kcal/mol. Contrast that with regular hydrogen bonding at  $\leq 2$  kcal/mol, and the amount of stabilization to be obtained on the formation of an LBHB is considerable.<sup>39, 40</sup> The consequence of a low barrier of exchange is the hydrogen bond becomes semi-covalent rather than simply electrostatic as in normal hydrogen bonding. Several requirements are usually outlined for the possible formation of LBHBs. (1) The distance between the heteroatoms of the species must be less than 2.55Å. A typical hydrogen bond length in water is 2.8Å, which classifies the classic water network as a set of weak hydrogen bonds.<sup>41</sup> However, even these weak hydrogen bonds are sufficient to make water a liquid at room temperature where hydrogen sulfide is a gas. (2) There must be a congruity of the  $pK_a$ s of the donor/accepter pair. In order for a situation like Figure 1.4B to occur, the zero point energies for the two heteroatom-H bonds must be similar or the energy difference will favor one covalency over the other and a scenario results in which the barrier for exchange to the disfavored covalency will be too large. (3) It has been shown that LBHBs will not form in competitive media such as water or other protic solvents. It has been strongly argued that the formation of LBHBs in enzymatic transformations is not feasible due to this last caveat.<sup>42</sup> However, calculations have shown that ordered water molecules, such as those found in enzyme active sites, will not interfere with low barrier hydrogen bonding.<sup>19</sup>

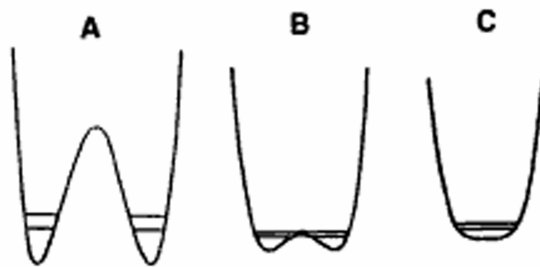
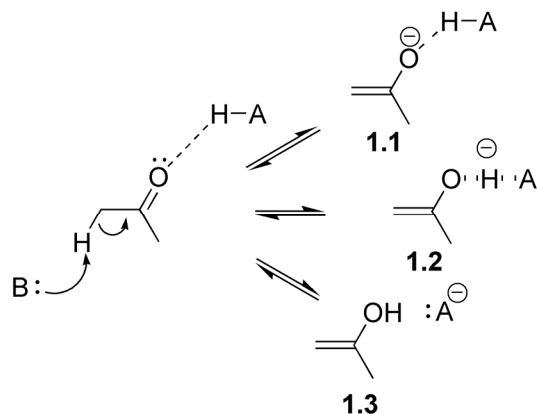


**Figure 1.4** A) Normal hydrogen bond  $A-H-A \geq 2.8 \text{ \AA}$ ; B) Low barrier hydrogen bond  $2.55 \text{ \AA} \geq A-H-A \geq 2.3 \text{ \AA}$ ; C) Single well hydrogen bond  $A-H-A \leq 2.3 \text{ \AA}$ .  
Reprinted from ref. 36

Gerlt and Gassman argued for the formation of LBHBs through the use of the Marcus formalism, which breaks the activation energy of a reaction  $\Delta G^\ddagger$  into two parts:  $\Delta G^\ddagger_{\text{int}}$ , the intrinsic kinetic barrier, and the contribution from thermodynamic barrier  $\Delta G^\circ$ .<sup>43, 44</sup>  $\Delta G^\ddagger_{\text{int}}$  is defined as the kinetic barrier of a reaction when  $\Delta G^\circ = 0$ . In order for catalysis to occur, an enzyme must ultimately lower the composite  $\Delta G^\ddagger$  in some fashion. The dilemma with proton transfer catalysis such as the case studies above, is that the calculated relative  $\Delta G^\ddagger$  is usually 13-17 kcal/mol based on their  $k_{\text{cat}}$ s. However, based on the  $pK_{\text{a}}$ s of the general bases involved in these reactions ( $\sim 6-7$ ), calculation of  $\Delta G^\ddagger$  in solution can be as high as 20 kcal/mol greater than the 13-17 kcal/mol seen with the enzyme. And so the question becomes, how does the enzyme achieve this fantastic reduction in the activation energy for these carbon acid processes? Gerlt and Gassman proposed that the data provided for such enzymes as those discussed above allows for the formation of an intermediate that is neither the anionic enolate (**1.1**) nor the neutral enol (**1.3**), but rather a structure in between stabilized by a low barrier hydrogen bond from the electrophilic catalyst residue (**1.2**)(Scheme 1.4).<sup>19</sup>

**Scheme 1.4**



For all three cases studied above, the evidence is favorable for the formation of a low barrier hydrogen bond. (1) The environmental perturbation of the  $pK_a$ s of His95 in TIM, Glu317 in MR, and His274 and His320 in CS, put all of these residues in close acidity matching with the proposed neutral enol intermediates. (2) All of these enzymes contain only ordered solvent molecules which would not interfere with a LBHB. (3) The neutral enol intermediates proposed are still too unstable to have the lifetimes suggested by empirical evidence.<sup>25</sup> (4) The distance requirements are well within reach based on the crystallographic evidence. The proposal was further broken down into how the interactions of the substrate/intermediate and general acid catalysts reduce both  $\Delta G^\circ$  and  $\Delta G^\ddagger_{\text{int}}$ .

The reduction in the free energy of the intermediate relies most heavily on the formation of the LBHB with the general acid catalyst. The  $pK_a$  matching of the would be neutral enol intermediates with the perturbed general acid catalysts help to facilitate much stronger hydrogen bonds with the intermediates than with the substrates ( $pK_a \sim -4$ ). This observation may also be tied to the previously mentioned theory of ground state



destabilization in which the enzyme is designed to destabilize the initial substrate in favor of strong binding to the intermediate.<sup>12</sup> By generating an intermediate with an intermolecular interaction, which can reduce its free energy by up to 20 kcal/mol versus a substrate with a stabilization of less than 2 kcal/mol, the enzyme facilitates a large reduction in the  $\Delta G^\circ$  of the reaction. This lowering of  $\Delta G^\circ$  results in a lower contribution of the free energy of the intermediate to the  $\Delta G^\ddagger$ . Thus the formation of the LBHB in the intermediate can help account for the  $k_{\text{cat}}$ s observed for these enzymes. The reduction of the intrinsic kinetic barrier,  $\Delta G^\ddagger_{\text{int}}$ , was proposed to arise from solvation effects of the general acid catalyst based on the Principle of Non-perfect Synchronization (PNS).

#### ***1.1.2.1 Principle of Non-perfect Synchronization***

It is fairly well known that the rate of deprotonation is much slower for carbon acids than acids of oxygen, sulfur, or other elements regardless of the  $\text{p}K_{\text{a}}$ . This observation has been attributed to the Principle of Non-perfect Synchronization (PNS), which is an extension of the Hammond Postulate.<sup>45</sup> PNS effects are seen in reactions in which two or more events are occurring during the same mechanistic step, such as in the deprotonation of a carbon acid. PNS is often described by Marcus formalism, which was originally based on electron/charge transfer reactions. To that end, an acid-base reaction can be thought of as a transfer of negative charge from the base to the acid. With a normal acid, such as  $\text{H}_3\text{O}^+$ , there is only one process occurring in the transition state, and the reaction can be thought of as completely symmetric. Carbon acids such as acetaldehyde or nitromethane, however, not only have a transfer of charge from the base, but also a delocalization of that charge through resonance and a rehybridization of the

resulting carbanion. The result is a situation in which one or more processes lag behind another during the reaction coordinate.

Perhaps the most widely known study of PNS with respect to carbon acids was conducted on aryl nitroalkanes and has been termed the nitroalkane anomaly.<sup>46, 47</sup> Hammett studies of the deprotonation of various aryl nitroalkanes with hydroxide revealed that the kinetic  $\rho(k)$ -value for deprotonation (1.28) was greater than  $\rho(K)$ -value for equilibrium (0.83). This result suggested that electron withdrawing groups have a greater stabilizing effect on the transition state than on the ionic product. Even more perplexing,  $\rho(k)$  in the reverse direction, i.e. protonation of the nitronate anion, was also found to be positive, 0.45, suggesting that electron withdrawing groups speed up protonation as well. In other words, the less basic the anion, the faster the proton transfer. When these values are normalized to Brønsted coefficients, the resulting values are highly irregular,  $\alpha = 1.54$ ;  $\beta = -0.55$ . Oddly,  $\beta$  values derived by changing the general base, are in the normal range between 0-1. Since the Brønsted coefficients can be thought of as a measure of the extent of proton transfer at the transition state, a 1.54  $\alpha$ -value suggests nearly complete deprotonation at the TS in the forward direction, and the -0.55  $\beta$ -value implies nearly no protonation in the reverse direction. The ultimate conclusion is that during the deprotonation, the transfer of charge/proton happens first while the rehybridization and delocalization through resonance lags behind such that most of it occurs on the down slope of the reaction coordinate. What this means, is that there is a localization of charge on the carbon, which raises the intrinsic kinetic barrier due to the high unfavorability of anionic carbon. Figure 1.5 gives a qualitative look at the anomaly which holds true for nearly all carbon acids in which resonance delocalization occurs.

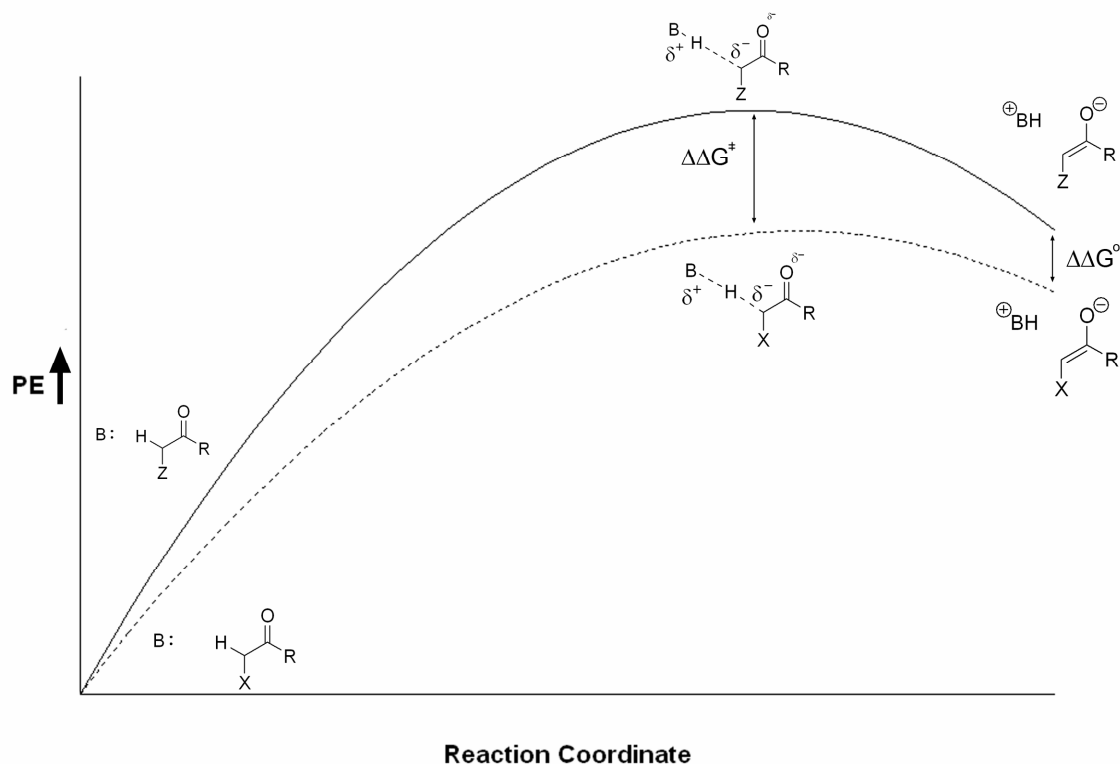


**Figure 1.5** The PNS dependence of carbon acid deprotonation leads to the situation in which electron withdrawing effects ( $X > Z$ ) have a greater affect on the transition state than the product.

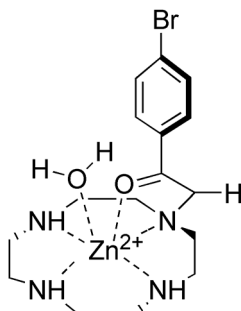
There have also been studies on the effects of solvation on the extent asynchronous proton transfer, which show that in disordered, hydrogen bonding solvents such as water and methanol, the PNS effect is much larger than in non-anion stabilizing solvents such as DMSO and acetonitrile.<sup>45</sup> The reason for this solvent dependence is that solvent reorganization in hydrogen bonding solvents again lags behind charge transfer. Fortunately, however, this behavior is observed for all acids, not just carbon acids. The lag time is thought to be entropic in nature, due to a greater  $\Delta S^\ddagger$  for solvent rotational changes than for vibrational mode changes. Hence in a solvent which reorients itself

around a charge as compared to a dipole, such as water, there is an added contribution to the  $\Delta G^\ddagger_{\text{int}}$  from the entropic cost of solvent reorientation that is not seen in less polar media. Gerlt and Gassman used this resolution effect to explain how the general acid catalysts in these enzyme mechanisms go about lowering the  $\Delta G^\ddagger_{\text{int}}$  of the deprotonation event.<sup>19</sup> They argued that the electrophilic general acid residue was preoriented to “solvate” the growing negative charge on the oxygen at the transition state whether it formed an LBHB or not. The preorientation would eliminate the entropic cost of solvent reorientation and remove it from  $\Delta G^\ddagger_{\text{int}}$ .

It is the opinion of this author, as well as others, that this reasoning is flawed for several reasons.<sup>42, 48, 49</sup> (1) If PNS is to be argued, the transition state of carbon acid deprotonation should show very little formation of negative charge on the oxygen. In other words, the bulk of  $\Delta G^\ddagger_{\text{int}}$  is determined by the fact that an excess of charge is growing on the *carbon* with very little progress towards rehybridization and delocalization. Hence, the entropic cost from solvent orientation lag is an effect related to the carbanion formation, not the delocalized charge. (2) As previously argued by Gerlt and Gassman themselves, there is very little disordered solvent present in the active site of the enzyme. Since the  $\Delta S^\ddagger$  contribution arises from the reorientation of disordered solvent, it is unlikely that this effect would be very large in the ordered binding pocket. These criticisms, however, are not intended to say that the ultimate proposition that  $\Delta G^\ddagger_{\text{int}}$  is lowered by the general acid is incorrect. However, the reasoning that the main contribution arises from the lessening of an entropic loss seems unlikely. This discussion will be revisited in a later section below.

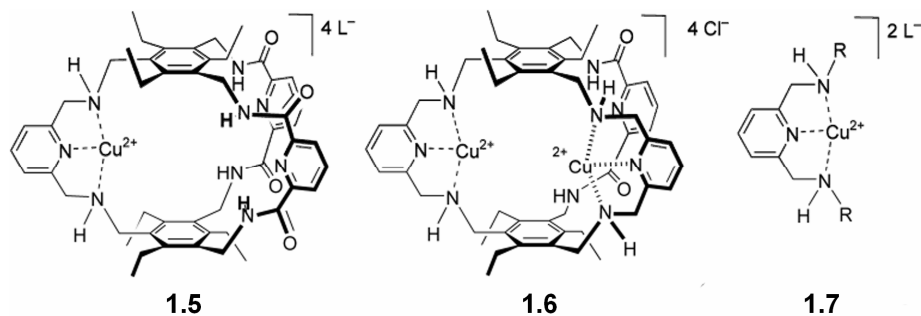
### 1.1.3 Beyond LBHBs

The low barrier hydrogen bond theory has had several critics and articles continue to be published which claim to show evidence either for or against the formation of LBHBs in enzyme mechanisms.<sup>50-57</sup> Several other theories have been proposed, either in lieu of or complimentary to the formation of LBHBs. One of these is the theory that the metal coordination that is necessary for catalytic action in enzymes such as MR plays a much larger role in reducing the overall kinetic barrier by reducing the  $pK_a$  of the  $\alpha$ -proton. Enolases, racemases, and aldolases in particular all contain at least one vital metal center at their active sites. Kimura *et al.* synthesized the 4-bromophenacyl-pendant cyclen system **1.4** to evaluate the mechanism of class II aldolases and the role of Zn(II) in the enolization step.<sup>58</sup> In a very similar fashion to the  $\alpha$ -proton transfer enzymes discussed above, class II aldolases from bacteria use a  $Zn^{2+}$  cation in their active sites to help stabilize the enolic intermediates generated in the reversible stereospecific aldol condensation which they catalyze. It was found that the presence of the Zn(II) in close proximity of the carbonyl oxygen in **1.4** was able to reduce the  $pK_a$  of the  $\alpha$ -proton to 8.41, nearly 10 orders of magnitude. The kinetic barrier towards deprotonation also appeared to be reduced with the half-life of H-D exchange reported at 25 minutes at 298K by  $^1H$ -NMR.



**1.4**

Studies in the Anslyn group using a series of hosts **1.5-1.7**, have shown that shifts of nearly 12  $pK_a$  units are observed for  $\alpha$ -hydrogens of various  $\beta$ -diketones.<sup>59</sup> The encapsulated host scaffolds, **1.5** and **1.6** showed slightly greater  $pK_a$  reduction due to better solvent exclusion from the interior. Yet in all cases, coordination to the Cu(II) affords a great deal of enolate stabilization. However, these findings do not account for enzymes such as TIM and CS in which no metals are present at the active site of enol(ate) formation. Another method of electrophilic stabilization, which may or may not occur through a low barrier interaction, has recently been postulated by the Anslyn group.



The active site of medium chain acyl-CoA dehydrogenase (MCADH) bound to the inhibitor 4-nitrophenyl-acetyl-CoA is shown in Figure 1.6A. The acyl-CoA dehydrogenase class of enzymes catalyze the  $\alpha,\beta$ -dehydrogenation of fatty acid acyl-CoA conjugates to the corresponding enoyl-CoA products. The reaction proceeds *via*  $\alpha$ -proton abstraction by Glu376 followed by  $\beta$ -hydride removal by the FAD cofactor. The crystal structure of wild-type medium chain acyl-CoA dehydrogenase shows no metal coordination in the active site, yet the substrate, like those in TIM, MR, and CS, must be highly activated for deprotonation to occur.<sup>60</sup> Looking at the active site in Figure 1.6A, there is a distortion in the hydrogen bonding geometry to the carbonyl oxygen from that which is generally accepted to be the most stable. That is, the hydrogen bonds indicated

from the backbone amide of Glu376 and the 2'-OH of the flavin are not in the plane of the oxygen's lone pairs. Likewise, 4-chlorobenzoyl-CoA dehalogenase, whose active site is shown in Figure 1.6B, catalyzes the hydrolytic removal of chloride from 4-chlorobenzoyl-CoA conjugates through a Meisenheimer complex intermediate.<sup>61</sup> Though the reaction does not involve an  $\alpha$ -proton abstraction, the Meisenheimer complex is enolic in form (Figure 1.6C). Notice again that the backbone amide hydrogen bonds are not in the plane described by the carbonyl oxygen's lone pairs. Looking back at the crystal structure of citrate synthase in Figure 1.3, there also appears to be a good deal of hydrogen bonding from His274, not toward the lone pairs of the thioester oxygen but rather to the  $\pi$ -bond.

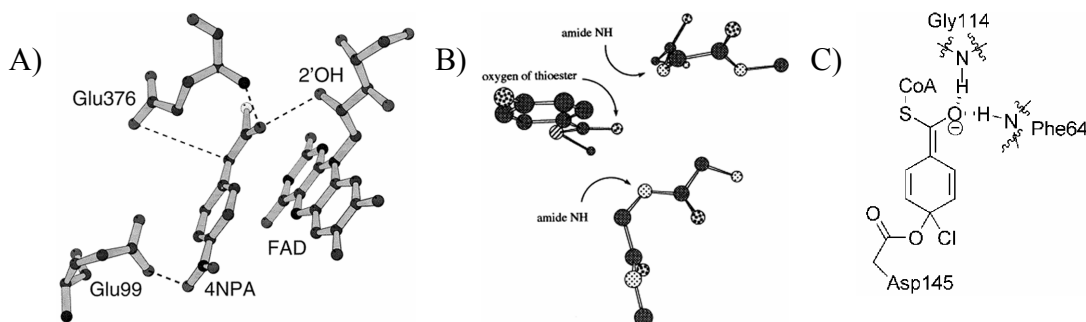
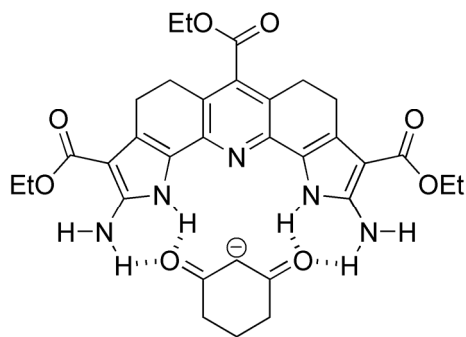


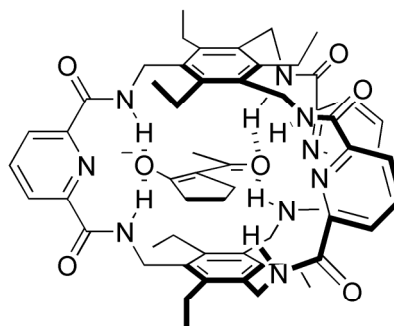
**Figure 1.6** A) Model of 4-(nitrophenyl)acetyl-CoA bound to MCADH with  $\pi$ -directed hydrogen bonds to the substrate analogue. Reprinted from ref. 60. B) Crystal structure of the active site of 4-Chlorobenzoyl-CoA dehalogenase with backbone amide hydrogen bonds to the  $\pi$ -face of the thioester. Reprinted from ref. 61. C) Enolic structure of the Meisenheimer intermediate from the mechanism of 4-Chlorobenzoyl-CoA dehalogenase.

In previous studies, our group has shown that placement of an electrophile in coordination with the  $\pi$ -system of a C=O bond can help to reduce the  $pK_a$ 's of  $\alpha$ -hydrogens by over 2  $pK_a$  units more than similar coordination to the carbonyl oxygen

lone pair.<sup>62, 63</sup> Receptor **1.8** was developed to model enolases and racemases. The crescent shaped receptor utilizes four amide-like hydrogen bond donors in a cavity to emulate an enzyme active site. **1.8** was screened for  $\beta$ -diketones and 1,3-cyclohexanedione was found to be most complementary with an association constant ( $K_a$ ) of  $1.35 \times 10^4 \text{ M}^{-1}$ . However, even with the cooperative binding of four hydrogen bonds, potentiometric titrations in acetonitrile revealed that **1.8** was only able to lower the  $pK_a$  of the active methylene of 1,3-cyclohexanedione by about 1 unit.<sup>64</sup> In a more competitive media, such as water, this stabilization would perhaps even be smaller.



**1.8**



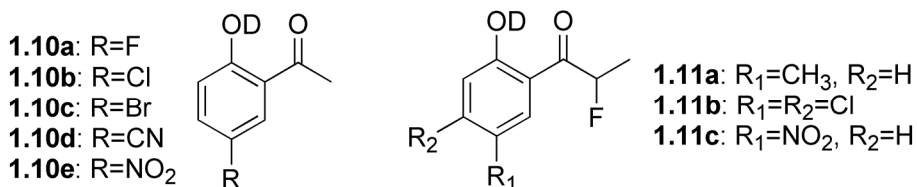
**1.9**

The bicyclic cyclophane **1.9** was used in a later study to test the effect of  $\pi$ -orbital hydrogen bond acceptance on  $pK_a$  shifting.<sup>62</sup> Because negative charge delocalization occurs mainly through the  $\pi$ -system, it was thought that greater stabilization could be gained by hydrogen bonding through the  $\pi$ -system rather than the lone pairs. In this study, 2-acetylcyclopentanone had the greatest complementarity to **1.9** ( $K_a = 3.06 \times 10^3 \text{ M}^{-1}$ ), and was chosen as the model carbon acid. The binding cavity of **1.9** is small enough (7.0 Å high) to constrain the guest to an horizontal orientation, which also constrains the hydrogen bonds to  $\pi$ -donation. It was found that, in acetonitrile, the  $pK_a$  of



2-acetylcyclopentanone in the presence of **1.9** was 22.5, 2.9 units lower than the free dione. These findings constitute a 300% increase in the stabilization of enolate formation based largely on the geometry of hydrogen bonding. Again, while impressive, there are some caveats to consider when looking at these findings. Though the electronics of the respective guests are fairly similar, those of the hosts are not. Cyclophane **1.9** contains amide hydrogen bonds, whereas **1.8** contains one set of vinylagous amide hydrogen bonds and one set of pyrrolic hydrogen bonds. The strengths of the inductions, which arise from these hydrogen bonds, are inherently different and are difficult to compare directly. There are also two more potential hydrogen bonding sites in **1.9** which will statistically add their inductive effects to the guest.

The previous two studies, while informative, are based solely on the thermodynamic advantages of hydrogen bond orientation, yet as seen in the nitroalkane anomaly, when it comes to carbon acids, kinetic effects are much more important. To determine the effects of lone pair directed hydrogen bonding on the rate of  $\alpha$ -proton abstraction, Anslyn and co-workers developed a series of 2-acylphenol probes **1.10** and **1.11** for Brønsted analysis of the rate of H-D exchange at the active carbon.<sup>65</sup> As a control, the phenol methyl ether versions of each compound in the **1.10** series were also synthesized and subjected to rate studies.



The kinetics experiments were conducted *via* <sup>1</sup>H-NMR in both 4:1 CD<sub>3</sub>OD/D<sub>2</sub>O (pD 5.83) and in acetonitrile. Both were buffered in a large excess of

imidazole/imidazolium chloride. These conditions ensured rapid and complete exchange of the phenolic proton for deuterium such that isotope effects could be dismissed. Rate constant versus pD analysis showed a leveling at pD~7; rate constant versus imidazole concentration increased linearly with increasing base. Both results are indicative of the desired general base catalysis. For Brønsted analysis, the  $pK_a$ s of the phenols were determined in both the methanol/water mixture (potentiometrically) and in acetonitrile (by comparison with known indicators). The Brønsted plots of series **1.10** and the methyl-ether analogues showed rather interesting results. The relative rate enhancement over the entire series was shown to be less than a single log unit, which is quite low for an intramolecular hydrogen bond.<sup>66</sup> Also, the  $\alpha$ -values in water determined from the slopes of the **1.10** series and the methyl ether controls are only 0.24 and 0.15 respectively. The difference of these two values gives a measure of the effect of hydrogen bond strength on the rate constant and only amounts to 0.09 in water. Strikingly, though the individual compounds showed rate enhancement, the same difference value arises for analysis in acetonitrile, in which one would by inspection expect larger contributions from the hydrogen bond in the stabilization of the enol(ate) intermediate. The **1.11** series was used to determine if lowering the  $pK_a$  of the enol intermediate would result in a greater effect due to better  $pK_a$  matching for possible LBHB formation. The results were similarly unimpressive, giving an  $\alpha$ -value of 0.24 in acetonitrile based on  $pK_a$ s determined in water.

These results were attributed once again to the Principle of Non-perfect Synchronization. Since there is very little negative charge developing on the carbonyl oxygen at the transition state of deprotonation, the overall strength of a hydrogen bond attempting to reduce the activation barrier makes very little difference. Though the

results of this study are based on intramolecular hydrogen bonds, some extrapolation to the intermolecular interactions found in enzymes can be made. The chief observation being that the formation of a low barrier hydrogen bond to the lone pair electrons of the substrate carbonyl oxygen would have very little effect on  $\Delta G^\ddagger$ . However, it is the ultimate purpose of the research presented below to examine whether placing a strong electrophilic coordination—whether it be a metal, LBHB, or normal hydrogen bond—directed toward the  $\pi$ -electron density could have a greater effect, not only on the thermodynamic stability of the resulting enol(ate), but also on the kinetics by perturbing the effects of the asynchronous nature of the transformation.

## 1.2 EXPERIMENTAL DESIGN

As mentioned above, Jencks proposed in the mid-70's the idea of ground-state destabilization in enzyme binding and catalysis.<sup>12</sup> In this case, the term “ground-state” refers to the initial form of the substrate rather than an electronic state of the molecule. The general premise is that an enzyme, or any catalyst for that matter, is primarily designed to lower the energy associated with  $\Delta G^\ddagger$  of the reaction it carries out. To do that, it has been postulated and empirically determined, that the enzyme active site should have a much higher affinity for either the transition state or high energy intermediate than the “ground-state” substrate. Mandelate racemase, for instance, has been shown to bind its mandelate substrates with  $K_a$ s on the order of  $10^3$ , yet determination of the  $K_a$  of MR to the common transition state of *R* and *S*-mandelate has been determined at close to  $10^{19}$ .<sup>67, 68</sup> Furthermore, the transition state binding thermodynamics have been broken down to show both favorable enthalpy *and* favorable entropy changes for the racemization reaction with enzyme assistance with respect to the non-enzymatic

reaction.<sup>67</sup> The overall binding enhancement was determined to be 26 kcal/mol for the transition state of the MR-mandelate complex.<sup>68</sup> This number will become significant in light of the findings described in the following sections.

On a fundamental level, the concept of ground-state destabilization can be described through qualitative analysis of the thermodynamic cycle of an enzyme catalyzed transformation shown in Figure 1.7. In this case, let us consider the enzyme assisted Brønsted acid dissociation of a carbon acid. In essence, there are two routes by which the reaction could proceed. The first, denoted by the  $K_1$ - $K_2$  route, involves deprotonation of the substrate before it binds to the enzyme or host. The second path goes through the host/guest binding event before deprotonation. Because the reactants and products of both routes are identical, the energies of both pathways must also be equivalent as shown in the first equation. Corollaries to the kinetics can also be drawn if the equilibrium constants are assumed to be in agreement with the Michaelis constant  $K_M$ . For a carbon acid,  $K_1$  is inherently small and the reaction is slow. Since  $K_1 = [S^-][H^+]/[SH]$ , there is no thermodynamic or kinetic dependence on the enzyme and the value can be assumed to be constant for the same carbon acid. All of the other equilibria are dependent on the enzyme, and as such, changing the enzyme in any way will affect all of them.  $K_4$  and  $K_2$  describe binding constants whereas  $K_3$  is the actual measure of the catalyzed deprotonation. The idea of ground state destabilization says that  $K_4$  should be small while  $K_2$  is large. In other words, the binding of the enzyme to the substrate should be weak—small  $K_4$ —compared to the binding of the transition state or, in this case, the intermediate—large  $K_2$ . Hence, the ratio of  $K_4/K_2$  on the right side of the second equation in Figure 1.7 should be less than 1. Thus, as this ratio becomes smaller

and smaller with increased affinity for the intermediate over the substrate,  $K_3$ , the rate or equilibrium of deprotonation, must increase in order to maintain a constant  $K_1$ .

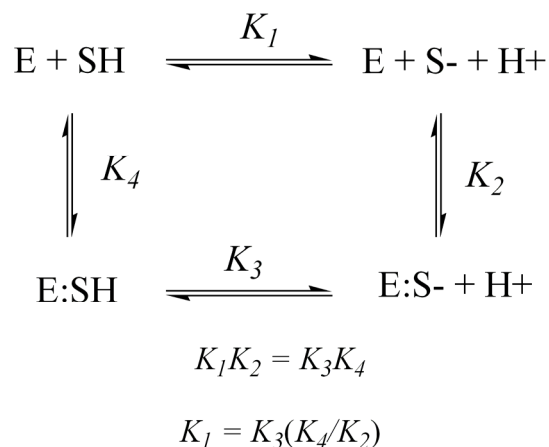


**Figure 1.7** Thermodynamic cycle of enzyme-assisted acid dissociation.

It is well established that, for a neutral carbonyl, electrophilic coordination to the lone pair orbitals is a stabilizing effect.<sup>2</sup> However, in light of the evidence presented above, lone pair coordination, at least from hydrogen bonding, has minimal effect on both the kinetics and thermodynamics of carbon acid deprotonation.<sup>62, 64, 65</sup> It should follow then, that the traditional mode of hydrogen bonding and other semi-weak electrophilic coordination to the oxygen lone pairs does not fulfill this notion of ground state destabilization as it increases the affinity for the neutral substrate ( $K_4$ ) and has little effect on the binding of the transition state/intermediate ( $K_2$ ). The results from the  $\pi$ -directed hydrogen bonding study are much more promising as they show better thermodynamic enhancement of the enol(ate) forming event.<sup>62, 63</sup> From a qualitative standpoint, this enhanced  $\text{p}K_{\text{a}}$  shift arises from two effects: (1) a destabilization of the neutral carbon acid through an induction of electron density away from a bonding orbital, hence reducing the

effective bond order and raising the energy of the bond, (2) stabilization of the resulting enolate by electrophilic induction of the  $\pi$ -delocalized negative charge. In the case of a proton transfer from a general acid to form the enol, the second effect is altered such that the best electrons to use in the new O-H bond are those from the breaking  $\pi$ -orbital due to energy matching. Following Jencks' logic then,  $\pi$ -bond coordination could well behoove an enzyme attempting to destabilize the initial carbon acid in favor of strong binding to an enolic transition state or intermediate. To semi-quantitatively assess the extent of this effect, a series of computational studies was performed on a simple electrophile coordinating to a simple carbon acid.<sup>69</sup>

### 1.3 THE LITHIUM-ACETALDEHYDE MODEL

In effect, we chose the simplest non-proton electrophile,  $\text{Li}^+$ , and the simplest carbon acid, acetaldehyde. A lithium cation was chosen as the model electrophile instead of a proton in order to ensure a coordinative bond distance from the carbonyl oxygen as opposed to the covalent bond that a proton would likely generate. Acetaldehyde was chosen to keep the CPU cost to a minimum while still allowing for  $\alpha$ -proton abstraction. With these two components, two potential energy surfaces were generated at an MP2 level with a 6-31G\* basis set using the ACES II quantum chemical program package developed by Stanton and collaborators.<sup>70</sup> The surfaces were generated by manually varying the Li-O-C bond angle against the Li-O-C-C dihedral angle in 5 degree increments as shown in Figure 1.8.

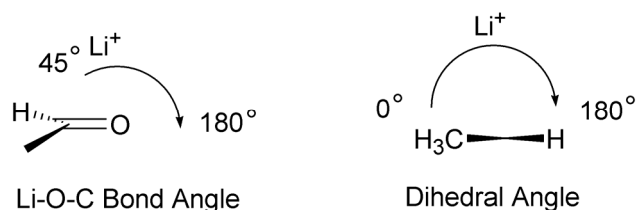


**Figure 1.8** Surfaces were obtained by iteration in 5 degree increments along both the Li-O-C bond angle (left) from  $45^\circ$ - $180^\circ$  and the Li-O-C-C dihedral angle (right) from  $0^\circ$ - $180^\circ$ .

Two surfaces were generated as composites of single-point energies for each combination of bond and dihedral angle listed in Figure 1.8, one for neutral acetaldehyde and the other for its enolate. Potential energy surfaces were compiled as opposed to fully optimized single-point energies because the goal was to predict the best placement of the electrophile to increase the acidity of a carbon acid. Such a geometry may not be a global energy minimum for either individual complex. Figure 1.9A shows the surface generated for the lithium cation coordinating to neutral acetaldehyde. As was expected, the global energy minimum geometry, Figure 1.9B, shows coordination of the lithium solely to the longitudinal lone pair of the carbonyl oxygen. Note, that for the neutral carbon acid, any coordination which deviates from the linear geometry predicted, results in a destabilization of the molecule. This observation is congruous with the theory of ground state destabilization in the enzymes discussed above for which there is evidence of  $\pi$ -directed hydrogen bonding to the substrate.

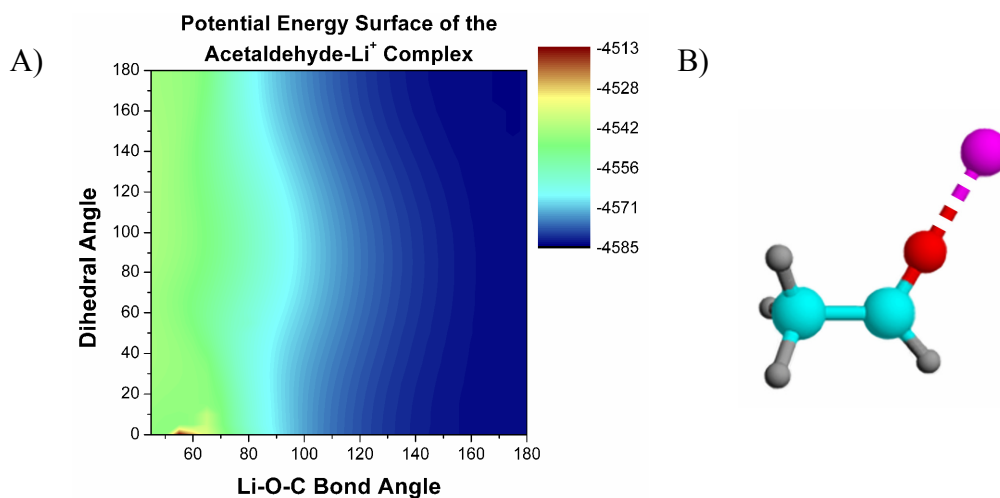


**Figure 1.9** A)  $\text{Li}^\oplus$  dihedral angle vs. Li-O-C bond angle enthalpy (kcal/mol) contour plot for the  $\text{Li}^\oplus$ -acetaldehyde complex generated at the MP2 level with a 6-31G\* basis set, and B) a graphical representation of the minimum energy structure.

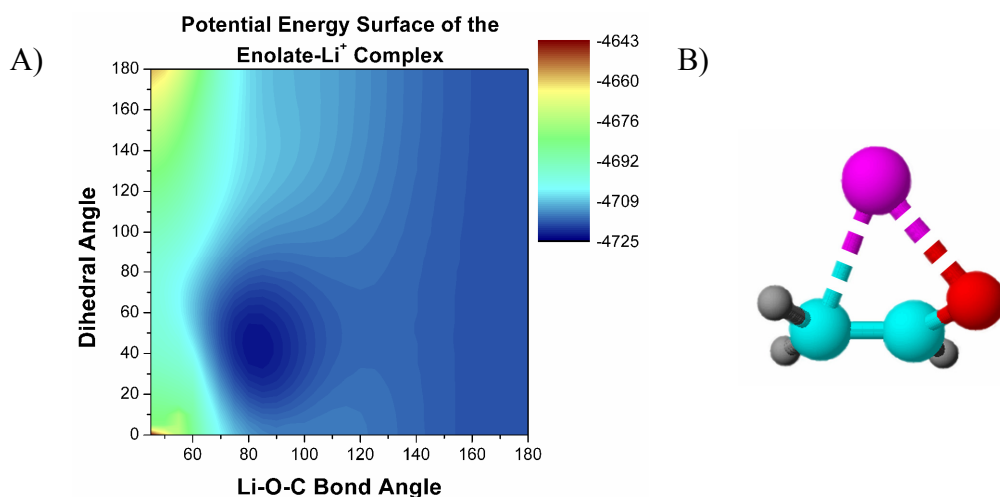


**Figure 1.10** A)  $\text{Li}^\oplus$ -dihedral angle vs. Li-O-C bond angle enthalpy (kcal/mol) contour plot for the  $\text{Li}^\oplus$ -enolate complex generated at the MP2 level with a 6-31G\* basis set. The global minimum structure (right) is shown with a dihedral angle of  $45^\circ$  and a Li-O-C bond angle of  $85^\circ$ .



Interestingly, the global energy minimum found from the enolate surface is quite different. In this case, the minimum geometry occurs at a Li-O-C bond angle of  $85^\circ$  and a Li-O-C-C dihedral angle of  $45^\circ$  (Figure 1.10). The first aspect to notice is the out-of-plane dihedral angle. This geometry suggests a significant amount of  $\pi$ -system coordination in the enolate system. The second important facet of this model is that based on rudimentary resonance analysis, the two centers of negative charge in an enolate reside at the oxygen and the  $\alpha$ -carbon. Hence, it is reasonable to assume this energy minimum arises due to coordination of the lithium ion to both the oxygen and the  $\alpha$ -carbon through the delocalized  $\pi$ -electrons.

These two surfaces alone say very little about which geometry is best to generate a substantive shift in the acid dissociation constant,  $K_a$ . As both of these surfaces were generated for gas phase systems, together they give an analysis of the relative gas phase acidity of this complex for all geometries, as well as the best geometry for enhancing the acidity of acetaldehyde by lithium coordination. The contour plot shown in Figure 1.11 arises from the difference of the enthalpies of lithium coordination to acetaldehyde and its corresponding enolate (see Figures 1.9 and 1.10). This contour represents the energy gained or lost at each single-point geometry upon enolate formation. Figure 1.11 does not technically represent a potential energy surface as with the two previous diagrams but should rather be thought of as a measure of the acid dissociation potential. Whereas the lowest energy conformation derived by inspection of the enolate surface resides at a bond angle of  $85^\circ$ , the gas phase acidity analysis reveals a new minimum occurring at  $70^\circ$ , while the dihedral angle remains  $45^\circ$  (Figure 1.12). The lithium now resides nearly perfectly anti-periplanar to the  $\alpha$ -hydrogen that will be deprotonated to create the enolate. Hence, backside electrophilic coordination to the orbital of the cleaving C-H bond as well

as  $\pi$ -system coordination to the carbonyl creates a more labile proton. Such a geometry does not exist as a global energy minimum for either individual complex.

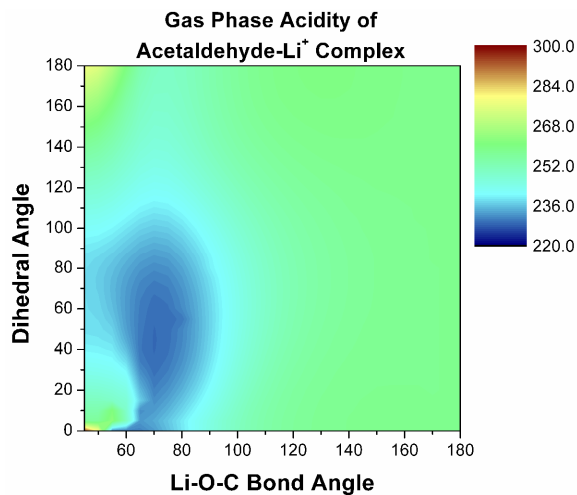


**Figure 1.11** Contour plot of the gas phase acidity (kcal/mol) of the acetaldehyde- $\text{Li}^+$  complex derived as the difference of the above acetaldehyde and enolate surfaces.

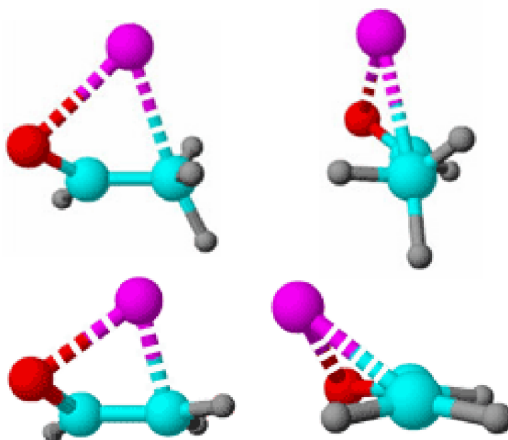


**Figure 1.12** (top) Front and side views of the optimum geometry for lithium coordination to enhance the acidity of acetaldehyde. (bottom) Analogous views of the enolate complex.

The calculated configuration for best enhancing acidity can be contrasted with the normally accepted geometry for enhancing acidity—coordination to the carbonyl lone pair. The acidity enhancement of the minimum depicted in Figure 1.12 versus lone pair coordination is the energy difference of the two single point enthalpies of the respective geometries. This difference amounts to 28.9 kcal/mol. At 0 K, this value results in a roughly 20 unit greater shift in  $pK_a$  with  $\pi$ -directed coordination of a Li cation as opposed to coordination to the lone pair. Previously, work conducted by Squires using  $BF_3$ -carbonyl complexes showed roughly 30-40% attenuation of the extent of the acidity enhancement garnered from the electrophilic coordination upon solvation in water.<sup>71</sup> Though this work was conducted on the absolute enhancement from coordination, it is reasonable to assume there would also be some extent of attenuation in the relative stabilization associated with the different geometries studied in this research. However, in an enzyme active site as discussed previously, the presence of solvent is generally in a highly ordered state with respect to bulk solvent. As such, the attenuation seen in bulk solvent should be higher than in the active site. Regardless of the actual value of the attenuation, this enhancement provides a clear understanding of the optimal geometry of coordination for maximum augmentation of acidity.

In addition, the discovery of the maximum acidity enhancement occurring at a coordination geometry in which the electrophile is heavily coordinated to the  $\alpha$ -carbon is of note in light of the Principle of Non-Perfect Synchronization. The effect of this coordination appears to be two-fold. First, a destabilizing interaction through backside C-H coordination increases the lability of the proton. Notice that the C-H bond in question is elongated indicating a weaker bond. Second, since the main contribution to the kinetic barrier of carbon acid deprotonation is the build up of negative charge on the

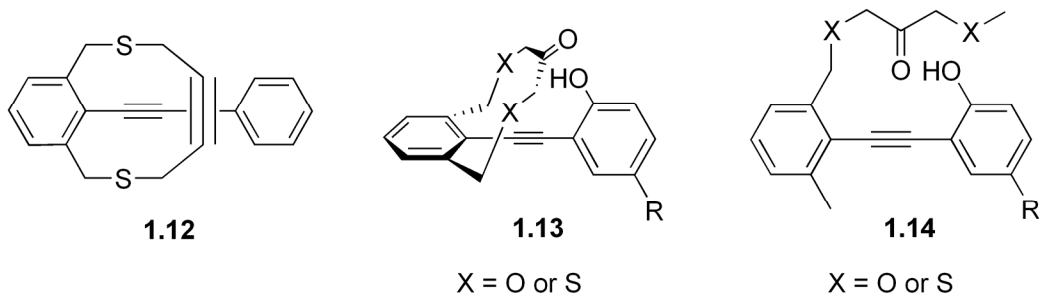
$\alpha$ -carbon resultant of a lag time in rehybridization and delocalization to the oxygen, coordination of an electrophile directly towards that building charge would help to significantly reduce  $\Delta G^\ddagger_{\text{int}}$  which was suggested to be necessary by Gerlt and Gassman.<sup>19</sup>

Since reaction coordinate and transition state modeling were not conducted, this analysis of the kinetic effects of this study is purely speculation. However, it is fair to say that the enzymes for which this type of interaction has been noted above take advantage of this ground state destabilization and the acidity enhancement which is garnered from  $\pi$ -directed electrophilic coordination. As discussed above, the reasoning put forth by Gerlt and Gassman for the reduction of  $\Delta G^\ddagger_{\text{int}}$  *via* entropic gain through preorganized coordination to the carbonyl oxygen does not strictly follow the Principle of Non-Perfect Synchronization which they exploit. As there is very little charge in the transition state on the oxygen, a preorganized coordination to the developing charge on the carbon or conformational change of the active site to facilitate this coordination would better fit a model for the reduction of  $\Delta G^\ddagger_{\text{int}}$ . From the study described above on the thermodynamics of MR transition state/intermediate binding and our findings, the 26 kcal/mol reduction in  $\Delta G^\ddagger$  could be achieved almost entirely by coordination to the  $\pi$ -system of the carboxylate of mandelate. The addition further coordination from the essential  $\text{Mg}^{2+}$  and the other stabilizing residues would more than allow this type of directed general acid catalysis to achieve the stabilization required to fit the observed kinetics and thermodynamics.

#### 1.4 DESIGN AND SYNTHESIS OF SCAFFOLD 1.13

In an effort to test the kinetic implications of these results with tangible experiments, we designed a molecular scaffold which would rigidly pre-orient an

intramolecular hydrogen bond towards the  $\pi$ -system of a carbon acid. Though it would not be feasible to generate the type of interactions described by the computational modeling, some constraint of the coordination through the  $\pi$ -bond should be possible. Ultimately, the scaffold chosen was based off of reports of several metacyclophanes similar to **1.12** synthesized by Cao *et al.*<sup>72</sup>

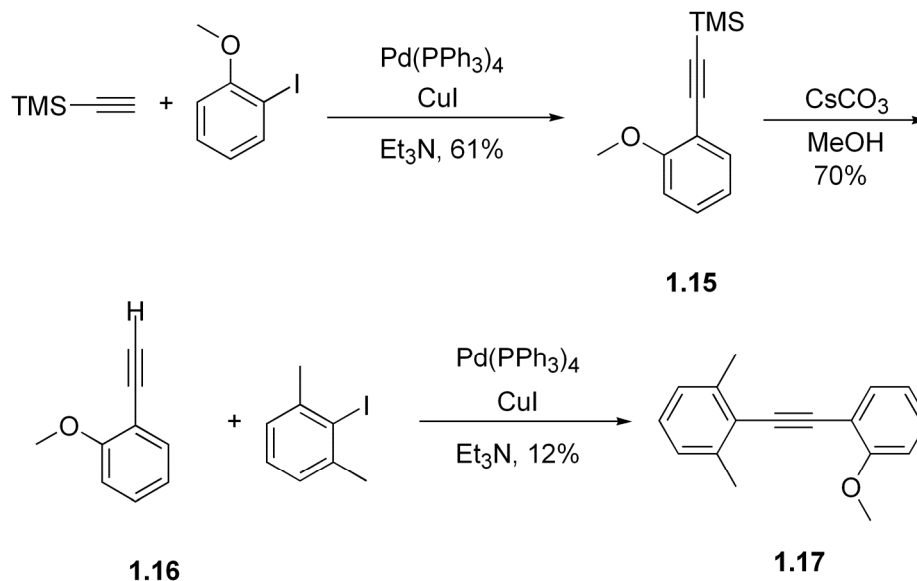


Cyclophane **1.13** incorporates all of the aspects desired for kinetic studies on the effect of  $\pi$ -directed hydrogen bonding on carbon acid deprotonation. Crystal structures of **1.12** show that upon appending the cyclophane arms, the two phenyls will reorient from a coplanar geometry to an orthogonal one.<sup>72</sup> Geometry minimizations using MacSpartan also indicate that in **1.13**, the phenyl rings will also be perpendicular to each other, constraining the phenolic hydrogen bond donor to point directly towards the  $\pi$ -system of the ketone acceptor. Based on the modeling, our original plan was to incorporate a pyridine moiety instead of the phenol in **1.13**. However, upon further review of the models, we found that the phenolic system gave interatomic distances between the heteroatoms of the hydrogen bond donor and acceptor which were closer to the requirements for LBHB formation. According to the models, the interatomic distance between the two oxygens is 2.65 Å for both the iterations of **1.13** (X = O or S). Similarly, using a pyridine moiety would have required a very strongly electron donating

group at the R position in order to achieve the proper  $pK_a$  matching required if LBHB effects were to be observed. Modeling of the enolate generated by deprotonation at the  $\alpha$ -carbon also gives a suitable geometry and the difference between the minimization energies calculated by molecular mechanics is roughly 35 kcal/mol. Since molecular mechanics does not take hydrogen bond stabilization, much less from LBHB or  $\pi$ -directed hydrogen bonding, this value was not distressing and matches well with calculated and experimental energies of typical enol(ate) formations.<sup>18, 25</sup> The structure of **1.13** is also convenient because its synthesis can be readily modified to give the free ketone **1.14**, which allows for lone pair hydrogen bonding studies as a control.

The synthesis of **1.13** was to be achieved by modifying the synthesis reported by Cao and coworkers as shown in Schemes 1 and 2.<sup>72</sup> Since the major synthetic steps consisted of two Sonogashira-type couplings, it was possible to start with either the phenol or the xylyl moieties. Our first route began with the anisole derivative shown in Scheme 1.5. 2-Iodoanisole and trimethylsilylacetylene were coupled under Sonogashira conditions with tetrakis(triphenylphosphine)palladium and copper(I)iodide in triethylamine at room temperature overnight to give trimethylsilyl-acetylene **1.15** in 65% yield. The trimethylsilyl (TMS) group is removed with cesium carbonate in dry methanol to yield 70% of acetylene **1.16**, which undergoes another palladium-catalyzed coupling with 2-iodo-*m*-xylene under the same conditions to give a disappointing 12% of diphenyl acetylene **1.17**.

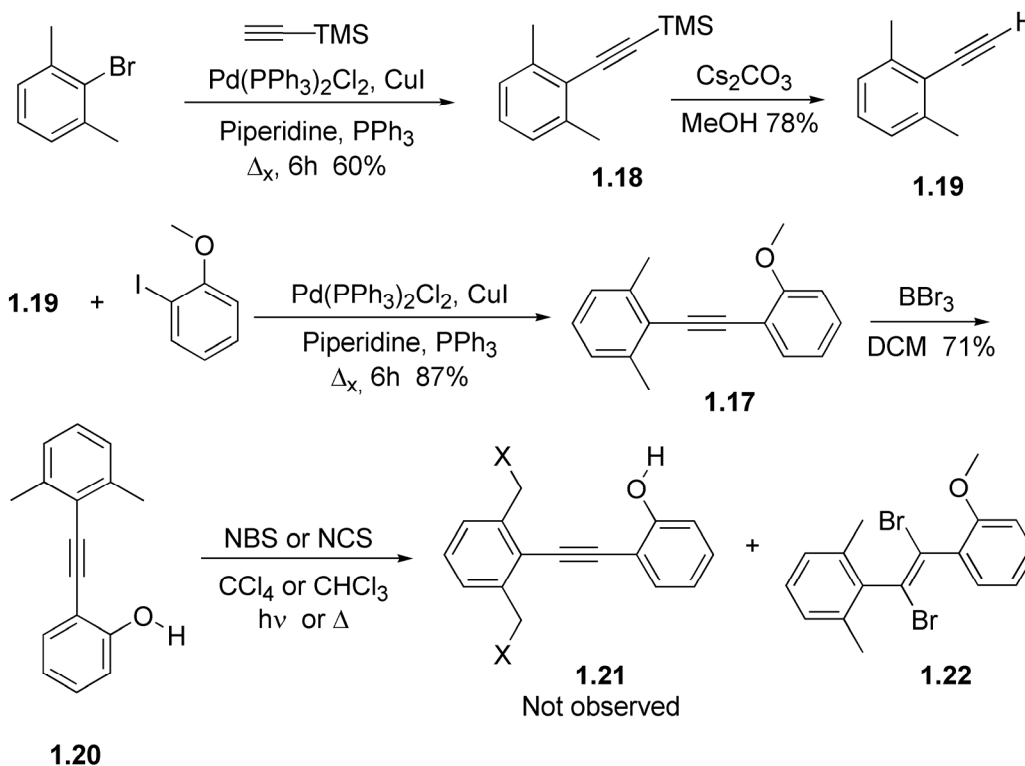
**Scheme 1.5**



Because of the instability of 2-iodo-*m*-xylene, the bromoxylene was used instead. Unfortunately, under these Sonogashira conditions, 2-bromo-*m*-xylene gave no reaction. However, Detty *et al.* reported coupling 2-bromo-*m*-xylene with trimethylsilylacetylene in moderate yields, so we rearranged our synthesis to incorporate their procedure (Scheme 1.6).<sup>73</sup> 2-Bromo-*m*-xylene and trimethylsilylacetylene undergo a Sonogashira coupling with bis(triphenylphosphine)palladium(II)chloride, copper(I)iodide, and triphenylphosphine in piperidine at reflux for 6 hours to give TMS-phenylacetylene **1.18** in 60% yield. The trimethylsilyl protecting group is then cleaved with cesium carbonate in methanol over 15 min. to give acetylene **1.19** in 78% yield. Under the same Sonogashira conditions (piperidine,  $\Delta_x$ ), **1.19** is coupled to 2-iodoanisole to give **1.17** in 87% yield. The methoxy group is then deprotected with boron tribromide in dichloromethane at -78 °C warming to ambient temperature overnight to give phenol **1.20**

in 71% yield. When **1.20** was subjected to NBS radical bromination conditions, the  $^1\text{H}$ -NMR of the products showed no allylic bromination products.

**Scheme 1.6**



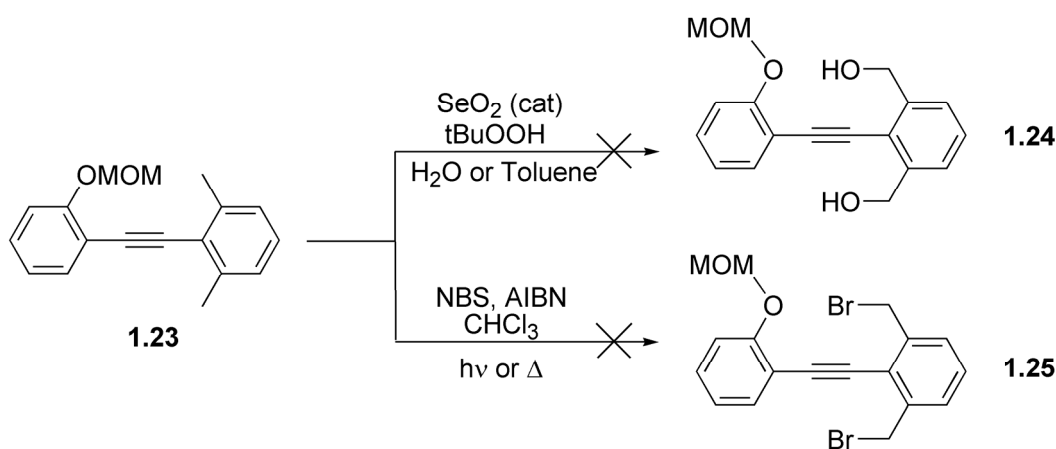
The low resolution mass spectrum, however, gave a 100% peak with the typical bromine isotope pattern at 2 m/z units higher than **1.21**. The  $^1\text{H}$ -NMR and  $^{13}\text{C}$ -NMR were inconclusive but the low resolution mass spectral data suggested that the major product was most likely **1.22** or a the tetrabrominated analogue.\* Both light and heat initiation procedures gave only **1.22**. When **1.18** was also subjected to the bromination conditions, similar results were obtained. This result sheds some doubt to the validity of

\* LRMS- $\text{Cl}^+$  m/z 381 (100%,  $\text{M}^+$ ) which is two mass units higher than bromination at the two allyl positions would suggest; evidence for 1,1,2,2-tetrabromo-product: 541 (21.1%,  $\text{M}^+$ ), 461 (26.8%,  $\text{M}^+-\text{Br}$ )



the findings of Cao *et al.* whose heat initiated conditions we used.<sup>72</sup> Out of concern that the free phenolic group might have been playing a role in the side reaction, phenol **1.20** was MOM-protected by reaction with MOMCl in dichloromethane in the presence of Hünig's base to give MOM ether **1.23** in 87% yield. Unfortunately, protection of the phenol did not help in functionalizing the xylyl positions.

**Scheme 1.7**

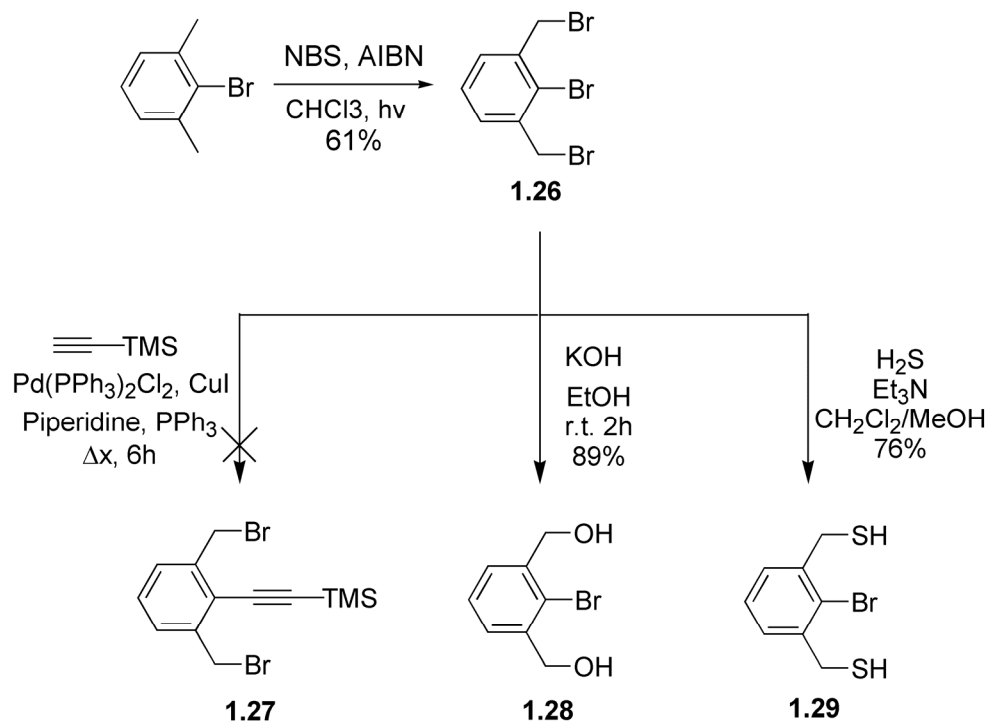


MOM ether **1.23** was subjected to the same bromination conditions as **1.20** with no better results (Scheme 1.7). In an attempt to bypass the halogenation of the alkynyl substrate, **1.23** underwent benzylic oxidation in water or toluene with selenium dioxide and *tert*-butylhydroperoxide, however, neither conditions led to diol **1.25**. We were thus forced to return to the beginning of our synthesis and devise new routes (Scheme 1.8).

Under light-initiated NBS bromination conditions, 2-bromo-*m*-xylene was bis(brominated) to give the tris(bromo)xylene **1.26** in 61% yield. Xylene **1.26** was subjected to the conditions above for Sonogashira coupling with trimethylsilylacetylene in an attempt to produce TMS-acetylene **1.27**, however, the desired product was not observed. It is probable that Pd(0) more readily inserts into the allylic C-Br than the

aromatic C-Br bond. The benzyl bromides were then subjected to substitution conditions to give both the bis-alcohol **1.28** and the bis-thiol **1.29** in 89% and 76% respectively.

**Scheme 1.8**



Unfortunately further progress proved difficult from this point. Attempts to attach the cyclophane portion of scaffold **1.13** at this point proved unsuccessful and all attempts at Sonogashira couplings were fruitless due to steric or electronic hinderances. Ultimately, this synthesis was tabled, though it is our opinion that a similar scaffold should be pursued in the future in order to further develop our understanding of the kinetic effects of this mode of electrophilic coordination.

## 1.5 CONCLUSIONS

We began this chapter with a series of case studies on three different classes of enzymes which all appear to have similar modes of operation. We looked at triose phosphate isomerase, mandelate racemase, and citrate synthase, which are all essential to metabolism and all catalyze the abstraction of an  $\alpha$ -proton of a carbon acid substrate. Studies on the mechanisms of these three enzymes revealed curious similarities in their catalytic mechanisms. All three showed that a general acid or electrophilic residue was essential for efficient turnover. Several of the main theories on how and why these general acid catalysts are so important in an apparent general base mechanism were given. The prominent theory discussed was that the electrophilic catalysts aid in the stabilization of the transition state and intermediate structures through the formation of very short, strong hydrogen bonds called low barrier hydrogen bonds. Whether or not these hydrogen bonds play a significant role is neither supported nor refuted, however, the use of the Principle of Non-Perfect Synchronization was used to dispute the reasoning put forth by Gerlt and Gassman—the main proponents of the LBHB theory—that the electrophilic residues help to reduce the intrinsic activation barrier for deprotonation through a decrease in negative entropy accumulation at the transition state. Computational studies on the effect of  $\pi$ -directed electrophilic coordination described in this chapter afford a different perspective on how an enzyme might thermodynamically stabilize  $\alpha$ -proton abstraction with possible implications towards the kinetic enhancement effects. It was shown that a coordination which took advantage of the growing negative charge on the  $\alpha$ -carbon as well as that on the carbonyl oxygen could offer a much greater acidity enhancement, and the models suggest that such coordination could help reduce the effective activation energy by weakening the cleaving C-H bond and stabilizing the

localized carbanionic transition state though this is speculative. Synthetic attempts to generate a scaffold containing a constrained, intramolecular,  $\pi$ -directed hydrogen bond were discussed in the hopes of creating a kinetic model to validate this speculation. However, this synthesis proved unsuccessful, and further evidence of the kinetic effects of  $\pi$ -directed electrophilic coordination needs to be accomplished.

## 1.6 EXPERIMENTAL SECTION

### 1.6.1 Computational Specifics

All calculations were performed using the ACES II software noted above. MP2 level calculations using a 6-31G\* basis set were performed on an acetaldehyde-Li<sup>+</sup> model system and the corresponding enolate system. The Li-O-C<sub>a</sub> bond angle was constrained to 5° intervals between 45° and 180° against constrained dihedral angles between the plane described by O-C<sub>a</sub>-C<sub>b</sub> and the Li<sup>+</sup> at 5° intervals between 0° and 180°. All other parameters in the z-matrix were allowed to optimize. SCF energies were obtained from the individual single-point output files and plotted to give the energy surfaces shown in Figures 1.9 and 1.10 above. The global minimum for the neutral acetaldehyde system (total charge = +1) lay at 180° for both the Li-O-C<sub>a</sub> bond angle and the dihedral angle. The global minimum for the enolate system (total charge = 0) lay at an 85° Li-O-C<sub>a</sub> bond angle and a 45° dihedral angle. The surface representing the gas phase acidity of the system was generated from a blanket subtraction of the enolate surface (Figure 1.10A) from the neutral surface (Figure 1.9A). This subtraction generated a set of positive enthalpies, which were plotted as a contour surface (Figure 1.11). Sample z-matrices for the acetaldehyde-Li<sup>+</sup> calculations (Figure 1.13A) and the enolate-Li<sup>+</sup> calculations (Figure 1.13B) are shown below.

A) LI  
 O 1 R1\*  
 C 2 R2\* 1 A  
 C 3 R4\* 2 A2\* 1 T  
 H 3 R3\* 2 A3\* 1 MT\*  
 H 4 R5\* 3 A4\* 2 T2\*  
 H 4 R6\* 3 A5\* 2 T3\*  
 H 4 R7\* 3 A6\* 2 T4\*

R1=2.1  
 R2=1.3  
 R3=1.1  
 R4=1.5  
 R5=1.1  
 R6=1.1  
 R7=1.1  
 A=90  
 A2=120  
 A3=120  
 A4=109.5  
 A5=109.5  
 A6=109.5  
 T=5  
 MT=-90  
 T2=0  
 T3=120  
 T4=-120

\*ACES2(BASIS=6-31G\*,CALC=MBPT[2],CHARGE=1,SCF\_MAXCYC=500,MEMORY=100000  
 00)

---

B) LI  
 O 1 R1\*  
 C 2 R2\* 1 A  
 C 3 R4\* 2 A2\* 1 T  
 H 3 R3\* 2 A3\* 1 MT\*  
 H 4 R5\* 3 A4\* 2 T2\*  
 H 4 R6\* 3 A5\* 5 T3\*

R1=2.1  
 R2=1.3  
 R3=1.1  
 R4=1.5  
 R5=1.1  
 R6=1.1  
 A=90

---

A2=120  
A3=120  
A4=120  
A5=120  
T=5  
MT=-90  
T2=0  
T3=0

\*ACES2(BASIS=6-31G\*,CALC=MBPT[2],SCF\_MAXCYC=400,MEMORY=10000000)

**Figure 1.13** Z-Matrix inputs for A) the acetaldehyde-Li<sup>+</sup> complex and B) the enolate-Li<sup>+</sup> complex. Parameter A is the Li-O-C<sub>a</sub> bond angle and parameter T is the Li-O-C<sub>a</sub>-C<sub>b</sub> dihedral angle. All starred parameters were fully optimized with each run. In the command line, BASIS sets the basis set for the calculation, CALC sets the calculation type/level, CHARGE sets the overall charge of the system, SCF\_MAXCYC sets the limit on the number of self-consistent field optimization cycles allowed before the job automatically cancels, and MEMORY sets the max number of memory words to be exploited for the calculation.

Table 1.1 below gives a list of the single-point optimization energies calculated using the above method. The energies are given in Hartrees with the bond angle on the horizontal axis and the dihedral angle on the vertical. For the generation of the individual surfaces, these energies were subtracted from the value of uncoordinated acetaldehyde (-153.348 H) or its enolate (-152.724 H) and converted to kcal/mol by the conversion factor 627.51 kcal·mol<sup>-1</sup>H<sup>-1</sup>. For the gas phase acidity analysis, the energies were differenced directly without factoring in the unliganded species.

**Table 1.1** Output energies for the acetaldehyde-Li<sup>+</sup> complex (top) and the enolate-Li<sup>+</sup> complex (bottom).  
Energies are given in Hartrees (H)

0	-160.421	-160.489	-160.572	-160.668	-160.774	-160.890	-161.016	-161.151	-161.294	-161.443	-161.597	-161.756	-161.919	-162.086	-162.256	-162.429	-162.604	-162.781	-162.959	-163.138	-163.318	-163.498	-163.677	-163.855	-164.033	-164.211	-164.388	-164.564	-164.739	-164.914	-165.088	-165.261	-165.433	-165.604	-165.774	-165.943	-166.111	-166.278	-166.443	-166.607	-166.770	-166.931	-167.091	-167.249	-167.405	-167.560	-167.713	-167.864	-168.014	-168.162	-168.308	-168.452	-168.594	-168.735	-168.873	-169.009	-169.143	-169.274	-169.404	-169.531	-169.656	-169.779	-169.899	-170.017	-170.132	-170.244	-170.353	-170.458	-170.560	-170.658	-170.752	-170.842	-170.928	-171.011	-171.090	-171.165	-171.236	-171.303	-171.366	-171.425	-171.480	-171.531	-171.578	-171.621	-171.660	-171.695	-171.726	-171.753	-171.776	-171.794	-171.808	-171.818	-171.824	-171.826	-171.824	-171.818	-171.808	-171.794	-171.776	-171.753	-171.726	-171.695	-171.660	-171.621	-171.578	-171.531	-171.480	-171.425	-171.366	-171.303	-171.236	-171.165	-171.090	-171.017	-170.928	-170.842	-170.752	-170.658	-170.560	-170.458	-170.353	-170.244	-170.132	-170.011	-169.899	-169.779	-169.656	-169.531	-169.404	-169.274	-169.143	-169.009	-168.873	-168.735	-168.594	-168.452	-168.308	-168.162	-168.014	-167.864	-167.713	-167.560	-167.405	-167.249	-167.091	-166.931	-166.770	-166.607	-166.443	-166.278	-166.111	-165.943	-165.774	-165.604	-165.433	-165.261	-165.088	-164.914	-164.739	-164.564	-164.388	-164.211	-164.033	-163.855	-163.677	-163.498	-163.318	-163.138	-162.959	-162.781	-162.604	-162.429	-162.256	-162.086	-161.919	-161.756	-161.597	-161.443	-161.294	-161.151	-161.016	-160.890	-160.774	-160.668	-160.572	-160.489	-160.421																																																																																																																																																																																																																																																																																																																																																																																																																																																																																																																																																																																																																																																																						
5	-160.187	-160.182	-160.176	-160.170	-160.164	-160.158	-160.152	-160.146	-160.140	-160.134	-160.128	-160.122	-160.116	-160.110	-160.104	-160.098	-160.092	-160.086	-160.080	-160.074	-160.068	-160.062	-160.056	-160.050	-160.044	-160.038	-160.032	-160.026	-160.020	-160.014	-160.008	-160.002	-159.996	-159.990	-159.984	-159.978	-159.972	-159.966	-159.960	-159.954	-159.948	-159.942	-159.936	-159.930	-159.924	-159.918	-159.912	-159.906	-159.900	-159.894	-159.888	-159.882	-159.876	-159.870	-159.864	-159.858	-159.852	-159.846	-159.840	-159.834	-159.828	-159.822	-159.816	-159.810	-159.804	-159.798	-159.792	-159.786	-159.780	-159.774	-159.768	-159.762	-159.756	-159.750	-159.744	-159.738	-159.732	-159.726	-159.720	-159.714	-159.708	-159.702	-159.696	-159.690	-159.684	-159.678	-159.672	-159.666	-159.660	-159.654	-159.648	-159.642	-159.636	-159.630	-159.624	-159.618	-159.612	-159.606	-159.600	-159.594	-159.588	-159.582	-159.576	-159.570	-159.564	-159.558	-159.552	-159.546	-159.540	-159.534	-159.528	-159.522	-159.516	-159.510	-159.504	-159.498	-159.492	-159.486	-159.480	-159.474	-159.468	-159.462	-159.456	-159.450	-159.444	-159.438	-159.432	-159.426	-159.420	-159.414	-159.408	-159.402	-159.396	-159.390	-159.384	-159.378	-159.372	-159.366	-159.360	-159.354	-159.348	-159.342	-159.336	-159.330	-159.324	-159.318	-159.312	-159.306	-159.300	-159.294	-159.288	-159.282	-159.276	-159.270	-159.264	-159.258	-159.252	-159.246	-159.240	-159.234	-159.228	-159.222	-159.216	-159.210	-159.204	-159.198	-159.192	-159.186	-159.180	-159.174	-159.168	-159.162	-159.156	-159.150	-159.144	-159.138	-159.132	-159.126	-159.120	-159.114	-159.108	-159.102	-159.096	-159.090	-159.084	-159.078	-159.072	-159.066	-159.060	-159.054	-159.048	-159.042	-159.036	-159.030	-159.024	-159.018	-159.012	-159.006	-159.000	-158.994	-158.988	-158.982	-158.976	-158.970	-158.964	-158.958	-158.952	-158.946	-158.940	-158.934	-158.928	-158.922	-158.916	-158.910	-158.904	-158.898	-158.892	-158.886	-158.880	-158.874	-158.868	-158.862	-158.856	-158.850	-158.844	-158.838	-158.832	-158.826	-158.820	-158.814	-158.808	-158.802	-158.796	-158.790	-158.784	-158.778	-158.772	-158.766	-158.760	-158.754	-158.748	-158.742	-158.736	-158.730	-158.724	-158.718	-158.712	-158.706	-158.700	-158.694	-158.688	-158.682	-158.676	-158.670	-158.664	-158.658	-158.652	-158.646	-158.640	-158.634	-158.628	-158.622	-158.616	-158.610	-158.604	-158.598	-158.592	-158.586	-158.580	-158.574	-158.568	-158.562	-158.556	-158.550	-158.544	-158.538	-158.532	-158.526	-158.520	-158.514	-158.508	-158.502	-158.496	-158.490	-158.484	-158.478	-158.472	-158.466	-158.460	-158.454	-158.448	-158.442	-158.436	-158.430	-158.424	-158.418	-158.412	-158.406	-158.400	-158.394	-158.388	-158.382	-158.376	-158.370	-158.364	-158.358	-158.352	-158.346	-158.340	-158.334	-158.328	-158.322	-158.316	-158.310	-158.304	-158.298	-158.292	-158.286	-158.280	-158.274	-158.268	-158.262	-158.256	-158.250	-158.244	-158.238	-158.232	-158.226	-158.220	-158.214	-158.208	-158.202	-158.196	-158.190	-158.184	-158.178	-158.172	-158.166	-158.160	-158.154	-158.148	-158.142	-158.136	-158.130	-158.124	-158.118	-158.112	-158.106	-158.100	-158.094	-158.088	-158.082	-158.076	-158.070	-158.064	-158.058	-158.052	-158.046	-158.040	-158.034	-158.028	-158.022	-158.016	-158.010	-158.004	-157.998	-157.992	-157.986	-157.980	-157.974	-157.968	-157.962	-157.956	-157.950	-157.944	-157.938	-157.932	-157.926	-157.920	-157.914	-157.908	-157.902	-157.896	-157.890	-157.884	-157.878	-157.872	-157.866	-157.860	-157.854	-157.848	-157.842	-157.836	-157.830	-157.824	-157.818	-157.812	-157.806	-157.800	-157.794	-157.788	-157.782	-157.776	-157.770	-157.764	-157.758	-157.752	-157.746	-157.740	-157.734	-157.728	-157.722	-157.716	-157.710	-157.704	-157.698	-157.692	-157.686	-157.680	-157.674	-157.668	-157.662	-157.656	-157.650	-157.644	-157.638	-157.632	-157.626	-157.620	-157.614	-157.608	-157.602	-157.596	-157.590	-157.584	-157.578	-157.572	-157.566	-157.560	-157.554	-157.548	-157.542	-157.536	-157.530	-157.524	-157.518	-157.512	-157.506	-157.500	-157.494	-157.488	-157.482	-157.476	-157.470	-157.464	-157.458	-157.452	-157.446	-157.440	-157.434	-157.428	-157.422	-157.416	-157.410	-157.404	-157.398	-157.392	-157.386	-157.380	-157.374	-157.368	-157.362	-157.356	-157.350	-157.344	-157.338	-157.332	-157.326	-157.320	-157.314	-157.308	-157.302	-157.296	-157.290	-157.284	-157.278	-157.272	-157.266	-157.260	-157.254	-157.248	-157.242	-157.236	-157.230	-157.224	-157.218	-157.212	-157.206	-157.200	-157.194	-157.188	-157.182	-157.176	-157.170	-157.164	-157.158	-157.152	-157.146	-157.140	-157.134	-157.128	-157.122	-157.116	-157.110	-157.104	-157.098	-157.092	-157.086	-157.080	-157.074	-157.068	-157.062	-157.056	-157.050	-157.044	-157.038	-157.032	-157.026	-157.020	-157.014	-157.008	-157.002	-156.996	-156.990	-156.984	-156.978	-156.972	-156.966	-156.960	-156.954	-156.948	-156.942	-156.936	-156.930	-156.924	-156.918	-156.912	-156.906	-156.900	-156.894	-156.888	-156.882	-156.876	-156.870	-156.864	-156.858	-156.852	-156.846	-156.840	-156.834	-156.828	-156.822	-156.816	-156.810	-156.804	-156.798	-156.792	-156.786	-156.780	-156.774	-156.768	-156.762	-156.756	-156.750	-156.744	-156.738	-156.732	-156.726	-156.720	-156.714	-156.708	-156.702	-156.696	-156.690	-156.684	-156.678	-156.672	-156.666	-156.660	-156.654	-156.648	-156.642	-156.636	-156.630	-156.624	-156.618	-156.612	-156.606	-156.600	-156.594	-156.588	-156.582	-156.576	-156.570	-156.564	-156.558	-156.552	-156.546	-156.540	-156.534	-156.528	-156.522	-156.516	-156.510	-156.504	-156.498	-156.492	-156.486	-156.480	-156.474	-156.468	-156.462	-156.456	-156.450	-156.444	-156.438	-156.432	-156.426	-156.420	-156.414	-156.408	-156.402	-156.396	-156.390	-156.384	-156.378	-156.372	-156.366	-156.360	-156.354	-156.348	-156.342	-156.336	-156.330	-156.324	-156.318	-156.312	-156.306	-156.300	-156.294	-156.288	-156.282	-156.276	-156.270	-156.264	-156.258	-156.252	-156.246	-156.240	-156.234	-156.228	-156.222	-156.216	-156.210	-156.204	-156.198	-156.192	-156.186	-156.180	-156.174	-156.168	-156.162	-156.156	-156.150	-156.144	-156.138	-156.132	-156.126	-156.120	-156.114	-156.108	-156.102	-156.096	-156.090	-156.084	-156.078	-156.072	-156.066	-156.060	-156.054	-156.048	-156.042	-156.036	-156.030	-156.024	-156.018	-156.012	-156.006	-155.999	-155.993	-155.987	-155.981	-155.975	-155.969	-155.963	-155.957	-155.951	-155.945	-155.939	-155.933	-155.927	-155.921	-155.915	-155.909	-155.903	-155.897	-155.891	-155.885	-155.879	-155.873	-155.867	-155.861	-155.855	-155.849	-155.843	-155.837	-155.831	-155.825	-155.819	-155.813	-155.807	-155.801	-155.795	-155.789	-155.783	-155.777	-155.771	-155.765	-155.759	-155.753	-155.747	-155.741	-155.735	-155.729	-155.723	-155.717	-155.711	-155.705	-155.699	-155.693	-155.687	-155.681	-155.675	-155.669	-155.663	-155.657	-155.651	-155.645	-155.639	-155.633	-155.627	-155.621	-155.615	-155.609	-155.603	-155.597	-155.591	-155.585	-155.579	-155.573	-155.567	-155.561	-155.555	-155.549	-155.543	-155.537	-155.531	-155.525	-155.519	-155.513	-155.507	-155.501	-155.495	-155.489	-155.483	-155.477	-155.471	-155.465	-155.459	-155.453	-155.447	-155.441	-155.435	-155.429	-155.423	-155.417	-155.411	-155.405	-155.399	-155.393	-155.387	-155.381	-155.375	-155.369	-155.363	-155.357	-155.351	-155.345	-155.339	-155.333	-155.327	-155.321	-155.315	-155.309	-155.303	-155.297	-155.291	-155.285	-155.279	-155.273	-155.267	-155.261	-155.255	-155.249	-155.243	-155.237	-155.231	-155.225	-155.219	-155.213	-155.207	-155.201	-155.195

### 1.6.2 General Synthesis

All reagents were obtained from Aldrich unless otherwise noted and were used without further purification. *N*-Bromosuccinimide was recrystallized from water prior to use. Piperidine was distilled from potassium hydroxide and triethylamine and dichloromethane were distilled from calcium hydride when noted. Analytical TLC was performed on precoated silica gel 60 F-254 plates. Preparative flash chromatography was performed on EM Science silica gel 60 with 230-400 mesh. Flash chromatography solvents are given in volume equivalents unless otherwise stated.  $^1\text{H}$ -NMR spectral data were obtained from a Varian Unity Plus 400 MHz spectrometer and are reported in parts per million (ppm) downfield from TMS.  $^{13}\text{C}$ -NMR were run at 75 MHz with C-H decoupling on a Varian Unity Plus spectrometer and reported in ppm referenced to the center of the chloroform triplet (77.0). A Finnigan VG analytical ZAB2-E spectrometer was used to obtain high-resolution mass spectra. Low resolution mass spectra were obtained on a Finnigan MAT TSQ700 spectrometer. All samples were placed under high vacuum for at least 12 hours before spectra were taken.

**(2-Methoxy-phenylethynyl)-trimethylsilane (1.15):** To a well stirred suspension of 2-iodoanisole (45.0g, 0.2 mol, 100 mol%), palladium(tetrakis)triphenylphosphine (2.3g, 0.002 mol, 1 mol%), and copper(I)iodide (0.4g, 0.002 mol, 1 mol%) in 200mL triethylamine in flame dried, argon flushed glassware was added trimethylsilylacetylene (37.5g, 0.4 mol 130 mol %). The solution was refluxed overnight after which time the solvent was evaporated under reduced pressure. The residue was chromatographed on silica gel with hexanes/dichloromethane (2:1) as eluant to yield 23.8g (0.12 mol, 60%)  $^1\text{H}$ -NMR ( $\text{CDCl}_3$ ):  $\delta$  7.44 (d,  $J = 3.2$ , 1H, Ar-H), 7.23 (t,  $J = 7.8$ , 1H, Ar-H), 6.86 (t,  $J =$



7.4, 1H, Ar-H), 6.79 (d,  $J = 8.0$ , 1H, Ar-H), 3.79 (s, 3H, OCH<sub>3</sub>), 0.28 (s, 9H, Si-CH<sub>3</sub>). <sup>13</sup>C-NMR (CDCl<sub>3</sub>):  $\delta$  160.0 (Ar-H, C-OMe), 133.8, 129.8, 120.1, 112.0 (Ar-C), 110.3 (Ar-C,  $\underline{\text{C}}\text{-C}\equiv\text{C}$ ), 101.2 (Ph- $\underline{\text{C}}\equiv\text{C}$ ), 97.4 (Ph-C $\equiv\text{C}$ -Si), 55.4 (OCH<sub>3</sub>), -0.1 (Si-CH<sub>3</sub>). LRMS-Cl<sup>+</sup>  $m/z$  205 (100%, M<sup>+</sup>). HRMS-Cl<sup>+</sup>  $m/z$  calcd for C<sub>12</sub>H<sub>17</sub>OSi: 205.104; obsd: 205.105.

**General Procedure for Trimethyl Silyl Deprotection:** Using flame dried glassware purged with argon, cesium carbonate (2 eq.) was added to a stirred solution of the TMS protected alkyne in dry methanol. The reaction was complete when the cloudy, opaque suspension became translucent. The reaction mixture was partitioned between dichloromethane and water. The aqueous layer was extracted again with dichloromethane. The combined organic layers were washed sequentially with saturated aqueous ammonium chloride, water, and brine. The organic layer was dried (Na<sub>2</sub>SO<sub>4</sub>) and the solvent was removed by rotary evaporation to yield 70-80% of the terminal alkyne.

**1-Ethynyl-2-methoxybenzene (1.16):** Yield: 72%. <sup>1</sup>H-NMR (CDCl<sub>3</sub>):  $\delta$  7.44 (m, 1H, Ar-H), 7.30 (m, 1H, Ar-H), 6.90 (m, 1H, Ar-H), 6.86 (d,  $J = 7.6$ , 1H, Ar-H), 3.88 (s, 6H, Ph(CH<sub>3</sub>)<sub>2</sub>), 3.29 (s, 1H, sp-CH). <sup>13</sup>C-NMR (CDCl<sub>3</sub>):  $\delta$  160.5 (Ar-C, C-OMe), 134.1, 130.3, 120.4, 111.1 (Ar-C), 110.5 (Ar-C,  $\underline{\text{C}}\text{-C}\equiv\text{C}$ ), 81.1 (Ph- $\underline{\text{C}}\equiv\text{C}$ ), 80.0 (Ph-C $\equiv\text{C}$ ), 55.7 (O-CH<sub>3</sub>). LRMS-Cl<sup>+</sup>  $m/z$  132 (100%, M<sup>+</sup>). HRMS-Cl<sup>+</sup>  $m/z$  calcd for C<sub>9</sub>H<sub>7</sub>O: 131.050; obsd: 131.050.

**2-Ethynyl-1,3-dimethylbenzene (1.19):** Yield: 78% <sup>1</sup>H-NMR (CDCl<sub>3</sub>):  $\delta$  7.12 (m, 1H, Ar-H), 7.03 (d,  $J = 7.6$ , 2H, Ar-H), 3.50 (s, 1H, sp-CH), 2.44 (s, 6H, Ph-CH<sub>3</sub>). <sup>13</sup>C-

NMR (CDCl<sub>3</sub>):  $\delta$  140.9 (Ar-C,  $\underline{\text{C}}\text{-CH}_3$ ), 128.1 (Ar-C), 126.6 (Ar-C), 121.9 (Ar-C,  $\underline{\text{C}}\text{-C}\equiv\text{C}$ ), 85.3 (Ph- $\underline{\text{C}}\equiv\text{C}$ ), 81.1 (Ph-C $\equiv\text{C}$ ), 21.0 (Ph-CH<sub>3</sub>). LRMS-Cl<sup>+</sup> m/z 131 (100%, M<sup>+</sup>). HRMS-Cl<sup>+</sup> m/z calcd for C<sub>10</sub>H<sub>11</sub>: 131.086; obsd: 131.086.

**2-(2-Methoxyphenylethynyl)-1,3-dimethylbenzene (1.17):**

*From 1.16:* Using flame dried glassware purged with N<sub>2</sub>, **1.16** (2.1g, 0.016 mol, 100 mol%) was added to a well stirred suspension of 2-iodo-*m*-xylene (4.6g, 0.02 mol, 130 mol%) obtained from Fluorochem, palladium(tetrakis)triphenylphosphine (216mg, 0.2 mmol, 1 mol%), and copper(I)iodide (54mg, 0.3 mmol, 1.5 mol%) in 50mL triethylamine. The solution was refluxed overnight. After 16 hours, the solvent was removed *via* rotary evaporation, and the residue was chromatographed on silica gel with hexanes/dichloromethane (2:1) as eluant to yield 0.47g (2 mmol, 12%) of **1.17**. Spectral data below.

*From 1.19:* Using flame dried glassware purged with N<sub>2</sub>, **1.19** (0.984 g, 8 mmol, 1.3 eq.) was added to a well stirred suspension of 2-iodoanisole (1.37 g, 6 mmol 1 eq.), (bis-triphenylphosphine)palladium(II)chloride (82 mg, 0.12 mmol, 0.02 eq.), copper(I)iodide (22 mg, 0.12 mmol, 0.02 eq.), and triphenylphosphine (153 mg, 0.6 mmol, 0.1 eq.) in 50mL dry piperidine under nitrogen. Upon addition of the alkyne, a rapid color change was observed from dark orange to light yellow. The reaction mixture was stirred under reflux for 6 hours during which time the color changed to a dark orange-brown and a yellow-grey crystalline precipitate formed. After completion, the resulting suspension was filtered through celite and partitioned between hexanes and water. The aqueous layer was further extracted with hexanes. The combined organic

layers were washed with brine, dried (Na<sub>2</sub>SO<sub>4</sub>), and the solvent was removed *via* rotary evaporation. The resulting oil was chromatographed on silica gel with hexanes/dichloromethane (3:1) as the eluant to give 1.21g (5 mmol, 87%) of **1.17**. <sup>1</sup>H-NMR (CDCl<sub>3</sub>): δ 7.50 (m, 1H, Ar-H), 7.31 (m, 1H, Ar-H), 7.11 (m, 1H, Ar-H), 7.06 (m, 2H, Ar-H), 6.96 (d, *J* = 10.4, 1H, Ar-H), 6.92 (d, *J* = 11.2, 2H, Ar-H, PhMe<sub>2</sub>), 3.92 (s, 3H, OCH<sub>3</sub>), 2.54 (s, 6H, sp<sup>3</sup>-CH, PhMe<sub>2</sub>). <sup>13</sup>C-NMR (CDCl<sub>3</sub>): δ 159.6 (Ar-C, C-OCH<sub>3</sub>), 139.8 (sp<sup>2</sup>-C-C), 132.7, 129.3, 127.4, 126.4 (Ar-C), 123.2 (Ar-C, MeOPh-C-C≡C), 120.1, 112.9 (Ar-C), 110.4 (Ar-C, Me<sub>2</sub>Ph-C-C≡C), 94.1 (sp-C, PhOMe), 91.2 (sp-C, PhMe<sub>2</sub>), 55.3 (OCH<sub>3</sub>), 20.9 (sp<sup>3</sup>-C). LRMS-Cl<sup>+</sup> *m/z* 237 (100%, M<sup>+</sup>). HRMS-Cl<sup>+</sup> *m/z* calcd for C<sub>17</sub>H<sub>17</sub>O: 237.127; obsd: 237.128.

**(2,6-Dimethylphenylethynyl)-trimethylsilane (1.18)**<sup>73</sup>: Prepared as prescribed in the literature. Spectral data is concurrent with that given.

**2-(2,6-Dimethyl-phenylethynyl)-phenol (1.20)**: Using flame dried glassware purged with N<sub>2</sub>, a solution of **1.17** (1.28g, 5.4 mmol, 1 eq.) in 20mL dry dichloromethane was prepared and cooled to -78 °C. 15mL of a 1M boron tribromide in dichloromethane (3 eq.) was added dropwise at -78 °C. The reaction was allowed to warm to room temperature overnight. The completed reaction mixture was partitioned between ethyl acetate and 1M HCl and the aqueous layer was washed further with ethyl acetate. The combined organic layers were washed with brine, collected, and dried (Na<sub>2</sub>SO<sub>4</sub>). The solvent was removed *via* rotary evaporation. The residue was chromatographed on silica gel with hexanes:dichloromethane (2:1) to give 0.61g (3 mmol 51%) of **1.20**. <sup>1</sup>H-NMR (CDCl<sub>3</sub>): δ 7.44 (m, 1H, Ar-H), 7.28 (m, 1H, Ar-H), 7.17 (m, 1H, Ar-H), 7.10 (d, *J* = 6.8,

2H, Ar-H, PhMe<sub>2</sub>), 7.00 (d,  $J$  = 8.4, 1H, Ar-H), 6.93 (m, 1H, Ar-H), 5.87 (s 1H, -OH), 2.53 (s, 6H, Ph(CH<sub>3</sub>)<sub>2</sub>). <sup>13</sup>C-NMR (CDCl<sub>3</sub>):  $\delta$  156.18 (Ar-C, C-OMe), 140.01 (Ar-C, PhC-CH<sub>3</sub>), 131.44, 130.34, 128.34, 126.92 (Ar-C), 122.22 (Ar-C, PhOMe-C-C $\equiv$ C), 120.43, 114.63 (Ar-C), 110.1 (Ar-C, Me<sub>2</sub>Ph-C-C $\equiv$ C), 94.1 (sp-C, MeOPh-C-C $\equiv$ C), 91.3 (Me<sub>2</sub>Ph-C-C $\equiv$ C), 21.3 (Ph(CH<sub>3</sub>)<sub>2</sub>). LRMS-Cl<sup>+</sup>  $m/z$  223 (100%, M<sup>+</sup>) HRMS-Cl<sup>+</sup>  $m/z$  calcd for C<sub>16</sub>H<sub>15</sub>O: 223.113; obsd: 223.112.

**2-(2-Methoxymethoxy-phenylethynyl)-1,3-dimethyl-benzene (1.23):** Using flame dried glassware purged with N<sub>2</sub>, (*i*Pr)<sub>2</sub>EtN (0.2 mL, 0.8 mmol) and chloromethyl methyl ether (MOMCl) (0.1mL, 0.8 mmol) was added to a well stirred solution of **1.20** (98.4 mg, 0.4 mmol) in 10mL dichloromethane at 0 °C. The solution was stirred at 0 °C for 4-6 hrs. The reaction mixture was then quenched with water and washed with brine. The organic layer was dried (Na<sub>2</sub>SO<sub>4</sub>) and the solvent is removed. No further purification was required, and 103 mg (0.39 mmol, 87%) of **1.23** was isolated. <sup>1</sup>H-NMR (CDCl<sub>3</sub>):  $\delta$  7.52 (d,  $J$  = 7.2, 1H, Ar-H), 7.28 (m, 1H, Ar-H), 7.12 (t,  $J$  = 7.6, 2H, Ar-H), 7.07 (m, 2H, Ar-H, PhMe<sub>2</sub>), 7.01 (m, 1H, Ar-H), 5.29 (d,  $J$  = 1.2, 2H, O-CH<sub>2</sub>-O), 3.53 (s, 3H, OCH<sub>3</sub>), 2.55 (s, 6H, Ph(CH<sub>3</sub>)<sub>2</sub>). <sup>13</sup>C-NMR (CDCl<sub>3</sub>):  $\delta$  157.3 (Ar-C, C-OMOM), 140.1, 132.9, 129.3, 127.6, 126.6 (Ar-C, PhC-CH<sub>3</sub>), 123.2 (Ar-C, PhMe<sub>2</sub>-C-C $\equiv$ C), 121.7, 114.7 (Ar-C), 114.2 (Ar-C, MOMPh-C-C $\equiv$ C), 94.5 (O-CH<sub>2</sub>-O), 94.0 (MOMPh-C-C $\equiv$ C), 91.2 (PhMe<sub>2</sub>-C-C $\equiv$ C), 56.1 (O-CH<sub>3</sub>), 20.9 (Ph(CH<sub>3</sub>)<sub>2</sub>).

**2-Bromo-1,3-bis-bromomethyl-benzene (1.26):** A stirred solution of 2-bromo-*m*-xylene (2.778 g, 15 mmol) in 150 mL CHCl<sub>3</sub> was illuminated with a 100W incandescent tungsten filament light source. To this solution *N*-bromosuccinimide (6.68 g, 38 mmol,

2.5 eq.) was added slowly over 16hrs. Each addition was followed by the addition of a small amount of AIBN. The reaction was allowed to continue under illumination for another 5hrs. 1-Hexene was added to sequester molecular bromine and the solvent was removed by rotary evaporation. The resulting dark orange oil was cooled overnight at 4 °C and the product crystallizes. The suspension was triturated from hexanes then dissolved in dichloromethane. The solvent was removed by rotary evaporation to yield 1.49g (4.4 mmol, 29%) of **18**. <sup>1</sup>H-NMR (CDCl<sub>3</sub>): δ 7.39 (d, *J* = 7.6, 2H, Ar-H), 7.27 (t, *J* = 7.6, 1H, Ar-H), 4.63 (s, 4H, CH<sub>2</sub>-Br). <sup>13</sup>C-NMR (CDCl<sub>3</sub>): δ 138.4, 131.3, 128.0 (Ar-C), 126.6 (Ar-C, C-Br), 33.8 (CH<sub>2</sub>-Br). LRMS-Cl<sup>+</sup> *m/z* 343 (2.54%, M<sup>+</sup>), 263 (100%, M<sup>+</sup>-Br). HRMS-Cl<sup>+</sup> *m/z* calcd for C<sub>8</sub>H<sub>7</sub>Br<sub>3</sub>: 339.809; obsd: 339.810.

**(2-Bromo-3-hydroxymethyl-phenyl)-methanol (1.28):** A solution of **1.26** (100 mg, 0.29 mmol, 1 eq.) and potassium hydroxide (33 mg, 5.9 mmol, 2 eq.) in 200 proof ethanol (10 mL) is stirred at ambient temperature for 2 hours. The reaction was quenched with 2N HCl and partitioned into ether. The aqueous layer was washed twice more with ether and the organic layers were combined, washed with water and brine, and concentrated to a viscous oil. The residue was placed under high vacuum overnight to yield 56 mg (0.26 mmol, 88% yield) **1.28**. The spectral and mass analysis was concurrent with the literature.<sup>74</sup>

**(2-Bromo-3-mercaptomethyl-phenyl)-methanethiol (1.29):** Hydrogen sulfide gas is bubbled through a flask containing solution of triethylamine (5 mL, 36 mmol, 12 eq.) obtained from J.T. Baker in methylene chloride/methanol 70/30 (100 mL) and equipped with an outlet into a 10% aqueous bleach trap until the basic solution is saturated. This

solution is cooled to 0-5° C in an ice-water bath. **1.26** (1 g, 2.9 mmol, 1 eq.) is dissolved in a minimal amount of methylene chloride and added to the cold reaction flask. The reaction is stirred at 0-5° C for 4 hours then quenched and partitioned with water. The aqueous layer is extracted twice with methylene chloride and the organic layers are combined. The combined organic layers are washed with saturated ammonium chloride, water and brine and the solvent is removed *via* rotary evaporation. The solid residue was recrystallized from ethanol and water to yield 552 mg (2.2 mmol, 76% yield) **1.29**. The spectral and mass analysis are concurrent with the literature.<sup>75</sup>

## 1.7 REFERENCES

- 1 Lehn, J. M., Supramolecular chemistry. *Science (Washington, DC, United States)* **1993**, 260, (5115), 1762-3.
- 2 Anslyn, E. V.; Dougherty, D. A., *Modern Physical Organic Chemistry*. 1 ed.; University Science Books: Sausalito, CA, 2006; Vol. 1.
- 3 Remington, S. J., Mechanisms of citrate synthase and related enzymes (triose phosphate isomerase and mandelate racemase). *Current Opinion in Structural Biology* **1992**, 2, (5), 730-5.
- 4 Voet, D.; Voet, J. G., *Biochemistry*. 3rd ed.; John Wiley & Sons Inc.: Hoboken, NJ, 2004.
- 5 Albery, W. J.; Knowles, J. R., Free-energy profile for the reaction catalyzed by triosephosphate isomerase. *Biochemistry* **1976**, 15, (25), 5627-31.
- 6 Rieder, S. V.; Rose, I. A., Mechanism of the triose phosphate isomerase reaction. *Journal of Biological Chemistry* **1959**, 234, 1007-10.
- 7 Gerlt, J. A., Understanding the mechanisms and rates of enzyme-catalyzed proton transfer reactions to and from carbon. *Bioorganic Chemistry: Peptides and Proteins* **1998**, 279-311, 500-501.
- 8 Komives, E. A.; Chang, L. C.; Lolis, E.; Tilton, R. F.; Petsko, G. A.; Knowles, J. R., Electrophilic catalysis in triosephosphate isomerase: the role of histidine-95. *Biochemistry* **1991**, 30, (12), 3011-19.

- 9 Davenport, R. C.; Bash, P. A.; Seaton, B. A.; Karplus, M.; Petsko, G. A.; Ringe, D., Structure of the triosephosphate isomerase-phosphoglycolohydroxamate complex: an analog of the intermediate on the reaction pathway. *Biochemistry* **1991**, 30, (24), 5821-6.
- 10 Nickbarg, E. B.; Davenport, R. C.; Petsko, G. A.; Knowles, J. R., Triosephosphate isomerase: removal of a putatively electrophilic histidine residue results in a subtle change in catalytic mechanism. *Biochemistry* **1988**, 27, (16), 5948-60.
- 11 Belasco, J. G.; Knowles, J. R., Direct observation of substrate distortion by triosephosphate isomerase using Fourier transform infrared spectroscopy. *Biochemistry* **1980**, 19, (3), 472-7.
- 12 Jencks, W. P., Binding energy, specificity, and enzymic catalysis: the Circe effect. *Advances in Enzymology and Related Areas of Molecular Biology* **1975**, 43, 219-410.
- 13 Richarz, R.; Wuethrich, K., Carbon-13 NMR chemical shifts of the common amino acid residues measured in aqueous solutions of the linear tetrapeptides H-Gly-Gly-X-L-Ala-OH. *Biopolymers* **1978**, 17, (9), 2133-41.
- 14 Creighton, T. E., *Proteins: Structures and Molecular Properties*. 2nd ed.; W.H. Freeman and Company: New York, 1993.
- 15 Hol, W. G. J., The role of the  $\alpha$ -helix dipole in protein function and structure. *Progress in Biophysics & Molecular Biology* **1985**, 45, (3), 149-95.
- 16 Lodi, P. J.; Knowles, J. R., Neutral imidazole is the electrophile in the reaction catalyzed by triosephosphate isomerase: structural origins and catalytic implications. *Biochemistry* **1991**, 30, (28), 6948-56.
- 17 Bruice, T. C.; Schmir, G. L., Imidazole catalysis. II. The reaction of substituted imidazoles with phenyl acetates in aqueous solution. *Journal of the American Chemical Society* **1958**, 80, 148-56.
- 18 Chiang, Y.; Kresge, A. J., Enols and other reactive species. *Science (Washington, DC, United States)* **1991**, 253, (5018), 395-400.
- 19 Gerlt, J. A.; Gassman, P. G., Understanding the rates of certain enzyme-catalyzed reactions: Proton abstraction from carbon acids, acyl transfer reactions, and displacement reactions of phosphodiester. *Biochemistry* **1993**, 32, (45), 11943-52.
- 20 Hegeman, G. D.; Rosenberg, E. Y.; Kenyon, G. L., Mandelic acid racemase from *Pseudomonas putida*. Purification and properties of the enzyme. *Biochemistry* **1970**, 9, (21), 4029-36.

- 21 Powers, V. M.; Koo, C. W.; Kenyon, G. L.; Gerlt, J. A.; Kozarich, J. W., Mechanism of the reaction catalyzed by mandelate racemase. 1. Chemical and kinetic evidence for a two-base mechanism. *Biochemistry* **1991**, 30, (38), 9255-63.
- 22 Landro, J. A.; Gerlt, J. A.; Kozarich, J. W.; Koo, C. W.; Shah, V. J.; Kenyon, G. L.; Neidhart, D. J.; Fujita, S.; Petsko, G. A., The role of lysine 166 in the mechanism of mandelate racemase from *Pseudomonas putida*: Mechanistic and crystallographic evidence for stereospecific alkylation by (R)- $\alpha$ -phenylglycidate. *Biochemistry* **1994**, 33, (3), 635-43.
- 23 Fee, J. A.; Hegeman, G. D.; Kenyon, G. L., Mandelate racemase from *Pseudomonas putida*. Subunit composition and absolute divalent metal ion requirement. *Biochemistry* **1974**, 13, (12), 2528-32.
- 24 Kenyon, G. L.; Hegeman, G. D., Mandelate racemase. *Advances in Enzymology and Related Areas of Molecular Biology* **1979**, 50, 325-60.
- 25 Kresge, A. J., Generation and study of enols and other reactive species. *Pure and Applied Chemistry* **1991**, 63, (2), 213-21.
- 26 Kallarakal, A. T.; Mitra, B.; Kozarich, J. W.; Gerlt, J. A.; Clifton, J. R.; Petsko, G. A.; Kenyon, G. L., Mechanism of the Reaction Catalyzed by Mandelate Racemase: Structure and Mechanistic Properties of the K166R Mutant. *Biochemistry* **1995**, 34, (9), 2788-97.
- 27 Mitra, B.; Kallarakal, A. T.; Kozarich, J. W.; Gerlt, J. A.; Clifton, J. R.; Petsko, G. A.; Kenyon, G. L., Mechanism of the Reaction Catalyzed by Mandelate Racemase: Importance of Electrophilic Catalysis by Glutamic Acid 317. *Biochemistry* **1995**, 34, (9), 2777-87.
- 28 Chiang, Y.; Kresge, A. J.; Pruszyński, P.; Schepp, N. P.; Wirz, J., Mandelic acid enols: determination of the acidity in aqueous solutions and estimation of keto-enol equilibrium constants and CH acidity of mandelic acid. *Angewandte Chemie* **1990**, 102, (7), 810-12.
- 29 Alter, G. M.; Casazza, J. P.; Zhi, W.; Nemeth, P.; Srere, P. A.; Evans, C. T., Mutation of essential catalytic residues in pig citrate synthase. *Biochemistry* **1990**, 29, (33), 7557-63.
- 30 Karpusas, M.; Branchaud, B.; Remington, S. J., Proposed mechanism for the condensation reaction of citrate synthase: 1.9-ANG. structure of the ternary complex with oxaloacetate and carboxymethyl coenzyme A. *Biochemistry* **1990**, 29, (9), 2213-19.



- 31 Karpusas, M.; Holland, D.; Remington, S. J., 1.9-Å. Structures of ternary complexes of citrate synthase with D- and L-malate: mechanistic implications. *Biochemistry* **1991**, 30, (24), 6024-31.
- 32 Man, W. J.; Li, Y.; O'Connor, C. D.; Wilton, D. C., Conversion of citrate synthase into citryl-CoA lyase as a result of mutation of the active-site aspartic acid residue to glutamic acid. *Biochemical Journal* **1991**, 280, (2), 521-6.
- 33 Zhi, W.; Srere, P. A.; Evans, C. T., Conformational stability of pig citrate synthase and some active-site mutants. *Biochemistry* **1991**, 30, (38), 9281-6.
- 34 Remington, S.; Wiegand, G.; Huber, R., Crystallographic refinement and atomic models of two different forms of citrate synthase at 2.7 and 1.7 Å resolution. *Journal of Molecular Biology* **1982**, 158, (1), 111-52.
- 35 Kurz, L. C.; Drysdale, G. R., Evidence from Fourier transform infrared spectroscopy for polarization of the carbonyl of oxaloacetate in the active site of citrate synthase. *Biochemistry* **1987**, 26, (9), 2623-7.
- 36 Cleland, W. W.; Kreevoy, M. M., Low-barrier hydrogen bonds and enzymic catalysis. *Science (Washington, DC, United States)* **1994**, 264, (5167), 1887-90.
- 37 Frey, P. A., Low-barrier hydrogen bonds. *Science (Washington, D. C.)* **1995**, 268, (5208), 189.
- 38 Frey, P. A.; Whitt, S. A.; Tobin, J. B., A low-barrier hydrogen bond in the catalytic triad of serine proteases. *Science (Washington, DC, United States)* **1994**, 264, (5167), 1927-30.
- 39 Hibbert, F.; Emsley, J., Hydrogen bonding and chemical reactivity. *Advances in Physical Organic Chemistry* **1990**, 26, 255-79.
- 40 Stahl, N.; Jencks, W. P., Hydrogen bonding between solutes in aqueous solution. *Journal of the American Chemical Society* **1986**, 108, (14), 4196-205.
- 41 Cleland, W. W., Low-barrier hydrogen bonds and enzymic catalysis. *Archives of Biochemistry and Biophysics* **2000**, 382, (1), 1-5.
- 42 Warshel, A.; Papazyan, A., Energy considerations show that low-barrier hydrogen bonds do not offer a catalytic advantage over ordinary hydrogen bonds. *Proceedings of the National Academy of Sciences of the United States of America* **1996**, 93, (24), 13665-13670.
- 43 Marcus, R. A., Unusual slopes of free energy plots in kinetics. *Journal of the American Chemical Society* **1969**, 91, (26), 7224-5.
- 44 Cohen, A. O.; Marcus, R. A., Slope of free energy plots in chemical kinetics. *Journal of Physical Chemistry* **1968**, 72, (12), 4249-56.

- 45 Bernasconi, C. F., The principles of nonperfect synchronization. *Advances in Physical Organic Chemistry* **1992**, 27, 119-238.
- 46 Bordwell, F. G.; Boyle, W. J., Jr., Kinetic isotope effects for nitroalkanes and their relation to transition-state structure in proton-transfer reactions. *Journal of the American Chemical Society* **1975**, 97, (12), 3447-52.
- 47 Bordwell, F. G.; Boyle, W. J., Jr., Acidities, Broensted coefficients, and transition state structures for 1-arylnitroalkanes. *Journal of the American Chemical Society* **1972**, 94, (11), 3907-11.
- 48 King, G.; Lee, F. S.; Warshel, A., Microscopic simulations of macroscopic dielectric constants of solvated proteins. *Journal of Chemical Physics* **1991**, 95, (6), 4366-77.
- 49 Warshel, A.; Papazyan, A.; Kollman, P. A., On low-barrier hydrogen bonds and enzyme catalysis. *Science (New York, N.Y.)* **1995**, 269, (5220), 102-6.
- 50 Frey, P. A., Isotope effects in the characterization of low barrier hydrogen bonds. *Isotope Effects in Chemistry and Biology* **2006**, 975-993.
- 51 Fuhrmann, C. N.; Daugherty, M. D.; Agard, D. A., Subangstrom Crystallography Reveals that Short Ionic Hydrogen Bonds, and Not a His-Asp Low-Barrier Hydrogen Bond, Stabilize the Transition State in Serine Protease Catalysis. *Journal of the American Chemical Society* **2006**, 128, (28), 9086-9102.
- 52 Ishida, T., Low-Barrier Hydrogen Bond Hypothesis in the Catalytic Triad Residue of Serine Proteases: Correlation between Structural Rearrangement and Chemical Shifts in the Acylation Process. *Biochemistry* **2006**, 45, (17), 5413-5420.
- 53 Pasqualato, S.; Cherfils, J., Crystallographic Evidence for Substrate-Assisted GTP Hydrolysis by a Small GTP Binding Protein. *Structure (Cambridge, MA, United States)* **2005**, 13, (4), 533-540.
- 54 Warshel, A., Calculations of enzymatic reactions: calculations of pKa, proton transfer reactions, and general acid catalysis reactions in enzymes. *Biochemistry* **1981**, 20, (11), 3167-77.
- 55 Warshel, A.; Aqvist, J., Electrostatic energy and macromolecular function. *Annual Review of Biophysics and Biophysical Chemistry* **1991**, 20, 267-98.
- 56 Warshel, A.; Levitt, M., Theoretical studies of enzymic reactions: dielectric, electrostatic and steric stabilization of the carbonium ion in the reaction of lysozyme. *Journal of Molecular Biology* **1976**, 103, (2), 227-49.
- 57 Yang, W.; Drueckhammer, D. G., Computational Study of the Citrate Synthase Catalyzed Deprotonation of Acetyl-Coenzyme A and Fluoroacetyl-Coenzyme A:

- Demonstration of a Layered Quantum Mechanical Approach. *Journal of Physical Chemistry B* **2003**, 107, (24), 5986-5994.
- 58 Kimura, E.; Kitamura, H.; Koike, T.; Shiro, M., Facile and selective electrostatic stabilization of uracil N(1)- anion by a proximate protonated amine: A chemical implication for why uracil N(1) is chosen for glycosylation site. *Journal of the American Chemical Society* **1997**, 119, (45), 10909-10919.
  - 59 Zhong, Z.; Postnikova, B. J.; Hanes, R. E.; Lynch, V. M.; Anslyn, E. V., Large pKa shifts of  $\alpha$ -carbon acids induced by copper(II) complexes. *Chemistry--A European Journal* **2005**, 11, (8), 2385-2394.
  - 60 Vock, P.; Engst, S.; Eder, M.; Ghisla, S., Substrate Activation by Acyl-Coenzyme A Dehydrogenases: Transition-State Stabilization and pKs of Involved Functional Groups. *Biochemistry* **1998**, 37, (7), 1848-1860.
  - 61 Benning, M. M.; Taylor, K. L.; Liu, R. Q.; Yang, G.; Xiang, H.; Wesenberg, G.; Dunaway-Mariano, D.; Holden, H. M., Structure of 4-chlorobenzoyl coenzyme A dehalogenase determined to 1.8 Å resolution: an enzyme catalyst generated via adaptive mutation. *Biochemistry* **1996**, 35, (25), 8103-9.
  - 62 Snowden, T. S.; Bisson, A. P.; Anslyn, E. V., A Comparison of NH- $\pi$  versus Lone Pair Hydrogen Bonding Effects on Carbon Acid pKa Shifts. *Journal of the American Chemical Society* **1999**, 121, (26), 6324-6325.
  - 63 Snowden, T. S.; Bisson, A. P.; Anslyn, E. V., Artificial receptors involved in enolization and pKa shifts. *Bioorganic & Medicinal Chemistry* **2001**, 9, (9), 2467-2478.
  - 64 Kelly-Rowley, A. M.; Lynch, V. M.; Anslyn, E. V., Molecular Recognition of Enolates of Active Methylene Compounds in Acetonitrile. The Interplay between Complementarity and Basicity and the Use of Hydrogen Bonding to Lower Guest pKas. *Journal of the American Chemical Society* **1995**, 117, (12), 3438-47.
  - 65 Zhong, Z.; Snowden, T. S.; Best, M. D.; Anslyn, E. V., Rate of Enolate Formation Is Not Very Sensitive to the Hydrogen Bonding Ability of Donors to Carboxyl Oxygen Lone Pair Acceptors; A Ramification of the Principle of Non-Perfect Synchronization for General-Base-Catalyzed Enolate Formation. *Journal of the American Chemical Society* **2004**, 126, (11), 3488-3495.
  - 66 Hartwell, E.; Hodgson, D. R. W.; Kirby, A. J., Exploring the Limits of Efficiency of Proton-Transfer Catalysis in Models and Enzymes. *Journal of the American Chemical Society* **2000**, 122, (38), 9326-9327.
  - 67 St. Maurice, M.; Bearne, S. L., Kinetics and Thermodynamics of Mandelate Racemase Catalysis. *Biochemistry* **2002**, 41, (12), 4048-4058.

- 68 Bearne, S. L.; Wolfenden, R., Mandelate Racemase in Pieces: Effective Concentrations of Enzyme Functional Groups in the Transition State. *Biochemistry* **1997**, 36, (7), 1646-1656.
- 69 Houk, R. J. T.; Anslyn, E. V.; Stanton, J. F., Carbonyl Coordination Chemistry from a New Angle: A Computational Study of  $\alpha$ -Carbon Acidity Based on Electrophile Coordination Geometry. *Organic Letters* **2006**, 8, (16), 3461-3463.
- 70 Stanton, J. F.; Gauss, J.; Watts, J. D.; Lauderdale, W. J.; Bartlett, R. J., The ACES II program system. *International Journal of Quantum Chemistry, Quantum Chemistry Symposium* **1992**, 26, (Proc. Int. Symp. At., Mol., Condens. Matter Theory Comput. Methods, 1992), 879-94.
- 71 Ren, J.; Cramer, C. J.; Squires, R. R., Superacidity and Superelectrophilicity of BF<sub>3</sub>-Carbonyl Complexes. *Journal of the American Chemical Society* **1999**, 121, (11), 2633-2634.
- 72 Cao, D. R.; Schollmeyer, D.; Meier, H., (Phenylethynyl)- and (phenylethenyl)metacyclophanes with p,p interactions. *European Journal of Organic Chemistry* **1999**, (4), 791-795.
- 73 Detty, M. R.; Virkler, P. R. Production of dye intermediates and polymethine dyes therefrom. 2001-US19981 2002000642, 20010622., 2002.
- 74 De Boer, H. J. R.; De Kanter, F. J. J.; Akkerman, O. S.; Bickelhaupt, F., 1-Bromo-2,6-bis(chloromagnesiomethyl)benzene from the attempted synthesis of a doubly benzylic 1,3,5-tri-Grignard reagent. *Main Group Metal Chemistry* **2001**, 24, (12), 841-844.
- 75 Fujihara, H.; Chiu, J. J.; Furukawa, N., Synthesis, conformation, and the stereoselective sulfur extrusion reaction of a new intraannular dibromo-substituted tetrathia[4.4]metacyclophane. *Chemistry Letters* **1991**, (1), 141-4.

## **Chapter 2: Luminescent Assays for Ketones and Aldehydes Employing Catalytic Signal Amplification**

### **2.0 INTRODUCTION**

Whereas Chapter 1 discussed in detail one of the types of interactions which supramolecular chemists can use to bind and/or modify a target, the current chapter looks mainly at the other half of a sensing or signal generating methodology. Namely this chapter will discuss the development of a new signaling methodology for sensing in a molecular recognition assay. A typical molecular signaling assay requires first a host or group of hosts that has some specific or generalized affinity for a target analyte, and second a method by which to detect the binding event of host and guest.<sup>1</sup> The trend in molecular recognition, as with many other application driven fields, is to generate the greatest output with the minimum size or detection limit. For example, when attempting to sense a disease marker, the earlier it can be discovered and hence, at lower concentration, the better. When attempting to decrease the limit of detection for an assay, two main questions must be addressed. The first is whether or not the recognition element has sufficient affinity for the target to attain favorable association at the desired detection level. To this end, supramolecular chemists turn to nature and attempt to mimic the interactions of strongly binding enzymes and antibodies. Though nowhere near to achieving the success of Mother Nature, chemists have become very proficient at

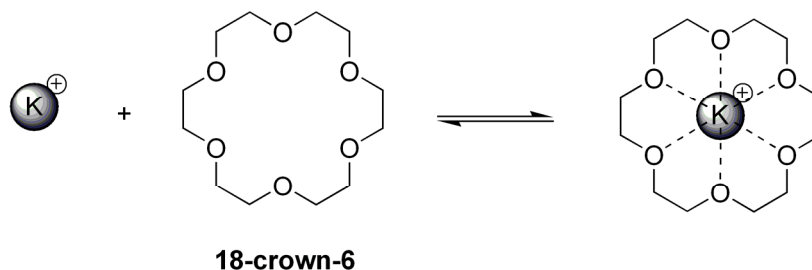
generating exceptional intermolecular interactions, and most assays today do not suffer from a lack of binding affinity.<sup>2,3</sup> The second question that must be answered is whether one will be able to observe the desired recognition event. Reconciling low analyte concentration with detectable signal output has received a good deal of attention in recent years,<sup>4</sup> and the following chapter will discuss some of the traditional methods of signal generation and the development of a new methodology by which this dilemma is being overcome.

## **2.1 BACKGROUND**

### **2.1.1 Supramolecular Chemistry and Molecular Recognition**

The term “supramolecular chemistry” was coined by Jean-Marie Lehn in the early 1990’s and was meant to encompass the vast field science associated with intermolecular noncovalent interactions.<sup>5</sup> Needless to say, this term is extremely broad in scope and comprises several other large fields, one of which is host-guest molecular recognition. As the name implies, in host-guest molecular recognition, a specific host or set of differential hosts is employed to bind and recognize a target guest molecule of interest through a noncovalent set of interactions. In more recent years, recognition events utilizing certain reversible covalent attachments, such as boronic esters, have also begun to appear and are assumed to fall under the supramolecular umbrella.<sup>6</sup> One of the most well known molecular recognition events is the binding of a metal cation into the center of a crown ether as shown in Scheme 2.1.<sup>7</sup>

**Scheme 2.1** Sequestration of a potassium cation by 18-crown-6



For many years, molecular recognition was a one step process involving only the recognition event as in the crown ether example. However, the field of abiotic molecular recognition has advanced considerably in the last few years with the advent of the chemosensor. A chemosensor derives its name from the biological system also known as a chemoreceptor in which sugars, proteins, enzymes, cells, and/or group of cells work in concert to detect a molecular signal which triggers a sensory response.<sup>8</sup> The best example of a biological chemosensor is the neuron. Receptors on the neuron receive chemical signals in the form of hormones and neurotransmitters, which upon binding, induce a signal transduction which passes on the signal to the next neuron. Similarly, an abiotic chemosensor describes a system in which the molecular recognition event or binding is transduced into a detectable signal.<sup>9</sup>

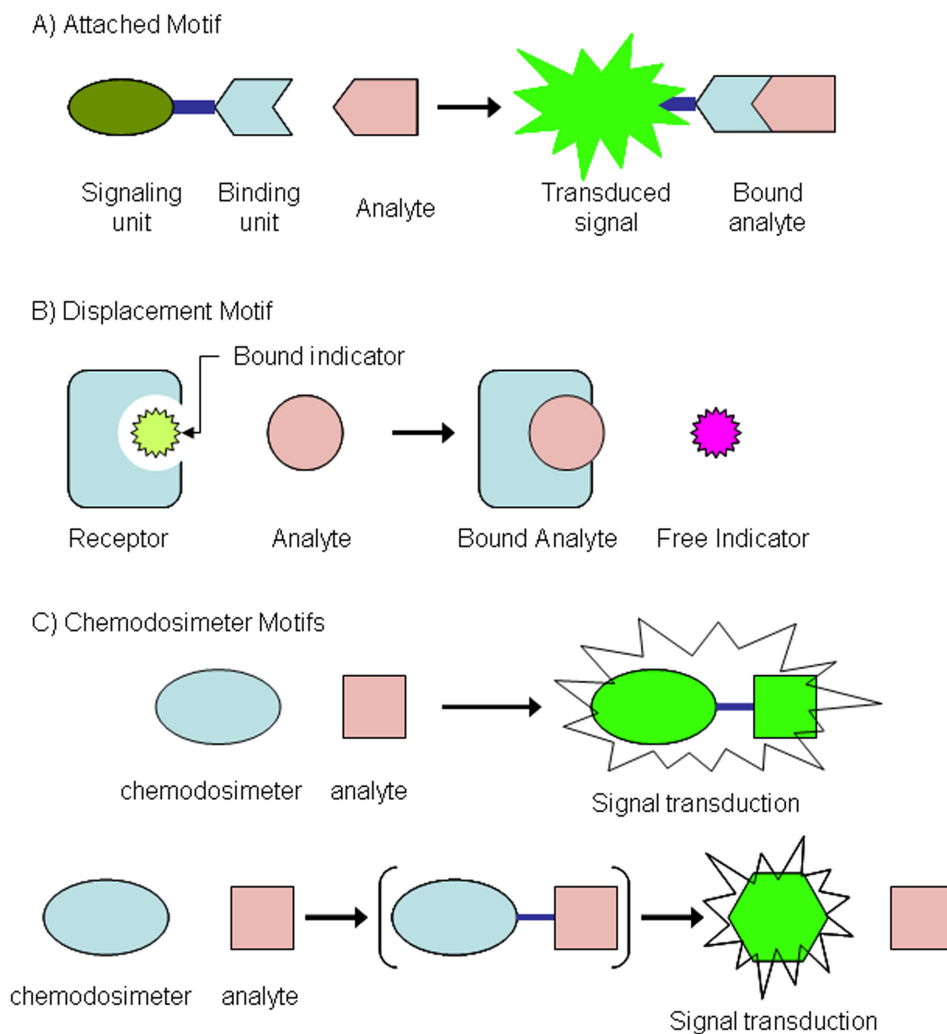


**Figure 2.1** A) Chemosensor design in which the binding unit and the signaling unit are covalently linked. B) The displacement design in which the analyte and indicator compete for the binding site. C) Two types of chemodosimeter in which an irreversible reaction occurs upon binding to generate a signal.

The vast majority of chemosensors produce fluorometric or colorimetric responses, though many instances of electrochemical chemosensors also exist.<sup>10</sup> There are three major types of chemosensor design which are shown in Figure 2.1. The first design incorporates a signaling unit and an analyte binding unit into the same molecule.



When an analyte binds, the signal is transduced through the molecule such that a recognizable signal is expelled from the signaling unit. This model will be called the attached approach. The second possibility is that of a displacement model, in which the analyte and an indicator are in a competitive equilibrium for the host receptor. In these cases there must be a significant change in the state of the indicator between its bound state and its free state. The third type of sensor described in Figure 2.1 is a chemodosimeter and cannot technically be called a chemosensor because analyte binding is not a reversible process. However, the general concept remains the same in that a reaction with an analyte occurs and a signal is generated. There are two main types of chemodosimeters, one in which the analyte covalently attaches to the chemodosimeter and the signal is generated directly, and the other in which the analyte catalyzes or promotes a transformation of the chemodosimeter into the active signal generator.<sup>11</sup>

The research discussed in this chapter and that in the next deals with chemodosimetric assays. However, for the purpose of discussion on signaling motifs, chemosensors will be discussed here. For a more in depth discussion on chemodosimeters and their use, please refer to the following chapter.

### **2.1.2 Chromogenic Sensing Motifs**

There are two main types of chromogenic signaling units in common use, organic dyes and metal complexes. Aggregation effects are also used to a slightly lesser and more specific degree with porphyrin and sapphyrin type systems.<sup>12</sup>

#### **2.1.2.1 Organic Dyes**

Organic dyes gain their color by absorbing electromagnetic radiation in the visible region of the spectrum from roughly 400-700 nm wavelengths. The extended  $\pi$ -

conjugation found in all organic dyes serves to reduce the HOMO-LUMO gap to within the relatively low energy range spanned by the visible region. There is a correlation between the length of the conjugation and the size of the HOMO-LUMO gap, with greater conjugation giving lower energy transitions. For instance anthracene absorbs light just outside the visible spectrum around 390 nm, whereas 9,10-bis(phenylethynyl)anthracene (BPEA) has a lower energy  $\lambda_{\text{maxabs}}$  near 470 nm (Figure 2.2). The difference arises solely from the extension of the conjugated  $\pi$ -system.

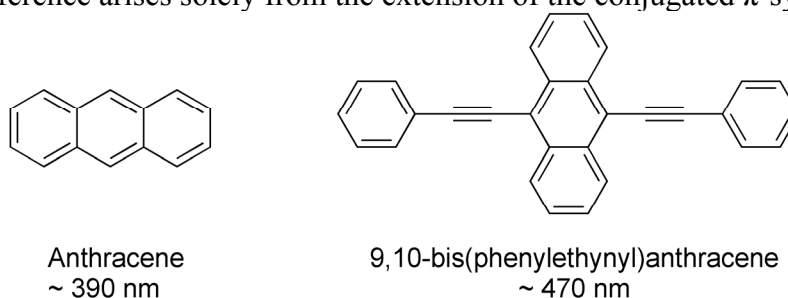


**Figure 2.2** The extension of the conjugated system in BPEA lowers the energy of the HOMO-LUMO gap to give a longer wavelength absorbance than anthracene.

The addition of an electron donating ( $-\text{NH}_2$ ,  $-\text{OH}$ ,  $-\text{OMe}$ ,  $-\text{X}$ , etc.) or withdrawing ( $-\text{NO}_2$ ,  $-\text{SO}_3\text{H}$ ,  $-\text{CO}_2\text{H}$ , etc.) substituent to the conjugated portion of an organic dye results in a modification of dye's absorbance. The extent and direction (batho or hypsochromic) of the modification depends on the dye in question and the group. In general, an electron donating group will raise the HOMO of the dye and should lead to a bathochromic shift, however, this is not always the case. The introduction of both an electron donor and acceptor connected through the conjugation can result in the formation of a charge transfer (CT) band. CT occurs more frequently as an intermolecular interaction when there is a donation of electron charge from a donor

molecule, such as tetrathiafulvalene, to an acceptor like tetracyanoethylene by a excitation from the donor HOMO to the acceptor LUMO.<sup>1</sup> The absorbance generated by this action is called a charge transfer band or CT band. Single dyes which contain both donating and accepting groups can undergo an intramolecular process that closely resembles traditional CT though the electronic transition is still technically a  $\pi$ - $\pi^*$  transition. Dyes such as squaraines and azobenzenes show distinct CT bands (Figure 2.3). Sensing with organic dyes is often accomplished through an interaction with a donating or withdrawing group which causes a modification in the absorbance based on how interaction with the guest or host alters the ability of the substituent to augment or shrink the HOMO-LUMO gap.<sup>11</sup>

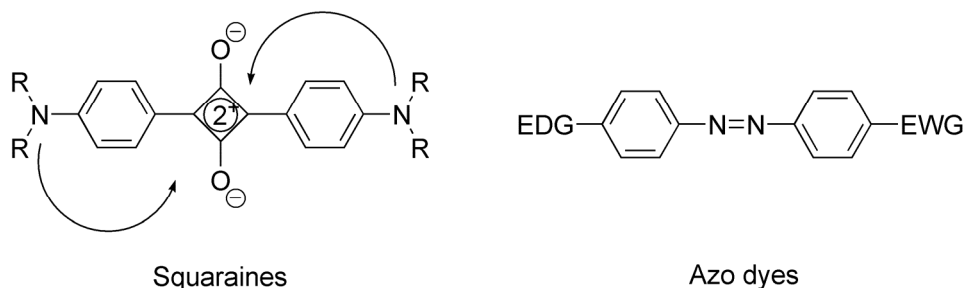
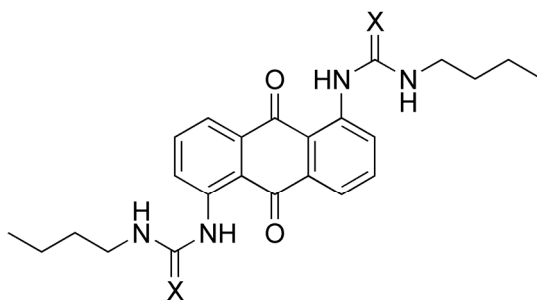


**Figure 2.3** Organic dyes such as azobenzenes and squaraines exhibit CT interaction between the donating and withdrawing groups attached to the conjugated  $\pi$ -system.

The anthraquinone based receptors **2.1** and **2.2** are examples of chromogenic chemosensors using the attached approach.<sup>13</sup> Anthraquinones are well established CT acceptor moieties, and the urea and thiourea groups are weakly donating substituents. In the presence of excess fluoride anion in acetonitrile, the thiourea version **2.1** showed a marked shift from orange to a deep brownish blue (490 nm to 670 nm) indicating an

increase in the charge donation from the fluoride bound substituents to the anthraquinone core. **2.1** was found to be very selective for fluoride, though **2.2** exhibited a wide range of different color changes in the presence of fluoride, dihydrogen phosphate, cyanide, acetate and benzoate.

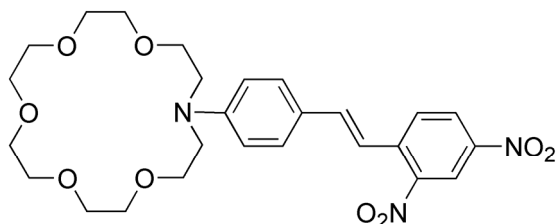


**2.1** X=S  $\lambda_{\text{max}} = 490\text{nm}$

**2.2** X=O  $\lambda_{\text{max}} = 490\text{nm}$

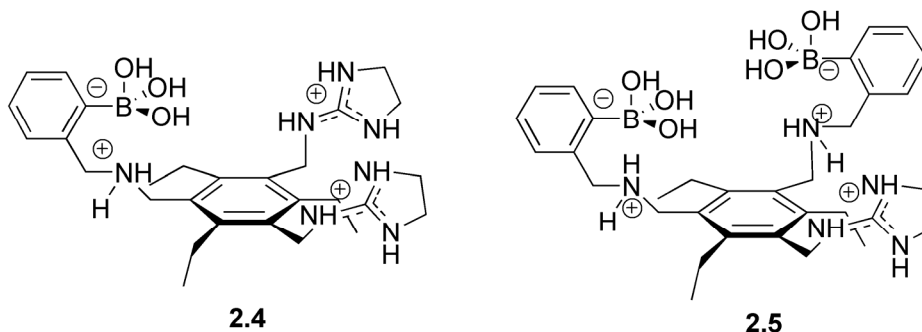
Though the term is rarely used in anion binding studies, the above anthraquinone receptors can be referred to as chromoionophores. Chromoionophores are described as chemosensors which contain a specific ionophilic subunit or ionophore which binds an ion and transduces a signal to the chromophore.<sup>14</sup> Stilbene dye **2.3** is a cation binding chromoionophore.<sup>15, 16</sup> Whereas the anion binding in the previous example resulted in better charge transfer from the donor to the acceptor, cation binding in this case reduces the ability of the nitrogen donor of the azacrown moiety to transfer electron charge to the nitro acceptors. This effect leads to a hypsochromic shift for cation binding whereas the anions caused a bathochromic shift in **2.1** and **2.2**. Chromoionophore **2.3** was used to study the effects of alkali and alkaline earth metal binding. In its native form, **2.3** absorbs at 476 nm. It was found, as expected, that alkaline earth metals with a +2 charge gave much greater shift in the absorbance maximum than the singly charged alkali metals. For instance, when sodium ions were bound to the crown receptor, only a modest

shift to 463 nm was observed. However, when barium was introduced, the hypsochromic shift was much more pronounced at 370 nm.



**2.3**

Two receptors reported by the Anslyn group (**2.4** and **2.5**) are used in the displacement model of chemosensor design and were used to target carboxylates containing vicinal diol functionalities such as tartrate, malate, and gallate. These carboxylates are present in all aged alcoholic beverages. Tartrate and malate are essential compounds for wine production since their concentrations over time can be traced to the proper aging of the wine. Gallate and similar cyclic carboxylates are found in the oak used in the aging barrels in scotch whiskey production and are extracted into the scotch during the aging process. Two receptors reported by Anslyn and coworkers were specifically designed to bind to vicinal diols which contain carboxylates. The triethylbenzene based receptor **2.4** consists of two aminodihydroimidazolium groups for carboxylate binding and a phenyl boronic acid which can form reversible boronic esters with a vicinal diol.<sup>17</sup>



Tartrate, with two carboxylate functionalities as well as a vicinal diol, was chosen as the target for **2.4**. This host was studied using an indicator-displacement assay with alizarin complexone because this indicator contains the same complimentary functionalities as tartrate. When the dye binds to the host through the formation of a boronic ester, the effect is similar to deprotonation of the hydroxyl groups which enhances the electron donation. This results in a bathochromic shift from yellow-orange ( $\lambda_{\text{max}}=450$  nm) to a deep red ( $\lambda_{\text{max}}=525$  nm). Upon release of the indicator by competition with tartrate, the donating ability is restored and the dye reverts to its native absorbance. Qualitative naked-eye experiments showed distinct color changes upon introduction of tartrate to a **2.4**-indicator solution. Quantitative analyses revealed that binding of tartrate ( $K_a = 5.5 \times 10^5 \text{ M}^{-1}$ ) in 25% water/methanol was selective over all other analytes except malate ( $K_a = 4.8 \times 10^5 \text{ M}^{-1}$ ). The host was successfully used to quantify the concentration of tartrate-malate in grape-based beverages such as wine. In a later study, the bis(boronic acid) analog **2.5** was studied for binding with gallate and similar structures.<sup>18</sup> Indicator displacement assays with pyrocatechol violet, which turned from yellow to maroon upon indicator binding and back to yellow with displacement, found binding constants between 100 (4-hydroxycinnamic acid) and 10,000 (gallic acid) for these targets. Interestingly, when the assay was applied to determination of the ages

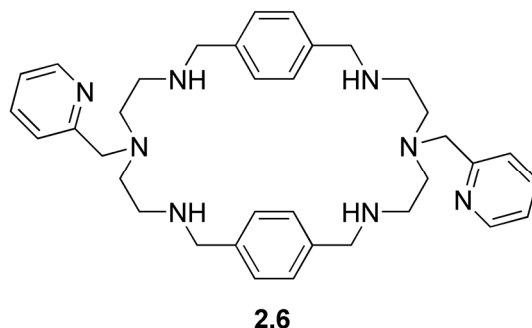
of scotch whiskeys, only the complex binding profile of all the analytes gave an accurate age to concentration ratio.

#### **2.1.2.2 Metal Complexes**

The second widely used chromogenic sensing motif utilizes transition metal complexation to bring about a color change. Transition metals have several ways of generating color. In metals with unfilled *d*-shells, *d-d*\* transitions are possible, however, these are usually either symmetry or spin forbidden transitions and give rather weak absorption bands. Complex formation with an analyte can lead to change in the symmetry which then makes *d-d*\* transition symmetry allowed. This type of interaction is often the reason for the presence or lack of color associated with copper(II). Another mode of color generation used in sensing applications with metals is the formation of CT complexes with the target analyte or indicator.<sup>11</sup> With low valent, high oxidation state metals bound to electron rich ligands, a charge transfer effect from the ligand to the unoccupied *d*-orbitals of the metal can occur, called ligand-to-metal charge transfer (LMCT). Charge transfer can also happen in the opposite direction if the metal has a relatively full *d*-shell, called metal-to-ligand charge transfer (MLCT). Since neither of these CT modes is spin or symmetry forbidden, the absorption arising from them is usually quite intense and in the visible spectrum. In the case of displacement type assays which use metal complexes, CT phenomena are generally undesirable as the color change of interest is derived from the organic dye rather than the metal complex so this discussion will focus on attached binding unit-signaling unit type scaffolds.

As most metals are somewhat electropositive, the vast majority of receptors built around metal complexation deal with anion binding.<sup>11</sup> Metal coordination presents an

interesting case in which the binding unit also serves directly as the signaling unit. The dicopper(II) complex of receptor **2.6** was used to select for the imidazolate anion.<sup>19</sup> Upon initial introduction of 2 equivalents of copper(II) at pH 9 in buffered water, the dimetallic complex shows a weak d-d\* band at 640 nm. Titration of imidazole generates a 1:1 complex with the imidazolate bridging the two Cu(II) centers. Accompanying the receptor-anion complex formation is a strong hyperchromic and bathochromic shift to 690 nm. The new absorbance at 690 nm corresponds to a perturbation in the d-orbital symmetry which makes the d-d\* transition allowed.



### 2.1.3 Fluorogenic Sensing Motifs

Even more widely used than chromogenic chemosensors, fluorescent assays have seen a wide array of uses in the past few decades.<sup>11</sup> Fluorescence has several advantages over absorbance, the most telling being a much higher level of sensitivity. In fluorescence, the emission signal is dependent on the concentration of the fluorophore and intensity of the incident light, whereas in absorbance, the signal is only dependent on the concentration. This is because absorbance is measured as a ratio of light in versus light out. If the intensity of the light is increased, more light is absorbed and the ratio remains the same for the same concentration. Fluorescence has a clear dependency on the excitation intensity as evidenced by the Beer-Lambert law for fluorescence shown



below in Equation 2.4. Hence, to a degree, the limit of detection for fluorescence can be decreased merely by turning up the power of the lamp.

#### **2.1.3.1 Fluorescence Phenomena**

There are several ways of exploiting the properties of fluorophores for the development of chemosensors. Electron or energy transfer effects have been commonly used in both biological and abiotic sensing.<sup>11, 20-22</sup> The first type of energy transfer mechanism is a photoinduced electron transfer or PET (Figure 2.4A-B). PET is a fluorescence quenching process and can occur in two different ways. The first is by interaction of the HOMO and LUMO of the fluorophore with the HOMO of a nearby molecule or of another part of the same molecule. Assuming the electron energy of the participating quencher lies between the HOMO-LUMO gap of the fluorophore, when the fluorophore is excited, an electron from the quencher transfers to the lower SOMO of the fluorophore. This transfer blocks the light-emitting relaxation pathway, and the electron from the upper, and now only, SOMO of the fluorophore transfers to the SOMO of the quencher to fill its HOMO. The other way PET can occur is through the interaction of the excited electron of the fluorophore with an empty orbital of a quencher (Figure 2.4B). Here the electron transfer is somewhat reversed in that the quencher is now an acceptor rather than a donor. The excited electron is transferred to the lower energy acceptor orbital and then relaxes non-radiatively down to the HOMO of the fluorophore. Again this interruption of the light emitting pathway causes either a decrease or complete quenching of fluorescence.<sup>11</sup>

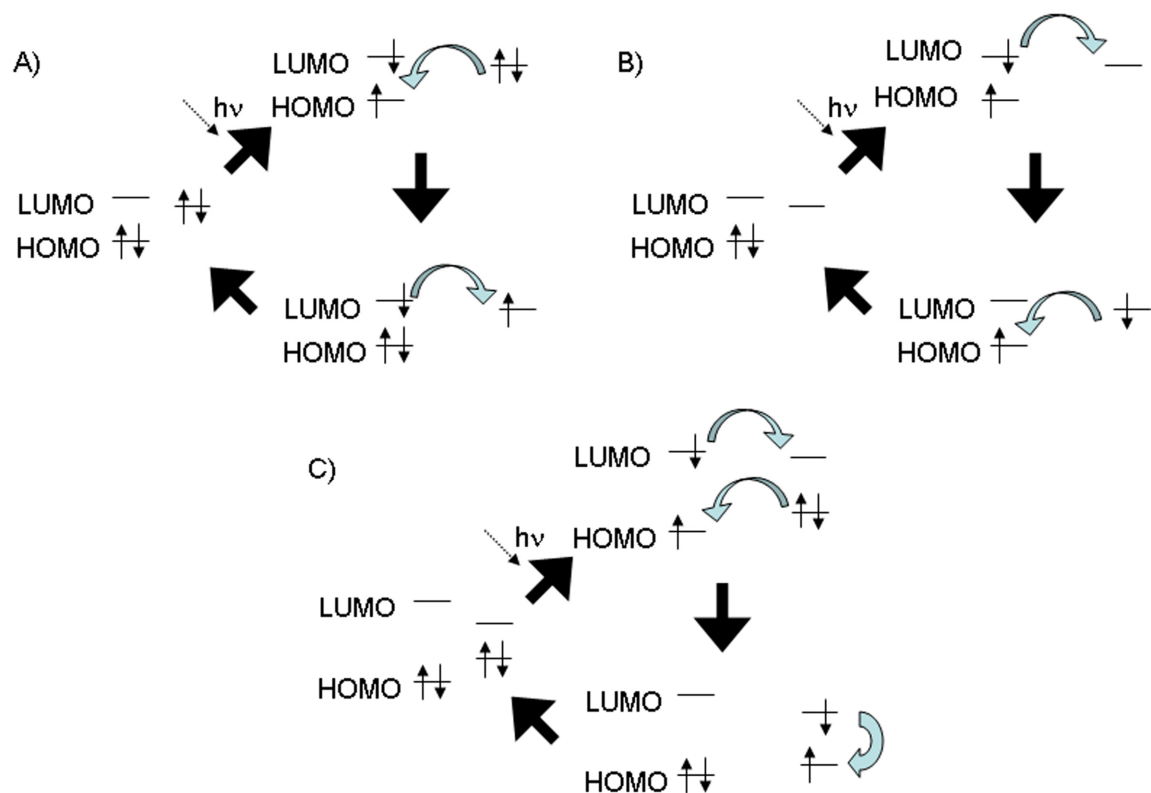


**Figure 2.4** A) PET quenching from a donor. B) PET quenching from an acceptor. C) EET mechanism that can result in quenching or sensitization

The third energy transfer mechanism, electronic energy transfer, is usually considered to be an intermolecular phenomenon and usually only happens in the solid state or in very rigid intramolecular systems. When a molecule with favorable orbital overlap as shown in Figure 2.4C comes into contact with an excited fluorophore, a double electron transfer occurs resulting in a ground state fluorophore and an excited state of the interfering molecule. This is known as the Dexter mechanism of electron exchange and has an exponential dependence on the distance between the interacting molecules.<sup>1</sup> If the initially excited molecule induces a triplet state in the acceptor molecule, the process is known as sensitization and is useful in phosphorescence based detection systems,

however, the strict intermolecular distance requirements have limited this mechanism's usefulness.

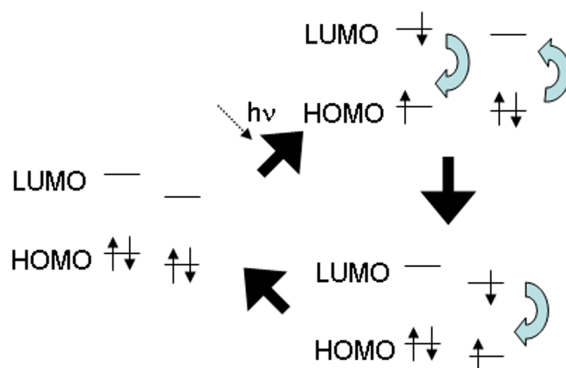
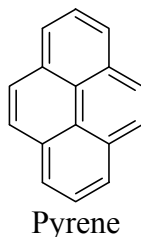


**Figure 2.5** Schematic of the Förster energy exchange mechanism

The last type of energy transfer mechanism is perhaps one of the most important and useful and is also the only one that is strictly an energy transfer. Figure 2.5 illustrates the Förster energy exchange mechanism which acts as a through space, non-radiative, energy transfer. Whereas the Dexter mechanism requires collisional distances and an overlap of the wavefunctions of the donor excited state and the acceptor ground state, the Förster process merely requires a coupling of the transition dipoles of the two molecules. Since, like any other dipole-dipole interaction, the strength of the interaction falls off as a function of  $1/r^3$ , the distance requirements for the energy transfer are much less restrictive than Dexter energy exchange. Though overlap of the wavefunctions is not required, there is a resonance condition applied to the donor and acceptor which stipulates that the acceptor will become excited at an energy that corresponds to the relaxation of the donor. In other words, the emission spectrum of the donor and the absorption spectrum of the acceptor must have some overlap.<sup>1</sup> The most powerful use of this type of energy transfer

is fluorescence resonance energy transfer or FRET. See Scheme 2.4 and its discussion for use of FRET in a signaling assay.

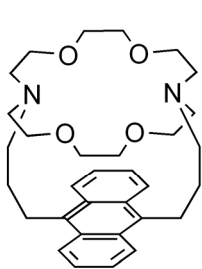
Another phenomenon associated with fluorescence is that of exciplex or excimer formation. Much like an intermolecular CT absorption complex, which acts as a whole to absorb a photon, an exciplex is an intermolecular complex which acts as one to emit a photon. When the members of the exciplex are two of the same molecule, it is called an excimer. Excimers and exciplexs consist of one molecule in the excited state and one in the ground state and the complex as a whole emits a photon at a longer wavelength than the monomeric fluorophore. Polyaromatic hydrocarbons such as pyrene show strong tendencies toward excimer formation, and their use will be discussed below.



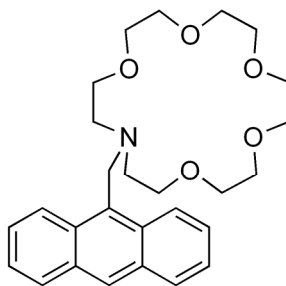
#### ***2.1.3.2 Fluorogenic Chemosensors***

Anthracene based chemosensors such as **2.7** and **2.8** have been widely studied due to the wide range of commercially available derivatives and well defined photophysical properties. Both receptors were studied for their cation binding properties and were found to undergo a turn on of fluorescence in the presence of analyte.<sup>23, 24</sup> Both studies are instrumental in demonstrating one of the most widely used devices in fluorogenic chemosensing. The lone pair electrons of amines are excellent donors for PET quenching of fluorescence. When those lone pairs are tied up in binding or if the amine becomes

protonated, the PET mechanism is interrupted and a turn on of the fluorescence is observed.

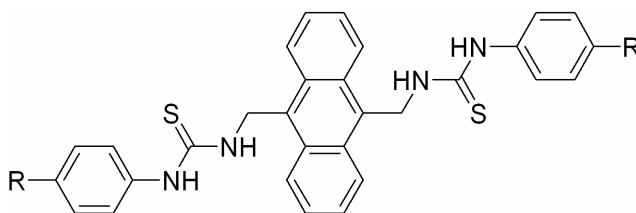


**2.7**



**2.8**

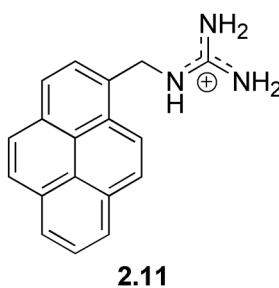
Also noteworthy is the fact that, unlike organic chromophores, it is generally undesirable to place heavily electron donating or withdrawing groups in direct conjugation with a fluorophore as it can lead to drastic changes in the fluorescence properties. Therefore, as in **2.7** and **2.8**, almost every instance of an attached motif fluorogenic chemosensor will have at least a methylene spacer between the signaling unit and the binding unit.



**2.9** R=H  
**2.10** R=CF<sub>3</sub>

Inducing PET quenching can also be an effective means of generating a viable signal. The bis-thiourea receptors **2.9** and **2.10** were reported to show fluorescence quenching upon the binding of both mono and bisanions.<sup>25</sup> The receptors were specifically designed to bind bisanions through the use of neutral binding sites. It was

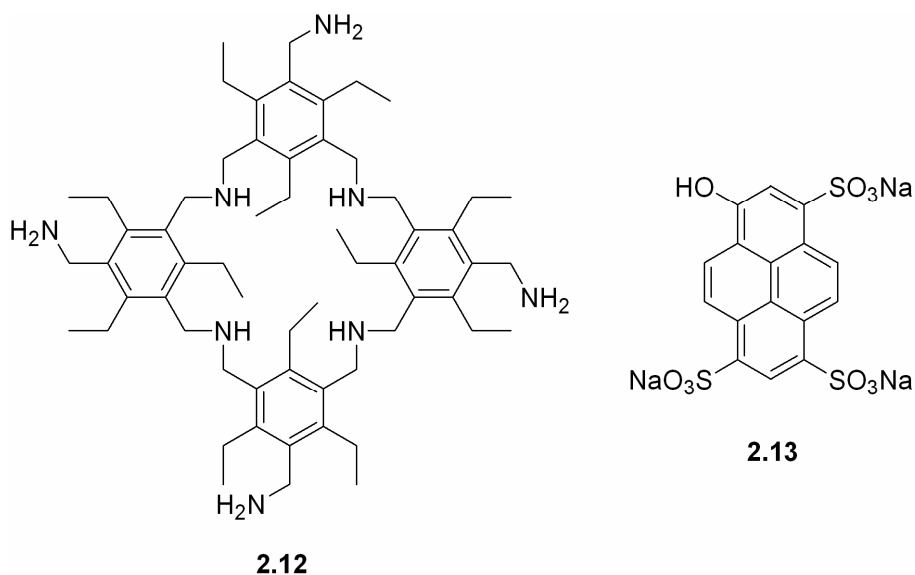
postulated that the binding of various carboxylate and phosphate anions and bisanions such as acetate, malonate, and pyrophosphate resulted in increasing the efficiency of electron transfer from the thiourea moieties by increasing their reduction potential. Though they were unable to prove this theory electrochemically, quenching only occurred upon binding complimentary guests and showed very little activity in the presence of spherical anions such as chloride and bromide.



As mentioned above, pyrene is often used in chemosensing assays for its ability to form strong excimers. A simple yet powerful receptor using pyrene is the guanidinium appended structure **2.11**.<sup>26</sup> In dilute methanolic solutions, monomer emission centered at 400 nm was observed. Upon addition of the bisanionic pyrophosphate, a broad band at 476 nm appeared associated with the pyrene-pyrene excimer. A 2:1 self-assembled complex with  $\pi$ -stacked pyrenes held together by interactions of the guanidinium binding units and the pyrophosphate anions was shown to form by <sup>1</sup>H-NMR titrations, and a clear isoemissive point was observed in fluorescence titrations.

A small number of displacement type assays have been reported with fluorescence as the signaling mechanism. The azacalixarene receptor **2.12** was reported by the Anslyn group in a competition assay with fluorophore **2.13** for the detection of the short lived inositol-triphosphate (IP<sub>3</sub>).<sup>27</sup> Complexation of **2.12** with **2.13** showed a decrease in the fluorescence emission. Introduction of IP<sub>3</sub> ejected **2.13** from the

azacalixarene and restored the full fluorescence intensity. **2.12** was studied with other anion guests such as fructose-1,6-diphosphate, gluconic acid, and adamantane-1,3-dicarboxylic acid, yet IP<sub>3</sub> was shown to have the greatest binding affinity.



Another final type of fluorogenic chemosensor employs the use of luminescent metal complexes of transition metals such as Ru, Re, Ir and Os and lanthanide metals like Eu and Tb.<sup>11</sup> These systems have a nice advantage that emission occurs at longer wavelengths that can be seen by the naked eye if necessary. Unfortunately, many of the assays designed around these complexes must be run in non-aqueous media due to water sensitivity of the metal complexes.

#### 2.1.4 Peroxyoxalate Chemiluminescence

In general, fluorogenic chemosensing and chemodosimetric assays are extremely powerful in the fact that a large number of different assays can be conceived using only a small number of different fluorescent cores and luminescence modification mechanisms.

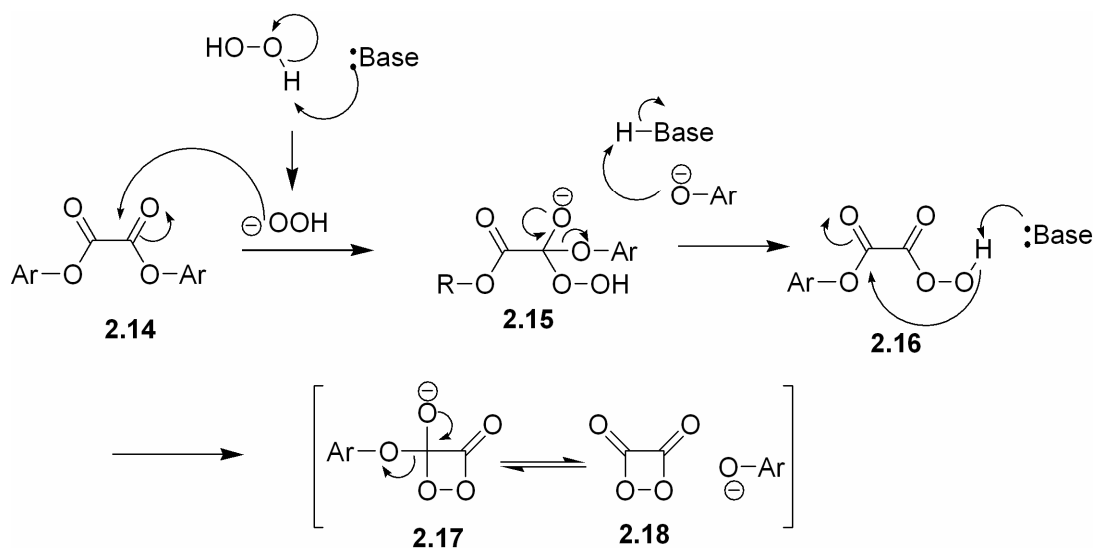
There is one type of fluorescence generating mechanism, however, which has never been used in a supramolecular sensing application. That mechanism is to use chemical means rather than optical to generate the fluorescence emission. Chemiluminescence, though often used in analytical chemistry, has yet to be linked to a molecular recognition process. For the research described below, the generation of a chemiluminescent signaling motif was studied and we have reported the first successful coupling of peroxyoxalate chemiluminescence to a molecular recognition event.<sup>28</sup>

#### ***2.1.4.1 The Mechanism***

Peroxyoxalate chemiluminescence (POCL) was first reported in 1963 by Edwin Chandross of Bell Telephone Laboratories.<sup>29</sup> When oxalyl chloride was allowed to react in solution with hydrogen peroxide, a vigorous gas-emitting reaction occurred, which gave off a faint blue-white glow. If a fluorescent sensitizer such as N-methyl acridone or anthracene was exposed to the vapors from the reaction, a much brighter luminescence was observed which corresponded to the fluorescence of the sensitizer. The technique and the name were later refined by Rauhut and coworkers in 1967 to the methods generally used today.<sup>30, 31</sup> It was reported that similar chemiluminescence could be achieved using both oxalyl anhydrides and electron deficient bis-aryl oxalate esters. Due to their stability and generation of good POCL quantum yields, the oxalate ester generated POCL mechanism is most often used today for a number of different applications ranging from highly sensitive HPLC and electrophoresis eluant detection<sup>32</sup> to commercially available glow sticks.



**Scheme 2.2** Generally accepted POCL mechanism involving an electron exchange step to generate the first singlet excited state of the fluorophore.



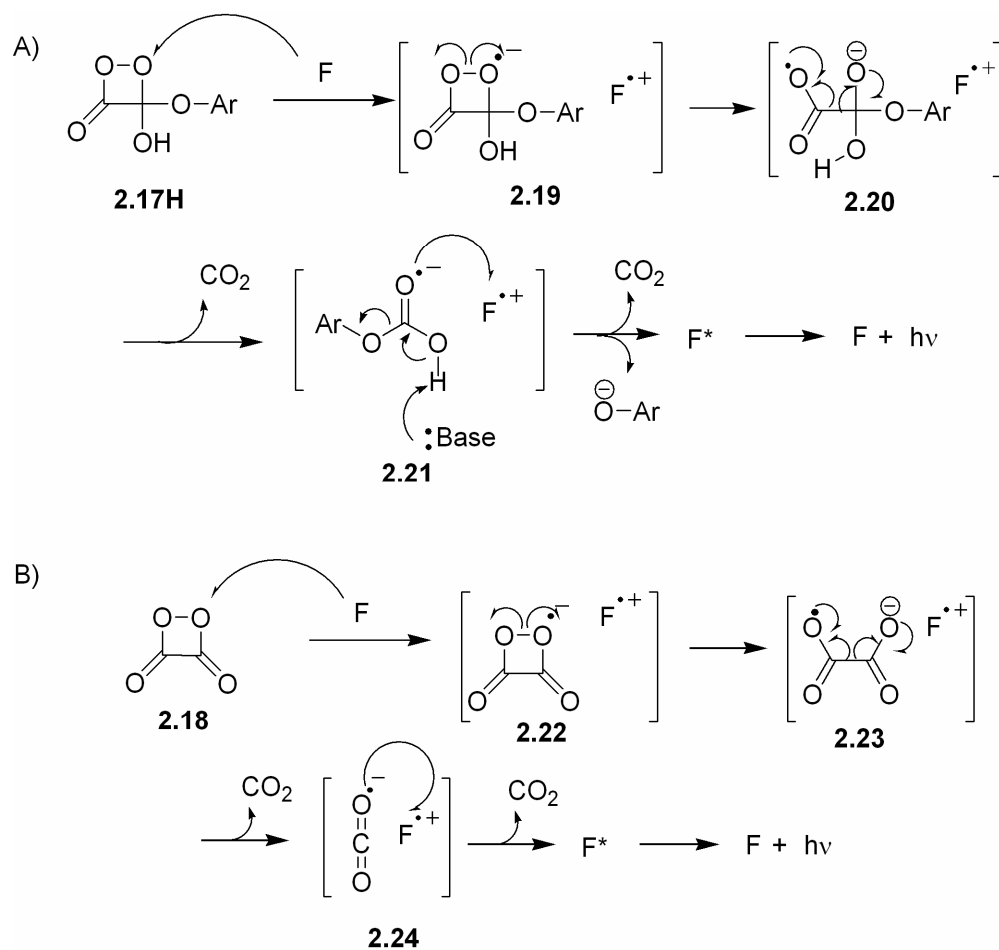
The mechanism first proposed by Rauhut is still generally accepted with a few slight modifications. Scheme 2.2 describes the mechanism for the formation of the key exciting intermediate in a basic medium. The reaction will proceed in neutral media as well, however, analytical results in neutral media tend to be erratic.<sup>33</sup> The peroxide anion generated by interaction between hydrogen peroxide and the exogenous base nucleophilically attacks the electron deficient oxalate ester **2.14** and displaces the phenol to give the monoperoxyoxalic ester **2.16**. Debate generally arises over the generation of the key metastable intermediate in the following step. The most widely accepted theory is that the 1,2-dioxetanedione **2.18** is the exciting intermediate,<sup>30, 34-40</sup> however there is debate that the excitation of the fluorescent activator is achieved by a structure in which the aryl leaving group is still attached as in **2.17**.<sup>33, 41-44</sup>

The most important, and unfortunately least well understood portion of the POCL mechanism is the chemiexcitation step in which the fluorophore is excited into its singlet ground state. Regardless of the key intermediate, **2.17(H)** or **2.18**, it is widely accepted that the chemiexcitation occurs through the chemically initiated electron exchange luminescence mechanism (CIEEL) proposed by Schuster.<sup>45</sup> The mechanism is based on the idea that oppositely charged radical ions can luminesce upon annihilation.<sup>46-48</sup> First discovered electrochemically, two molecules of a potential lumophore can be ionized oppositely at a cathode and an anode, and the radical ions produced will annihilate each other to produce a ground state and an excited state fluorophore. When the excited state relaxes, luminescence is observed. The electroluminescence quantum yields can be easily determined by the redox potential of the lumophore. CIEEL adheres to the annihilation of oppositely charged radical ions theory, however the generation of the radical species is thought to occur through chemical means rather than electronically.

Scheme 2.3 shows the mechanism thought to occur in the CIEEL step in POCL for the intermediates proposed by the two major schools of thought. In both cases, the initial step is a single electron transfer from the fluorophore, F, to the peroxy structure, **2.17H** or **2.18**. Hence, the rate of this electron transfer should be proportional to the oxidation potential of the fluorophore. Several studies have shown that this proportionality is linear, which is perhaps the most telling argument that POCL and other peroxide-based chemiluminescent systems proceed through the CIEEL mechanism.<sup>37, 45</sup> The next few steps proceed in a stepwise homolytic fashion rather than through a concerted and electronically forbidden pericyclic ring opening.<sup>49</sup> This ring opening and the entropic favorability of the loss of carbon dioxide serve to raise the energy of the resulting radical anion, **2.21** or **2.24**. The true chemiexcitation step then occurs from the

back electron transfer of the now high energy radical anion into the LUMO of the fluorophore to produce the first singlet excited state. In a successful luminescing pathway, the relaxation of this excited state results in the emission of a photon.

**Scheme 2.3** CIEEL mechanism applied to two of the major intermediates thought to be responsible for chemiexcitation in POCL



#### 2.1.4.2 Detection using POCL

Though the debate continues on the mechanistic basis for chemiexcitation in POCL, the usefulness of the process as a whole has gone far from unnoticed. Since the latter 1970's, chemiluminescence has been exploited as a highly sensitive detection method in the analysis of liquid and gel chromatography as well as a direct sensor for hydrogen peroxide and native fluorescent compounds.<sup>32</sup> Use in direct analysis of hydrogen peroxide is perhaps the most easily understood application. Direct measurement of hydrogen peroxide in sodas using pyrimido[5,4-*d*]pyrimidines as the fluorescent activators in a flow injection system was reported to show extremely high luminescence intensities.<sup>50</sup> Using solid supported fluorophores such as 3-aminofluoranthene<sup>51</sup> and perylene<sup>52</sup> on glass beads, hydrogen peroxide in rain water was detected as low as 10 nM.<sup>53</sup> Several other direct hydrogen peroxide determinations have also been reported.<sup>32</sup>

The first use of POCL for the indirect detection of enzymatic substrates by hydrogen peroxide evolution was reported by Williams *et al.* in 1976.<sup>54</sup> They used the reaction of immobilized glucose oxidase to detect the conversion of glucose into hydrogen peroxide in a flow injection analysis (FIA). Since then, many other substrates and enzymes have been probed using the indirect detection of hydrogen peroxide such as D and L-amino acids, cholesterol, uric acid, acetylcholine, and choline.<sup>32</sup>

HPLC coupled with automated post column POCL analysis of natively fluorescent compounds such as polyaromatic hydrocarbons (PAH) in coal tar extract was first reported in 1983 and was found to have higher sensitivity than UV-Vis or fluorescence spectroscopic analysis.<sup>55</sup> This analysis was then used in the determination of amino-PAH in shale oil, coal oil and coal gasifier.<sup>56</sup> Introducing a short column

packed with zinc allowed for detection of nitro-PAH by reducing the nitro groups to amines to allow for sufficient activation of the POCL pathway.<sup>57</sup> Similar systems have been used to detect nitro and amino-PAH in fossil fuels and fossil fuel by-products such as car exhaust and precipitation.<sup>32</sup>

In addition to these direct and semi-direct detection methods using chemiluminescence, many reports using fluorescently labeled compounds have been reported using HPLC and capillary electrophoresis.<sup>32</sup> Usually POCL-coupled methods generate 10-100 fold more sensitive detection than traditional fluorescence detection. The main reason for the increased sensitivity is that, unlike fluorescence or UV-Vis spectroscopy, chemiluminescence does not require an external light source.<sup>58</sup> The lack of a source eliminates errors from excitation light scattering, background absorbance or fluorescence, and fluctuations in source intensity. This allows for a much darker baseline than sourced spectroscopy resulting in very high signal to noise ratio. As an example, catecholamines, which play important roles as neurotransmitters and hormones, are routinely monitored in urine or plasma as a marker for diseases such as hypertension. Highly sensitive detection is required, since normal concentrations of catecholamines are on the pmol/mL order in plasma. HPLC coupled with POCL detection of on-line labeled catecholamines was found to be as sensitive as 1 fmol/mL.<sup>59</sup>

To date, very little work has been completed on coupling this extremely powerful signaling motif to chemosensing or chemodosimetric assays. Because of the high level of sensitivity and the selectivity for low oxidation potential fluorophores, the use of a POCL reaction as a signal auxiliary to a binding event could be very advantageous. Hence, we chose to couple peroxyoxalate chemiluminescence into an assay using another relatively unexplored signal augmenting technique, transition metal catalyzed signal amplification.

### 2.1.5 Enzymatic Signal Amplification

To deal with low signal output in recognition assays, organic chemists have begun to incorporate catalytic processes to generate a greater yield of the signaling indicator. In this arena, biochemists and microbiologists have been exploiting enzymatic processes for a number of years. Perhaps the most famous use of this paradigm is the enzyme-linked immunosorbent assay or ELISA depicted in cartoon form in Figure 2.6.<sup>60-67</sup> In this type of assay, an antibody, which is specific to the desired analyte, is bound to a solid phase resin or other solid phase substrate. The solid phase antibody is subjected to a sample containing the specific antigen. After a washing step the resin bound antibody/antigen complex is hybridized with a solution phase enzyme-linked antibody which binds to a separate epitope of the now resin bound antigen. The entire solid phase complex is then allowed access to a chromogenic or fluorogenic substrate, which upon contact with the linked enzyme, produces respectively a colorimetric or fluorometric response. Many standard disease screenings, such as HIV, utilize this powerful method.

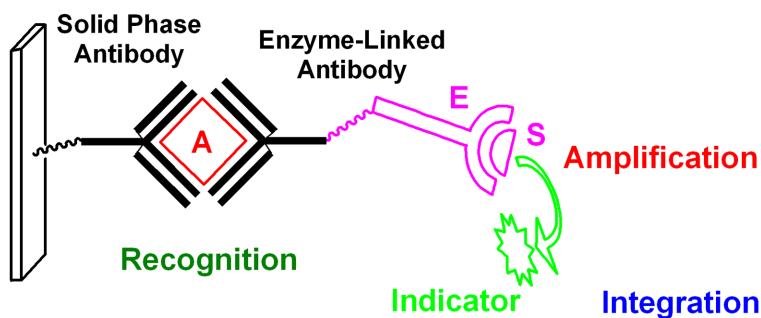


**Figure 2.6** A cartoon of an ELISA assay. HIV is routinely detected via this method.

More recently, other enzyme linked assays have begun to surface. Ghadiri and coworkers described the allosteric ssDNA sensor described in Figure 2.7 in which an inhibitor is covalently linked to an enzyme *via* a flexible ssDNA linker.<sup>68</sup> In the absence of the complimentary strand of DNA, the inhibitor is able to wrap around and block the active site. Upon integration of the ssDNA target, the inhibitor is removed from the active site and the fluorogenic substrate is catalytically transformed into the fluorescent product. Using this method, the authors were able to detect the target ssDNA at concentrations as low as 10 pM. Due to the high fidelity of DNA base pairing, non-complimentary strands were found to have no effect on the rate of enzyme throughput. The clear advantage of high tunability with near complete selectivity makes an assay of this type extremely attractive to molecular biologists. However, like the ELISA assay, it is limited in scope to large biomolecules.

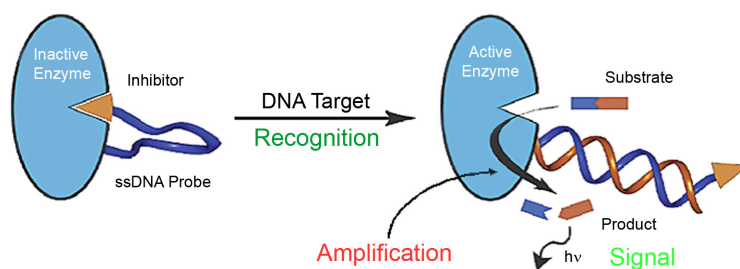


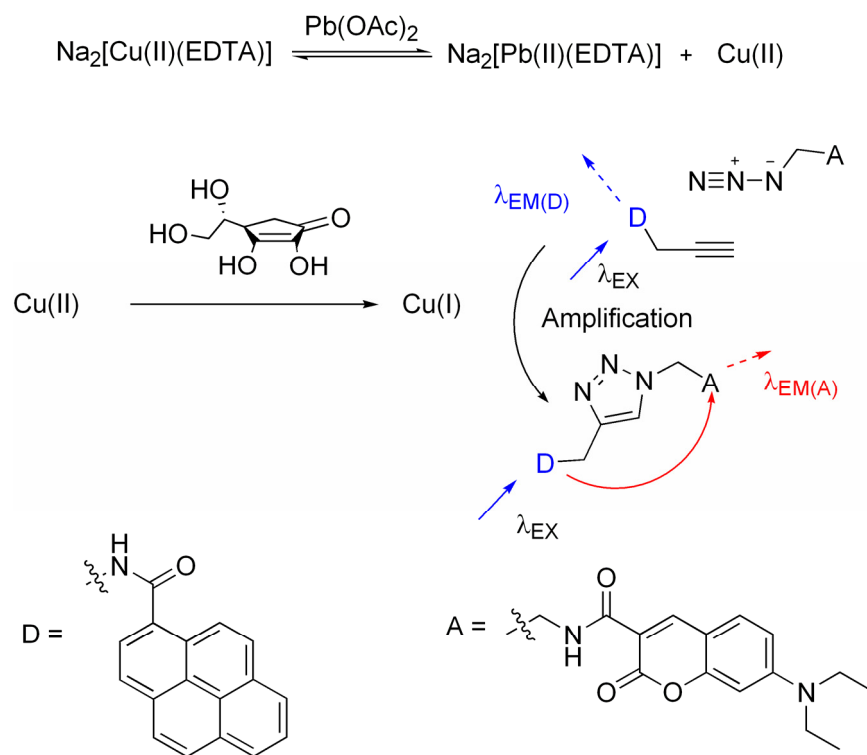
**Figure 2.7** A selective sensor for ssDNA incorporating enzymatic signal amplification.

### 2.1.6 Transition Metal Signal Amplification

Recently, however, chemists have begun to exploit the vast wealth of transition metal catalysts for sensing purposes. The first instance of a transition metal catalyst used in a recognition assay was reported by the Anslyn group.<sup>69</sup> Scheme 2.4 describes a competition assay for the detection of heavy transition metal analytes using EDTA as a universal host developed by Dr. Lei Zhu. Initially bound to copper(II), the addition of an analyte metal with a higher binding affinity, such as lead(II), forces the equilibrium towards the right. In the presence of ascorbate, the newly freed Cu(II) is reduced *in situ* to catalytically active Cu(I). When the assay is conducted in the presence of an azide and an alkyne, each respectively labeled with one member of a fluorescence resonance energy transfer (FRET) pair, the reduced Cu(I) catalyzes a Huisgen cycloaddition, which brings the FRET pair into close contact.<sup>70, 71</sup> The rate of FRET emission increase can be monitored and used to quantify the amount of initial heavy metal analyte present. In the case of lead detection, this assay was found to be sensitive to millimolar concentrations. Though not terribly sensitive, the assay demonstrated the first use of a transition metal-catalyzed reaction being exploited to amplify signal output upon analyte recognition.



**Scheme 2.4** Competition assay for detection of heavy transition metals based on FRET signal amplification from Cu(I) catalyze Huisgen cyclization.

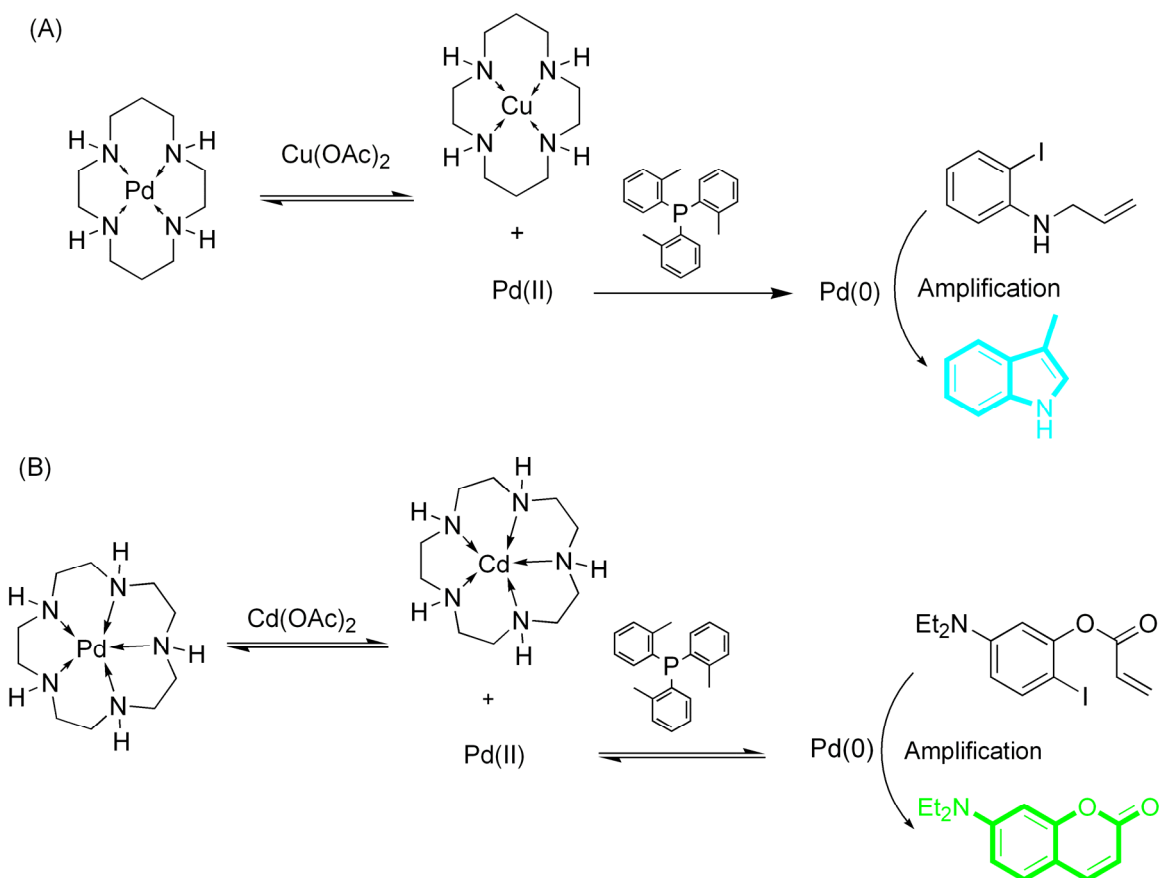


Further studies in our group by Ms. Joy Wu for the detection of copper and cadmium using a Heck cross-coupling reaction were later reported.<sup>72, 73</sup> Scheme 2.5 shows two similar methods designed as competition assays between the respective metal analytes and a palladium(II) catalyst. Both assays utilize cyclic polyamines as hosts/inhibitors, which were shown to completely turn off the catalytic activity of palladium (II) acetate in the absence of analyte. In both methods, the analyte metal is added prior to the addition of the palladium catalyst due to the slow kinetic exchange of palladium out of the azamacrocycles. In the first assay, Cu(II) is added and allowed to

chelate with the tetracyclam host/inhibitor. Upon the addition of Pd(II), any remaining tetracyclam chelates a portion of the catalyst while the remainder is left uninhibited to facilitate the intramolecular Heck cross-coupling reaction, which forms the fluorescent indole product. The rate of increase of indole emission is monitored and can be used to analyze the amount of Cu(II) initially added. Due to the size of the tetracyclam, the assay was selective for Cu(II) by 3-fold over Co(II) and 6-fold over Ni(II) and Cd(II). The sensitivity of the assay was also a vast improvement over the Huisgen cyclization methodology giving detectable results as low as 30 nM Cu(II).

The second assay employs much the same methodology, however the pentacyclam host is used to select for the larger Cd(II) species and the fluorescent marker was changed to coumarin to increase both the efficiency of the cross-coupling and the overall quantum yield. In this case, Cd(II) was detectable to as low as  $\mu\text{M}$  concentrations which suggests a higher binding affinity of the pentacyclam for the palladium catalyst than in the previous assay or perhaps a lower binding affinity of the cadmium guest. Regardless, both assays represented significant steps forward in the development of transition metal catalytic signal amplification. The technique has begun to garner interest from other research groups as well.

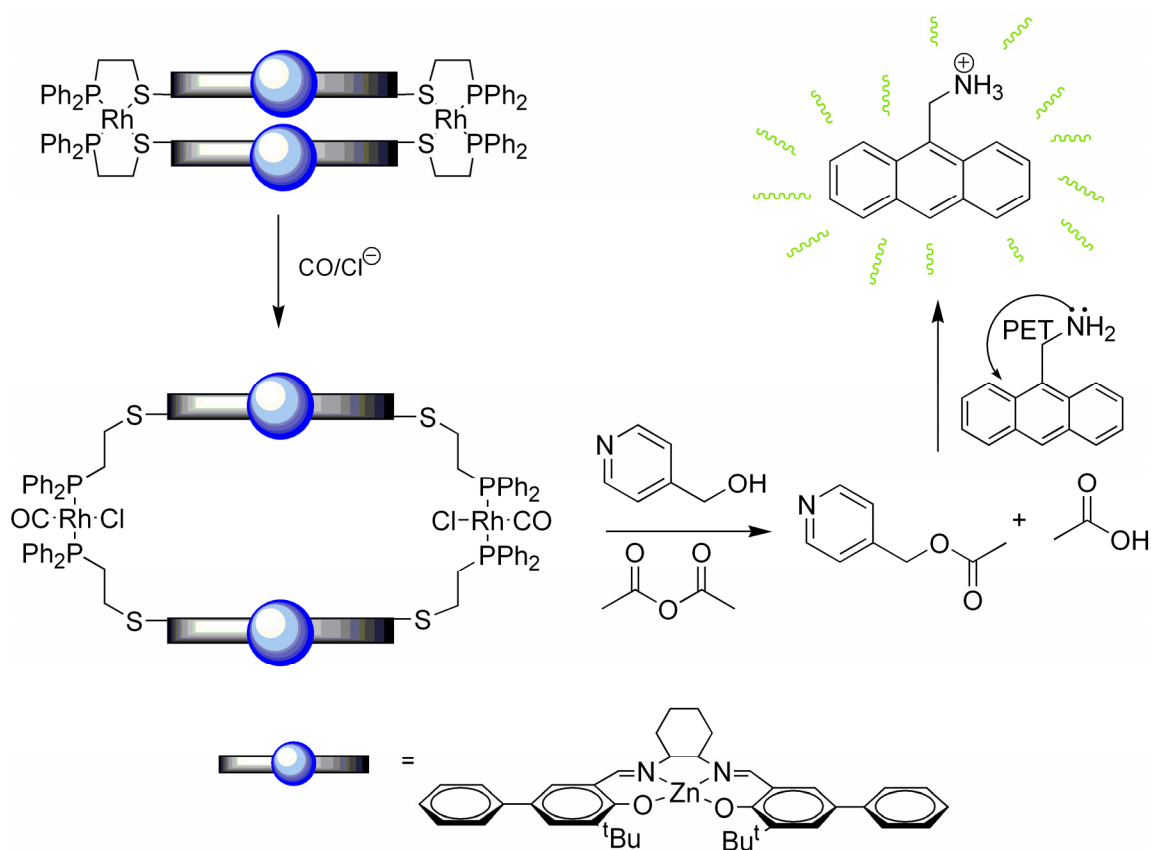
**Scheme 2.5** Two assays which utilize the Heck cross-coupling reaction to enhance signal output in the detection of (A) Copper(II) at nM concentrations and (B) Cadmium(II) at  $\mu\text{M}$  concentrations.



Mirkin and coworkers have reported an assay for chloride anions through the clever use of their signature “weak-link” approach to allosteric macrocyclic ring expansion/constriction.<sup>74</sup> In this assay, shown in Scheme 2.6, a heterometallic macrocycle containing two zinc(II) and two rhodium(I) centers was created. In its synthesized state, each rhodium center is coordinated by the two appended sulfide linkages. In this conformation, the macrocyclic cavity is closed, and the rate of

acetylation of 4-hydroxymethylpyridine is essentially zero. However, in the presence of chloride under a carbon monoxide atmosphere, the sulfide “weak-links” are broken and replaced by one carbonyl and one chloride per rhodium center.

**Scheme 2.6** An allosteric catalyst scaffold reported by Mirkin et al. used as a chloride anion sensor at concentrations as low as .8  $\mu\text{M}$  by “naked-eye” detection



The macrocycle then adopts an open conformation, which fosters much more facile conversion of acetic anhydride and 4-hydroxymethylpyridine to 4-acetylmethylpyridine and acetic acid *via* the catalytic zinc centers. Interestingly, this

assay relies on a doubly indirect signaling motif. Rather than directly measuring the production of acetic acid potentiometrically, the assay is conducted in the presence of 9-(aminomethyl)anthracene, which is self-PET quenched in the absence of acid. The creation of acetic acid protonates the appended amine and disrupts the PET quenching mechanism, thus leading to a turn on of the anthracene fluorescence. It was found that chloride anion was detectable by the “naked-eye” under a handheld UV lamp as low as 0.8  $\mu\text{M}$ . One slight disadvantage was the need for two different turn on species rather than the single analyte. No efforts have been reported to use this scaffold as a carbon monoxide sensor.

Another recent report has been published for the detection of ssDNA using transition metal based catalytic signal amplification as well.<sup>68, 75</sup> The assay is similar to the inhibitor-linked enzyme based detector discussed above, however, Cu(II) is used as the signal amplifying catalyst here. Cu(II) is sequestered by two terpyridine ligands attached at opposite ends of a ssDNA probe. Integration of the target strand in this case, frees the copper(II) and allows for the catalytic oxidation of 2,7-dichlorohydrofluorescein to 2,7-dichlorofluorescein which turns on a fluorescent signal. Sensitivities were reported in the nanomolar range for this system.

All of these assays are each quite powerful and groundbreaking in their own way. As yet, however, no instances of any type of catalytic signal amplification have been reported to detect small organic analytes. The remainder of this chapter will discuss the first such assays to utilize chemical catalysis methods in the analysis of ketones and

aldehydes. In the process, the first use of peroxyoxalate initiated chemiluminescence as a signaling motif in a molecular signaling assay is discussed.<sup>28, 40, 76</sup>

## **2.2 TARGET CHOICE AND ASSAY DESIGN**

All previously reported attempts to use transition metal catalysis for signal enhancement describe analyses of inorganic or large biological substrates.<sup>69</sup> The quandary which arises when dealing with a small organic analyte is that the strength of organic intermolecular noncovalent binding forces is generally much weaker than those associated with metal interactions.<sup>1</sup> As such, a competitive equilibrium between a metal and an organic molecule for a common ligand will generally be strongly skewed in favor of metal coordination. This disparity leads to the major difficulty in designing this type of assay for small organic substrates. It then becomes apparent that using a purely supramolecular approach entailing noncovalent interactions would not be sufficient to achieve satisfactory results. The goal became to discover a system in which the inhibiting ligand would have a strong covalent interaction with the target analyte and a strong but not scavenging interaction with the metal catalyst.

Based on previous research discussed in Chapter 1, it was determined to continue work on palladium catalyzed cross-couplings as the signal amplifying step. The previously described cyclam ligands would not be sufficient for use in the detection of organics, so a new class of inhibitor had to be found. The poisoning interaction between thiols and palladium catalysts is well known.<sup>77</sup> In heterogeneous catalyst systems, sulfur

is often used as an additive to control the exothermicity of hydrogenations. The porous palladium surface acts as a sponge for the soft sulfur nucleophiles, which form very strong metal-sulfide bonds. Thiols, and especially dithiols, have also long been known to organic chemists. The interaction of dithiols with carbonyls represents one of the first protecting groups a student learns in introductory organic chemistry.<sup>78</sup> When 1,3-propanedithiol is condensed with aldehydes to form 1,3-dithiolanes, so called “umpolung” reactions can be performed by deprotonation of the otherwise intractable aldehyde proton.<sup>79</sup>

## **2.3 SONOGASHIRA ASSAY**

With both processes well established, the assay was designed for ketones and aldehydes based on the thioacetal condensation with a palladium-catalyzed Sonogashira cross-coupling reaction as a signal amplification method.

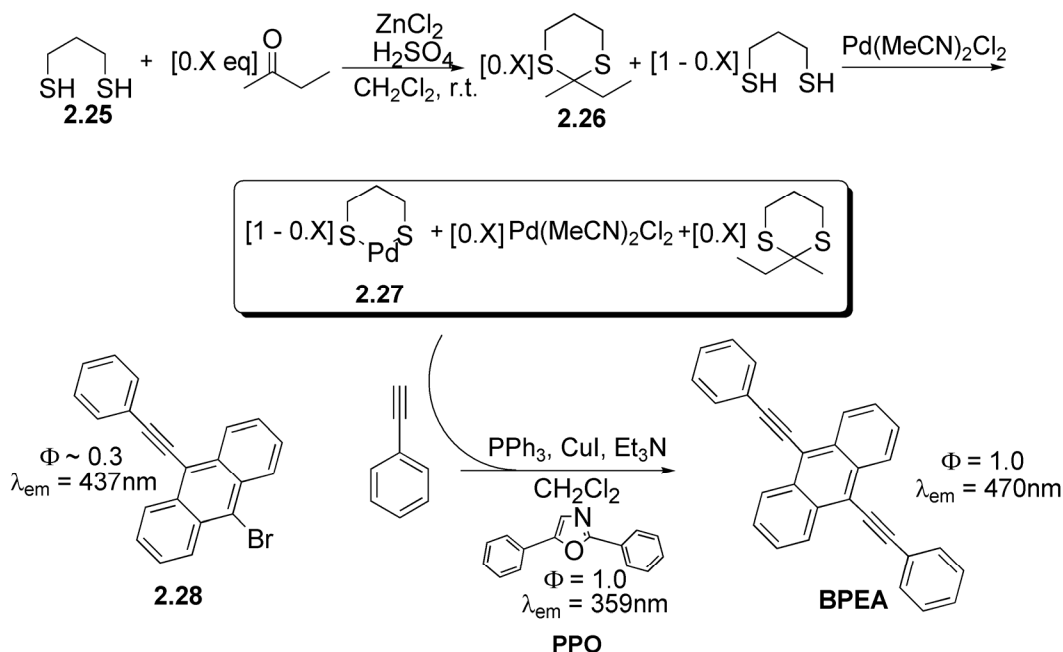
### **2.3.1 Design**

Scheme 2.7 describes the assay. In a procedure adapted from the literature, 1,3-propanedithiol is condensed with an analytical amount of a representative ketone, 2-butanone, in acidic methylene chloride with the Lewis acid catalyst zinc(II)chloride to give a mixture of the dithiolane and a remainder of free dithiol.<sup>80</sup> As mentioned briefly above, because the interaction between the host and the analyte is irreversible, this assay would technically be described as a chemodosimeter. The standard conditions for this condensation with boron trifluoride diethyletherate were unacceptable due to by-products

which prevent the subsequent Sonogashira coupling. After quenching the condensation with triethylamine, bis(acetonitrile)palladium(II)chloride is added such that an equimolar amount of palladium with respect to original dithiol is present. The residual dithiol chelates and poisons some of the palladium precatalyst while the rest remains unspoiled. Hence, the unpoisoned amount of palladium catalyst is the same or proportional to the initial amount of 2-butanone. To this mixture, triphenylphosphine is added to displace the acetonitrile ligands for more effective catalysis. To commence the Sonogashira cross-coupling reaction, 9-bromo-10-(phenylethynyl)anthracene, copper(I) iodide, and an internal standard 2,5-diphenyloxazole (PPO) are added and the mother liquor is brought to a gentle reflux. Phenylacetylene is added as a final step and the reaction is monitored over a 2 hour period.



**Scheme 2.7** Schematic of the assay for ketones based on a Sonogashira cross-coupling reaction as the signal amplification process. Reactions were conducted at millimolar concentrations for tenable reaction kinetics.



### 2.3.2 Choice of Fluorophores

The Sonogashira coupling described in the final step of Scheme 2.7 produces the well known fluorophore 9,10-bis(phenylethynyl)anthracene (BPEA). It has been reported to have  $\Phi_F = 1.0$ .<sup>81</sup> At concentrations lower than  $10^{-6}$  M, monomer  $\lambda_{\text{max}}\text{em}$  occurs near 470 nm in most common organic solvents and shows very little solvatofluoric effect. At higher concentrations, BPEA shows a strong tendency towards excimer formation with a  $\lambda_{\text{max}}\text{em}$  near 500 nm. The excimer emits the characteristic lime green

color found in many commercially available glowsticks. Excitation and emission spectra of all fluorophores used in this assay are shown in Figure 2.8.

Initial work with this system utilized the Sonogashira starting material 9,10-dibromoanthracene (**2.35**). It was attractive as a starting point due to the lower observed quantum yield than the monocoupled **2.28** and an even further blue shifted initial emission near 410 nm. The absorbance  $\lambda_{\text{max}}$  for **2.35** at 403 nm also made solutions of starting material nearly colorless to the naked eye. Initially the assay did work with the **2.35** starting material for the cross-coupling, however, since we were monitoring the kinetics of BPEA formation, we could not discount the formation of the **2.28** intermediate. The derivation of the rate law was much more complicated, and the effort was found to be unnecessary if the assay was conducted using the monocoupled **2.28** as the starting material.

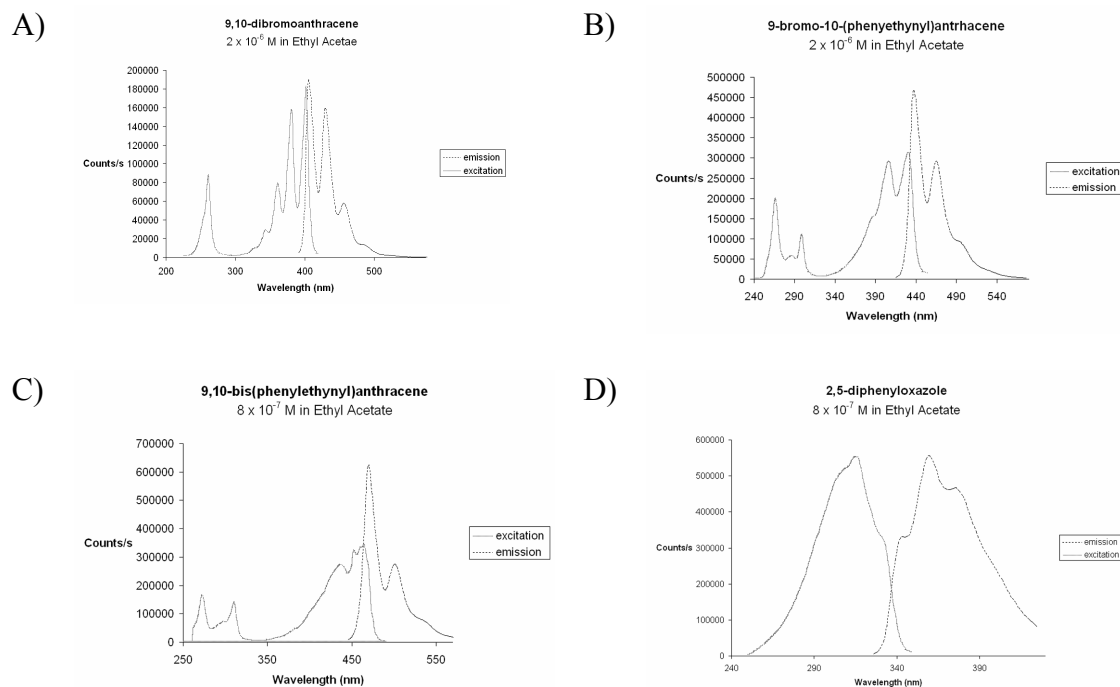


**Figure 2.8** Excitation and emission spectra in ethyl acetate of  
 A) 9,10-dibromoanthracene 2.10 at  $2 \times 10^{-6}$  M,  
 B) 9-bromo-10-(phenylethynyl)anthracene 2.4 at  $2 \times 10^{-6}$  M,  
 C) 9,10-bis(phenylethynyl)anthracene (BPEA) at  $8 \times 10^{-7}$  M, and  
 D) 2,5-diphenyloxazole (PPO) at  $8 \times 10^{-7}$  M.

### 2.3.3 Measurement

Due to PET quenching from the large amount of triethylamine present in the reaction, direct fluorescence and chemiluminescence measurements on the system were impossible. Thus, the assay was conducted on a semi-preparative scale with aliquots taken at precise timed intervals over a two hour period. The aliquots were partitioned between ethyl acetate and 2N HCl to remove the offending amine base, and samples for

fluorescence were diluted in ethyl acetate to less than  $10^{-6}$  M of fluorophore assuring a safe range of emission even at full conversion to BPEA. Samples to be used for chemiluminescence measurements were taken without dilution from the acid wash and washed with 2M NaOH to remove the acid. The chemiluminescent reaction does not proceed under acidic conditions; hence, the extra washing step was necessary. Due to potential imprecision in aliquot acquisition and solvent evaporation over the two hour reaction time at reflux, we added the soluble internal standard 2,5-diphenyloxazole (PPO). PPO has been shown to have extremely high quantum efficiency and was an attractive choice as its excitation  $\lambda_{\text{max}}$  overlays well with the troughs in the anthracene-dye excitation profiles. The use of this non-reactive internal standard negates the need for rigorous attention to volumetrics concerning aliquot acquisition(see derivation below). The following discussion of the fluorescence based kinetics relies heavily on the use of PPO in this assay.

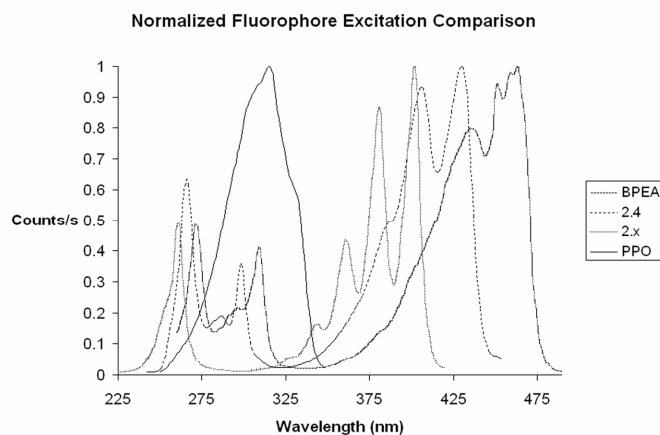


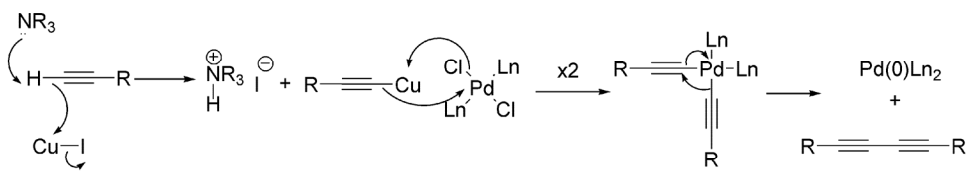
**Figure 2.9** Overlaid comparison of the normalized excitation spectra of the anthracene dyes versus the internal standard 2,5-diphenyloxazole (PPO).

### 2.3.4 Derivation of Kinetics

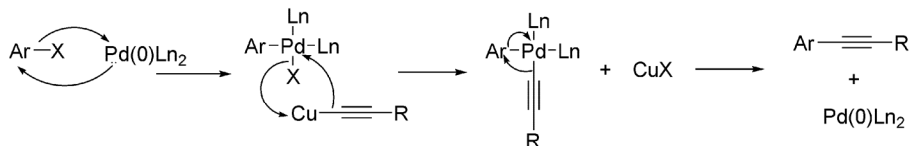
Determination of the sensitivity of this detection method depends upon a good understanding of the kinetics of the Sonogashira coupling. The generally accepted mechanism is shown in Scheme 2.8.<sup>82</sup> When using a Pd(II) precatalyst, there are two theories as to how the reduction to the active Pd(0) occurs. There is stronger evidence for the first method proposed in that the diacetylene by-product is usually isolable from the reaction. Because the diacetylene is also produced when using a Pd(0) catalyst, the alternate mode of reduction has been proposed as well.<sup>82</sup>

**Scheme 2.8** The generally accepted mechanism for the Sonogashira cross-coupling reaction. Two proposed methods of reducing a Pd(II) precatalyst to the active Pd(0) species have been proposed.

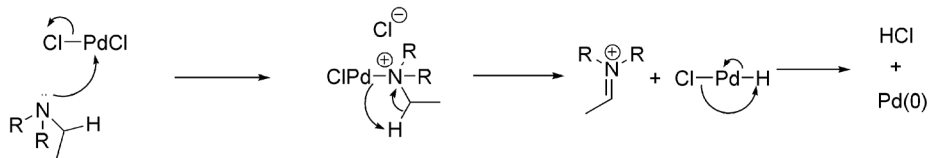
#### Generation of Cu-acetylene and Pd(0)



#### Coupling



#### Alternate Catalyst Preparation



Regardless of which reduction mechanism occurs, the process is fast on the timescale of this assay and can be ignored in the rate law. The formation of the Cu-acetylene complex is also quite rapid and does not limit the rate of reaction. In essence, this reaction is a trimolecular process with dependencies on the catalyst, aryl halide, and the acetylene, where for the majority of the reaction time, the catalyst is the rate determining reagent. A proposed rate law is given by equation **2.1**, where A is phenylacetylene, B is **2.28**, P is BPEA, and “cat” represents the Pd-catalyst or alternatively the ketone/aldehyde concentration.

$$\frac{dP}{dt} = k[\text{cat}]^x [A][B] \quad (2.1)$$

$$\frac{dP}{dt} = k'[\text{cat}]^x \quad (2.2)$$

where  $k' = [A][B]$  and  $[A][B] = [A]_0[B]_0$

If we assume initial rate kinetics we can make the simplification given in equation **2.2**, where  $[A]_0$  and  $[B]_0$  represent the initial concentrations of A and B. As mentioned above, a work up step prior to fluorescence measurement results in an unknown amount of fluorophore loss. To solve this problem and eliminate the need for any volumetric congruity between aliquots, an internal standard (PPO) was added to the reaction, represented here as S. If we divide both sides of equation **2.2** by the concentration of the internal standard we arrive at a rate law based on the change in the ratio of P to S, equation **2.3**.

$$\frac{\frac{dP}{dt}}{[S]} = \frac{d\left(\frac{P}{S}\right)}{dt} = \frac{k'[\text{cat}]^x}{[S]} \quad (2.3)$$

However, since neither concentration is absolutely known, the rate law needs to be expressed in terms of fluorescence intensity. Equation **2.4** represents the Beer-Lambert Law for fluorescence where  $I_0$  is the intensity of the incident light,  $\phi$  is the quantum yield of the fluorophore,  $\varepsilon$  is the molar absorptivity,  $c$  is the concentration, and  $b$  is the path length.

$$F = I_0 \phi (1 - 10^{-\varepsilon cb}) \quad (2.4)$$

$$F = I_0 \phi 2.3 \varepsilon cb \quad (2.5)$$

At low concentrations, only the first term of the expanded Taylor series for equation **2.4** remains important, and the Law can be simplified to equation **2.5**. A ratio of the fluorescence of P to S is given by equation **2.6**. Equation **2.6** can then be reduced to equation **2.7** where  $\kappa$  is a constant representing the ratio of  $I_0 \phi \varepsilon$ .

$$\frac{F_p}{F_s} = \frac{I_0 \phi_p 2.3 \varepsilon_p c_p b}{I_0 \phi_s 2.3 \varepsilon_s c_s b} = \frac{I_0 \phi_p \varepsilon_p}{I_0 \phi_s \varepsilon_s} \times \frac{[P]}{[S]} \quad (2.6)$$

$$\frac{F_p}{F_s} = \kappa \frac{[P]}{[S]} \quad (2.7)$$

Substituting equation **2.7** into equation **2.3** gives equation **2.8**.

$$\frac{d\left(\frac{P}{S}\right)}{dt} = \frac{d\left(\frac{F_p}{F_s}\right)}{dt} \kappa = \frac{k'[\text{cat}]^x}{[S]} \quad (2.8)$$

We now have a rate law expressed in terms of fluorescence instead of concentration. Separating the derivative and combining the constants sets up the integrated rate law given in equation **2.9** with the new apparent rate constant,  $k''$ , given by equation **2.10**.

$$\int d\left(\frac{F_p}{F_s}\right) = \int \frac{k'[\text{cat}]^x}{[S]\kappa} dt = \int k''[\text{cat}]^x dt \quad (2.9)$$

$$k'' = k \frac{[A]_0 [B]_0}{[S] \frac{I_0 \phi_p \varepsilon_p}{I_0' \phi_s \varepsilon_s}} \quad (2.10)$$

The integrated rate law, equation **2.11**, shows that the rate can be sufficiently described by a plot of the ratio of fluorescence intensities of P to S vs. time.

$$\frac{F_p}{F_s} = k''[\text{cat}]^x t \quad (2.11)$$

Finally, a plot of the rates vs. catalyst/ketone concentration will elucidate the order in catalyst and the apparent rate constant,  $k''$ .



### 2.3.4 Rate Studies

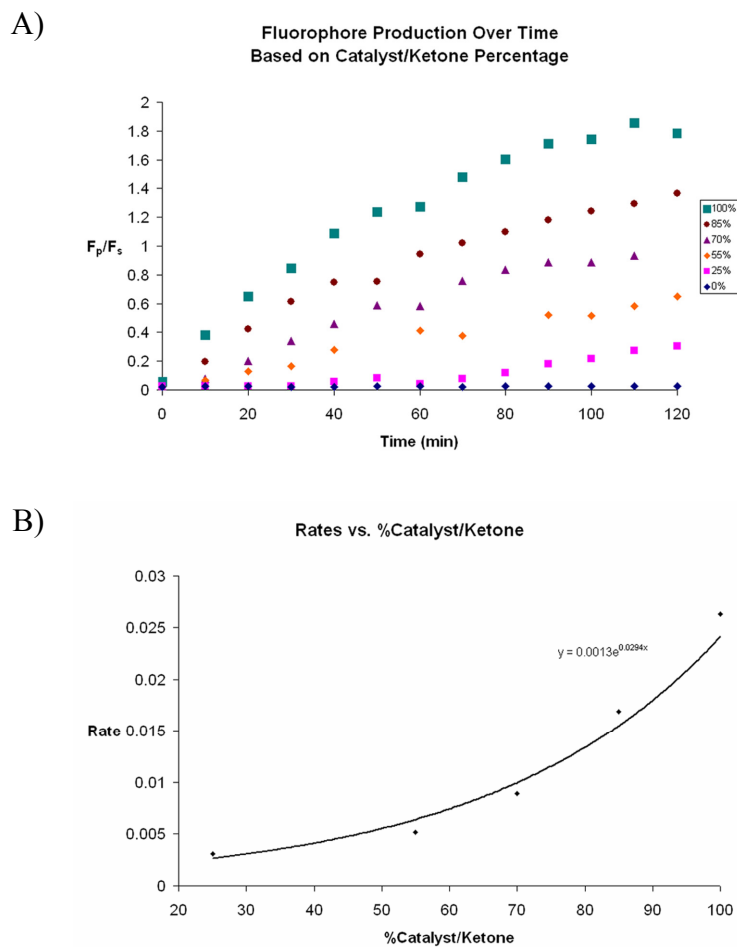


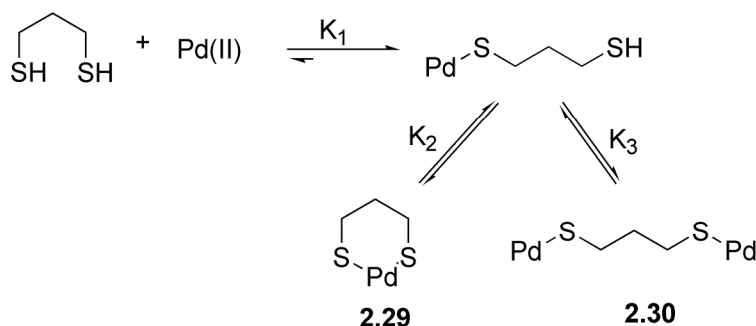
**Figure 2.10** A) Plot of the ratio of BPEA emission to PPO emission vs. time for 1-10mM 2-butanone. For all: 1,3-propanedithiol: initial  $8.60 \times 10^{-3}$  M; after dilution  $7.17 \times 10^{-4}$  M;  $\text{Pd}(\text{MeCN})_2\text{Cl}_2$   $7.17 \times 10^{-4}$  M; 9-bromo-10-(phenylethynyl)anthracene  $4.00 \times 10^{-3}$  M; phenylacetylene  $1.49 \times 10^{-2}$  M; copper(I) iodide  $8.75 \times 10^{-4}$  M; 2,5-diphenyloxazole  $6.33 \times 10^{-3}$  M. B) Plot of the rates from (A) vs. %catalyst/ketone

Rate studies were conducted by varying the amount of 2-butanone from 0% to 100% versus 1,3-propanedithiol. This represents a concentration range of roughly 1-10 mM of 2-butanone. Theoretically, a 0% assay should show no formation of BPEA whereas a 100% assay should give very fast conversion. A plot of the rate determinations for representative concentrations as a function of the ratio of product fluorescence to PPO emission versus time is shown in Figure 2.10(A). PPO is excited at 316 nm and read at 357 nm and BPEA is excited at 451 nm and read at 472 nm. As expected with no ketone present, no increase in product emission is observed over the 2 hour reaction time. As the amount of analyte increases so too does the rate of conversion to BPEA. At 85% ketone loading and above, the rates begin to plateau, indicating a departure from initial rate kinetics at a time dependent on the amount of catalyst present.

The rate profile is shown in Figure 2.10(B). The plot of rate versus catalyst/ketone concentration shows a marked nonlinearity. This deviation from linearity can be explained by the complex equilibrium proposed in Scheme 2.9, which can occur for the palladium-dithiol interaction. It can be assumed that the equilibrium constant of the initial strong Pd-S bond,  $K_1$ , will be very large due to the electron deficiency of the Pd(II)Cl<sub>2</sub> center. Upon binding the first sulfur, however, the palladium center becomes much less electrophilic and the second bond formation occurs less readily, allowing a more balanced equilibrium described by  $K_2$ . It is proposed that  $K_2$  still favors the bidentate chelation such that at the high concentrations of residual dithiol brought about by low ketone equivalency, the equilibrium is driven towards **2.29**. As the concentration

of dithiol drops relative to palladium, a second equilibrium begins to build up in which the Pd:dithiol binding becomes 2:1 as with **2.30**. It is proposed that **2.30** still retains a modest amount of catalytic activity.

**Scheme 2.9** The complex equilibrium is proposed to account for the nonlinear increase in reaction rate at high catalyst concentrations.

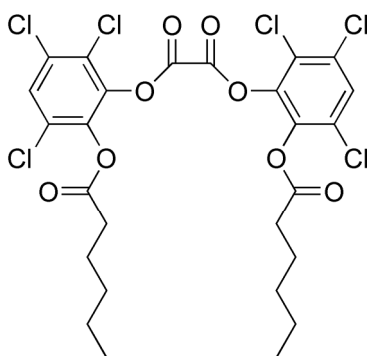


Since this phenomenon occurred for both the Sonogashira assay above and the Suzuki assay described below, this theory was tested with a Suzuki reaction using 1 mmol of 9-bromoanthracene, 1.5 mmol phenylboronic acid, 2 mmol sodium carbonate, and  $4.5 \times 10^{-3}$  mmol each of  $\text{Pd}(\text{OAc})_2$  and 1-propanethiol, which can only monothiolate one palladium. The reaction was run in a 3:3.5 acetone-water mix. The reaction shows moderate conversion to 9-phenylanthracene over a 2 hour period based on TLC and CI-MS analysis. Thus, as the concentration of **2.30** increases due to decreasing dithiol concentration, the fraction of active palladium increases non-stoichiometrically.

### 2.3.5 Chemiluminescence Measurements

Due to the inherent drop in quantum efficiency, chemiluminescence measurements were conducted at a higher concentration than fluorescence. And, as

mentioned earlier, a second basic wash of the aliquot from the reaction was necessary to remove any acid from the organic layer. The oxalic ester used to produce chemiluminescence was bis(2-carbopentyloxy-3,5,6-trichlorophenyl)oxalate, **2.31**.



**2.31**

Figure 2.11 shows a side by side comparison of the rate of **BPEA** formation determined from fluorescence and chemiluminescence. The data were recorded on the same fluorometer in the absence of an excitation source. Chemiluminescence data were treated in the same fashion as that from fluorescence and the plot in Figure 2.11B is of the ratio **BPEA** luminescence to **PPO** luminescence. Unfortunately, the chemiluminescence data for this assay was inconsistent and showed no fidelity of rate versus catalyst/ketone concentration. This failure along with several practical issues led us to pursue the Suzuki cross-coupling based assay discussed below.

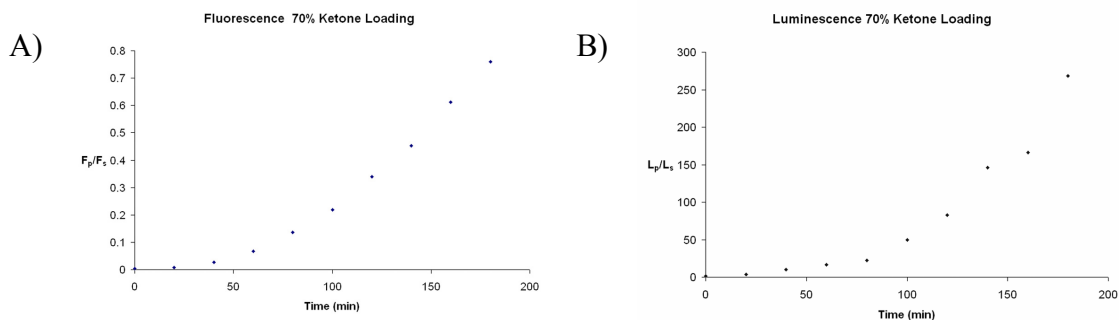


**Figure 2.11** A) Fluorescence measurement an assay with 70% analyte loading. B) Chemiluminescence measurement for an assay with 70% analyte loading. All reaction conditions are as given in Figure 2.10. For B) 2 mL of aliquot solution, 50 mg (.074 mmol) 2.31, 10  $\mu$ L 0.1 M NaOH, 50  $\mu$ L 30% H<sub>2</sub>O<sub>2</sub>.

## 2.4 SUZUKI BASED ASSAY

As a proof of concept, the Sonogashira assay worked well, however, several pragmatic issues arise from the use of this particular catalytic process. The first problem is the reaction's intolerance to water, which makes the assay rather impractical to apply. Another issue is the necessity of an amine base to facilitate reduction of the Pd(II) salt to the active Pd(0) species. The side effect of PET quenching prohibits the direct monitoring of the Sonogashira by fluorescence again making the assay less applicable. Collisional quenching also occurs from the chloride anions released upon reduction of the palladium catalyst. The catalyst itself is also less stable than some other non-chloride palladium salts, introducing an unpredictable source of error. Also, the ultimate goal of generating a chemiluminescent sensing motif is impaired by the need for an extended work up of the aliquots. All of these concerns led us to ponder a new potential catalytic system.

### 2.4.1 Design

The Suzuki cross-coupling reaction appeared to solve many of the problems associated with the previous assay. Suzuki's are often run in water, they require only a carbonate base, and the catalyst,  $\text{Pd}(\text{OAc})_2$  is comparatively cheap and very stable. The product, 9,10-diphenylanthracene (DPA), of the Suzuki coupling shown in Scheme 2.10, is similar to its counterpart, BPEA, in many of its optical properties. A blue emitter with  $\Phi_F = 1.0$ , DPA is the lumophore found in most commercial blue glowsticks. Unlike BPEA, however, DPA shows very little tendency towards excimer formation and maintains emission near 410 nm over a wide concentration range. Unfortunately as shown in Figure 2.12, the precursor **2.35** also emits near 410 nm, however, the observed quantum efficiency of **2.35** is much lower than that of DPA which allows for the determination of emission increase.

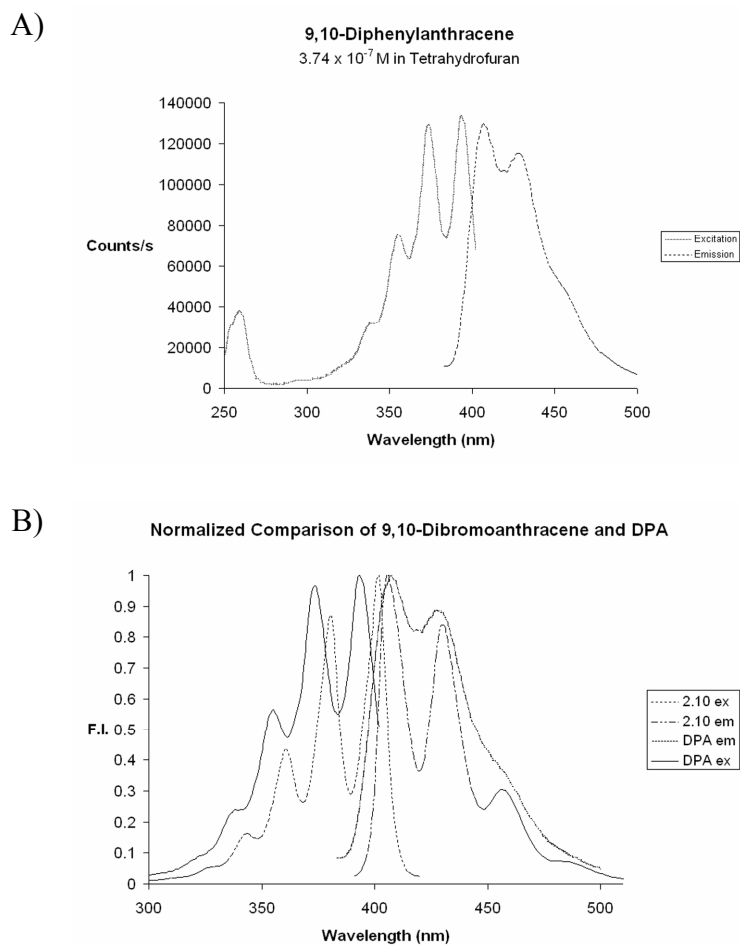
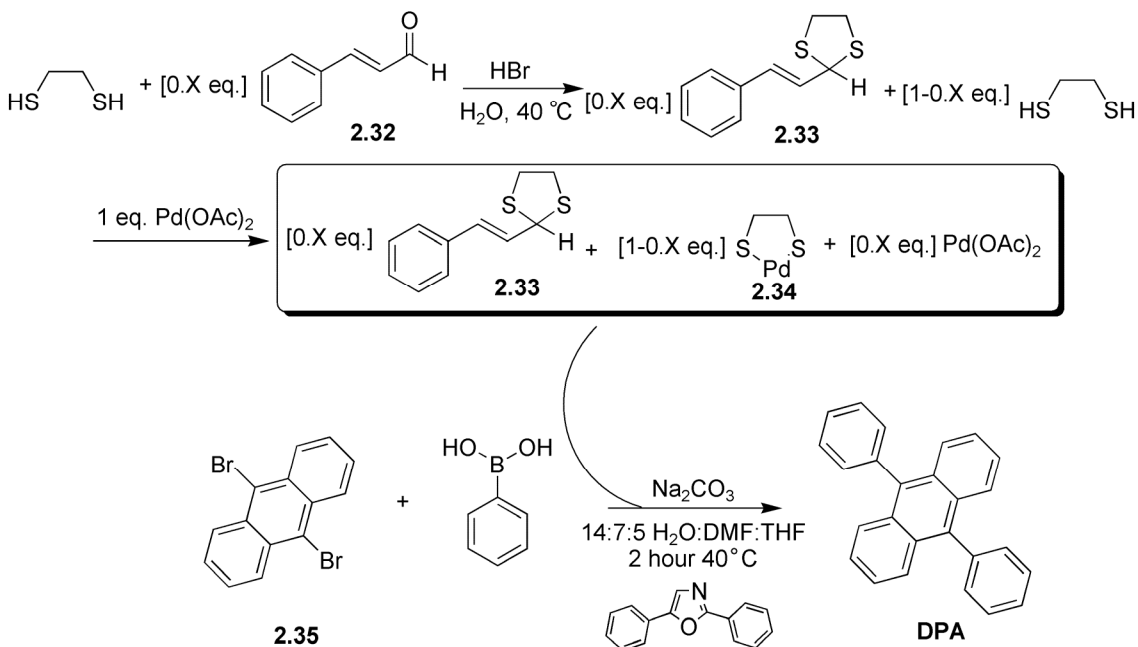


**Figure 2.12** A) Excitation and emission spectra for 9,10-diphenylanthracene (DPA) in THF at  $3.74 \times 10^{-7}$  M, and B) normalized spectral overlay of 9,10-dibromoanthracene and DPA showing very little shift in emission.

The Suzuki based assay is described by Scheme 2.10. Using an extremely simplified dithiane formation procedure reported by Wakharkar, 1,2-ethanedithiol was condensed with cinnamaldehyde, **2.32** in water in the presence of hydrobromic acid.<sup>83</sup>

The reaction is extremely fast and forms a white precipitate which at low analyte concentrations, redissolves in the remaining immiscible ethanedithiol over the course of the reaction time. Upon completion, the reaction is quenched with 6N NaOH to sequester the hydrobromic acid and deprotonate the dithiol to allow homogeneous mixing. Basifying the mixture also causes any dissolved dithiane product, **2.33**, to precipitate again.

**Scheme 2.12** Schematic of the assay for aldehydes using a Suzuki coupling.



Unfortunately, the low concentrations of the extremely efficient fluorophore product required for safe fluorescence determination again prevented this assay from direct monitoring in the fluorometer. At nanomolar catalyst concentrations, the Suzuki reaction proceeds extremely slowly if at all. Thus, the reaction was again run on a semi-



preparative scale. Analogous to the previous assay, initial attempts were performed using 9-bromo-10-phenylanthracene as a starting material, however, results for this reaction were erratic and inconclusive. 9,10-dibromoanthracene, **2.35**, gave much better results for both fluorescence and chemiluminescence detection. Based on mass spectral and TLC analysis of an aliquot of a Suzuki reaction with **2.35** as the starting material and with no inhibitor after 2 hours, it was determined that very little formation of DPA had actually occurred. Rather, the vast majority of fluorescing product was found to be the 9-bromo-10-phenylanthracene intermediate. This conclusion is supported in the literature from which the conditions were adapted, in that the authors report that while mono-couplings were quick and nearly quantitative, attempts to use these parameters for di-, tri-, or polymer couplings gave low yields beyond the initial coupling product.<sup>84</sup> Hence it was determined that the rate for the “double reaction” could be described in the same fashion as the single coupling as in the previous assay since most likely only a single coupling is actually occurring.

Apart from low catalyst concentration disallowing direct monitoring of the fluorescence turn on, the insolubility of the anthracenes also prevented accurate aliquot measurement. To overcome these difficulties, two identical reactions were set up in parallel, one as a control and one as the sample. Two side by side reaction vessels were charged with palladium acetate in DMF, and a small aliquot of the completed dithiane mixture was added such that the palladium to original dithiol ratio was 1:1. Then both flasks were given equal amounts of **2.35**, PPO, and sodium carbonate. The control flask

was allowed to stir for 20 minutes at 40 °C. The sample flask was charged with 3 eq. of phenylboronic acid and allowed to react for 2 hours at 40 °C. The Suzuki reaction conditions were modified from the literature and run in a 7:5:14 mixture of DMF:THF:H<sub>2</sub>O.<sup>84</sup> THF was added for initial solubility of **2.35** before the addition of water. Upon completion, the reactions were directly diluted with ethyl acetate to partition the solvents and dissolve the anthracenes. The organic layer was then diluted for fluorescence and chemiluminescence measurements.

#### **2.4.2 Fluorescence vs. Chemiluminescence**

The solution resulting from the control experiment where no phenylboronic acid was added was used as a time zero measurement. A 120 minute measurement was taken with the solution garnered from the full reaction flask. For fluorescence measurements, the samples were diluted to 5 µM of total anthracene species. Chemiluminescence samples were prepared at 200 µM of total anthracene containing species. Data were observed over aldehyde loadings from 0-90% versus 1,2-ethanedithiol. This represents a concentration range starting at 10 mM. The results are plotted as a percent increase in fluorescence and chemiluminescence (Figure 2.13).

Though single point measurements are insufficient to fully characterize the kinetics of the reaction, a similar nonlinear dependence on the catalyst concentration appears to be present in this assay as well. The reasons for this observation have already been discussed. Fluorescence data were taken in THF exciting at 393 nm and reading at

407 nm. The data show a modest 13% intensity increase for the lowest concentration up to nearly 200% increase for the highest concentration studied. Perhaps even more interesting is the chemiluminescence data.

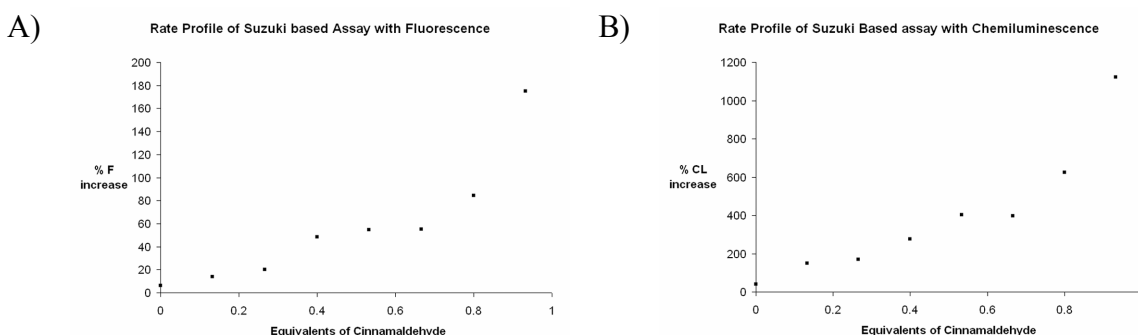


**Figure 2.13** Rate profiles of the Suzuki assay for cinnamaldehyde using A) fluorescence and B) chemiluminescence

As with the Sonogashira assay, chemiluminescence data were recorded in the same fluorometer instrument with the excitation shutter closed. The increase in chemiluminescence is nearly an order of magnitude higher than that detected by fluorescence, with the lowest concentration tested giving an astounding 150% intensity increase. It is interesting to note that even though **2.35** has roughly the same excitation and emission profile as DPA and the mono-coupled intermediate, its chemiluminescence efficiency is essentially non-existent as is evidenced by the large difference in intensity changes between fluorescence and chemiluminescence. This assay demonstrates the power of using chemiluminescent sensors for high sensitivity in molecular sensing assays.

## 2.5 CONCLUSIONS

In this chapter, we have discussed the formulation of a new signaling methodology for use in chemosensing and chemodosimetric assays. This research actually represents two major breakthroughs in signaling modalities for use with molecular recognition assays. Though transition metal catalytic signal amplification has been described in the recent literature, its use has been limited to the detection of other metals and biological macromolecules. This research represents the first use of this novel signal enhancing technique for the detection of a small organic analyte. As with the first example of using transition metal catalysis in sensing, the assay here is not terribly sensitive nor selective.<sup>69</sup> The goal of this research, however, was in the further development of this signal generating modality toward applicability for a wider range of targets. This achievement is crucial in the development of this field as a molecular recognition scaffold. Further work needs to be conducted on the extension of this methodology towards ever wider ranging analytes and catalysts. One promising pathway for the recognition of small organics is through the use of organic catalysts. One such system discussed in Chapter 3 reports that the target analytes, conformationally constrained dicarboxylates, produce a signal transduction in a catalytic fashion (see Scheme 3.5).<sup>85</sup>

The second breakthrough described by this study is the first coupling of the highly sensitive technique of peroxyoxalate chemiluminescence with a molecular recognition assay. As evidenced in Figure 2.13, the lack of a light source and the specificity of the activator help to bring about an enhanced level of sensitivity. Work is ongoing in our laboratory to promote the use of this signaling methodology in a wide variety of analyte

determinations. The work in Chapter 3, which utilizes a highly fluorescent squaraine dye, is currently being explored as a chemiluminescent chemodosimeter.

In the first two chapters, we have looked at both aspects of molecular sensing, the binding, albeit circuitously, and the signaling. The first chapter looked in depth at just one of the many intermolecular interactions supramolecular and molecular recognition chemists use to bind two or more molecules together. The current chapter looked at the ways in which the binding of those molecules are observed in a sensing aspect. That is with optical signals. The next and final chapter will tie it all together for the development of a whole and complete assay with sensitive binding *and* exquisite signal output.

## **2.6 EXPERIMENTAL SECTION**

### **2.6.1 Materials and Methods**

All reagents were obtained through Sigma-Aldrich or Acros Fine Organics and used without further purification unless noted. Bis(acetonitrile)palladium(II)chloride, 9,10-dibromoanthracene, and 9-bromo-10-phenylanthracene were prepared as described in the literature.<sup>86-88</sup> Triethylamine and dichloromethane were distilled over calcium hydride prior to use. Fluorescence and chemiluminescence measurements were performed on a Photon Technology International QuantaMaster Cuvet-Based spectrofluorometer.

**9-bromo-10-(phenylethynyl)anthracene (2.28):** 4.0g (12 mmol) 9,10-dibromoanthracene, 83.5 mg (0.12 mmol) bis(triphenylphosphine)palladium(II) chloride, and 23

mg (0.12 mmol) copper (I) iodide were added to 250 mL of freshly distilled triethylamine and brought to 40 °C. To this solution was added dropwise over 6 hours 12.7 mmol phenylacetylene in 50 mL dry triethylamine. The reaction was allowed to stir overnight at 40 °C after addition was complete. Upon completion of the reaction by TLC, the mother liquor was filtered with hexanes through celite and partitioned into 2N HCl. The organic extract was washed again with 2N HCl until slightly acidic by pH paper. The organic layer was then washed with water, saturated NaCl, and dried ( $\text{Na}_2\text{SO}_4$ ). 10 mg of chromatography grade silica gel was added to the dried organic layer and the solvent was removed. The silica adsorbed residue was chromatographed on silica gel with 100% hexanes to give 2.2 g (6.1 mmol, 52% yield). Characterization is reported in the literature and is concomitant with our analysis.<sup>89</sup>

## **2.6.2 Kinetics Determination in the Sonogashira Assay**

The trial using 55% 2-butanone to catalyst is used as an example procedure.

### ***2.6.2.1 Dithiolane Formation***

Under inert argon atmosphere, 2.5 mL of an  $8.60 \times 10^{-3}$  M solution of 1,3-propanedithiol in dichloromethane is mixed with 2.5 mL of a  $4.73 \times 10^{-3}$  M solution of 2-butanone in dichloromethane. To the solution is added 10  $\mu\text{L}$  concentrated sulfuric acid and 10 mg zinc chloride. The reaction is stirred under argon at room temperature for 1 hour and then quenched by adding 5 mL dichloromethane and 5 mL triethylamine.

#### ***2.6.2.2 Palladium Poisoning and Sonogashira***

Then 2.5 mL of an  $8.60 \times 10^{-3}$  M solution of  $\text{Pd}(\text{MeCN})_2\text{Cl}_2$  in dichloromethane is added to the quenched solution and stirred for five minutes under argon. A 12.5 mL solution containing 0.19 mmol 9-bromo-10-(phenylethynyl)anthracene and 0.12 mmol 2,5-diphenyloxazole along with 5 mg neat CuI are then added and the 30 mL solution is brought to gentle reflux. Finally, 50  $\mu\text{L}$  of phenylacetylene is added and 250  $\mu\text{L}$  aliquots are taken and worked up every 10 min. for 2 hr.

#### ***2.6.2.3 Aliquot Work-up***

250  $\mu\text{L}$  of the reaction liquor is partitioned between 4 mL ethyl acetate and 2 mL 2N HCl. For fluorometry, the organic layer is then directly diluted by roughly  $10^{-3}$  in ethyl acetate. Preparation of the aliquot for chemiluminescence requires further washing of the organic layer with 2M NaOH followed by drying ( $\text{Na}_2\text{SO}_4$ ).

#### ***2.6.2.4 Fluorescence***

Spectra were taken for 2,5-diphenyloxazole, 9-bromo-10-(phenylethynyl)anthracene, and 9,10-bis(phenylethynyl)anthracene in ethyl acetate exciting at 316nm, 406nm, and 451nm respectively for each aliquot. 2,5-diphenyloxazole was read at 357 nm, **2.28** at 432, and BPEA at 471. Slit widths were set at 2nm for excitation and emission giving average fluorescence intensities of  $>10^5$

counts/s. Data from each spectrum was collected *via* integration from -5 to +5 nm about the respective emission  $\lambda_{\text{max}}$  using the Felix32 v1.0 software package.

#### ***2.6.2.5 Chemiluminescence***

To a standard 1 cm path length quartz fluorescence cuvet was placed 2 mL of the base washed sample in ethyl acetate, 50 mg **2.31**, and 10  $\mu\text{L}$  0.1 M NaOH. The cuvet was equipped with a stir bar and placed in the fluorometer with the excitation shutter closed. The chemiluminescence reaction was started with the addition of 50  $\mu\text{L}$  30% hydrogen peroxide and data collection was begun at 357 nm for PPO, 432 nm for **2.28**, and 470 nm for BPEA. Data was collected as the average over a 60 second time period once the emission intensity had plateaued.

#### **2.6.3 Kinetics Determination for the Suzuki Assay**

The trial with 13.3% cinnamaldehyde is used as an example.

##### ***2.6.3.1 Dithiane Condensation***

To a 5 mL round bottom flask are added 1 mL thoroughly degassed water, 50  $\mu\text{L}$  (0.6 mmol) ethanedithiol, 10  $\mu\text{L}$  (0.08 mmol) cinnamaldehyde, and 25  $\mu\text{L}$  48% hydrobromic acid in water. The reaction is stirred at 40 °C for 2hr during which time a small amount of white precipitate forms and is redissolved in the remaining insoluble ethanedithiol. The reaction is quenched with 3 mL of 6N sodium hydroxide which reforms the white precipitate as the ethanedithiol is deprotonated and dissolved in the



aqueous layer. At this time the total concentration of disulfur species (ethanedithiol and the condensed dithiolane) is 0.147 M. This solution is labeled solution **A**.

#### 2.6.3.2 Suzuki Coupling

In 10 mL volumetric flask is placed 101.3 mg (0.3 mmol) 9,10-dibromoanthracene and 25.3 mg (0.1 mmol) 2,5-diphenyloxazole (PPO), which were then diluted to 10 mL with a 1:1 DMF:THF solution. The resulting solution was labeled solution **B**. 83.5 mg (0.37 mmol) of palladium (II) acetate was diluted to 50 mL in DMF in a separate volumetric flask and labeled solution **C**. To each of *two parallel reaction* flasks were added 3.5 mL degassed water, 0.5 mL of solution **C**, and 25  $\mu$ L of solution **A**. The solution turned from a light brown to burnt orange instantaneously. The each of these solutions were then added 2.5 mL of solution **B** which precipitated upon contact with water. The reaction vessels were then brought to 40 °C. To the first reaction flask labeled **time 120**, was added 31.6 mg (0.3 mmol) sodium carbonate and 25.3 mg (0.2 mmol) phenylboronic acid and the timer was started. To the second flask labeled **time 0**, was added only 31.5 mg (0.3 mmol) sodium carbonate. The **time 0** flask was stirred for 20 min. and the **time 120** flask was stirred for 2 hours. Final concentrations in the reaction flask prior to reaction were as follows: 9,10-dibromoanthracene 0.012 M; PPO 0.004 M; palladium (II) acetate  $5.7 \times 10^{-4}$  M; phenylboronic acid 0.032 M; ethanedithiol based on no dithiolane formation  $5.7 \times 10^{-4}$  M; sodium carbonate 0.046 M. Upon completion of the reaction both flasks were treated in the following manner. 7 mL of

ethyl acetate were added to quench the reaction giving a 10 mL organic layer on the assumption that all DMF was partitioned. From the organic layer, a 0.25 mL aliquot was diluted to 10 mL with THF and labeled **Lum0** and **Lum120** respectively.

#### ***2.6.3.3 Fluorescence***

Fluorescence measurements were taken by diluting 50  $\mu\text{L}$  of **Lum0** or **Lum120** respectively to 2 mL with THF in a quartz fluorescence cuvet. This dilution gives a maximum  $4.9 \times 10^{-6}$  M solution of fluorophore based on the initial amount of 9,10-dibromoanthracene. Scans of each sample were taken with excitations at 316 nm for PPO and 393 nm for the anthracene fluorophores. The emission outputs at 357 and 407 respectively were integrated as with the previous method and taken as a ratio of product emission to PPO emission. The percent fluorescence increase from time 0 to time 2 hours was then calculated and plotted versus the initial concentration of cinnamaldehyde.

#### ***2.6.3.4 Chemiluminescence***

Chemiluminescence measurements were conducted using undiluted portions of **Lum0** and **Lum120** using the same fluorometer. To a cuvet equipped with a magnetic stirring rod was added 1.89 mL of the respective sample, 50 mg (0.075 mmol) bis(2-carbopentyloxy-3,5,6-trichlorophenyl)oxalate, and 10  $\mu\text{L}$  of 0.1 N sodium hydroxide. With the shutter to the excitation lamp closed 100  $\mu\text{L}$  of 30% hydrogen peroxide solution was added followed quickly by initiation of a time based data collection protocol. When luminescence levels plateaued, a spectrum scan was initiated, which took a 3-fold

average at each wavelength. The data was integrated as before and the percent increase from time 0 to 2 hours was calculated and plotted versus the initial concentration of cinnamaldehyde.

## 2.7 REFERENCES

1. Anslyn, E. V.; Dougherty, D. A., *Modern Physical Organic Chemistry*. 1 ed.; University Science Books: Sausalito, CA, 2006; Vol. 1.
2. Gokel, G. W.; Editor, *Advances in Supramolecular Chemistry, Volume 9*. 2003; p 263 pp.
3. Steed, J. W.; Atwood, J. L., *Supramolecular Chemistry: A Concise Introduction*. 2000; p 400 pp.
4. Prodi, L., Luminescent chemosensors: from molecules to nanoparticles. *New Journal of Chemistry* **2005**, 29, (1), 20-31.
5. Lehn, J. M., Supramolecular chemistry. *Science (Washington, DC, United States)* **1993**, 260, (5115), 1762-3.
6. Wang, W.; Gao, X.; Wang, B., Boronic acid-based sensors. *Current Organic Chemistry* **2002**, 6, (14), 1285-1317.
7. Sutherland, I. O., Crown compounds. Molecule and cation recognition by synthetic host molecules. *Crown Compd.* **1992**, 235-60.
8. Dorland, W. A. N., *Dorland's Illustrated Medical Dictionary*. 31st ed.; W.B. Saunders: Philadelphia, PA, 2007; Vol. 1.
9. Desvergne, J. P.; Czarnik, A. W.; Editors, *Chemosensors of Ion and Molecule Recognition. (Proceedings of the NATO Advanced Research Workshop, held 31 August-4 September 1996, in Bonas, France.) [In: NATO ASI Ser., Ser. C, 1997; 492]*. 1997; p 245 pp.
10. Beer, P. D.; Cadman, J., Electrochemical and optical sensing of anions by transition metal based receptors. *Coordination Chemistry Reviews* **2000**, 205, 131-155.
11. Martinez-Manez, R.; Sancenon, F., Fluorogenic and Chromogenic Chemosensors and Reagents for Anions. *Chemical Reviews (Washington, DC, United States)* **2003**, 103, (11), 4419-4476.

12. Sessler, J. L.; Weghorn, S. J., *Expanded, Contracted and Isomeric Porphyrins*. 1 ed.; Pergamon: Oxford, UK; New York, NY, 1997; Vol. 1.
13. Jimenez, D.; Martinez-Manez, R.; Sancenon, F.; Soto, J., Selective fluoride sensing using colorimetric reagents containing anthraquinone and urea or thiourea binding sites. *Tetrahedron Letters* **2002**, 43, (15), 2823-2825.
14. Loehr, H. G.; Voegtle, F., Chromo- and fluoroionophores. A new class of dye reagents. *Accounts of Chemical Research* **1985**, 18, (3), 65-72.
15. Dix, J. P.; Voegtle, F., New chromoionophores. *Chemische Berichte* **1981**, 114, (2), 638-51.
16. Dix, J. P.; Voegtle, F., Ligand structure and complexation. L. Ion-selective crown ether dyes. *Chemische Berichte* **1980**, 113, (2), 457-70.
17. Lavigne, J. J.; Anslyn, E. V., Teaching old indicators new tricks: a colorimetric chemosensing ensemble for tartrate/malate in beverages. *Angewandte Chemie, International Edition* **1999**, 38, (24), 3666-3669.
18. Wiskur, S. L.; Anslyn, E. V., Using a Synthetic Receptor to Create an Optical-Sensing Ensemble for a Class of Analytes: A Colorimetric Assay for the Aging of Scotch. *Journal of the American Chemical Society* **2001**, 123, (41), 10109-10110.
19. Fabbrizzi, L.; Pallavicini, P.; Parodi, L.; Perotti, A.; Taglietti, A., Molecular recognition of the imidazole residue by a dicopper(II) complex with a bisdien macrocycle bearing two pendant arms. *Journal of the Chemical Society, Chemical Communications* **1995**, (23), 2439-40.
20. Jares-Erijman, E. A.; Jovin, T. M., Imaging molecular interactions in living cells by FRET microscopy. *Current Opinion in Chemical Biology* **2006**, 10, (5), 409-416.
21. Li, I. T.; Pham, E.; Truong, K., Protein biosensors based on the principle of fluorescence resonance energy transfer for monitoring cellular dynamics. *Biotechnology Letters* **2006**, 28, (24), 1971-1982.
22. Snowden, T. S.; Anslyn, E. V., Anion recognition: synthetic receptors for anions and their application in sensors. *Current Opinion in Chemical Biology* **1999**, 3, (6), 740-746.
23. de Silva, A. P.; de Silva, S. A., Fluorescent signaling crown ethers: switching on of fluorescence by alkali metal ion recognition and binding in situ. *Journal of the Chemical Society, Chemical Communications* **1986**, (23), 1709-10.

24. Konopelski, J. P.; Kotzyba-Hibert, F.; Lehn, J. M.; Desvergne, J. P.; Fages, F.; Castellan, A.; Bouas-Laurent, H., Synthesis, cation binding, and photophysical properties of macrobicyclic anthracenocryptands. *Journal of the Chemical Society, Chemical Communications* **1985**, (7), 433-6.
25. Gunnlaugsson, T.; Davis, A. P.; O'Brien, J. E.; Glynn, M., Fluorescent Sensing of Pyrophosphate and Bis-carboxylates with Charge Neutral PET Chemosensors. *Organic Letters* **2002**, 4, (15), 2449-2452.
26. Nishizawa, S.; Kato, Y.; Teramae, N., Fluorescence Sensing of Anions via Intramolecular Excimer Formation in a Pyrophosphate-Induced Self-Assembly of a Pyrene-Functionalized Guanidinium Receptor. *Journal of the American Chemical Society* **1999**, 121, (40), 9463-9464.
27. Niikura, K.; Anslyn, E. V., Azacalixarene: synthesis, conformational analysis, recognition behavior toward anions. *Journal of the Chemical Society, Perkin Transactions 2: Physical Organic Chemistry* **1999**, (12), 2769-2775.
28. Houk, R. J. T.; Anslyn, E. V., Luminescent assays for ketones and aldehydes employing catalytic signal amplification. *New Journal of Chemistry* **2007**, In press.
29. Chandross, E. A., A new chemiluminescent system. *Tetrahedron Letters* **1963**, 1963, (12), 761-5.
30. Rauhut, M. M.; Bollyky, L. J.; Roberts, B. G.; Loy, M.; Whitman, R. H.; Iannotta, A. V.; Semsel, A. M.; Clarke, R. A., Chemiluminescence from reactions of electronegatively substituted aryl oxalates with hydrogen peroxide and fluorescent compounds. *Journal of the American Chemical Society* **1967**, 89, (25), 6515-22.
31. Bollyky, L. J.; Whitman, R. H.; Roberts, B. G.; Rauhut, M. M., Chemiluminescence from reactions of oxalic anhydrides with hydrogen peroxide in the presence of fluorescent compounds. *Journal of the American Chemical Society* **1967**, 89, (25), 6523-6.
32. Tsunoda, M.; Imai, K., Analytical applications of peroxyoxalate chemiluminescence. *Analytica Chimica Acta* **2005**, 541, (1-2), 13-23.
33. Catherall, C. L. R.; Palmer, T. F.; Cundall, R. B., Chemiluminescence from reactions of bis(pentachlorophenyl) oxalate, hydrogen peroxide, and fluorescent compounds: kinetics and mechanism. *Journal of the Chemical Society, Faraday Transactions 2: Molecular and Chemical Physics* **1984**, 80, (7), 823-36.
34. Baader, W. J.; Silva, S. M.; Oyamaguchi, K. H.; Ciscato, L. F. L. M.; Stevani, C. V., Further studies on the mechanism of the peroxyoxalate reaction. *Chemiluminescence at the Turn of the Millennium* **2001**, 33-38.

35. Bos, R.; Barnett, N. W.; Dyson, G. A.; Lim, K. F.; Russell, R. A.; Watson, S. P., Studies on the mechanism of the peroxyoxalate chemiluminescence reaction. Part 1. Confirmation of 1,2-dioxetanedione as an intermediate using  $^{13}\text{C}$  nuclear magnetic resonance spectroscopy. *Analytica Chimica Acta* **2004**, 502, (2), 141-147.
36. Silva, S. M.; Casallanovo, F., Jr.; Oyamaguchi, K. H.; Ciscato, L. F. L. M.; Stevani, C. V.; Baader, W. J., Kinetic studies on the peroxyoxalate chemiluminescence reaction: determination of the cyclization rate constant. *Luminescence* **2002**, 17, (5), 313-320.
37. Silva, S. M.; Wagner, K.; Weiss, D.; Beckert, R.; Stevani, C. V.; Baader, W. J., Studies on the chemiexcitation step in peroxyoxalate chemiluminescence using steroid-substituted activators. *Luminescence* **2002**, 17, (6), 362-369.
38. Stevani, C. V.; Baader, W. J., Kinetic studies on the chemiluminescent decomposition of an isolated intermediate in the peroxyoxalate reaction. *Journal of Physical Organic Chemistry* **1997**, 10, (8), 593-599.
39. Stevani, C. V.; Da Silva, S. M.; Baader, W. J., Studies on the involvement of the CIEEL sequence in the peroxyoxalate reaction. *Bioluminescence and Chemiluminescence: Perspectives for the 21st Century, Proceedings of the International Symposium on Bioluminescence and Chemiluminescence, 10th, Bologna, Sept. 4-8, 1998* **1999**, 53-56.
40. Stevani, C. V.; Silva, S. M.; Baader, W. J., Studies on the mechanism of the excitation step in peroxyoxalate chemiluminescence. *European Journal of Organic Chemistry* **2000**, (24), 4037-4046.
41. Alvarez, F. J.; Parekh, N. J.; Matuszewski, B.; Givens, R. S.; Higuchi, T.; Schowen, R. L., Multiple intermediates generate fluorophore-derived light in the oxalate/peroxide chemiluminescence system. *Journal of the American Chemical Society* **1986**, 108, (20), 6435-7.
42. Catherall, C. L. R.; Palmer, T. F.; Cundall, R. B., Chemiluminescence from reactions of bis(pentachlorophenyl) oxalate, hydrogen peroxide, and fluorescent compounds. Role of the fluor and nature of chemielectronic process(es). *Journal of the Chemical Society, Faraday Transactions 2: Molecular and Chemical Physics* **1984**, 80, (7), 837-49.
43. Koike, R.; Motoyoshiya, J.; Takaguchi, Y.; Aoyama, H., The key intermediates that interact with the fluorophores in the peroxyoxalate chemiluminescence reaction of 2,4,6-trichlorophenyl N-aryl-N-tosyloxamates. *Chemical Communications (Cambridge, United Kingdom)* **2003**, (6), 794-795.

44. Orlovic, M.; Schowen, R. L.; Givens, R. S.; Alvarez, F.; Matuszewski, B.; Parekh, N., A simplified model for the dynamics of chemiluminescence in the oxalate-hydrogen peroxide system: toward a reaction mechanism. *Journal of Organic Chemistry* **1989**, 54, (15), 3606-10.
45. Schuster, G. B., Chemiluminescence of organic peroxides. Conversion of ground-state reactants to excited-state products by the chemically initiated electron-exchange luminescence mechanism. *Accounts of Chemical Research* **1979**, 12, (10), 366-73.
46. Chandross, E. A.; Sonntag, F. I., Novel chemiluminescent electron transfer reaction. *Journal of the American Chemical Society* **1964**, 86, (15), 3179-80.
47. Hercules, D. M., Chemiluminescence resulting from electrochemically generated species. *Science (Washington, DC, United States)* **1964**, 145, (3634), 808-9.
48. Santhanam, K. S. V.; Bard, A. J., Chemiluminescence of electrogenerated 9,10-diphenylanthracene anion radical. *Journal of the American Chemical Society* **1965**, 87, (1), 139-40.
49. Richardson, W. H.; Montgomery, F. C.; Yelvington, M. B.; O'Neal, H. E., Kinetics of the thermal decomposition of 3,3-diphenyl- and 3,3-dibenzyl-1,2-dioxetane. Consideration of stepwise and concerted mechanisms. *Journal of the American Chemical Society* **1974**, 96, (24), 7525-32.
50. Kenichiro Nakashima, K. M. S. A. K. I., Evaluation of pyrimido[5,4-*d*]pyrimidine derivatives as peroxyoxalate chemiluminescence reagents using a flow injection system. *Biomedical Chromatography* **1990**, 4, (3), 105-107.
51. Gubitz, G.; Van Zoonen, P.; Gooijer, C.; Velthorst, N. H.; Frei, R. W., Immobilized fluorophores in dynamic chemiluminescence detection of hydrogen peroxide. *Analytical Chemistry* **1985**, 57, (11), 2071-4.
52. Van Zoonen, P.; Kamminga, D. A.; Gooijer, C.; Velthorst, N. H.; Frei, R. W.; Gubitz, G., A solid-state chemiluminescence detector for hydrogen peroxide based on an immobilized luminophore. Application to rain water. *Analytica Chimica Acta* **1985**, 174, 151-61.
53. Stigbrand, M.; Ponten, E.; Irgum, K., 1,1'-Oxalyldiimidazole as Chemiluminescence Reagent in the Determination of Low Hydrogen Peroxide Concentrations by Flow Injection Analysis. *Analytical Chemistry* **1994**, 66, (10), 1766-70.
54. Williams, D. C., III; Huff, G. F.; Seitz, W. R., Evaluation of peroxyoxalate chemiluminescence for determination of enzyme generated peroxide. *Analytical Chemistry* **1976**, 48, (7), 1003-6.

55. Sigvardson, K. W.; Birks, J. W., Peroxyoxalate chemiluminescence detection of polycyclic aromatic hydrocarbons in liquid chromatography. *Analytical Chemistry* **1983**, 55, (3), 432-5.
56. Sigvardson, K. W.; Kennish, J. M.; Birks, J. W., Peroxyoxalate chemiluminescence detection of polycyclic aromatic amines in liquid chromatography. *Analytical Chemistry* **1984**, 56, (7), 1096-102.
57. Sigvardson, K. W.; Birks, J. W., Detection of nitro-polycyclic aromatic hydrocarbons in liquid chromatography by zinc reduction and peroxyoxalate chemiluminescence. *Journal of Chromatography* **1984**, 316, 507-18.
58. Lancaster, J. S., Chemiluminescence detection in analytical chemistry. *Endeavour* **1992**, 16, (4), 194-200.
59. Prados, P.; Higashidate, S.; Imai, K., A fully automated HPLC method for the determination of catecholamines in biological samples utilizing ethylenediamine condensation and peroxyoxalate chemiluminescence detection. *Biomedical Chromatography* **1994**, 8, (1), 1-8.
60. Geymayer, P.; Bahr, N.; Reymond, J.-L., A general fluorogenic assay for catalysis using antibody sensors. *Chemistry--A European Journal* **1999**, 5, (3), 1006-1012.
61. Hang, H. C.; Yu, C.; Pratt, M. R.; Bertozzi, C. R., Probing Glycosyltransferase Activities with the Staudinger Ligation. *Journal of the American Chemical Society* **2004**, 126, (1), 6-7.
62. Los, M., Virus detection today. *Modern Bacteriophage Biology and Biotechnology* **2006**, 131-152.
63. MacBeath, G.; Hilvert, D., Monitoring Catalytic Activity by Immunoassay: Implications for Screening. *Journal of the American Chemical Society* **1994**, 116, (14), 6101-6.
64. Oguri, H.; Hiram, M.; Tsumuraya, T.; Fujii, I.; Maruyama, M.; Uehara, H.; Nagumo, Y., Synthesis-Based Approach toward Direct Sandwich Immunoassay for Ciguatoxin CTX3C. *Journal of the American Chemical Society* **2003**, 125, (25), 7608-7612.
65. Taran, F.; Gauchet, C.; Mohar, B.; Meunier, S.; Valleix, A.; Renard, P. Y.; Creminon, C.; Grassi, J.; Wagner, A.; Mioskowski, C., Communications: High-throughput screening of enantioselective catalysts by immunoassay. *Angewandte Chemie, International Edition* **2002**, 41, (1), 124-127.



66. Ueda, H.; Tsumoto, K.; Kobota, K.; Suzuki, E.; Nagamune, T.; Nishimura, H.; Schueler, P. A.; Winter, G.; Kumagai, I.; Mahoney, W. C., Open sandwich ELISA: a novel immunoassay based on the interchain interaction of antibody variable region. *Nature Biotechnology* **1996**, 14, (13), 1714-1718.
67. Weizmann, Y.; Patolsky, F.; Katz, E.; Willner, I., Amplified DNA sensing and immunosensing by the rotation of functional magnetic particles. *Journal of the American Chemical Society* **2003**, 125, (12), 3452-3454.
68. Saghatelian, A.; Guckian, K. M.; Thayer, D. A.; Ghadiri, M. R., DNA Detection and Signal Amplification via an Engineered Allosteric Enzyme. *Journal of the American Chemical Society* **2003**, 125, (2), 344-345.
69. Zhu, L.; Lynch, V. M.; Anslyn, E. V., FRET induced by an allosteric cycloaddition reaction regulated with exogenous inhibitor and effectors. *Tetrahedron* **2004**, 60, (34), 7267-7275.
70. Rostovtsev, V. V.; Green, L. G.; Fokin, V. V.; Sharpless, K. B., A stepwise Huisgen cycloaddition process: copper(I)-catalyzed regioselective \"ligation\" of azides and terminal alkynes. *Angewandte Chemie, International Edition* **2002**, 41, (14), 2596-2599.
71. Tornøe, C. W.; Christensen, C.; Meldal, M., Peptidotriazoles on Solid Phase: [1,2,3]-Triazoles by Regiospecific Copper(I)-Catalyzed 1,3-Dipolar Cycloadditions of Terminal Alkynes to Azides. *Journal of Organic Chemistry* **2002**, 67, (9), 3057-3064.
72. Wu, Q.; Anslyn, E. V., Catalytic Signal Amplification Using a Heck Reaction. An Example in the Fluorescence Sensing of Cu(II). *Journal of the American Chemical Society* **2004**, 126, (45), 14682-14683.
73. Wu, Q.; Anslyn, E. V., Heavy metal analysis using a Heck-catalyzed cyclization to create coumarin. *Journal of Materials Chemistry* **2005**, 15, (27-28), 2815-2819.
74. Gianneschi, N. C.; Nguyen, S. T.; Mirkin, C. A., Signal Amplification and Detection via a Supramolecular Allosteric Catalyst. *Journal of the American Chemical Society* **2005**, 127, (6), 1644-1645.
75. Graf, N.; Goeritz, M.; Kraemer, R., A metal-ion-releasing probe for DNA detection by catalytic signal amplification. *Angewandte Chemie, International Edition* **2006**, 45, (24), 4013-4015.
76. Zhang, Z.; Zhang, S.; Zhang, X., Recent developments and applications of chemiluminescence sensors. *Analytica Chimica Acta* **2005**, 541, (1-2), 37-46.
77. Dunleavy, J. K., Sulfur as a catalyst poison. *Platinum Metals Review* **2006**, 50, (2), 110.

78. Brown, W. H.; Foote, C. S.; Iverson, B. L., *Organic Chemistry*. 4th ed.; Brooks/Cole: Belmont, CA, 2005; Vol. 1, p 1168.
79. Seebach, D.; Kolb, M., Umpolung (dipole inversion) of carbonyl reactivity. *Chemistry & Industry (London, United Kingdom)* **1974**, (17), 687-92.
80. Sheehan, J. C.; Coderre, R. A.; Cruickshank, P. A., The formation of five- and six-membered rings by the acyloin condensation. IV. The natural estrogenic steroids. *Journal of the American Chemical Society* **1953**, 75, 6231-33.
81. Du, H.; Fuh, R.-C. A.; Li, J.; Corkan, L. A.; Lindsey, J. S., Photochem CAD: a computer-aided design and research tool in photochemistry. *Photochemistry and Photobiology* **1998**, 68, (2), 141-142.
82. Li, J. J., *Name Reactions*. 2nd ed.; Springer-Verlag: Berlin, Germany, 2003; Vol. 1, p 465.
83. Shinde, P. D.; Borate, H. B.; Wakharkar, R. D., Thioacetalization of the carbonyl function, transthioacetalization of acetals, ketals, oximes and hydrazones catalyzed by aqueous hydrobromic acid. *ARKIVOC (Gainesville, FL, United States)* **2004**, (14), 110-117.
84. Liu, L.; Zhang, Y.; Xin, B., Synthesis of Biaryls and Polyaryls by Ligand-Free Suzuki Reaction in Aqueous Phase. *Journal of Organic Chemistry* **2006**, 71, (10), 3994-3997.
85. Sancenon, F.; Martinez-Manez, R.; Miranda, M. A.; Segui, M.-J.; Soto, J., Towards the development of colorimetric probes to discriminate between isomeric dicarboxylates. *Angewandte Chemie, International Edition* **2003**, 42, (6), 647-650.
86. Zhang, X. M.; Bordwell, F. G.; Bares, J. E.; Cheng, J. P.; Petrie, B. C., Homolytic bond dissociation energies of the acidic carbon-hydrogen bonds in a-substituted and 10-substituted 9-methylanthracenes and their related radical anions. *Journal of Organic Chemistry* **1993**, 58, (11), 3051-9.
87. Andres, M. A.; Chang, T. C. T.; Cheng, C. W. F.; Kapustay, L. V.; Kelly, K. P.; Zweifel, M. J., Nitration of alkenes by palladium nitro complexes. *Organometallics* **1984**, 3, (10), 1479-84.
88. Heilbron, I. M.; Heaton, J. S., 9,10-Dibromoanthracene. *Organic Syntheses* **1923**, III, 41-3.
89. Swager, T. M.; Gil, C. J.; Wrighton, M. S., Fluorescence Studies of Poly(p-phenyleneethynylene)s: The Effect of Anthracene Substitution. *Journal of Physical Chemistry* **1995**, 99, (14), 4886-93.

## **Chapter 3: A Diagnostic Colorimetric Sensor for Residual Pd(II) in Cross-Coupling Reactions**

### **3.0 INTRODUCTION**

As has been stated previously, there are two main components to the design of a molecular sensing or signaling assay: the recognition unit and the signaling unit. Depending on the class of recognition element that is chosen, there are a number of intermolecular non-covalent or covalent interactions which can be employed to affect strong binding affinity between the host molecule and the designated target. Chapter 1 discussed in detail some of the nuances associated with one widely employed non-covalent interaction, electrophilic coordination, when we looked at the effects of unusually strong hydrogen bonds and nonclassically oriented electrophiles on the stabilization of carbon acids. Other commonly utilized binding elements are ion-pairing, other dipole-dipole interactions, hydrophobic effects, and to a lesser degree Van der Waals forces. The second part of a sensing assay involves the signaling motif. Chapter 2 discussed the different types of signaling motifs often employed for molecular recognition based sensing, and saw the development of a new type of signal in peroxyoxalate chemiluminescence coupled with catalytic signal amplification. Whereas Chapter 1 focused on binding forces and Chapter 2 on signaling modes, the current chapter will see the development of a full and complete molecular signaling application.

Herein, we will discuss the development of a regenerative chemodosimetric assay for the detection of trace Pd(II) from industrial process cross-coupling reactions. The chapter will begin with a brief introduction to chemodosimeters and their uses followed by a look at some of the general properties and uses of the squaraine class of organic

dyes. Some previously unpublished preliminary studies on the thermodynamic and spectroscopic properties of the squaraine-based dosimetric complexes conducted by Dr. Karl Wallace, formerly of the Anslyn research group, will be presented as a corollary to the research presented by this author on the highly sensitive chromogenic and fluorogenic detection of Pd(II).

### **3.1 CHEMODOSIMETERS**

As described in Chapter 2, the difference between a chemosensor and a chemodosimeter relies on the reversibility of the binding interaction between the host and the analyte. If the binding which leads to signal transduction is reversible, as with non-covalent supramolecular receptors and a few types of covalent interactions, the host may be termed a chemosensor. If an irreversible or effectively irreversible reaction occurs between the host and analyte, the receptor is called a chemodosimeter.<sup>1</sup> A caveat of this distinction is that because chemodosimeters almost always involve the formation of covalent bonds, they do not technically fall under the supramolecular umbrella. One of the greatest advantages of chemodosimeters is that because an irreversible reaction occurs between the dosimeter and the target, extremely high specificity can usually be obtained. The major disadvantage also arises from the irreversibility of dosimetric assays, in that they can only be used once. Chemodosimeters are also restricted by the kinetic and thermodynamic viability of the sensing reaction. As such, many dosimetric assays are conducted as time-based assays. Unlike chemosensors which can measure analyte concentration at equilibrium or dynamically with changing analyte concentration, chemodosimeters are usually concerned with the detection of cumulative analyte concentration.<sup>2, 3</sup>

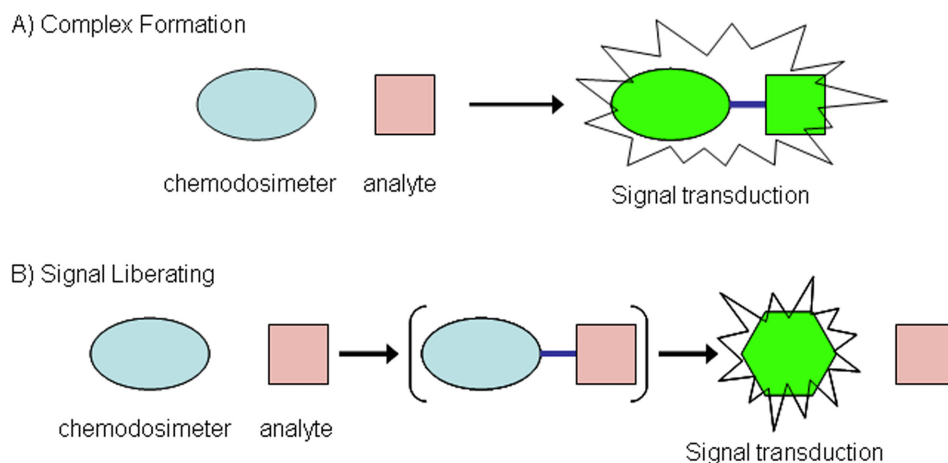


**Figure 3.1** Two types of chemodosimeters. A) The analyte reacts with the dosimeter to generate a new signal producing complex which integrates both original pieces. B) The analyte reacts with the dosimeter to change its constitution such that the signal generating species is liberated.

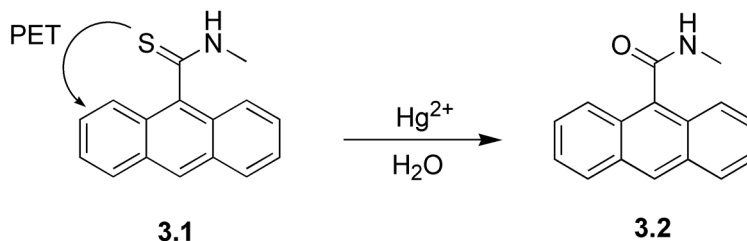
Figure 3.1 shows the two major types of chemodosimeters. The first type involves a system in which the analyte reacts with the dosimeter to generate a signal transducing complex (Figure 3.1A). This type of dosimeter, also called a chemoreactant, is primarily used in the sensing of neutral and anion targets.<sup>4</sup> The dosimeter molecules used in this type of assay are often colored or fluorescent dyes which undergo a spectral shift or turn-on/off upon creating a covalent bond with the target. The second type (Figure 3.1B) occurs when the target analyte catalyzes or promotes the release of a chromo- or fluorogenic moiety from the original dosimeter molecule. This method is the primary choice for cationic sensing as most target cations of interest are transition metals which are often capable of catalysis or the promotion of chemical reactions. The assay described in Chapter 2 is an intricate version of this signal liberating type of chemodosimeter. The application described in this chapter is a combination of both varieties. The following subsections take a short look at some examples of both types of

chemodosimeter to gain a better understanding of the strategies employed and the types of analytes for which this methodology is best suited.

### 3.1.1 Signal Liberating Dosimeters

This strategy for chemodosimetric applications is by far the most widely used. As mentioned above, it is widely used for the detection of cationic metals, though several examples of anion detection have been recently reported. Of the metal targets most often screened with these assays, mercury(II) and copper(II) have received the most attention.<sup>5-15</sup> Silver(I) has also been a target in some cases.<sup>5, 16</sup> Often the mode of action for these applications involves a coordinative promotion of the removal or addition of an optical quencher/modifier. This type of assay can also be used for the detection of various neutral and anionic nucleophiles through a substitution type reaction or through the anionic promotion of a cyclization reaction. Cyanide, fluoride, dicarboxylates, phosphates, thiols, and other divalent sulfur containing targets have been sensed *via* the signal liberating methodology.<sup>17-26</sup>

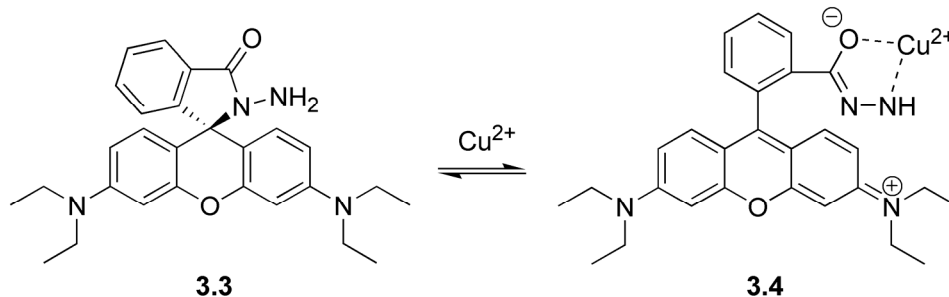
**Scheme 3.1**



The first dosimeter reported for the selective detection of Hg(II) and to a lesser extent Ag(I) was reported by Czarnik in the early 90's.<sup>5</sup> The thioamide group of **3.1** strongly quenches the anthracene fluorescence due to the enhanced contribution of the thiolate resonance form. The introduction of the extremely thiophilic Hg(II) salt in the presence of water serves to desulfurize the thioamide to the non-quenching amide **3.2**.

The stoichiometry for mercury was 1:1 by the formation of HgS and 2:1 for silver with the formation Ag<sub>2</sub>S. Time based measurement showed 87% completion and 73% completion after 10 minutes with stoichiometric amounts of Hg(II) and Ag(I) respectively. This study represented the first instance of a fluorescence turn-on for the detection of what would normally have been a quenching metal. Since both HgS and Ag<sub>2</sub>S are insoluble in water, their precipitation prevented collisional heavy-metal quenching of the anthracene signaling unit.

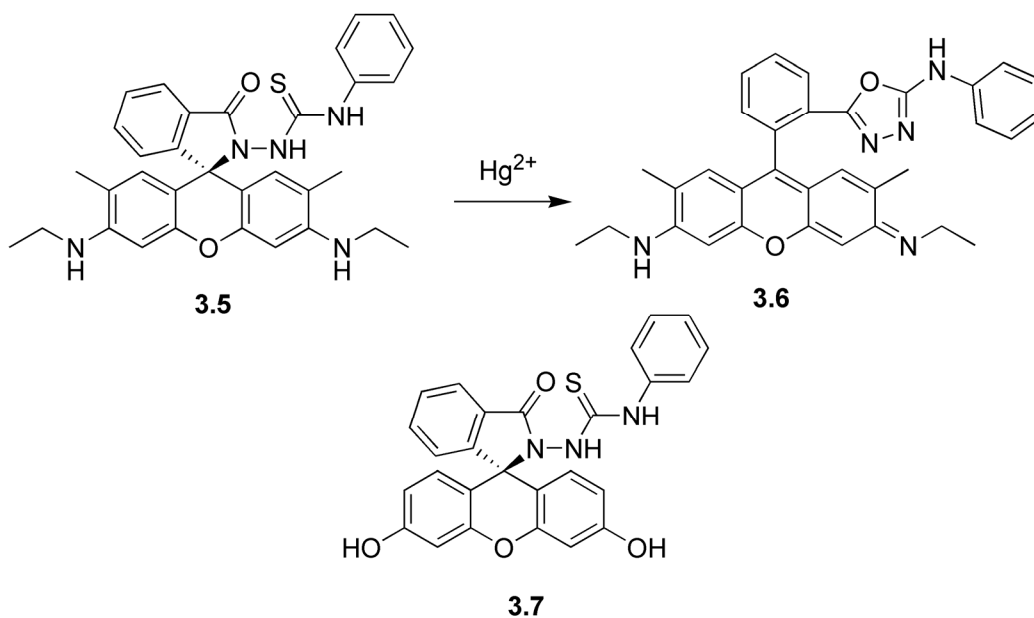
### Scheme 3.2



Rhodamine and fluorescein based dyes are attractive for use as dosimeters due to the built in turn-off mechanism through lactone or lactam formation and have been described in the detection of some metal cations. The rhodamine B derivative **3.3** was designed as a selective chemodosimeter for the detection of copper(II) in aqueous media.<sup>6</sup> The *N*-amino lactam **3.3** is both colorless and nonfluorescent in acetonitrile/water mixtures. Based on the fact that Cu(II) coordination, as opposed to other metals, has a unique rate enhancing effect on the hydrolysis of  $\alpha$ -amino esters, a dosimetric assay was derived from the hydrazidolactam moiety in **3.3**. Addition of  $\text{Cu}(\text{OAc})_2$  rapidly resulted in the pink color and characteristic emission of rhodamine B.<sup>27-29</sup> It was found that in pure acetonitrile, the addition of excess Cu(II)-scavenging ligands such as cyclen resulted in quenched fluorescence and color once again, indicating an equilibrium process. Upon

the addition of water, however, the hydrazide **3.4** was hydrolyzed to yield true rhodamine B as determined analytically. Upon testing against other metals it was found that only Hg(II) showed any similar activity, yet at a much slower rate. In all cases, down to submicromolar concentrations, full response by copper was achieved within 2 minutes, whereas Hg(II) samples took over 50 hours to complete.

**Scheme 3.3**

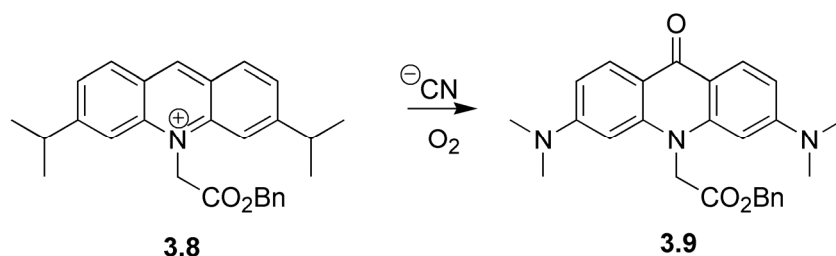


The rhodamine 6G based **3.5** and later the fluorescein based **3.7** were used for the detection of Hg(II) ions.<sup>13, 14</sup> The highly thiophilic nature of mercury was exploited by incorporating the elements required for mercury assisted formation of the 1,3,4-oxadiazole moiety in **3.6**.<sup>30</sup> Upon addition of  $\text{Hg}^{2+}$  salts, the spirolactam is opened by the formation of a chelate complex between the  $\text{Hg}^{2+}$  ion and the carbonyl and sulfonyl. Irreversible mercury assisted desulfurization *via* the formation of the 1,3,4-oxadiazole then occurs. Titrations of  $\text{Hg}^{2+}$  salts showed a stoichiometric dependence of the dosimeter with mercury with saturation occurring at 1 equivalent. For compound **3.5** the



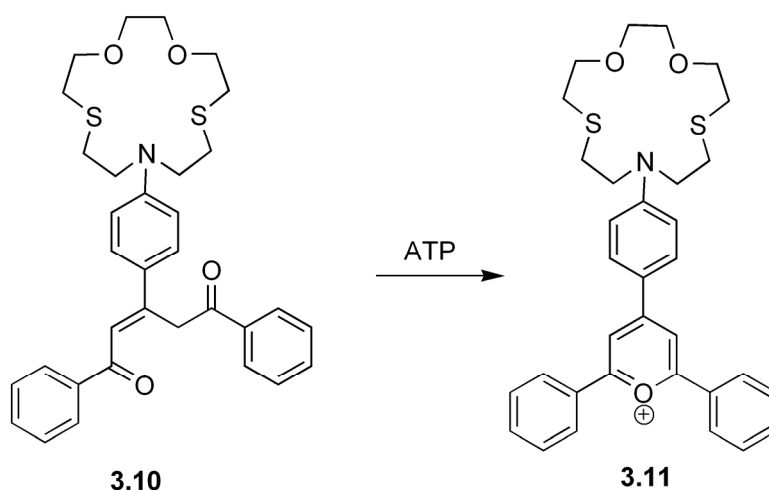
detection limit in water-methanol solutions (80/20 v/v) was less than 2 ppb or roughly  $10^{-8}$  M and showed very little if any response to other metals.<sup>13</sup> In a later study, the fluorescein analogue **3.7** showed similar reactivity. Studies on the fluorescence intensity versus reaction time indicated that effective completion was reached after less than 10 minutes. The fluorescein derivative was also found to be more stable to aqueous conditions and had a sub-nanomolar detection limit.<sup>14</sup>

#### Scheme 3.4



Quenching of fluorescence upon reaction with analyte has also been used in dosimetric assays. The acridine derivative **3.8** was synthesized as a selective cyanide anion detector.<sup>23</sup> In promoting media (95/5 v/v DMSO:H<sub>2</sub>O), in the presence of cyanide anion, **3.8** undergoes a stark colorimetric change from orange to very pale blue accompanied by a nearly complete turn off of fluorescence emission. The CN nucleophilically adds at the 9-position, and in the presence of oxygen, is further displaced by oxidation of the acridine to the acridinone **3.9**. **3.8** was screened against a variety of other anions and nucleophiles, all of which showed no change in the absorbance or fluorescence spectra of the acridine. The sensitivity was found to be less than micromolar by naked eye colorimetric detection.

**Scheme 3.5**



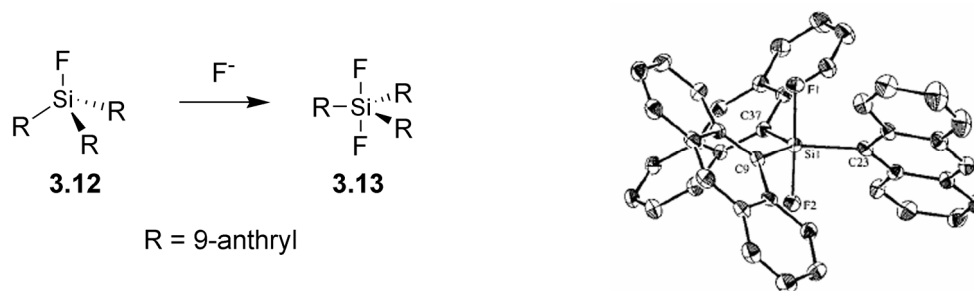
Scheme 3.5 shows a recent class of chromogenic dosimeters developed for selective anion recognition.<sup>24</sup> The “inactivated” structure **3.10** has an absorbance maximum of roughly 380 nm (pale yellow) in buffered pH 6 dioxane/water solutions. It was found that cyclization to the 2,4,6-triphenylpyrylium ion **3.11**—which induces a stark color change to magenta—was pH dependent, and was facilitated in the absence of anionic triggers in the pH 2-5 range. This assay is somewhat unique in that the signal generating reaction is not induced by a covalent interaction of the target with the dosimeter. Rather, this approach combines the function of chemodosimeters with supramolecular binding. In the presence of ATP and, to a lesser extent sulfate, the binding mode of the anions is such that sequestration of the anilino lone pair occurs at higher pH than found with the receptor alone. In other words, binding of the guests raises the  $pK_a$  of the aniline nitrogen. It was found that only ATP and sulfate were capable of inducing the color change, while solutions containing halogens, phosphate, GMP, and ADP, remained yellow. These dosimeters were later adapted to sense for conformationally constrained dicarboxylates, such as oxalate, maleate and malonate,

which again induced the dosimetric reaction through noncovalent interactions.<sup>22</sup> In this case, the binding mode was determined to be in a tweezer-like fashion through formation of strong hydrogen bonds to the enolic tautomer of the 1,5-diketone moiety. Analogues of **3.10** were found to be selective for maleate over fumarate based on the conformational restriction of the double bond. In addition, the dicarboxylates were found to induce the formation of the pyrylium cation in a catalytic fashion. As briefly mentioned in the concluding remarks in Chapter 2, this particular dosimeter could be coupled as an auxiliary to a separate molecular recognition event which releases these dicarboxylates to act as organic catalysts in a signal amplification assay.

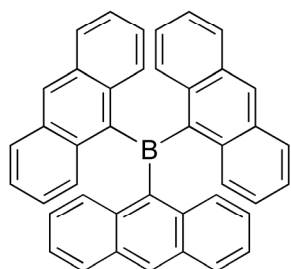
### **3.1.2 Complex Forming Dosimeters**

The examples above—which take advantage of the unique reactivity of their targets to induce an optical change without incorporating that target into the signaling motif—represent the majority of chemodosimetric assays described in the literature. However, there are several examples in which the covalent or other strong, essentially irreversible attachment of the target to the sensing molecule is the trigger for optical change. Whereas the signal liberating motif has been more focused on cationic recognition, the complexation approach has seen fairly common use in the detection of neutral or anionic targets. The nucleophilic nature of many anions and some neutral functional groups (i.e. thiols, alcohols, amines) makes them suitable targets for either removing a quenching moiety by substitution or inducing quenching or color change by addition or substitution.

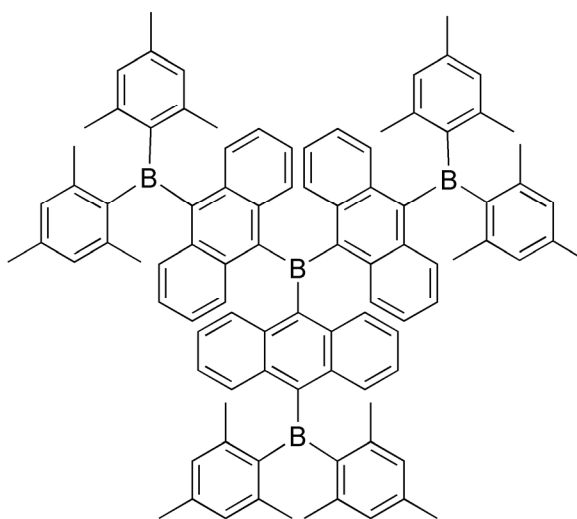
**Scheme 3.6** The crystal structure of 3.13 is reprinted from ref. 31



Perhaps the most widely targeted anion for dosimetric detection has been fluoride. The spectral properties of trianthrylfluorosilane **3.12** were studied as a function of hypercoordination in the presence of fluoride anion.<sup>31</sup> The affinity of silicon for fluoride is well known, and the formation of hypercoordinate “Ate-complexes” with fluoride is a widely used technique for the deprotection of alkylsilane protecting groups in organic synthesis. While there was a slight (10 nm) chromogenic shift in the absorption spectrum with increasing fluoride concentration, the changes in fluorescence were much more striking. It was found that upon reconfiguration from the four coordinate tetrahedral structure to the trigonal bipyramidal **3.13**, the emission showed a 20 nm hypsochromic shift and a nearly 20-fold increase in quantum efficiency ( $\Phi_{3.12} = 0.033$  to  $\Phi_{3.13} = 0.64$ ). Based on controls with varyingly substituted arylsilanes, the large shift was attributed less to the hypercoordination and more to a lengthening of the Si-C bonds upon pyramidalization which increased the distance between the anthryl groups and optimized their through-space interactions.<sup>32</sup>

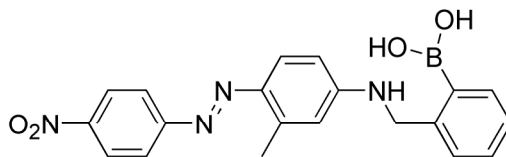


**3.14**



**3.15**

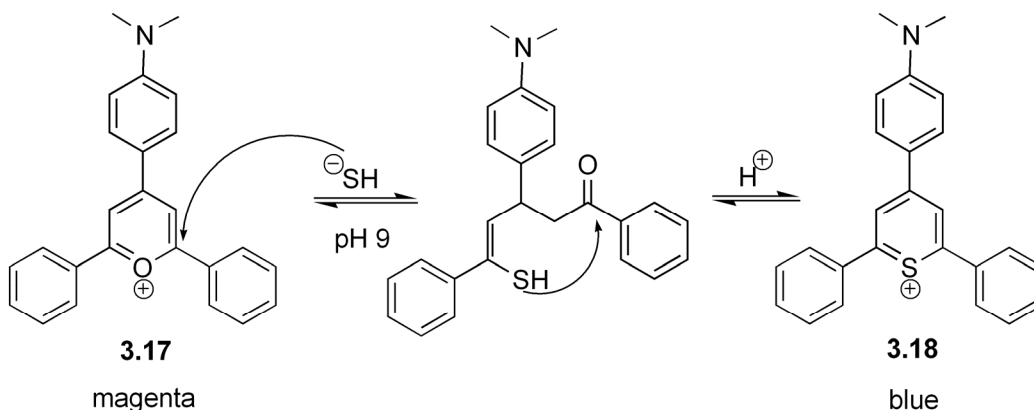
Boron also has a high affinity for fluoride ions, and several dosimeters have been designed to exploit this interaction. In a series of boro-centric structures similar to **3.14** and **3.15**, a distinct colorimetric change was observed upon introduction of fluoride.<sup>33</sup> In an opposite fashion to the silyl receptor above, the addition of fluoride causes the color to turn off due to a conformational change from trigonal planar  $sp^2$  boron to the  $sp^3$  tetrahedral boronate anion. Thusly, solutions of **3.14** turned from orange to colorless in the presence of fluoride, while the further  $\pi$ -extended **3.15** exhibited a marked hypsochromic absorbance shift and turned from bright yellow to orange. The introduction of other anions such as chloride, bromide, iodide, perchlorate, and tetrafluoroborate showed no color change.



**3.16**

Another boron based fluoride detector is the boronic acid **3.16**.<sup>34</sup> It was found that the addition of potassium fluoride in methanolic solutions of **3.16** induced a color change from orange to a deep red wine color. Other halides induced only an increase in absorbance at the original wavelength due to changes in the dielectric medium. The color change was attributed to the formation of the monofluoroboronate anion. Interaction of the aniline nitrogen with the boronate is suspected to alter the energies of the n and  $\pi^*$  orbitals involved in the internal charge transfer associated with the color of azo-dyes. This receptor has also been studied as a saccharide sensor through the formation of boronic or boronate esters with the diol functionalities found in nearly all saccharides.<sup>35</sup> However, due to the highly reversible nature of boronic ester formation, real-time concentration measurements can be achieved for diol recognition with boronic acids. As such, when used for saccharide and other diol detection, boronic acids are categorized as chemosensors.

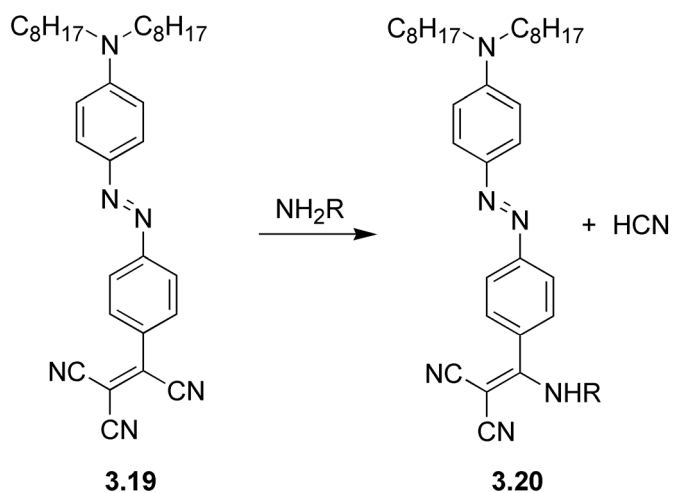
**Scheme 3.7**



Though fluoride has received a good deal of attention in this arena, other anions have been targets for this type of chemodosimeter. Using a similar set of chromogenic reagents as those presented in Scheme 3.5, the presence of sulfide anion can be selectively detected in aqueous solutions.<sup>36</sup> As described above, the 2,4,6-

triphenylpyrylium derivatives such as **3.11** and **3.17** show a unique intramolecular CT band near 540 nm which gives them a distinct magenta color. Unlike other pyrylium chromophores, which are usually yellow, the presence of the aniline donor moiety allows for the CT band to appear. Utilizing known chemistry, the pyrylium ion **3.17** can be converted to the thiopyrylium analogue **3.18**.<sup>37</sup> The conversion is pH dependent once again and requires two steps, one at basic pH to allow the attack of the sulfide anion, followed by acidification to facilitate ring closure. Upon formation of the thiopyrylium core, the solution changes from magenta to blue, indicating a significant bathochromic shift in the CT band. This color change was only observed for sulfide anions, though the presence of amines, cyanide, and the constrained dicarboxylates discussed above was shown to be inhibitory and the blue color upon acidification was not as strong.

### Scheme 3.8

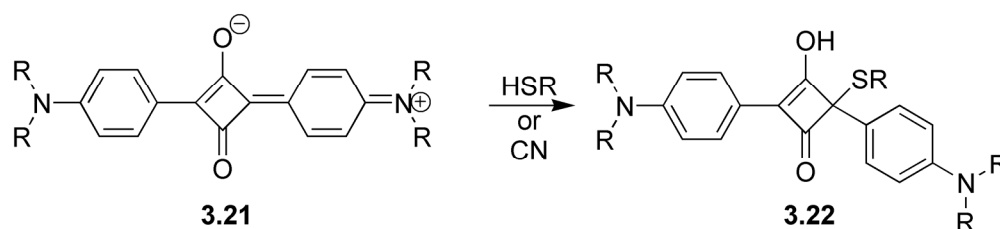


Neutral substrates are also detectable through dosimetric methods. The tricyanovinyl azo-dye **3.19** has been used as a sensor for primary amines.<sup>4</sup> Using a dipstick type assay in which **3.19** was adsorbed in PVC plasticized with 2-nitrophenyloctyl ether the absorbance of the dye shifted from 642 nm (blue) to 470 nm

(yellow-orange) when the test stick was dipped into solutions containing primary amines. The color change arises from nucleophilic displacement of the benzyl cyano group by the amine to effectively generate an equivalent of hydrogen cyanide, and the amine appended dye, **3.20**.

Of particular pertinence to the research described in this chapter, a series of squaraine dyes have been shown to have selective interactions with cyanide and thiols under certain conditions in water.<sup>38, 39</sup> Under basic conditions, the blue squaraines **3.21** were decolorized on the addition of cyanide anion, though the presence of other anions had little to no effect. In a later study at pH 6, it was found that selectivity for thiols was obtained. In a screen against nearly all of the natural  $\alpha$ -amino acids, only cysteine showed decolorization of the squaraine. Attack of the electron deficient central four membered ring by the respective nucleophiles causes a break in the conjugation and a breakdown of the intramolecular charge transfer that is responsible for the blue color. In the latter study, it was found that the squaraine-based chemodosimeter was capable of accurately detecting the concentration of aminothiols in human blood. This interaction is exploited in the research discussed below and hence, an understanding of the photophysical properties and common uses of squaraine dyes is necessary and will be discussed in more detail in the following section.

**Scheme 3.9**

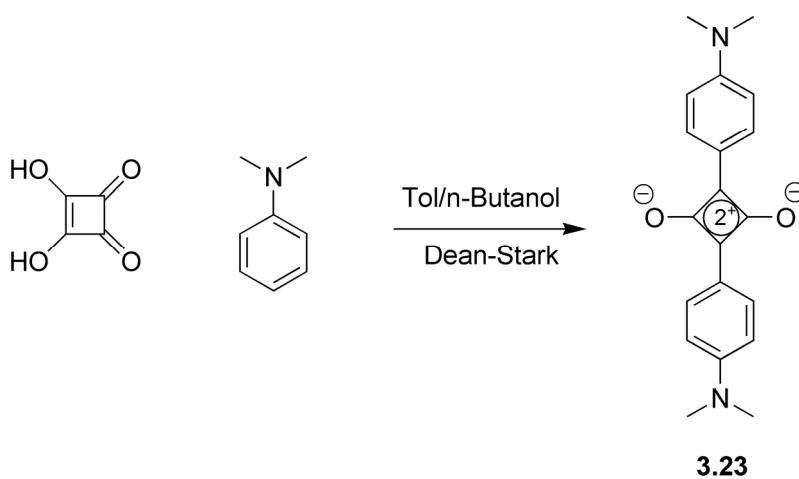




### 3.2 SQUARAIN DYES

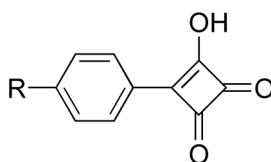
Squaraine dyes result from the coupling of electron rich aromatic nucleophiles with squaric acid. The first synthesis and description of this class of organic dye was reported by Treibs and Jacob in the mid-60's and they were called at the time cyclotrimethine dyes.<sup>40</sup> The molecules have undergone a number of different name changes, yet for the last 25 years or so, a systematic nomenclature based on the term squaraine has been adopted almost entirely.<sup>41</sup> The most common synthetic route towards symmetrical squaraines is *via* electrophilic aromatic condensation under azeotropic conditions as originally described by Treibs and Jacob. Scheme 3.10 shows this synthetic route in which the major product is a 1,3-disubstituted squaraine such as **3.23**. Other synthetic routes to symmetrical squaraines have been proposed. For use in some photoconducting applications, the squaraines derived from squaric acid are unsuitable, and synthesis from alkyl squarates has been described.<sup>42</sup> Starting with squaric acid diesters can also selectively yield 1,2-disubstituted dyes.<sup>43</sup>

**Scheme 3.10**



Unsymmetrical squaraines have also been synthesized through several routes. One of the major routes involves a [2+2] cycloaddition of an aryl ketene with

tetraethoxyethylene to ultimately yield after acidic reflux the monoadduct **3.24**.<sup>44</sup> This intermediate can then be condensed with various other nucleophiles to give the unsymmetrical product. A second route to the **3.24** intermediate was described involving electrophilic aromatic substitution of the aryl nucleophile with 1,2-squaraine dichloride.<sup>45</sup> A large number of both symmetrical and unsymmetrical squaraines have been synthesized for a number of differing applications. The discussion below is somewhat limited in scope and is confined to a small subset of bis-phenyl squaraines. For more information on other types of squaraines and their properties, several excellent reviews have been published.<sup>46, 47</sup>



**3.24**

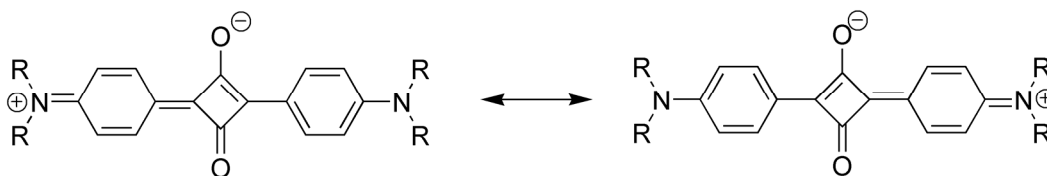
### 3.2.1 Photophysical Properties and Applications

#### 3.2.1.1 Solvent Effects

Squaraines are often described as donor-acceptor-donor type structures in which the donors are the electron rich aryl groups and the acceptor is the central C<sub>4</sub>O<sub>2</sub> moiety. These dyes exhibit strong absorbances and can be quite fluorescent. Often squaraines are described by the cross-conjugation resonance structures shown in scheme 3.11, however crystallographic evidence of the common anilino-squaraines suggests that the true structure contains a considerable amount of cyclobutadienylium dicationic character. On the other hand the C-C bond lengths of the aromatic ring also show lengths of 1.366 Å indicative of quinoid character.<sup>48</sup> This somewhat contrasting evidence suggests that the true form is a complex mixture of the two cross-conjugated resonance forms and the

dication form as in **3.23**. MNDO and CNDO semi-empirical calculations have confirmed this complex electronic nature. The aryl groups again showed quinoid-like character. Evidence for the cyclobutadienylium character arose from the fact that the ground and excited states of squaraines exists as charge transfer states, which are confined mostly to the interior C<sub>4</sub>O<sub>2</sub> moiety.<sup>49</sup> It was found that about 80% of the CT character arises from donation by the oxygens while only 20% comes from the outer donors. However, this confined CT character along with the extended  $\pi$ -delocalization gives rise to the characteristic sharp low energy solution phase absorbance, which is characteristic of all squaraines.

**Scheme 3.11**

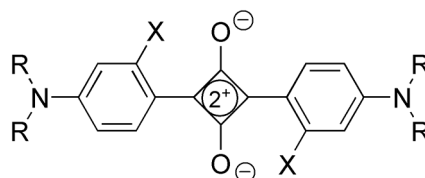


A result of the reduced effect of the remote donor groups in CT states, is that within the same class of squaraines (i.e. anilines vs. anisoles) changes to the donor group have only a small effect on the photophysical properties of these dyes. Table 3.1 lists the absorbance spectral properties for some symmetrical aniline based squaraines in methylene chloride. Notice that the full range of absorbance values only shifts by about 25 nm over a myriad of differing substitutions. The series from Sq1-Sq5 only shifts by 12.4 nm even though the stabilizing power of the aniline donors is increasing significantly.

It has been postulated that the small bathochromic shifts that arise from increasing the chain length of the *N*-alkyl substituents arise not from better donation into the CT

state, but rather from an increase in absorption from a solute-solvent complex.<sup>50</sup> From Table 3.1, several anomalies can be found to discount the idea that the spectral changes are resultant of CT enhancement due to structural changes in the peripheral donors. For instance, one would expect the addition of a strongly donating group at the C-2 position (X) to give rise to large shifts in the absorbance maxima and  $\epsilon_{\max}$ . However the change from Sq7-Sq9 is actually less pronounced than that from Sq1-Sq4 suggesting that the addition of the hydroxyl group at C-2 is less important to the photophysical properties of these squaraines than the *N*-alkyl groups.

**Table 3.1** Spectral data of symmetrical aniline squaraines in methylene chloride.<sup>50</sup>



Squaraine	Substituents	$\lambda_{\max}$ (nm)	$\log \epsilon_{\max}$
Sq1	R=CH <sub>3</sub> , X=H	627.6	5.49
Sq2	R=C <sub>2</sub> H <sub>5</sub> , X=H	634.1	5.51
Sq3	R=C <sub>3</sub> H <sub>7</sub> , X=H	638.8	5.53
Sq4	R=C <sub>4</sub> H <sub>9</sub> , X=H	640.0	5.53
Sq5	R=C <sub>18</sub> H <sub>37</sub> , X=H	641.8	5.52
Sq6	R=CH <sub>3</sub> , X=F	630.0	5.09
Sq7	R=CH <sub>3</sub> , X=OH	635.0	5.52
Sq8	R=C <sub>2</sub> H <sub>5</sub> , X=OH	641.1	5.57
Sq9	R=C <sub>4</sub> H <sub>9</sub> , X=OH	648.2	5.56
Sq10	R=CH <sub>3</sub> , X=CH <sub>3</sub>	643.5	5.42
Sq11	R=C <sub>2</sub> H <sub>5</sub> , X=CH <sub>3</sub>	651.0	5.49
Sq12	R=C <sub>4</sub> H <sub>9</sub> , X=CH <sub>3</sub>	657.1	5.47
Sq13	R=CH <sub>3</sub> , X=OCH <sub>3</sub>	631.8	5.40
Sq14	R=C <sub>2</sub> H <sub>5</sub> , X=OCH <sub>3</sub>	638.8	5.48
Sq15	R=C <sub>4</sub> H <sub>9</sub> , X=OCH <sub>3</sub>	643.5	5.40
Sq16	R=CH <sub>3</sub> , X=C <sub>2</sub> H <sub>5</sub>	643.0	5.42

This implication is further supported by looking at derivatives with the same *N*-alkyl substituents but varying C-2 substitution. If the donor-acceptor-donor (D-A-D) CT enhancement is occurring the expected magnitude of the bathochromic shift with respect to Sq1 should go in the order OH  $\sim$  OCH<sub>3</sub> > F > CH<sub>3</sub>  $\sim$  C<sub>2</sub>H<sub>5</sub>. However the order is reversed experimentally. Sq13 is only shifted by 4.2 nm whereas the shifts observed for the alkyl substituted Sq10 and Sq16 are close to 16 nm. The large shift associated with the alkyl substituted examples is attributed to a conformational change to a non-planar ground state. Interestingly, this leads to a decrease in the CT donation by the peripheral groups as evidenced by lower  $\epsilon_{\text{max}}$  values for Sq10-12 and Sq16. The small shifts with the strongly donating groups such as hydroxyl and methoxy lend some doubt to the idea that these shifts arise from increasing CT donation.

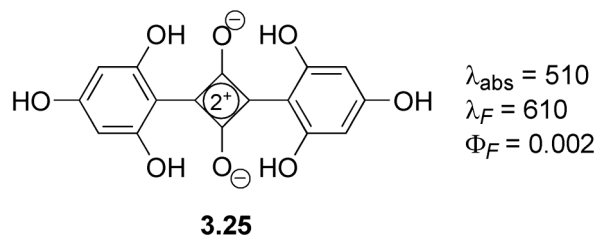
Strong evidence that the formation of solute-solvent complexes results in these optical properties came from a series of spectral determinations of Sq4 in a myriad of differing solvents.<sup>50</sup> It was found that a strong linear correlation between the absorbance  $\lambda_{\text{max}}$  and the coordinating ability of the solvent ( $\pi^*$ -value) exists. The  $\pi^*$  solvent polarity scale is arranged based on a solvent's ability to stabilize the excited state of a molecule and is generally a good prediction of solvatochromicity.<sup>51</sup> Note that this scale does not necessarily adhere to the dielectric polarity of a solvent. The absorbance maximum for Sq4 could be shifted from  $\sim$ 620 nm to nearly  $\sim$ 660 nm. These solvatochromic effects were more pronounced in the fluorescence emission spectra. Switching to fluorescence, in less coordinating solvents such as diethyl ether and *p*-xylene, three distinct bands can be seen in the emission of nearly all squaraines. These emission bands have been termed the  $\alpha$ ,  $\beta$ , and  $\gamma$  bands and have been determined to correspond not to vibrational fine structure, but rather to three different environmental and conformational states of the

squaraine. The  $\alpha$ -band, which has the smallest Stokes shift, corresponds to Franck-Condon type relaxation of the uncomplexed squaraine in solution. This determination was made by noting that as conditions became more favorable for solvent coordination (i.e. lengthened *N*-alkyl chains, greater solvent  $\pi^*$  value), the  $\alpha$ -band disappeared. Temperature effect experiments with Sq4 in diethyl ether found that at room temperature, absorbance and emission were dominated by the uncomplexed squaraine, but at 77 K, both excitation and emission were significantly red shifted indicating the formation of a temperature dependent state which exhibited stronger stabilization of the CT. The resulting emission  $\lambda_{\text{max}}$  at low temperature resembled the  $\beta$ -emission at room temperature, while the absorbance was characteristic of Sq4 in solvents with high  $\pi^*$  values.

The origin of  $\beta$ -emission was determined with a mixed solvent experiment using a ternary system of diethyl ether, *n*-hexane and chloroform. As chloroform was titrated into an Sq4 solution in ether and hexane, both the absorbance and emission spectra showed a marked bathochromic shift. In fact, at low concentrations of chloroform, isosbestic and isoemissive points were observed and indicated the formation of a distinct complex between the coordinating solvent, chloroform and the squaraine with a 1:1 stoichiometry. A further shift was seen at higher concentrations of chloroform and fidelity of the isosbestic and isoemissive points was lost indicating preferential solvation of the squaraine with the coordinating solvent. The emission band which grew in was determined to be the  $\beta$ -band and was said to originate from emission of the solvent-solute complex. The final emissive band, the  $\gamma$ -band, was postulated to arise from emission of a twisted, non-planar conformation of the squaraine as evidenced by its pronounced observation with squaraines such as Sq10-15, which were previously determined to have some amount of non-planarity.

The explanation of a solvent-solute complex giving rise to the spectral shifts upon *N*-alkyl chain lengthening is also supported by the previously mentioned semi-empirical molecular orbital calculations.<sup>49</sup> The electronic structure of the squaraine molecule was found to be highly polarized, with the central ring having a localized charge of +0.37 e and the oxygens and nitrogens have localized charges of -0.35 e and -0.4 e. Despite the significant charge on the peripheral nitrogens, the effective increase in positive charge during the  $S_0$  to  $S_1$  transition is only 0.019 e as opposed to 0.094 e for the central oxygens. Due to the disparity between the highly polarized nature of the periphery and the amount of effective charge transfer in the electronic transition, it was postulated that stabilizing the localized charges would result in an increase in the D-A-D CT character of the molecule. Hence, forming a solvent-solute complex, whose stabilizing effects would not be as strong as adding donating groups directly to the molecule, could account for the small increase in CT character that gives the bathochromic shift in the absorbance.

Similar effects have been observed for other types of squaraine dyes and though substituent effects are somewhat small within the same class of squaraines, the differences between classes (i.e. aniline versus phenol) can be quite large. For instance, phenol-based squaraines such as **3.25** show remarkable hypsochromic absorbance shifts. In ethanol, **3.25** has a  $\lambda_{\text{max}}$  of 510 nm even though the hydroxyl donating groups are much stronger than the aniline nitrogens of the squaraines in Table 3.1.<sup>52</sup> The emissive properties of phenolic and anisolic squaraines are greatly reduced as well. Whereas the quantum efficiencies of the aniline squaraines are generally quite high (0.2-1.0), phenolic and anisolic squaraines tend to have very low fluorescence yields.<sup>46</sup>



### 3.2.1.2 Aggregation and Solid State Applications

In addition to the solvent complexes which are characteristic of most squaraines, these dyes have also been shown to aggregate with themselves even at low concentrations.<sup>53-55</sup> The aggregation can occur in two ways, which yield opposite chromatic effects. In accordance with exciton theory, upon aggregation, the monomeric excited state energy level splits into two new energy levels, one that is higher and one that is lower in energy than the monomeric form.<sup>56</sup> Depending on the orientation of the two dye molecules, only one of the energy transitions is electronically allowed. For head-to-tail “J-type” dimers, the higher energy transition is forbidden and this type of aggregate will see a bathochromic absorbance shift corresponding to the lower energy transition. Conversely, the low energy transition is forbidden for face-to-face “H-type” aggregates, which leads to a hypsochromic shift corresponding to a transition to the high energy excited state.

The type of aggregate formed is dependent on the phenyl substituents. For instance, phenolic squaraines such as **3.25** often show formation of J-type aggregates at high concentrations. Studies in acetonitrile show that at low concentration ( $<5 \mu\text{M}$ ), **3.25** exists as a monomer with maximum absorbance at 480 nm with  $\epsilon_{\text{max}} = 6.5 \times 10^4 \text{ L cm}^{-1}\text{mol}^{-1}$ . However, higher concentrations see the growth of a new, more intense band centered at 563 nm.<sup>57</sup> The bathochromic shift indicates the formation of head-to-tail aggregates for which the lower energy transition is allowed. Furthermore, these aggregates dissociated in the excited state, and the emission occurs only from the



monomer. Presumably, the aggregation arises from intermolecular hydrogen bonding among the peripheral hydroxyl groups since the aggregates were shown to dissipate upon addition of a competitive solvent such as water.

Anilino squaraines have also been shown to aggregate in solution, however the mechanism of dimerization is quite different from phenolic squaraines. A study using Sq9 from Table 3.1 was conducted on the solvent effects on aggregation.<sup>58</sup> Sq9 exhibited a strong, sharp absorbance at 664 nm with a slight hypsochromic shoulder in pure DMSO to 70% DMSO-water (see titration data below for this curve shape). With increasing concentrations of water, two different types of aggregates formed. Between 50-70% DMSO-H<sub>2</sub>O, the main absorbance peak shifts to ~530 nm with a significantly reduced extinction coefficient. The hypsochromic and hypochromic shifts were attributed to the formation of H-type face-to-face aggregates for which only the high energy transition is allowed. A second type of aggregate occurred in higher water concentrations and gave a broad peak that spanned from 550-700 nm. This aggregate form was still mainly blue shifted and was attributed to intermolecular interactions between the electron-rich anilino moieties and the electron-deficient C<sub>4</sub>O<sub>2</sub> core. This type of interaction has less face-to-face character and as a result induces less hypsochromicity. In a later study, several other anilino squaraines were subjected to similar tests.<sup>59</sup> In most cases, formation of the first H-type aggregate was observed, and on squaraines with longer *N*-alkyl chains, the second type of dimer was seen. The conclusion was that the full H-type aggregate is thermodynamically more stable and that formation of the lesser aggregate occurs under kinetic control. The small shoulder observed in the pure DMSO samples was also attributed to a small amount of H-type aggregation. Clearly these aggregation effects arise more from hydrophobic interactions than hydrogen bonding. For the purposes of

the research discussed below, aggregation effects are minimal, but any that are formed are promoted by hydrophobic/van der Waals forces.

Much of this discussion has focused on the importance of solvent in the photophysics of squaraine dyes. In solution, as shown below, squaraines exhibit sharp absorption and emission bands, however in the solid state, the absorbance is panchromatic.<sup>47</sup> For instance, the sharp absorbance bands between 630 and 660 of the squaraines in Table 3.1 give them intense blue colors indicative of long wavelength absorption. However in the absence of solvent, the dyes often have a metallic green color indicative of absorbance both at long wavelength and at short wavelength.<sup>60</sup> Though the research described below deals with solution phase chemistry of squaraines, this class of organic dye has seen much wider application for its solid state properties.

Due to their highly polarized nature and panchromatic solid state absorption, squaraines have desirable semiconductive and photoconductive properties. These properties have led to a large number of device applications such as photosensitizing materials in xerographic devices and optical sound recording devices, light harvesting layers in organic photovoltaic cells, electroluminescent diodes, and in the case of unsymmetrical squaraines, nonlinear optical devices.<sup>61-70</sup> More recently, polymeric squaraines have been utilized for improved performance in many similar types of devices.<sup>71, 72</sup> The alternating regions of donor and acceptor moieties along the polymer back bone is useful for many semiconductive and photoconductive devices. In solution phase, squaraines have seen use as dyes for several biological and ionic sensing applications.<sup>73-95</sup> The research described below applies the advantageous properties of solution phase squaraine dyes with the strength and sensitivity of a chemodosimetric analysis to the problem of detecting residual heavy metals in industrial process chemistry products such as pharmaceuticals.

### 3.3 DESIGN OF A PALLADIUM SENSOR

Palladium complexes represent some of the more useful facilitators of organic transformations known. Palladium(II) salts, such as  $\text{PdCl}_2$ ,<sup>96</sup>  $\text{Pd}(\text{OAc})_2$ <sup>97</sup> and  $\text{Pd}(\text{PPh}_3)_2\text{Cl}_2$ ,<sup>98</sup> are predominantly used as oxidizing reagents, as well as catalysts for cross-coupling reactions. The wide array of commonly used reactions catalyzed by these complexes,<sup>99</sup> such as Suzuki, Heck, and aromatic amination reactions, are processes that would otherwise be infeasible or impractical. Many of these methodologies are widely utilized in pharmaceutical research and development for the discovery and production of drugs.<sup>100</sup> However, governmental restrictions on the levels of residual heavy metals in end products are very strict. Typical contamination levels of palladium remaining in the organic phase after experimental work up range from 5 to 100 ppm.<sup>99</sup> Due to its utility as well as its inherent stickiness, palladium poses a difficult challenge both for its detection and removal. The most popular current method for detecting the presence of such metals utilizes ICP-MS to vaporize the metal ions and obtain a quantitative mass spectrum.\* Though very precise even in the ppt and ppq range, the instruments are somewhat expensive to run, and the need for highly acidic samples in palladium detection tends to corrode the cones faster than normal. Hence, new, milder methods for the sensitive detection of trace palladium is desirable.

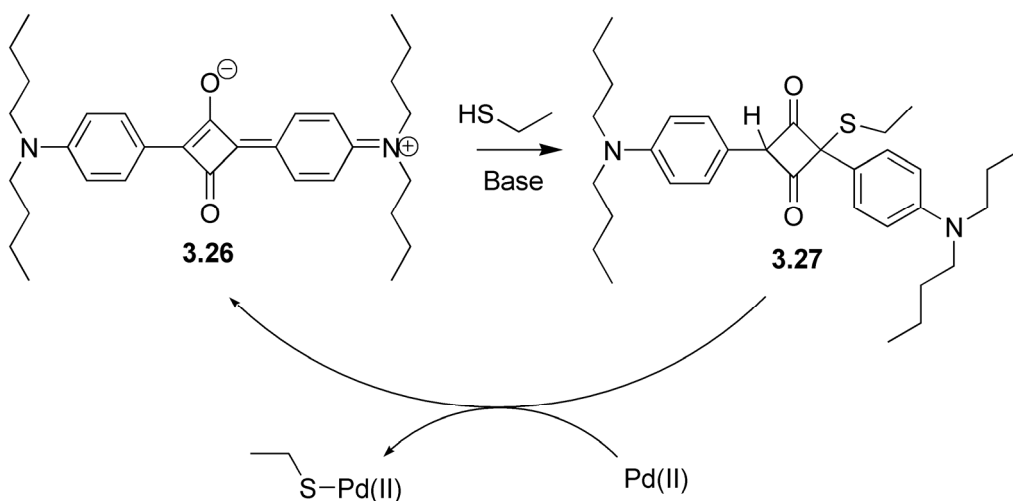
As discussed above, exploitation of reversible covalent bond formation for use as a tool in the detection of analytical targets has become an area of much interest in the last few years.<sup>88</sup> Based on the work of Soto and coworkers shown above in Scheme 3.9, we postulated that a sufficiently thiophilic metal, such as palladium would be capable of scavenging the thiol and restoring the conjugation and CT character to the parent squaraine (Scheme 3.12).<sup>38, 39</sup> Concurrent with our work in this area, Soto and coworkers

---

\* According to sources at Merck Pharmaceuticals

reported a similar system for the selective detection of mercury in aqueous media.<sup>85</sup> Whereas Soto's work shows selectivity for mercury in aqueous solutions, our own work in organic media suggests that little selectivity among heavy metal(II) salts is achieved.<sup>101</sup> Preliminary results show that the current method is sensitive not only to Pd(II) but also several other commonly used transition metals such as tin and common pollutants such as lead, cadmium, and of course mercury. For the application we envision, however, it is unlikely that a lack of specificity will be detrimental as generally only one or two different metals will be present in a sample taken from a pharmaceutical process plant.

**Scheme 3.12**



### 3.3.1 Synthesis and Characterization of **3.26**

The synthesis of the squaraine dye **3.26** was prepared in a one pot procedure as described previously (Scheme 3.10).<sup>48, 55</sup> Two equivalents of N,N-dibutylaniline were refluxed with one equivalent of squaric acid under Dean-Stark conditions in 1:1 n-butanol/toluene for 6-8 hours at which time the solution is a deep blue-green color. Literature procedures describe the purification as a simple extraction and solvent removal, however, the low yield always associated with **3.26** forced a more stringent

work up method to remove the myriad side products. Column chromatography of the resulting residue with hexanes and ethyl acetate produced a green solid which was recrystallized from methylene chloride and hexanes to give small, fluffy, blue-green needles. Compound **3.26** was characterized by  $^1\text{H}$  NMR,  $^{13}\text{C}$  NMR, and high-resolution mass spectrometry, which were all consistent with the proposed structure. Compound **3.26** is symmetrical and shows very simple  $^1\text{H}$  and  $^{13}\text{C}$  NMR spectra. Both low and high resolution ESI mass spectra show a significant amount of dimerization with a 70% intensity peak at 976 m/z.

UV-Vis spectral analysis of **3.26** in DMSO is shown in Figure 3.2. Beer's law analysis shows a  $\lambda_{\text{max}}$  at 656 nm over the concentration range tested. The absorbance curve is unsymmetrical with a slight hypsochromic shoulder. This shoulder, as mentioned above, corresponds to the slight amount of H-type face-to-face dimer present in solution. Linear adherence to the Beer plot was maintained as high as 2 absorbance units. The molar extinction coefficient in DMSO was determined to be  $2.3 \times 10^5 \text{ L mol}^{-1} \text{ cm}^{-1}$  from the slope of the plot of absorbance at 656 nm versus the concentration of **3.26**.

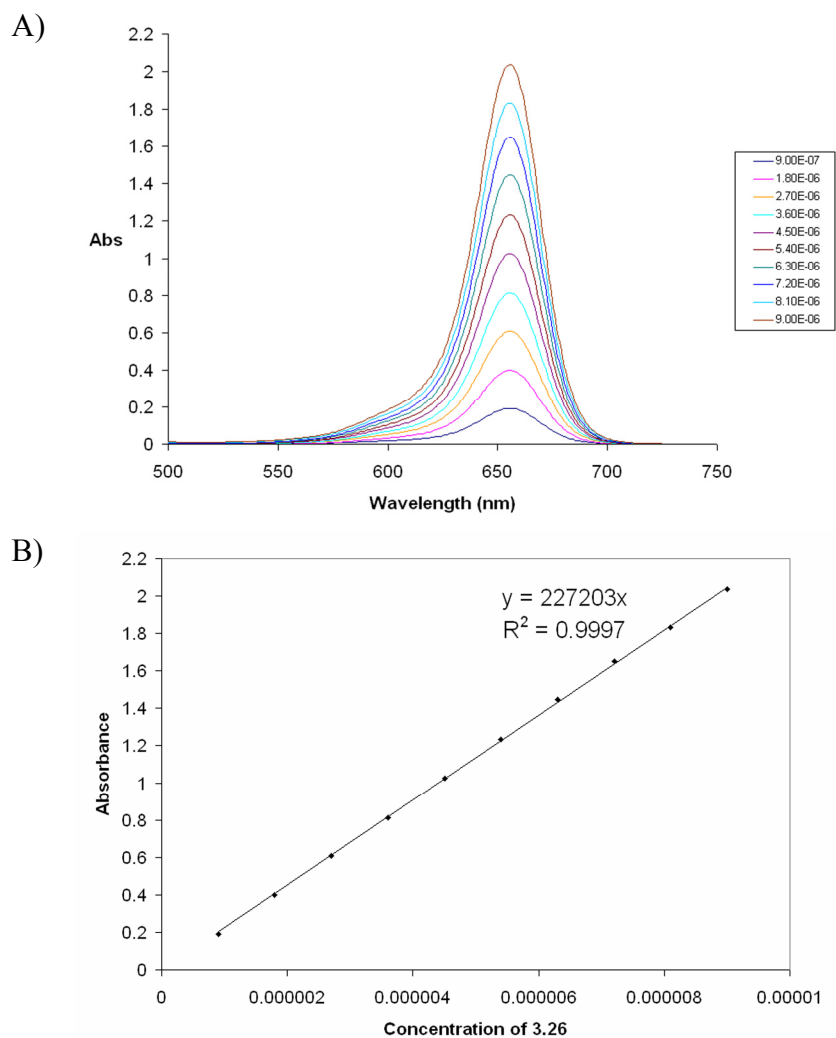


**Figure 3.2** Beer's law analysis of squaraine **3.26** from  $9 \times 10^{-7}$  M to  $9 \times 10^{-6}$  M. Linearity is maintained as high as 2 absorbance units and an extinction coefficient of  $2.3 \times 10^5$  L mol<sup>-1</sup>cm<sup>-1</sup> was obtained.<sup>102</sup>

### 3.3.2 Understanding the Squaraine-Thiol Interaction

Though several reports have now been published on the interactions of squaraines with various nucleophiles, very little is known about the affinity of the nucleophile-squaraine interaction.<sup>38,39</sup> Since work with cyanide anions and thiols by Soto and

coworkers was conducted in water, the interaction was perceived to be complete and not at equilibrium. However, our studies have shown that in organic media, this “dosimetric” system is fairly dynamic and has equilibrium-like properties. Thus, an understanding of this equilibrium is of considerable importance.

### **3.3.2.1 <sup>1</sup>H-NMR Studies**

A former group member, Dr. Karl Wallace, conducted a series of <sup>1</sup>H-NMR studies to fully characterize the nucleophilic addition of the thiol nucleophile to the central four-membered ring. The NMR studies and previous reported literature have shown that squaraine molecules desymmetrize upon the addition of nucleophiles.<sup>39, 85, 101, 103, 104</sup> <sup>1</sup>H-NMR titration studies are thus a viable tool in determining the stability of the complex. For the conditions to be optimal for the nucleophilic attack in chloroform a base was added to facilitate deprotonation of the thiol for greater nucleophilicity. In these preliminary studies, the base 1,8-diazabicyclo[5.4.0]undec-7-ene (DBU) was employed.

Upon the addition of small aliquots of ethanethiol in the presence of DBU (Figure 3.3) to a 37 mM solution of **3.26**, four distinct signals appear at  $\delta$  6.51, 6.59, 7.48 and 7.74 ppm, and are assigned to the aromatic protons of the **3.27** complex. The aromatic protons for **3.26** appear at  $\delta$  6.71 and 8.36. The immediate appearance of signals assigned to the aromatic hydrogen atoms upon each addition of thiol, suggests that **3.27** is a tightly formed covalent complex.

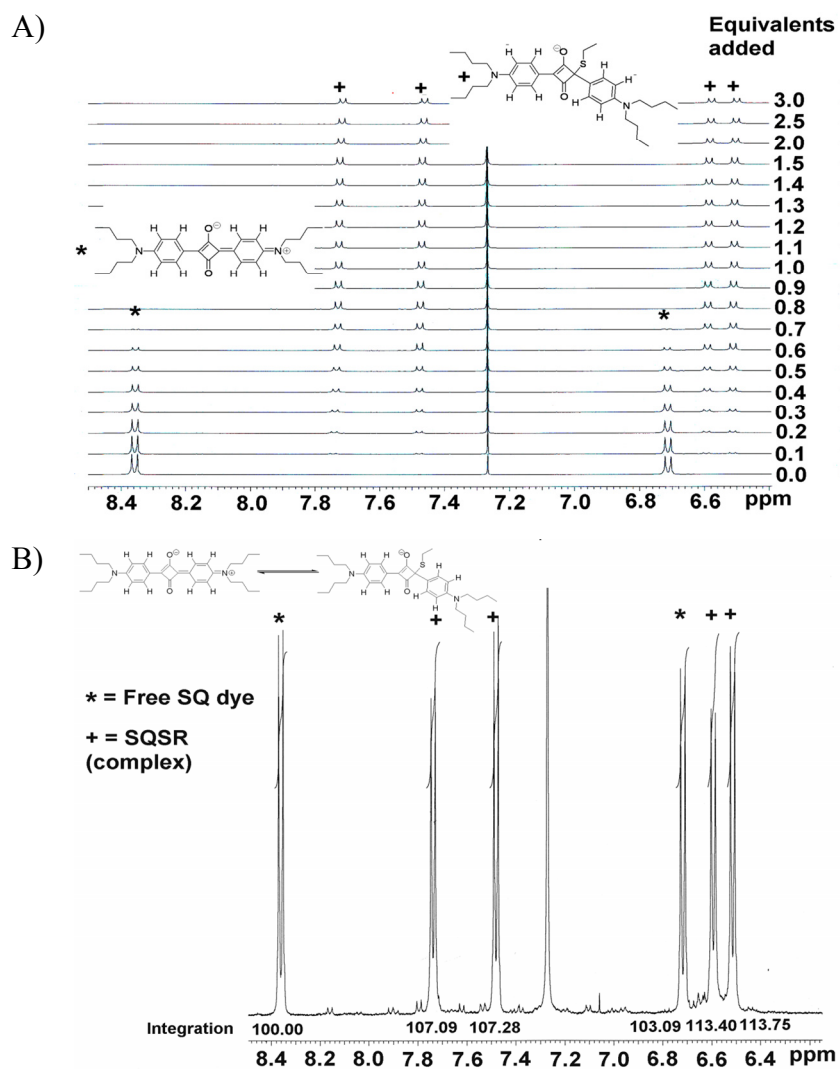


**Figure 3.3**  $^1\text{H}$ -NMR titrations of **3.26** with ethanethiol in the presence of DBU in  $\text{CHCl}_3\text{-}d$ .  $[\mathbf{3.26}]_0 = 37 \text{ mM}$ ;  $[\text{DBU}]_0 = 37 \text{ mM}$ .<sup>101</sup>

### 3.3.2.2 *van't Hoff Analysis*

Further studies on the thermodynamics of the **3.27** complex were later carried out by this author through the use of van't Hoff techniques. Chemical insight into the formation of **3.27** can be gained by measuring the enthalpy ( $\Delta H$ ) and entropy ( $\Delta S$ ), by determining  $K_{\text{eq}}$  at different temperatures. A van't Hoff analysis garners a plot of  $\ln K_{\text{eq}}$



versus  $1/T$  which gives  $\Delta H$  from the slope of the graph and  $\Delta S$  is from the intercept. In this case, **3.27** was first generated by reaction of 1 equivalent each of **3.26** and ethanethiol in DMSO facilitated by the 0.75 equivalents of the base 2,8,9-trimethyl-2,5,8,9-tetraaza-1-phosphabicyclo[3.3.3]undecane, **3.31** (a Verkade base). The use of this base over DBU will be discussed in more detail in a later section. The absorbance of unbound **3.26** was measured at regularly increasing temperature from 288.5 K to 317.8 K to monitor the change in the complex formation. Higher temperatures were not used due to the low boiling point of ethanethiol. The results are shown in Figure 3.4, and they are quite remarkable. Not only did temperature affect the intensity of the absorbance, but there was a slight hypsochromic shift from 656 nm to 654 nm over even this limited temperature range. This blue shifted absorbance indicates that the solvent-solute complex with **3.26** formed in DMSO is breaking up at the relatively low temperatures used here.

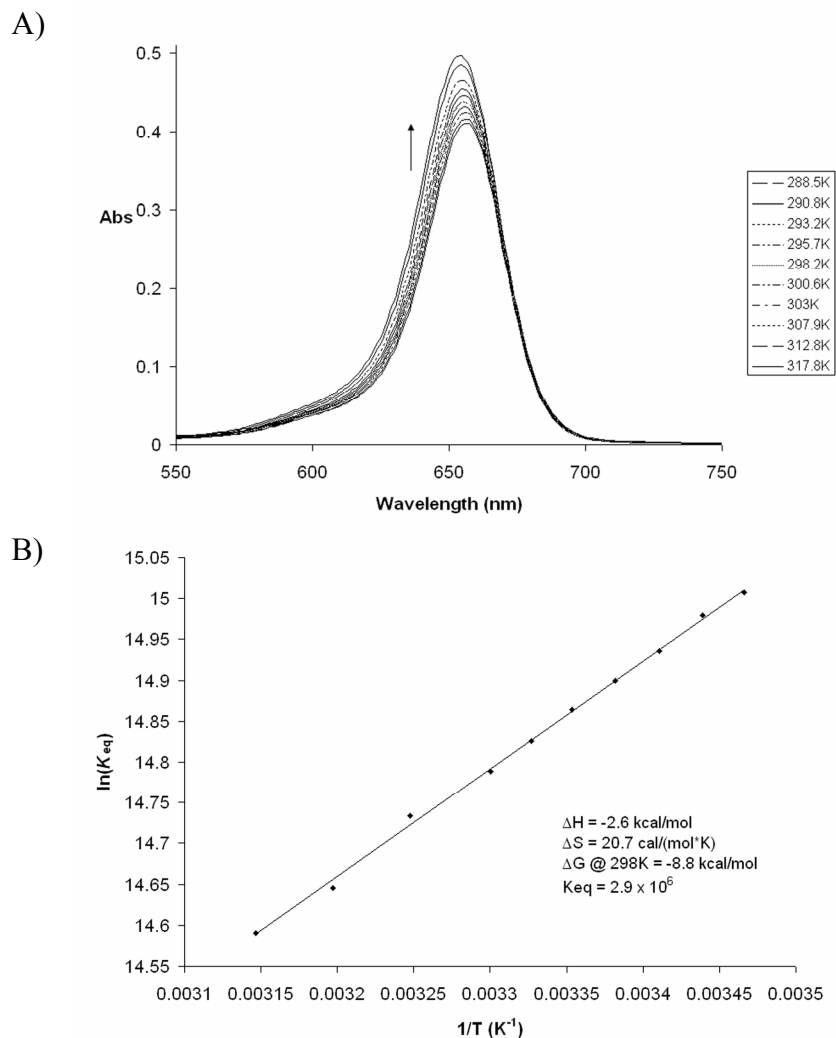


**Figure 3.4** van't Hoff analysis of **3.27** at  $1.2 \times 10^{-5}$  M. A) Spectral data of free **3.26** at temperatures from 288.5 K to 317.8 K showing a break up of the solvent-solute complex. B) van't Hoff plot of  $\ln K_{eq}$  vs.  $1/T$  showing an overall association constant of  $2.9 \times 10^6$  M<sup>-1</sup>.<sup>102</sup>

The thermodynamic parameters garnered from the van't Hoff plot in Figure 3.4B are also quite interesting. The temperature dependent equilibrium constants were derived as follows. The concentration of free **3.26** was calculated from the absorbance at 656 nm based on the extinction coefficient derived above. The bound complex **3.27** and free

thiol concentrations were extrapolated from the concentration of free **3.26** assuming a 1:1 association of thiol with the squaraine. With these concentrations the equilibrium constants at each temperature could be calculated as  $K_{eq} = [\mathbf{3.27}]/([\mathbf{3.26}][\text{RSH}])$ . The plot of the natural log of these values versus  $1/T$  gives the plot shown in Figure 3.4B.

The  $\Delta H$  determined from the slope of the van't Hoff plot was found to be -2.6 kcal/mol whereas  $\Delta S$  taken from the intercept is  $20.7 \text{ cal mol}^{-1}\text{K}^{-1}$ . Thus at 298 K, this association is entropy driven with  $T\Delta S$  contributing 6.2 kcal/mol versus only -2.6 kcal/mol from the enthalpy term. The overall  $\Delta G^\circ$  at 298 K is -8.8 kcal/mol with an association constant of  $2.9 \times 10^6$ . At first glance, these results seem to be quite odd. However, looking back at the mixed solvent study conducted on this same squaraine derivative at high concentrations of the coordinating solvent, a preferential solvation phenomenon occurred in which a 2:1 or 3:1 solvent-solute complex was forming, which shifted the absorbance out of the isosbestic region.<sup>50</sup> Hence, if the introduction of a nucleophile to the electron deficient core serves to break up a higher order solvent-solute complex, the solvent release upon binding would be more entropically favorable than the cost of bringing the squaraine and the nucleophile together. It is also reasonable to imagine that the formation of this bond would not be greatly enthalpically favorable. The bond dissociation energies of C-S single bonds are generally quite low, usually less than 75 kcal/mol, compared even to aliphatic S-H bonds which are usually around 83 kcal/mol.<sup>105</sup> Couple that with the breaks in conjugation and favorable charge transfer interactions that accompany the formation of **3.27**, and it becomes plain that any enthalpic gain in this reaction is surprising. Perhaps the most striking observation is how rare it is to find entropically driven associations in supposedly non-competitive media such as DMSO.

### 3.3.3 Initial Attempts at Pd(II) Detection

Initial work on the Pd(II) chemodosimeter was performed again by Dr. Karl Wallace. Based on the Beer's Law and van't Hoff analyses, it was determined that when ethanethiol and **3.26** were mixed in equimolar quantities in DMSO, the amount of free **3.26** at equilibrium was roughly 1/10 the total concentration. In order to keep the absorbance intensity within the limits of Beer's Law, the total concentration of **3.26** both bound and unbound should be less than  $10^5$  M. However, in an effort to develop "naked eye" qualitative detection of palladium, the concentrations used were such that a large color turn-on would occur at low analyte concentration. Initial studies were conducted in a DMSO-based solution containing a small amount chloroform for solubility purposes. As before, the **3.27** complex was prepared by reacting a thiol (ethanethiol) with a solution of **3.26** in a one-to-one ratio in the presence of a suitable base (DBU) to prepare a complex in situ that has a concentration of 47  $\mu$ M. Upon completion of the reaction, the absorbance at 656 nm is greatly reduced or "switched off". The formation of **3.27** gives rise to a new absorbance band centered at roughly 317 nm. Due to the transient nature of this complex, an accurate extinction coefficient could not be determined, however, it is much less absorbent than the parent squaraine **3.26**. The formation of **3.27** is kinetically slow and takes approximately 24 hours to come to equilibrium. The **3.27** complex must be formed prior to Pd(II) analysis and can be stored briefly for use. When stored in the dark, the solution is stable for roughly 48 hours and is able to retain a response to Pd(II).

#### 3.3.3.1 UV-Vis Titrations

Two palladium salts were used in the initial study.  $\text{Pd}(\text{OAc})_2$  and  $\text{Pd}(\text{PPh}_3)_2\text{Cl}_2$  were chosen due to their extensive use in cross-coupling reactions. Titrations of both palladium species into solutions of **3.27** formed with DBU are shown in Figure 3.5.

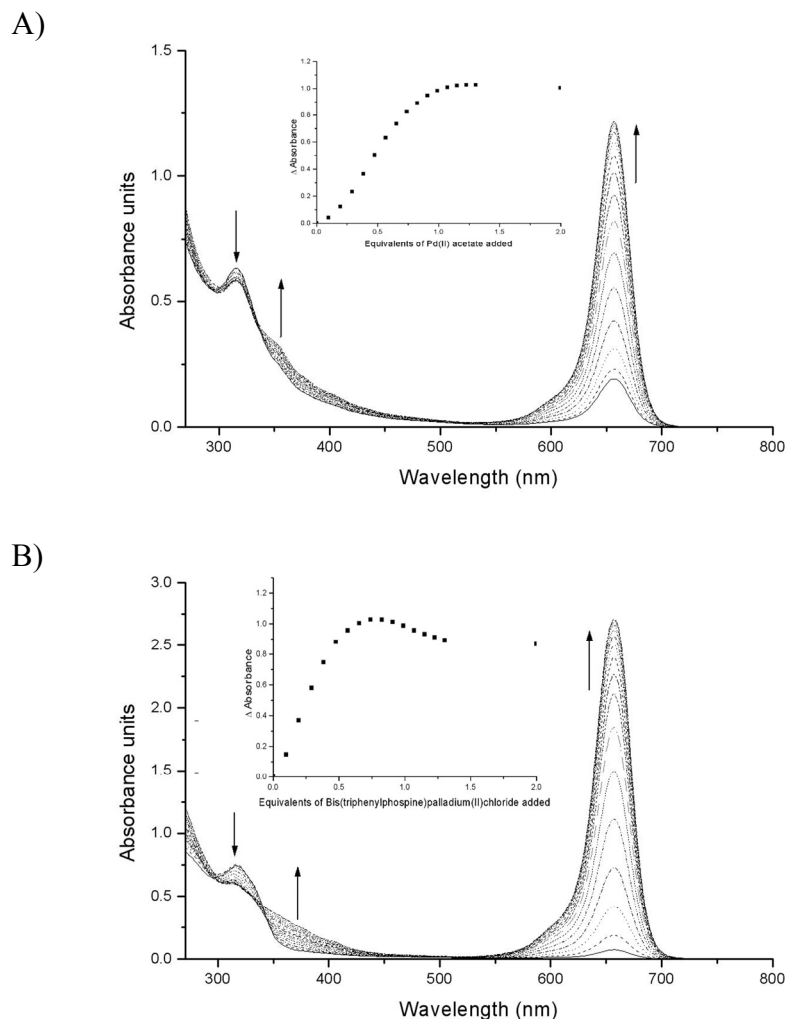


**Figure 3.5** Titrations of A)  $\text{Pd}(\text{OAc})_2$  and B)  $\text{Pd}(\text{PPh}_3)_2\text{Cl}_2$  into solutions of **3.27** at  $2.35 \times 10^{-5}$  M in DMSO. **3.27** complexation was facilitated with 1 equivalent of ethanethiol and 2 equivalents of DBU.<sup>101</sup>

Upon the addition of the palladium(II) salts, the band at 317 nm decreases and the band at 656 nm increases, switching “on” the color. An isosbestic point is observed near 344 nm indicating the interconversion of two distinct species with absorbances in that region. The small band that appears at 373 nm was assigned to a palladium-thiol species forming in solution. The isotherms obtained for the titration experiments are sigmoidal in

shape because at equilibrium, thiol complexation to the squaraine is not complete. Thus, small amounts of uncomplexed thiol exist in solution, and the initial palladium that is added binds first to the “free” thiol. Once the free thiol has been bound the remaining palladium then scavenges thiol away from the **3.27** complex and turns on the colorimetric response. The saturation at one equivalent of palladium suggests that the species responsible for the absorbance at 373 nm is a monothiolated palladium species. Interestingly, the isotherm for the  $\text{Pd}(\text{PPh}_3)_2\text{Cl}_2$  does not plateau but instead a slight decrease in absorbance is seen again at 656 nm as more  $\text{Pd}(\text{II})$  salt was added. The formation of a covalent Pd-S bond liberates a chloride anion, however from previous studies on nucleophilic addition to squaraines, the probability that this chloride is responsible for the subsequent “re-quenching” of **3.26** is small.<sup>39</sup> A more likely scenario is that the formation of the Pd-S bond significantly reduces the electrophilicity of the Pd center causing one or both of the triphenylphosphine ligands to dissociate. A similar effect was observed in the previous chapter (Scheme 2.9).<sup>106</sup> The  $\text{PPh}_3$  group thus indirectly displaced by the thiol is itself slightly nucleophilic and attacks the electron deficient 4-membered ring system of **3.26**. This result was confirmed by preparing a solution of **3.26** and adding one equivalent of  $\text{PPh}_3$  with the observation of a color “turn-off”. The ultimate sensitivity for these two  $\text{Pd}(\text{II})$  salts using this method was roughly  $10^{-6}\text{M}$ .

### **3.3.3.2 Fluorescence Titrations**

Even though there is an inherent interest in “naked eye detection” the sensitivity is limited even when chromophores with large extinction coefficients, such as squaraines, are used. In an attempt to lower the sensitivity from the above mentioned  $\mu\text{M}$  range, Dr. Wallace performed a series of fluorescence titrations. Squaraine **3.26** has been shown to

have very strong fluorescence emission in many organic solvents.<sup>46</sup> Analogously to the colorimetric studies, it was anticipated that once the thiol attacks the electron deficient ring the fluorescence would be “switched off.” The break in conjugation and the deviation from planarity accompanying the addition of the nucleophile should introduce a number of new non-radiative decay pathways. As was seen in the UV-Vis studies, the solution of **3.27** is still slightly fluorescent due to the small amount of free **3.26**. A 0.24  $\mu\text{M}$  solution of **3.27** was prepared in a similar fashion to the UV-Vis studies in  $\text{DMSO}:\text{CHCl}_3$ , and a  $\lambda_{\text{Ex}}$  at 660 nm was observed (Figure 3.6). The initial fluorescence spectrum shows a slight fluorescent signal at 660 nm indicating that complex formation is once again not complete. Figure 3.6 shows the fluorescence titration curves obtained for both palladium salts. As with the colorimetric titrations, the fluorescence signal shows a “turn on” upon the addition of palladium. Again a sigmoidal curve is seen in each case, and again there is a decrease in the fluorescence signal upon the addition of  $\text{Pd}(\text{PPh}_3)_2\text{Cl}_2$ . This decrease is more dramatic than observed in the UV-Vis titrations and can be attributed to the addition of slight PET quenching from the free phosphine. Nevertheless, the two techniques compliment each other and are in good agreement.

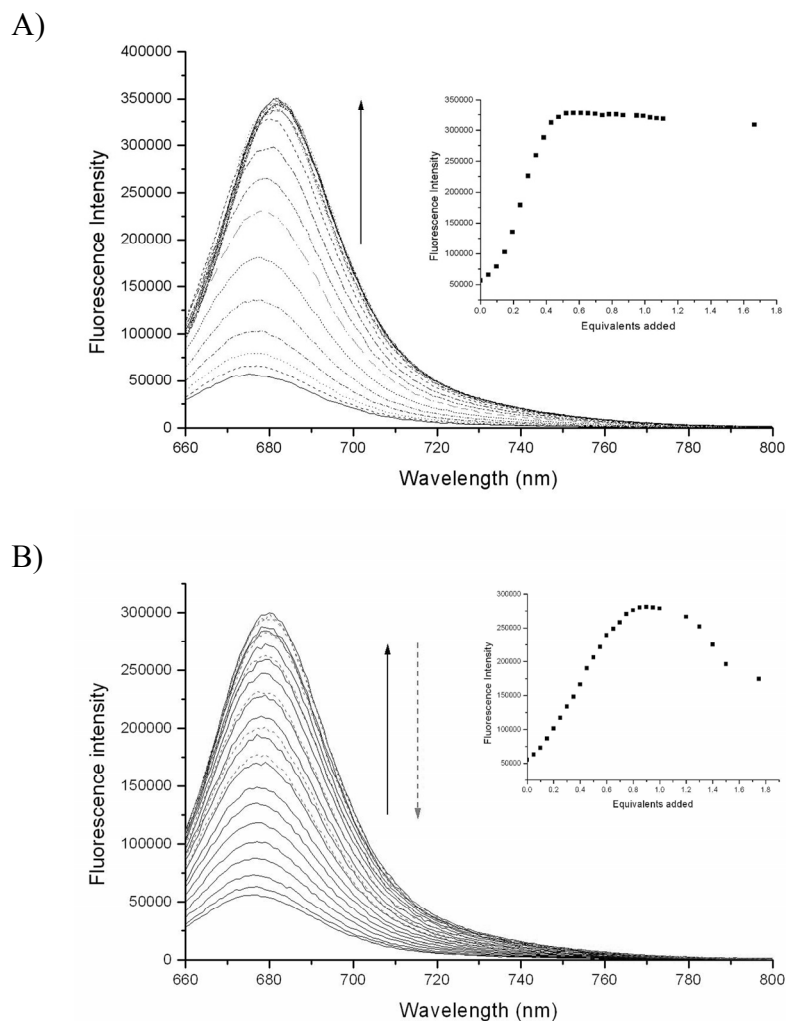


**Figure 3.6** Fluorescence titrations of A)  $\text{Pd}(\text{OAc})_2$  and B)  $\text{Pd}(\text{PPh}_3)_2\text{Cl}_2$  in DMSO. Complex **3.27** was formed with ethanethiol and 2 equivalents DBU. Theoretical  $[\mathbf{3.27}] = 2.35 \times 10^{-7} \text{ M}$ .  $\lambda_{\text{ex}} = 650 \text{ nm}$ ;  $\lambda_{\text{max}F} = 660 \text{ nm}$ .<sup>101</sup>

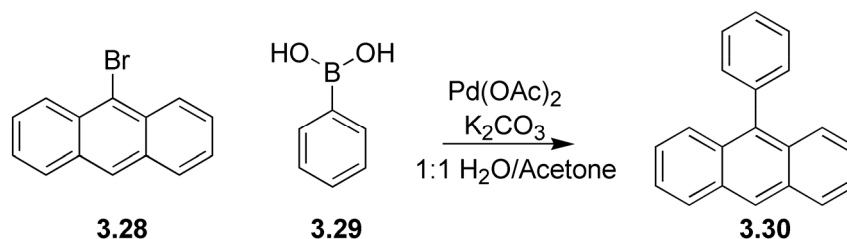
### 3.3.3.3 Testing Unknowns

It was quite apparent that this system could be used in a controlled situation to quantitatively detect Pd(II) salts. However, no tests had been conducted for the use of this assay on actual samples taken from a cross-coupling reaction. First, calibration



curves using both UV-Vis and fluorescence were created using several solutions containing known quantities of  $\text{Pd}(\text{OAc})_2$ . The resulting curves are shown in Figure 3.7. To perform real sample tests, several Suzuki coupling reactions were run as shown in Scheme 3.13. The Suzuki coupling was chosen because it uses the palladium(II) acetate catalyst and a non-nucleophilic carbonate base. When aliquots were taken directly from the reaction and administered to the **3.27** solutions, the result was a moderate turn-on of the 656 nm band corresponding to free **3.26** (Figure 3.7c). However, the calculated concentration did not match up well with the calibration curve. Furthermore, administration of samples taken from the quenched or worked up Suzuki reaction, showed no turn-on at all.

**Scheme 3.13**



It was observed that, often during the course of a palladium catalyzed reaction, much of the palladium is converted to  $\text{Pd}(0)$ , and that upon quenching, all remaining active catalyst is either precipitated as palladium black or tied up in bulky, intractable ligands created during the reaction. These palladium species are usually either insoluble or undetectable by this chemodosimeter. One possibility to remedy this problem is to generate a uniform  $\text{Pd}(\text{II})$  species *via* oxidation or ligand exchange with nitric acid to form the highly soluble nitrate salt. To characterize this assay for use with nitric acid digested samples, several titrations were performed with  $\text{Pd}(\text{NO}_3)_2$ .

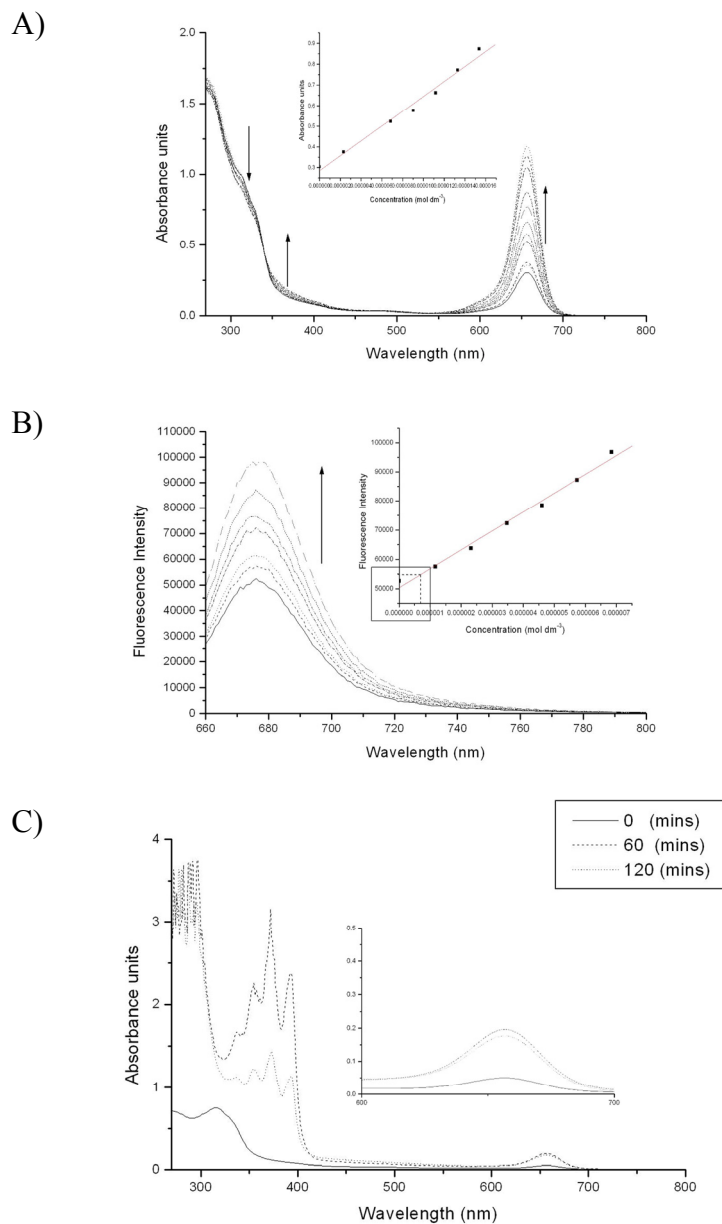


**Figure 3.7** A) Colorimetric calibration curve for  $\text{Pd}(\text{OAc})_2$  in DMSO.  $[\text{3.27}] = 2.35 \times 10^{-5} \text{ M}$ . B) Fluorescence calibration curve for  $\text{Pd}(\text{OAc})_2$  in DMSO.  $[\text{3.27}] = 2.35 \times 10^{-7} \text{ M}$ . C) UV-Vis spectra of  $\text{3.27}$  solution with addition of 25  $\mu\text{L}$  aliquots from the Suzuki coupling in Scheme 3.13 at 0, 60, and 120 minutes reaction time.<sup>107</sup>

### 3.3.4 Pd(NO<sub>3</sub>)<sub>2</sub> Characterization

To test the viability of nitric acid digestion as a means to homogenize the residual palladium in the product of a coupling reaction, a series of four Suzuki couplings according to Scheme 3.13 were conducted. Each reaction was allowed to react until completion, at which point the reactions were quenched and each was handled in a different manner. The first reaction was given no work up or purification; the second reaction was filtered through celite with hexanes; the third reaction was passed through an alumina plug with hexanes; the fourth reaction was run down a full silica column with hexanes and only the product fraction was collected. The residues remaining from each of these reactions after work up, were subjected to 4N HNO<sub>3</sub> at 80 °C for 30 minutes. After neutralization and extraction with methylene chloride, the samples were tested against the assay. The results are shown in Figure 3.8 and show that the formation of the nitrate salt indeed allows for spectroscopic determination with this assay.

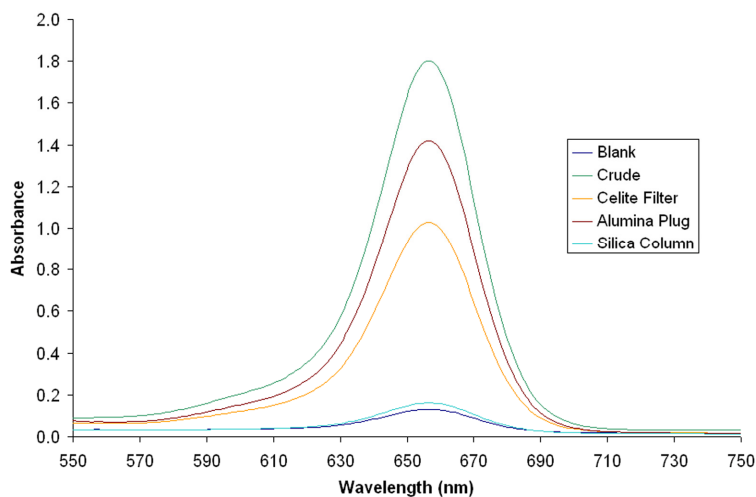


**Figure 3.8** Spectral data for samples from Suzuki couples digested with nitric acid. The samples were subjected to different work up conditions prior to nitration as shown. [3.27] =  $2.35 \times 10^{-5}$  M.

With the usefulness of the method tested, the displacement assay, which had only been tested previously with  $\text{Pd}(\text{OAc})_2$  and  $\text{Pd}(\text{PPh}_3)_2\text{Cl}_2$ , required characterization with  $\text{Pd}(\text{NO}_3)_2$ . Initially, the **3.27** complex was formed as described above using a 1:9 v/v chloroform:DMSO solvent mixture in the presence of 2 equivalents of DBU. The titration of  $\text{Pd}(\text{NO}_3)_2$  into a 24  $\mu\text{M}$  solution of **3.27** is shown in Figure 3.9. Interestingly, saturation occurred at 0.5 equivalents of palladium(II) nitrate suggesting a novel 2:1 interaction. We attributed this anomaly to the increased electrophilicity of the nitrated palladium center, however upon further review of the spectral data, it was observed that we were not achieving full turn on of **3.26** even after reaching saturation. A plot of the calculated concentration of **3.26** from absorbance at 635 nm ( $\epsilon \approx 99,000$ ) versus the concentration of palladium(II) added (Figure 3.10) should have a slope of 2 based on the saturation point of the titration. However, the slope is found to be 1 suggesting 1:1 binding. In fact, extrapolation of the initial slope on the isotherm in Figure 3.9b gives 1:1 binding based on Beer's Law equivalence.

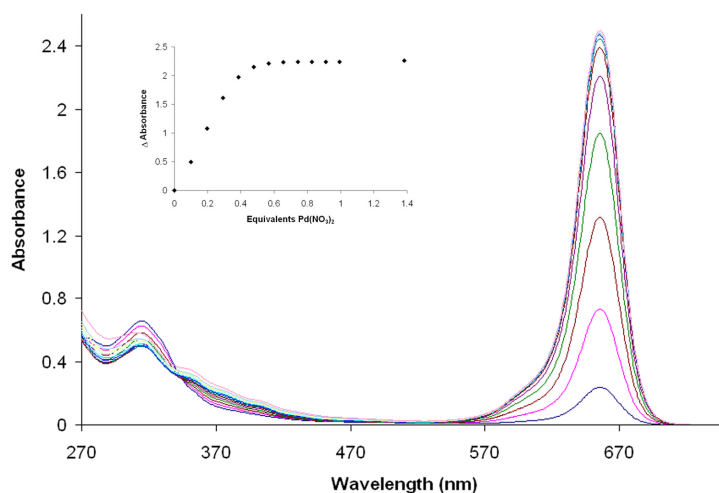


**Figure 3.9** Titration data for  $\text{Pd}(\text{NO}_3)_2$  into **3.27** ( $2.35 \times 10^{-5}$  M in DMSO) formed with ethanethiol and 2 equivalents DBU.

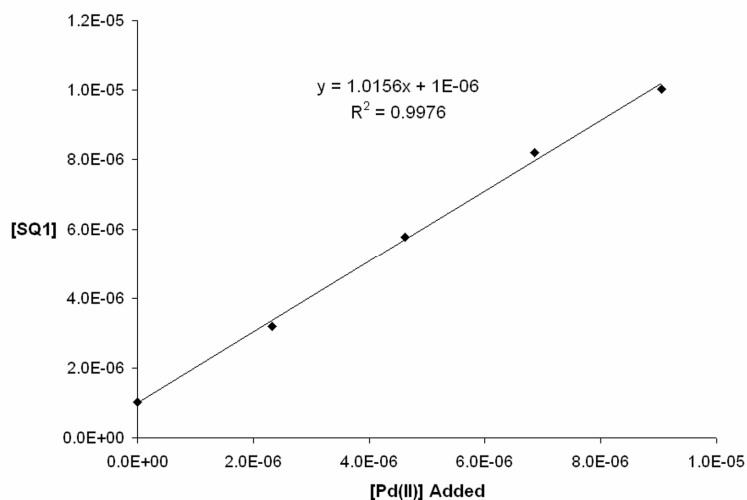
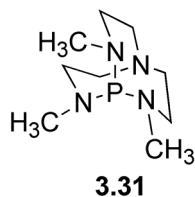


**Figure 3.10** Plot of the concentration of **3.26** calculated from the extinction coefficient versus the concentration of palladium added in the titration from Figure 3.9.

To solve this quandary, we looked into all aspects of the assay. All reagents were found to be analytically clean by NMR and mass spectral analysis. In addition to degassing, the solvents were dried as well, which gave similar results. We examined the base, DBU, and discovered that we had made a poor selection. In aqueous solution, the  $pK_a$  of  $H\text{-DBU}^+$  is roughly 12, and that of a typical aliphatic thiol is close to 10.<sup>108</sup> Hence, in water DBU is a suitable base to produce the thiolate anion. However, the polar aprotic environment of DMSO drastically changes this relationship. In the cationophilic DMSO medium, the  $pK_a$  of  $H^+\text{-DBU}$  does not differ very much, however, that of a thiol is dramatically increased to near 18.<sup>109</sup> Thus, with DBU in DMSO, the complex formation is occurring under general base catalysis rather than the expected specific base catalysis. In other words, the sulfur-squaraine bond must show a significant amount of formation before the S-H proton is acidic enough for DBU deprotonation. This revelation explains why the complex formation was kinetically slow under these conditions. In addition to being inadequate as a base, it was also discerned that DBU was

too nucleophilic and when added to **3.26** in excess (4+ equivalents), fairly rapid decolorization ensued. Our first instinct then, led us to assume that the discrepancy between the saturation isotherm and the Beer's Law equivalency arose from a deactivation of a portion of the squaraine through irreversible nucleophilic attack by DBU.

### 3.3.3.1 The Verkade Base



To resolve both the basicity and nucleophilicity issues we turned to the so-called “super bases.” In particular, we chose the tricyclic phosphatrane base, **3.31** also known as a Verkade base.<sup>110</sup> Reported to have a protonated  $pK_a$  of 26.8 in DMSO, **3.31** is basic enough to act as a general base catalyst for the **3.27** complex formation.<sup>111</sup> Several tests were conducted to determine the best ratio of base to thiol to achieve both facile complex formation and full recovery of **3.26** upon introduction of analytes. Using 0.75 equivalents of **3.31** gave the best results shown the spectra and isotherm of a titration conducted at 4 hours after starting the formation of **3.27** in Figure 3.11. For this new system, titrations were performed at a lower concentration of **3.27** ( $8.8 \times 10^{-6}$  M) to maintain Beer's Law linearity over the complete titration range. Interestingly, after 4 hours of reaction time, full turn on and 1:1 binding were observed, however, when longer wait periods were used, both diminishing recovery and saturation points closer to the 0.5 equivalents were observed in the DBU systems.

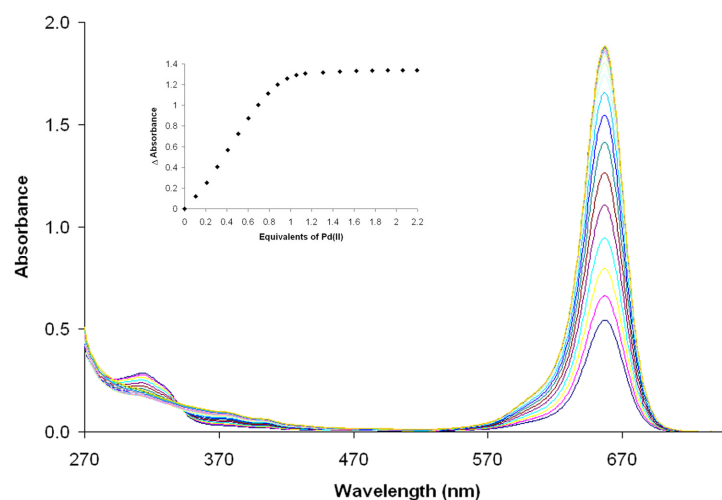


**Figure 3.11** Titration of  $\text{Pd}(\text{NO}_3)_2$  into  $8.8 \times 10^{-6}$  M **3.27** in DMSO formulated with ethanethiol and Verkade base **3.31**. Titration was conducted after 4 hours reaction time between squaraine **3.26** and ethanethiol.

Several repeats of this titration were conducted for reproducibility, yet the system proved to be erratic and even strict adherence to a 4 hour limit on the interaction between the thiol and **3.26** was unreliable. Fortunately, if the system was allowed to come to a true equilibrium over a 12-15 hour period, the data were much more stable from trial to trial. However, as stated above, longer reaction time led to lower color recovery and apparent 2:1 stoichiometry. Since this base is very non-nucleophilic it is unclear from what source the loss arises. In fact, these data suggest that our earlier assumptions dealing with the nucleophilicity of DBU might also have been incorrect. Regardless of which system is being used, the reason for the loss of signal remains a mystery. Our theory for the 2:1 binding stoichiometry once again arises from the increased electrophilicity of the palladium(II) nitrate salt. Figure 3.12 gives titration data with the Verkade system in DMSO after 12-15 hours of complexation time.

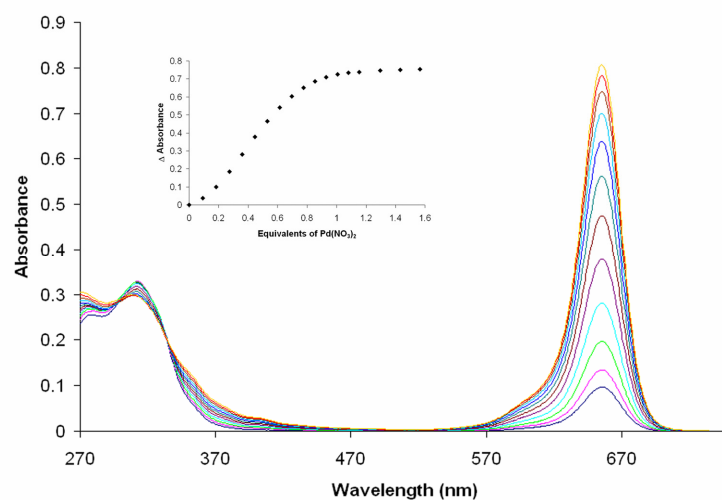


**Figure 3.12** Titration of  $\text{Pd}(\text{NO}_3)_2$  into  $1.2 \times 10^{-5}$  M **3.27** in DMSO formulated with ethanethiol and Verkade base **3.31**. Titrations were conducted after 12-15 hours reaction time between squaraine **3.26** and ethanethiol

### 3.3.3.2 Calibration Curves for DMSO-Verkade System

Samples of known  $\text{Pd}(\text{NO}_3)_2$  concentration were prepared and tested against the titration data to determine its usefulness as a calibration curve for unknown samples. Unfortunately, in all cases using the standard 5 minute wait period between sample injection and scan, the samples tested came well short of their theoretical turn on quantity. Though much of the work described above focused on the thermodynamics of these associations, the discrepancies between the titration data and the known samples arises from a kinetic effect. Throughout the course of a titration such as the one shown in Figure 3.12, each aliquot injected is given a 5 minute interval during which equilibration was though to be reached. While the titration data is a good measure of the overall turn on one should expect, when applied to a sample with an intermediate concentration, it is indeterminate how long the thiol-scavenging reaction will take to complete.



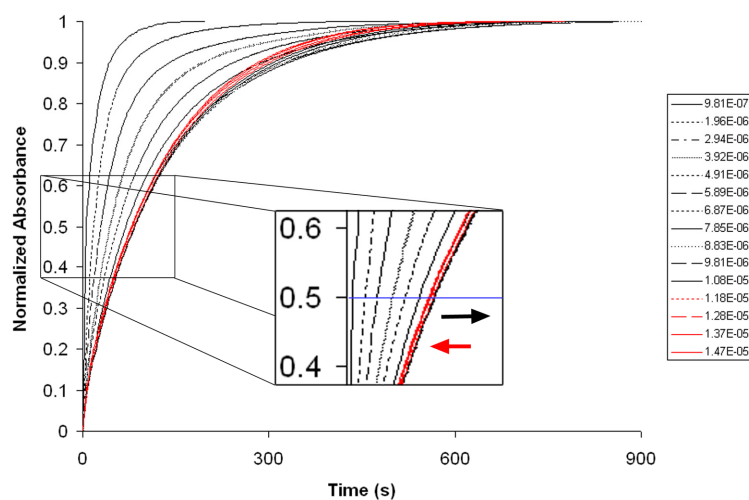


**Figure 3.13** A) Normalized kinetic traces of calibration curve data using a series of samples of increasing palladium concentration. Below 1 equivalent shown in black, above shown in red. The inset shows the half-time.  $[3.27] = 1.2 \times 10^{-5}$ ;  $[Pd]$  range =  $9.1 \times 10^{-7}$  to  $1.5 \times 10^{-5}$

To remedy this error and generate a truer calibration curve, a series of samples with steadily increasing Pd(II) concentrations was prepared. Each sample was assigned a fresh solution of complexed **3.27**, and upon injection of a 20  $\mu$ L aliquot, the color turn on was monitored over time at 656 nm. The normalized kinetic traces are shown in Figure 3.13. The time to full equilibrium was found to increase as the concentration of Pd(II) increased until saturation as described by the isotherm in Figure 3.14A. After the saturation point, the time to full color turn on for each sample decreased as expected. The inset in Figure 3.13 shows the region at which the traces reach the half-time to full turn on. The line drawn at 0.5 normalized absorbance units in the inset shows that as the concentration of the sample increases, the half-time to completion becomes steadily longer until the isotherm of maximum absorbance reaches saturation ( $\sim 0.6$  equivalents Pd). Past this saturation point, the half-time stabilizes briefly then begins to shorten past a 1:1 equivalency. The traces shown in red are those of samples containing greater than 1

equivalent of Pd(II). Since a large concentration range gives a regular increase in the half-time to reaction completion, the implication is that for unknown samples containing less than a full equivalency of palladium, the half-time to full turn on could be used as a secondary validation in concentration determination (Figure 3.14). When using newly formulated **3.27** to test known samples of arbitrary concentration, the half-time isotherm gave results that were much more accurate.

The results for a set of arbitrarily selected samples of known  $\text{Pd}(\text{NO}_3)_2$  concentration with this system are shown in Table 3.2. The first two sets of data are derived against the absorbance calibration curve shown in Figure 3.14A, and against the half-time calibration curve shown in Figure 3.14B. The kinetics of the color turn on were monitored for every sample to ensure the true maximum absorbance was reached. For the samples measured against the absorbance calibration curve, the error was quite large with an average of ~27%, yet the error was consistently underachieving, suggesting fairly good precision. Since these results were taken using a newly made stock solution of **3.27**, the large error could possibly be attributed to inaccuracies in weighing and dilution in the stock preparation. We have seen that the absolute absorbance values can vary significantly from titration to titration using different stock solutions. Usually there is good correlation in the relative absorbance values between stock solutions, however in this manner of data collection there appears to be a systematic error based on the total absorbance value.

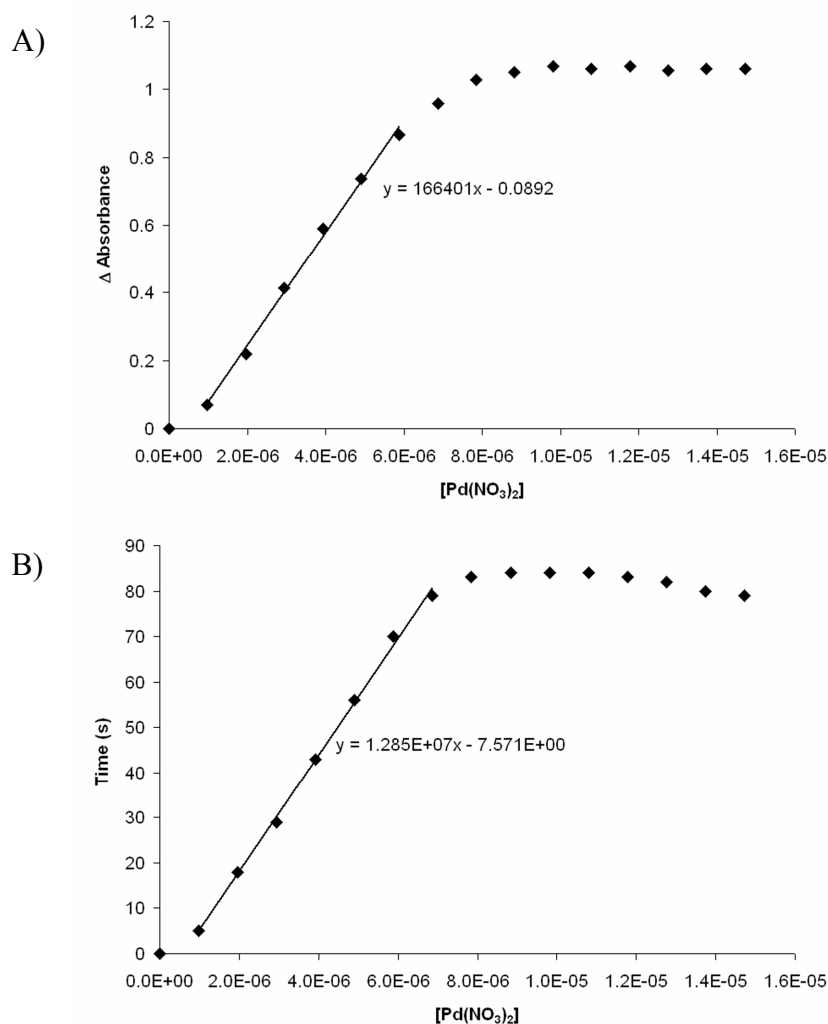


**Figure 3.14** A) Maximum absorbance calibration curve with linear fit and B) half-time calibration curve with linear fit for kinetics determination shown in Figure 3.13.

Determination of these known samples against the half-time calibration curve (Figure 3.14B) gave an overall better average error at  $\sim 14\%$ , however, the precision was quite poor, and there did not appear to be any systematic deviation as with the absorbance values. Since there was no apparent trend to the error, it is doubtful whether this method would actually be a viable recourse for concentration determination of unknown samples.

**Table 3.2** A) Four samples of known concentration tested against the absorbance calibration curve (first column), the half-time calibration curve (second column). B) Data for arbitrary known samples tested against a fully equilibrated titration isotherm generated from the same stock solution of 3.27.

A)	Sample	Concentration (M)	$\Delta$ Absorbance	Half-time (s)	
	1	1.56E-06	0.1000	15	
	2	2.61E-06	0.2148	26	
	3	5.73E-06	0.6376	43	
	4	6.78E-06	0.7623	66	
	Sample	[Pd] from Abs Calibration	[Pd] from Half-time Calibration		
	1	1.14E-06	1.76E-06		
	2	1.83E-06	2.61E-06		
	3	4.37E-06	3.94E-06		
	4	5.12E-06	5.73E-06		
	Sample	% Error	% Error		
	1	27.3	12.3		
	2	29.9	0.2		
	3	23.8	31.4		
	4	24.5	15.5		
	Average Error	26.4	14.9		
B)	Sample	Known [Pd]	[Derived #1]	[Derived #2]	Average %Error
	1	1.62E-06	1.62E-06	1.48E-06	4.6
	2	2.70E-06	2.87E-06	2.58E-06	5.3
	3	4.33E-06	4.74E-06	4.51E-06	6.8
	4	6.49E-06	7.36E-06	7.07E-06	11.1
	Average Error				6.9
Average Relative Deviation				3.6	

To alleviate the systematic error from the absorbance calibration, we conducted a third round of tests. In this case, a titration was performed just prior to determinations of the arbitrary samples and all experiments were conducted from the same stock solution of 3.27. The calibration titration was conducted with kinetic monitoring of each aliquot injection and gives the spectra and isotherm shown in Figure 3.12. Two determinations were conducted at each test sample concentration, and the absorbance values were then

applied to the sigmoidal Richards type 1 function curve fit of the isotherm. In this fashion the average error over the concentration range tested was greatly reduced to 7%. At low concentrations, the error tended to be low, whereas higher concentrations lead to over estimation; however the extent of the error is fairly uniform with an average relative deviation of roughly 4%. Thus for practical use we recommend that calibration *via* titration should be conducted for every new stock solution of **3.27** prepared.

#### **3.3.4 UV-Vis Studies in DMF**

An unfortunate side effect of using basified DMSO to perform a study involving thiols is that several factors converge to create a virtual perfect storm for disulfide bond formation. DMSO is inherently oxidative in nature even apart from its ability to dissolve large quantities of molecular oxygen. As disulfide bond formation requires oxidation of the two sulfurs, DMSO is a perfect solvent to facilitate the reaction. In the presence of base, the reaction, which involves a thiol deprotonation step, is further enhanced. Disulfide formation is prohibitive of this assay being successful, and drastically shortens the lifetime of the **3.27** complex. Also, based on the work in the previous chapter, the squaraine **3.26** was tested for its peroxyoxalate chemiluminescent (POCL) behavior. Through a qualitative assessment, **3.26** appears to have extremely high chemiluminescence yields and gives the striking effect of looking blue in lighted areas and red in the dark. Unfortunately, the POCL reaction is inhibited in DMSO solutions. In order to find a suitable solvent system which was less beneficial for disulfide bond formation yet advantageous for both Pd(II) detection and chemiluminescence measurement, the formation of **3.27** was attempted in several different polar aprotic solvents. Neither acetonitrile, THF, chloroform, nor ethyl acetate gave appropriate decolorization. Of all solvents tested only DMF was shown to facilitate complete

complex formation. Our first attempts at complex formation using DMF and the Verkade base **3.31** as in the DMSO system proved disastrous, as the complex **3.27** was too tight to be disrupted by the Pd(II) salt. It was determined through a series of experiments using various amounts of the Verkade base **3.31** that no exogenous base was required for complex formation in DMF.

Unfortunately, DMF alone has the unfortunate attribute of decolorizing the squaraine **3.26**. DMF is often produced from a catalytic coupling of carbon monoxide and dimethyl amine, and under favorable conditions, DMF can degrade back to those starting materials. Heat, acid, and base have all been shown to facilitate this degradation.<sup>112</sup> The slight presence of dimethyl amine in even the purest DMF plays two opposite roles with regards to this dosimeter. It first and foremost acts as the base to facilitate the **3.27** complex formation, allowing for the process to occur without adding an extra reagent. Adversely, this amine has proven nucleophilic enough to attack the squaraine and destroy its usefulness. We have found qualitatively that the rate of nucleophilic attack of dimethyl amine is slow with respect to thiol addition. The rate difference is probably due to two main factors. The first and most obvious, is that when using relatively pure DMF, there is very little of this amine present. The second factor is that the amine is a neutral nucleophile which is more basic than it is nucleophilic.<sup>113</sup> The thiol on the other hand, while not very acidic in aprotic media, is a very good nucleophile. As with DBU in DMSO, it is expected that dimethyl amine facilitates the nucleophilic attack *via* general acid catalysis. The stability of the **3.27** complex in DMF as opposed to the amine-squaraine coupling allows the solutions to be usable for 2-3 days after initial preparation. An unfortunate consequence of the presence of an auxiliary nucleophile in this system, is that a true Beer's Law analysis could not be performed. However, based on qualitative assessments, the extinction coefficient of **3.26** in DMF is

reduced by about half from the value in DMSO. The absorbance  $\lambda_{\text{max}}$  sees a hypsochromic shift to 649 nm as expected from the lowering of the  $\pi^*$  value of DMF (0.875) versus DMSO (1.000).<sup>50, 51</sup> This reduction of excited state coordination by the solvent may also explain the diminished absorptivity. The small hypsochromic shoulder still appears indicating the presence of a small amount of H-type aggregates in the DMF solution.

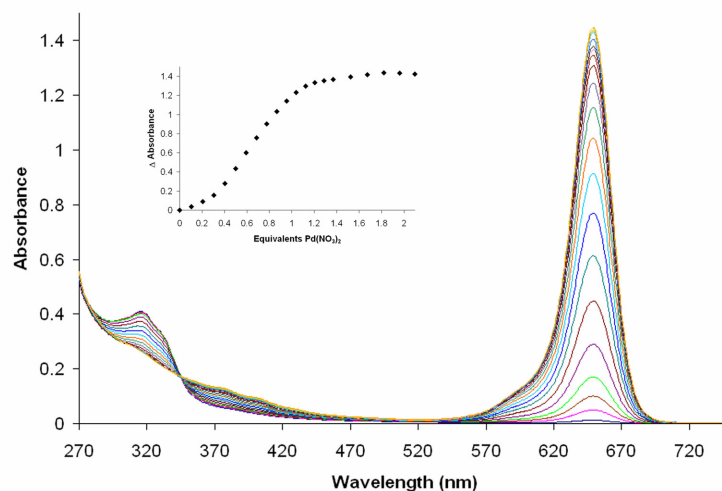


**Figure 3.15** Titration of  $\text{Pd}(\text{NO}_3)_2$  into **3.27** ( $1.2 \times 10^{-5}$  M) in DMF with no exogenous base.

Several titrations were conducted to assess the viability of the palladium sensing assay in DMF. Figure 3.15 shows the results of a typical titration with  $\text{Pd}(\text{NO}_3)_2$ , and shows a 1:1 isotherm. It was found that the best data arose from titrations conducted when the **3.27** complex solutions were 10-24 hours old. Though the complex formation appears to only require 2-3 hours to come to equilibrium, titrations conducted after only 4 hours showed poor binding stoichiometry at 1.3:1. It is unclear why this phenomenon occurs. The return to 1:1 binding, as opposed to the apparent 2:1 seen in DMSO, most likely arises from a decrease in the nucleophilicity of the thiol in DMF and the increase in

strength of the **3.27** complex. All titrations in DMF showed remarkable isosbestic fidelity at 344 nm as compared to previous experiments in DMSO which showed deviation after saturation. Experiments in DMF were conducted at a slightly higher concentration to account for lower absorptivity. Due to either a higher affinity of the **3.27** complex or residual dimethyl amine complexing to the initial aliquots of Pd(II), the isotherms for experiments run under these conditions exhibit a much stronger sigmoidal character than previously observed in DMSO.

#### ***3.3.4.1 Calibration Curve for the DMF system***

With the new solvent system well characterized, calibration of the DMF system against unknowns was attempted. As with the DMSO-Verkade system, calibration against the titration data gave erroneous results due to the reaction time of thiol scavenging. These results were much more pronounced in the DMF solvent system, and the reason became apparent from the kinetics experiments. In a set of experiments analogous to those described for the DMSO-Verkade system, a set of 14 samples of increasing Pd(II) concentration were tested, each with fresh mixtures of **3.27** at  $1.2 \times 10^{-5}$  M. The normalized kinetic traces are shown in Figure 3.16A.



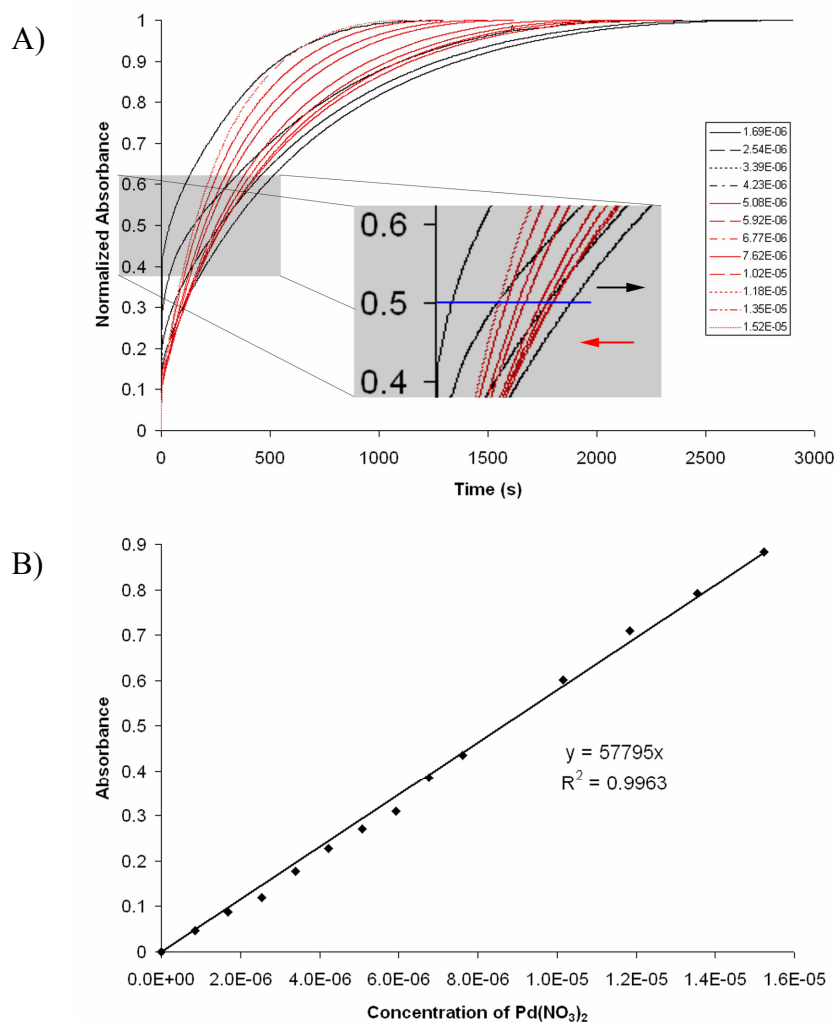


**Figure 3.16** A) Normalized kinetic traces for  $\text{Pd}(\text{NO}_3)_2$ -induced color turn-on of the 3.27 complex. Inset shows the trend in the half-times to completion.  $[\text{3.27}] = 1.2 \times 10^{-5} \text{ M}$  B) Isotherm of absolute absorbance values for kinetics in A showing no saturation.

The most obvious difference from the previous study is that the reaction times for full turn on are significantly longer, on the order of 45 minutes for intermediate concentrations. The second major difference is that the reaction half-times began to shorten at a much lower concentration than with the DMSO system. This result precludes any possible use of the reaction half-times as a diagnostic tool. Finally,

looking at the absorbance calibration curve in Figure 3.16B, there is no appreciable saturation curvature even well passed a full equivalent of Pd(II) has been added. It is unclear from where this apparent 1:X ( $X>1$ ) binding equivalency arises. Saturation is always observed in titration data, yet the linear fit of the calibration curve in Figure 3.16B is reasonably accurate over a wide concentration range.

Table 3.3 shows the results of three arbitrary samples of known Pd(II) concentration tested against the calibration curve in Figure 3.16B. Note that with this calibration curve, the absolute absorbance values gave better accuracy and precision than relative absorbance values, albeit judged only on these three samples. The average error over the concentration range tested is 13% which is somewhat worse than the DMSO-Verkade system when tested against a titration. Since the titrations with the DMF system are all relatively uniform in both relative and absolute absorbances, it can be assumed that this calibration curve could be used as is without the need to conduct a titration with each new formulation of **3.27**.

**Table 3.3** Data for three samples of known Pd(II) concentration tested against the calibration curve in Figure 3.16B.

Sample	Known [Pd] (M)	Maximum Abs	Calculated [Pd] (M)	% Error
1	2.96E-06	0.1417	2.58E-06	13.1
2	6.35E-06	0.4202	7.18E-06	14.7
3	9.73E-06	0.6551	1.12E-05	13.0
Average Error				13.6%

### 3.4 CONCLUSIONS

In this chapter we have discussed the combination of the two main components of a molecular sensing/signaling assay. The recognition element chosen was of the chemodosimeter type, which is extremely powerful in determining the cumulative

amount of an analyte present in a given system. In this case as in the previous chapter, the chemodosimetric element took advantage of the strong affinity of thiols for palladium. Whereas previously, palladium was “displaced” in order to facilitate a signal transduction, this assay uses palladium in the opposite way. In other words, palladium is the displacer which released the signaling motif. As stated above, this assay represents a combination of the two major types of chemodosimeter. There is a complexation type dosimeter in the formation of **3.27** followed by a signal liberating chemodosimeter in the thiol scavenging by the palladium analyte. The signaling motif utilizes one member of a novel class of organic dyes, a squaraine, which interacts with the thiolic “host” through an electrophilic addition. The squaraine **3.26** has a very large extinction coefficient which allows very sensitive detection.

Further work on this system is ongoing in our laboratory. The first step is to continue to lower the limit of detection through a more detailed exploration into fluorescence. Because the quantum efficiency of **3.26** is also quite high, an estimation of 3 orders of magnitude greater sensitivity could possibly be achieved through the use of fluorometry. Other aspects which are under investigation are the quantification of other thiophilic metals with this assay. Through qualitative inspection, this chemodosimeter is active for at least Pb(II), Cd(II), Cu(II) and Zn(II), all of which are targets of interest for their environmental, biological, and/or chemical activity. The search for a palladium sensor arises from its wide use in industrial processes, and hence, metals such as tin, rhodium, ruthenium, and platinum would also be of interest. Assuming success with these efforts the ultimate goal is to incorporate a variety of thiolic “hosts” with differing peripheral substitutions for use in pattern recognition of multiple metals.<sup>114-118</sup> The research presented in this chapter sees the fulfillment of a number of in depth studies on the various aspects of molecular/atomic recognition.

### 3.5 EXPERIMENTAL SECTION

$^1\text{H}$  and  $^{13}\text{C}$  NMR spectra were recorded on a Varian Unity Plus 300 MHz spectrometer in  $\text{CHCl}_3$ -*d*. Chemical shifts are reported in parts per million ( $\delta$ ) downfield from tetramethylsilane (0 ppm) as the internal standard and coupling constants (*J*) are recorded in Hertz (Hz). The multiplicities in the  $^1\text{H}$  NMR are reported as (br) broad, (s) singlet, (d) doublet, (dd) doublet of doublets, (ddd) doublet of doublet of doublets, (t) triplet, (sp) septet, (m) multiplet. All spectra are recorded at ambient temperatures. UV-Vis experiments were performed on Beckman DU-70 and DU-800 UV-Vis spectrophotometers. Low and High-resolution mass spectra were measured with a Finnigan TSQ70 and VG Analytical ZAB2-E instruments, respectively. Compound **3.26** was synthesized according to a slight modification of the reference method.<sup>55</sup> All chemicals and reagents were brought from Aldrich or Fluka and used without further purification. DMSO was degassed *via* displacement with  $\text{N}_2$  and dried over molecular sieves for at least 6 hours prior to use. DMF was obtained purified through filter-based solvent delivery system. Dilutions and aliquots were performed using FisherBrand Finnpiquette autopipets calibrated by mass.

**Bis[(N,N-dibutyl phenyl) squaraine (3.26):** Under a dry atmosphere of nitrogen, a mixture of squaric acid (1.5 g, 13.5 mmol, 1 eq.) and *N,N*-dibutylaniline (6 mL, 27 mmol, 2 eq.) were dissolved in a mixture of toluene (20 mL) and 1-butanol (20 mL). The mixture was refluxed with azeotropic distillation of water for 6-8 h. During this time period the solution turned an intense blue color. The solvent was removed under reduced pressure, and the dark blue oil was then subjected to column chromatography using 3:2 v/v ethyl acetate and hexanes and the blue band was collected. The solvent was immediately reduced to form a green solid. This residue was precipitated from

methylen chloride with hexanes the green solid was filtered and washed with pentane (100 mL). The filtrate was then refiltered and washed with hexanes (100 mL) then diethyl ether (20 mL) and dried under hi-vacuum overnight to give (120 mg, 0.25 mmol, 2% yield).  $^1\text{H}$ -NMR ( $\text{CHCl}_3$ -*d*, *J* / Hz,  $\delta$  / ppm): 0.98 (t, 12H,  $\text{CH}_3$ ); 1.43 (m, 8H,  $\text{CH}_2$ ); 1.64 (m 8H,  $\text{CH}_2$ ), 3.43 (m, 8H,  $\text{CH}_2$ ), 6.70 (d, *J* = 9.2 Hz, 4H, ArH), 8.35 (d, *J* = 9.2 Hz, 4H, Ar);  $^{13}\text{C}$ -NMR ( $\text{CHCl}_3$ -*d*), 75 MHz,  $\delta$  / ppm): 13.9, 20.2, 29.6, 51.2, 112.2, 119.6, 133.2, 153.4, 183.5, 187.7 HRMS (CI): *m/z* calcd for  $\text{C}_{32}\text{H}_{44}\text{N}_2\text{O}_2$ ; 488.704; found:  $\text{C}_{32}\text{H}_{45}\text{N}_2\text{O}_2$ ; 489.702. UV-Vis (DMSO)  $\lambda_{\text{max}}$  ( $\epsilon$ ) =  $2.3 \times 10^5 \text{ cm}^{-1} \text{ M}^{-1}$  (656 nm)

### 3.5.1 UV-Vis Titrations in DMSO with DBU

A stock solution of **3.26** ( $6.0 \times 10^{-4} \text{ M}$ ) was prepared by dissolving **3.26** (3 mg, 6  $\mu\text{mol}$ ) in 10 mL 1:9  $\text{CHCl}_3/\text{DMSO}$ . This stock solution was then used to prepare a  $4.7 \times 10^{-5} \text{ M}$  solution of **3.26** using pure DMSO. A separate stock solution of ethanethiol ( $2.7 \times 10^{-3} \text{ M}$ ) and (2 eq. of DBU) was also prepared in pure DMSO. This second solution was then used to prepare a  $4.7 \times 10^{-5} \text{ M}$  solution of ethanethiol. Equal volumes (2 mL) were added together and left for 24 hours to form a theoretical  $2.35 \times 10^{-5} \text{ M}$  solution of **3.27**. A 1 mL aliquot of the **3.27** complex was transferred to the UV-Vis cuvet. A separate solution of the Pd(II) salts were prepared at 10 times palladium concentration and 10  $\mu\text{L}$  aliquots were added and the spectrum was recorded 5 minutes after each aliquot injection.

### 3.5.2 UV-Vis Titrations in DMSO with Verkade Base

A  $4.7 \times 10^{-5} \text{ M}$  solution of **3.26** was prepared in DMSO analogously to the previous method. A separate solution of  $4.7 \times 10^{-5} \text{ M}$  ethanethiol and 0.75 eq ( $3.53 \times 10^{-5} \text{ M}$ ) **3.31** was also prepared. Complex **3.27** formation was achieved by combining 1 part each of the above solutions with 2 parts DMSO. The resulting concentrations of **3.26** and

ethanethiol were each  $1.18 \times 10^{-5}$  M. Decolorization proceeded quickly, though the solution was allowed to come to equilibrium for 12-15 hours prior to use. The complex thus prepared and stored over molecular sieves was stable for titration use up to 48 hours.

The palladium(II) nitrate titrant solution was prepared by dilution of 2.5 mg of  $\text{Pd}(\text{NO}_3)_2 \cdot 2\text{H}_2\text{O}$  in 10 mL DMSO. 100  $\mu\text{L}$  of this solution is combined with 750  $\mu\text{L}$  of the **3.27** complex solution and 150  $\mu\text{L}$  DMSO to give a 1 mL solution containing roughly 10 eq. of Pd(II) to squaraine. A standard, quartz, 3 mL volume, 1 cm pathlength UV-Vis cuvet was charged with 750  $\mu\text{L}$  of the  $1.18 \times 10^{-5}$  M solution of **3.27** and 250  $\mu\text{L}$  DMSO giving a final concentration of  $8.82 \times 10^{-6}$  M. The titration was performed by administering successive 10  $\mu\text{L}$  aliquots of the Pd(II) solution.

### 3.5.3 van't Hoff Analysis

500  $\mu\text{L}$  of the above prepared solution of **3.27** with the Verkade base and 500  $\mu\text{L}$  DMSO were placed in a standard 1 cm pathlength cuvet. UV-Vis spectra were collected upon equilibration of the **3.27** at iteratively increasing temperatures. The temperature was set using a built in Peltier apparatus and independently monitored in cuvet using a FisherBrand digital K-thermocouple. The absorbance readings at 656 nm and 635 nm were used for separate determinations of the thermodynamic parameters as described in section 3.3.2.2.

### 3.5.4 UV-Vis Titrations in DMF

Dry, degassed DMF was obtained through a high-pressure filter-type solvent delivery system and kept over 4A molecular sieves. 1 mg ( $2.0 \times 10^{-6}$  mol) **3.26** was diluted to 10 mL in DMF to give a  $5.9 \times 10^{-4}$  M solution. A separate  $4.1 \times 10^{-2}$  M solution of ethanethiol in DMF was prepared *via* dilution of 30  $\mu\text{L}$  of ethanethiol to 10mL of DMF. 2.875 mL of the **3.26** solution is mixed with 14.5  $\mu\text{L}$  of the ethanethiol

solution and the resulting mixture is diluted to 25 mL with fresh DMF. The resulting  $2.35 \times 10^{-5}$  M solution of **3.27** was allowed to react for 12-15 hours after which time the solution was completely colorless to the naked eye.

6.96 mg ( $2.61 \times 10^{-5}$  mol)  $\text{Pd}(\text{NO}_3)_2 \cdot 2\text{H}_2\text{O}$  was diluted to 10 mL in DMF resulting in a  $2.61 \times 10^{-3}$  M solution. A small vial is charged with 45  $\mu\text{L}$  of the Pd(II) solution, 455  $\mu\text{L}$  DMF, and 500  $\mu\text{L}$  of the prepared **3.27** complex solution to yield a  $1.18 \times 10^{-5}$  M solution of **3.27** and  $1.18 \times 10^{-4}$  M in Pd(II). This solution is labeled “titrant.” To standard 1cm path length 3 mL UV-Vis cuvet is added 500 $\mu\text{L}$  each of DMF and the prepared **3.27** complex solution resulting in a  $1.18 \times 10^{-5}$  M solution of the **3.27** complex. The titration was performed with successive 10  $\mu\text{L}$  injections of the titrant solution. A five minute equilibration period was allowed between injection and spectral scan.

#### **3.5.4 Kinetics and Calibration Curve Determination**

For both kinetics determinations, the **3.27** solutions were prepared as described for the respective titrations. For the DMSO study, 4 mg  $\text{Pd}(\text{NO}_3)_2$  was dissolved 10 mL DMSO to give a  $1.5 \times 10^{-3}$  M solution. 15 vials labeled 1-15 were given 10  $\mu\text{L}$  increasing amounts of the Pd(II) stock solution such that vial 1 contained 10  $\mu\text{L}$  and vial 15 contained 150  $\mu\text{L}$ . The vials were then charged with DMSO to bring the total volume in each vial to 150  $\mu\text{L}$ . Directly before each kinetics determination, each vial was charged with 150  $\mu\text{L}$  of the **3.27** solution to give a total volume of 300  $\mu\text{L}$  and **3.27** concentration  $1.2 \times 10^{-5}$  M. For the DMF study, 5.75 mg  $\text{Pd}(\text{NO}_3)_2$  was diluted to 10 mL in fresh DMF to give a  $2.2 \times 10^{-3}$  M solution. 15 vials labeled 1-15 were give aliquots of the stock solution as follows: vials 1-10 were given volumes increasing by 10  $\mu\text{L}$  such that vial 1 contained 10  $\mu\text{L}$  and vial 10 contained 100  $\mu\text{L}$ ; vials 11-15 were increased to 20  $\mu\text{L}$  increasing volumes such that vial 11 was given 120  $\mu\text{L}$  and vial 15 had 200  $\mu\text{L}$ .

Each vial was then filled with DMF to a total volume of 250  $\mu\text{L}$ . Directly before each kinetics determination, each vial was charged with 250  $\mu\text{L}$  of the prepared **3.27** solution to give a total volume of 500  $\mu\text{L}$  and concentration of **3.27** of  $1.2 \times 10^{-5}$  M.

The trials were identical from this point onward. The cuvet was charged with 500  $\mu\text{L}$  of the **3.27** solution and 500  $\mu\text{L}$  of the respective solvent to give  $1.2 \times 10^{-5}$  M solutions of **3.27**. The UV-Vis sample holder was kept at a constant temperature of 25  $^{\circ}\text{C}$  by a built-in Peltier apparatus. Once the sample had equilibrated to temperature (5-10 minutes depending on ambient temperature), an initial wavelength scan was collected. The UV-Vis was then switched into kinetics mode and set to acquire. A timer set to count down 5 seconds was on hand. A 20  $\mu\text{L}$  aliquot of the vial being sampled was injected into the cuvet while simultaneously starting the 5 second timer. The cuvet was shaken vigorously to mix and replaced in the cell holder within the 5 second countdown. The kinetics collection at 656 nm was started at the completion of the 5 second countdown and the absorption was monitored until it leveled off. Upon completion, another wavelength scan was collected for verification of the final absorbance value. The Kinetic traces were then normalized such that the maximum absorbance was set equal to 1. 5 seconds was added to the start of trace to account for the time from injection to the start of data collection.

### 3.6 REFERENCES

1. Martinez-Manez, R.; Sancenon, F., Fluorogenic and Chromogenic Chemosensors and Reagents for Anions. *Chemical Reviews (Washington, DC, United States)* **2003**, 103, (11), 4419-4476.
2. Bell, T. W.; Hext, N. M., Supramolecular optical chemosensors for organic analytes. *Chemical Society Reviews* **2004**, 33, (9), 589-598.



3. Czarnik, A. W., Fluorescent chemosensors for metal and non-metal ions in aqueous solution based on the CHEF paradigm. *Advances in Supramolecular Chemistry* **1993**, 3, 131-57.
4. Mohr, G. J., Chromo- and fluororeactands: indicators for detection of neutral analytes by using reversible covalent-bond chemistry. *Chemistry--A European Journal* **2004**, 10, (5), 1082-1090.
5. Chae, M. Y.; Czarnik, A. W., Fluorometric chemodosimetry. Mercury(II) and silver(I) indication in water via enhanced fluorescence signaling. *Journal of the American Chemical Society* **1992**, 114, (24), 9704-5.
6. Dujols, V.; Ford, F.; Czarnik, A. W., A Long-Wavelength Fluorescent Chemodosimeter Selective for Cu(II) Ion in Water. *Journal of the American Chemical Society* **1997**, 119, (31), 7386-7387.
7. Hennrich, G.; Walther, W.; Resch-Genger, U.; Sonnenschein, H., Cu(II)- and Hg(II)-Induced Modulation of the Fluorescence Behavior of a Redox-Active Sensor Molecule. *Inorganic Chemistry* **2001**, 40, (4), 641-644.
8. Kovacs, J.; Roedler, T.; Mokhir, A., Chemodosimeter for CuII detection based on cyclic peptide nucleic acids. *Angewandte Chemie, International Edition* **2006**, 45, (46), 7815-7817.
9. Liu, B.; Tian, H., A selective fluorescent ratiometric chemodosimeter for mercury ion. *Chemical Communications (Cambridge, United Kingdom)* **2005**, (25), 3156-3158.
10. Ros-Lis, J. V.; Marcos, M. D.; Martinez-Manez, R.; Rurack, K.; Soto, J., A regenerative chemodosimeter based on metal-induced dye formation for the highly selective and sensitive optical determination of Hg<sup>2+</sup> ions. *Angewandte Chemie, International Edition* **2005**, 44, (28), 4405-4407.
11. Song, K. C.; Kim, J. S.; Park, S. M.; Chung, K.-C.; Ahn, S.; Chang, S.-K., Fluorogenic Hg<sup>2+</sup>-Selective Chemodosimeter Derived from 8-Hydroxyquinoline. *Organic Letters* **2006**, 8, (16), 3413-3416.
12. Wu, J.-S.; Hwang, I.-C.; Kim, K. S.; Kim, J. S., Rhodamine-Based Hg<sup>2+</sup>-Selective Chemodosimeter in Aqueous Solution: Fluorescent OFF-ON. *Organic Letters* **2007**, 9, (5), 907-910.
13. Yang, Y.-K.; Yook, K.-J.; Tae, J., A Rhodamine-Based Fluorescent and Colorimetric Chemodosimeter for the Rapid Detection of Hg<sup>2+</sup> Ions in Aqueous Media. *Journal of the American Chemical Society* **2005**, 127, (48), 16760-16761.
14. Yang, X.-F.; Li, Y.; Bai, Q., A highly selective and sensitive fluorescein-based chemodosimeter for Hg<sup>2+</sup> ions in aqueous media. *Analytica Chimica Acta* **2007**, 584, (1), 95-100.

15. Zhang, G.; Zhang, D.; Yin, S.; Yang, X.; Shuai, Z.; Zhu, D., 1,3-Dithiole-2-thione derivatives featuring an anthracene unit: new selective chemodosimeters for Hg(II) ion. *Chemical Communications (Cambridge, United Kingdom)* **2005**, (16), 2161-2163.
16. Liang, J.-G.; Ai, X.-P.; He, Z.-K.; Pang, D.-W., Functionalized CdSe quantum dots as selective silver ion chemodosimeter. *Analyst (Cambridge, United Kingdom)* **2004**, 129, (7), 619-622.
17. Chow, C.-F.; Chiu, B. K. W.; Lam, M. H. W.; Wong, W.-Y., A trinuclear heterobimetallic Ru(II)/Pt(II) complex as a chemodosimeter. Selective for sulfhydryl-containing amino acids and peptides. *Journal of the American Chemical Society* **2003**, 125, (26), 7802-7803.
18. Chow, C.-F.; Lam, M. H. W.; Sui, H.; Wong, W.-Y., Design and synthesis of heterobimetallic donor-acceptor chemodosimetric ensembles for the detection of sulfhydryl-containing amino acids and peptides. *Dalton Transactions* **2005**, (3), 475-484.
19. Chow, C.-F.; Lam, M. H. W.; Wong, W.-Y., A Heterobimetallic Ruthenium(II)-Copper(II) Donor-Acceptor Complex as a Chemodosimetric Ensemble for Selective Cyanide Detection. *Inorganic Chemistry* **2004**, 43, (26), 8387-8393.
20. Chung, Y.; Lee, H.; Ahn, K. H., N-Acyl Triazenes as Tunable and Selective Chemodosimeters Toward Cyanide Ion. *Journal of Organic Chemistry* **2006**, 71, (25), 9470-9474.
21. Descalzo, A. B.; Jimenez, D.; Haskouri, J. E.; Beltran, D.; Amoros, P.; Marcos, M. D.; Martinez-Manez, R.; Soto, J., A new method for fluoride determination by using fluorophores and dyes anchored onto MCM-41. *Chemical Communications (Cambridge, United Kingdom)* **2002**, (6), 562-563.
22. Sancenon, F.; Martinez-Manez, R.; Miranda, M. A.; Segui, M.-J.; Soto, J., Towards the development of colorimetric probes to discriminate between isomeric dicarboxylates. *Angewandte Chemie, International Edition* **2003**, 42, (6), 647-650.
23. Yang, Y.-K.; Tae, J., Acridinium salt based fluorescent and colorimetric chemosensor for the detection of cyanide in water. *Organic letters* **2006**, 8, (25), 5721-3.
24. Sancenon, F.; Descalzo, A. B.; Martinez-Manez, R.; Miranda, M. A.; Soto, J., A colorimetric ATP sensor based on 1,3,5-triarylpent-2-en-1,5-diones. *Angewandte Chemie, International Edition* **2001**, 40, (14), 2640-2643.
25. Kim, T.-H.; Swager, T. M., A fluorescent self-amplifying wavelength-responsive sensory polymer for fluoride ions. *Angewandte Chemie, International Edition* **2003**, 42, (39), 4803-4806.

26. Roeschlaub, C. A.; Maidwell, N. L.; Reza Rezai, M.; Sammes, P. G., A fluorescent probe for the detection of NAD(P)H. *Chemical Communications (Cambridge)* **1999**, (17), 1637-1638.
27. Kroll, H., Manganous complexes of several amino acids. *Journal of the American Chemical Society* **1952**, 74, 2034-6.
28. Kroll, H., The participation of heavy-metal ions in the hydrolysis of amino acid esters. *Journal of the American Chemical Society* **1952**, 74, 2036-9.
29. Bender, M. L.; Turnquest, B. W., The kinetics and oxygen exchange of the cupric ion-catalyzed hydrolysis of  $\alpha$ -amino esters. *Journal of the American Chemical Society* **1957**, 79, 1889-93.
30. Zou, X.; Jin, G., Synthesis of pyridazinone-substituted 1,3,4-thiadiazoles, -1,3,4-oxadiazoles and -1,2,4-triazoles. *Journal of Heterocyclic Chemistry* **2001**, 38, (4), 993-996.
31. Yamaguchi, S.; Akiyama, S.; Tamao, K., Photophysical Properties Changes Caused by Hypercoordination of Organosilicon Compounds: From Trianthrylfluorosilane to Trianthryldifluorosilicate. *Journal of the American Chemical Society* **2000**, 122, (28), 6793-6794.
32. Yamaguchi, S.; Akiyama, S.; Tamao, K., Synthesis, Structures, Photophysical Properties, and Dynamic Stereochemistry of Tri-9-anthrylsilane Derivatives. *Organometallics* **1998**, 17, (20), 4347-4352.
33. Yamaguchi, S.; Akiyama, S.; Tamao, K., Colorimetric fluoride ion sensing by boron-containing  $\pi$ -electron systems. *Journal of the American Chemical Society* **2001**, 123, (46), 11372-5.
34. Ward, C. J.; Patel, P.; James, T. D., A molecular colour sensor for fluoride. *Chemistry Letters* **2001**, (5), 406-407.
35. Arimori, S.; Bosch, L. I.; Ward, C. J.; James, T. D., Fluorescent internal charge transfer (ICT) saccharide sensor. *Tetrahedron Letters* **2001**, 42, (27), 4553-4555.
36. Jimenez, D.; Martinez-Manez, R.; Sancenon, F.; Ros-Lis, J. V.; Benito, A.; Soto, J., A New Chromo-chemodosimeter Selective for Sulfide Anion. *Journal of the American Chemical Society* **2003**, 125, (30), 9000-9001.
37. Staunton, J., *Pyrylium salts*. Pergamon: Oxford, UK, 1979; Vol. 4, p 607-27.
38. Ros-Lis, J. V.; Garcia, B.; Jimenez, D.; Martinez-Manez, R.; Sancenon, F.; Soto, J.; Gonzalvo, F.; Valdecabres, M. C., Squaraines as fluoro-chromogenic probes for thiol-containing compounds and their application to the detection of biorelevant thiols. *Journal of the American Chemical Society* **2004**, 126, (13), 4064-4065.

39. Ros-Lis, J. V.; Martinez-Manez, R.; Soto, J., A selective chromogenic reagent for cyanide determination. *Chemical Communications (Cambridge, United Kingdom)* **2002**, (19), 2248-2249.
40. Treibs, A.; Jacob, K., Cyclotrimethine dyes derived from quadratic acid [1,2-dihydroxycyclobutenedione]. *Angew. Chem.* **1965**, 77, (15), 680-1.
41. Schmidt, A. H., *Oxocarbons*. Academic Press: New York, 1980; p 185-231.
42. Law, K. Y.; Bailey, F. C., Squaraine chemistry. Synthesis of bis[4-(dimethylamino)phenyl]squaraine from dialkyl squarates. Mechanism and scope of the synthesis. *Canadian Journal of Chemistry* **1986**, 64, (12), 2267-73.
43. Sprenger, H. E.; Ziegenbein, W., Cyclobutenediylum cation, a novel chromophore from squaric acid. *Angewandte Chemie, International Edition in English* **1967**, 6, (6), 553-4.
44. Bellus, D., Synthesis and reactivity of compounds with cyclobutane ring(s). 11. [2 + 2] Cycloadditions of tetraalkoxyethylenes with ketenes: a general route to 2-substituted 1-hydroxycyclobut-1-ene-3,4-diones. *Journal of the American Chemical Society* **1978**, 100, (25), 8026.
45. Wendling, L. A.; Koster, S. K.; Murray, J. E.; West, R., Syntheses and properties of 1,2- and 1,3-diquinocyclobutanediones. *Journal of Organic Chemistry* **1977**, 42, (7), 1126-30.
46. Law, K.-Y., *Absorption, fluorescence emission, and photophysics of squaraines*. Marcel Dekker, Inc: New York, 1997; Vol. 1, p 519-584.
47. Das, S.; Thomas, K. G.; George, M. V., *Photophysical and photochemical properties of squaraines in homogeneous and heterogeneous media*. Marcel Dekker, Inc: New York, 1997; Vol. 1, p 467-517.
48. Dirk, C. W.; Herndon, W. C.; Cervantes-Lee, F.; Selnau, H.; Martinez, S.; Kalamegham, P.; Tan, A.; Campos, G.; Velez, M.; et al., Squarylium Dyes: Structural Factors Pertaining to the Negative Third-Order Nonlinear Optical Response. *Journal of the American Chemical Society* **1995**, 117, (8), 2214-25.
49. Bigelow, R. W.; Freund, H. J., An MNDO and CNDO/S(S + DES CI) study on the structural and electronic properties of a model squaraine dye and related cyanine. *Chemical Physics* **1986**, 107, (2-3), 159-74.
50. Law, K. Y., Squaraine chemistry: effects of structural changes on the absorption and multiple fluorescence emission of bis[4-(dimethylamino)phenyl]squaraine and its derivatives. *Journal of Physical Chemistry* **1987**, 91, (20), 5184-93.
51. Kamlet, M. J.; Abboud, J. L.; Taft, R. W., The solvatochromic comparison method. 6. The p\* scale of solvent polarities. *Journal of the American Chemical Society* **1977**, 99, (18), 6027-38.

52. Scott, G. W.; Tran, K., Squaraine Photophysics in Polymer Films. *Journal of Physical Chemistry* **1994**, 98, (44), 11563-9.
53. Chen, H.; Law, K.-Y.; Perlstein, J.; Whitten, D. G., Amphiphilic Squaraine Dye Aggregates: Evidence for a Cyclic Chiral Structure as a General Supramolecular Structure for Aggregates of Dyes and Aromatic Molecules. *Journal of the American Chemical Society* **1995**, 117, (27), 7257-8.
54. Evens, C. E.; Bohn, P. W., Characterization of an Aggregate-Sensitive Single-Component Energy-Transfer System. *Journal of the American Chemical Society* **1993**, 115, 3306-3311.
55. Tian, M.; Furuki, M.; Iwasa, I.; Sato, Y.; Pu, L. S.; Tatsuura, S., Search for Squaraine Derivatives That Can Be Sublimed without Thermal Decomposition. *Journal of Physical Chemistry B* **2002**, 106, (17), 4370-4376.
56. Kasha, M.; Rawls, H. R.; El-Bayoumi, M. A., Exciton model in molecular spectroscopy. *Pure and Applied Chemistry* **1965**, 11, (3-4), 371-92.
57. Das, S.; Thanulingam, T. L.; Thomas, K. G.; Kamat, P. V.; George, M. V., Photochemistry of squaraine dyes. 5. Aggregation of bis(2,4-dihydroxyphenyl)squaraine and bis(2,4,6-trihydroxyphenyl)squaraine and their photodissociation in acetonitrile solutions. *Journal of Physical Chemistry* **1993**, 97, (51), 13620-4.
58. Buncel, E.; McKerrow, A. J.; Kazmaier, P. M., Solvent-controlled aggregation of a photoconductive dye. *Journal of the Chemical Society, Chemical Communications* **1992**, (17), 1242-3.
59. McKerrow, A. J.; Buncel, E.; Kazmaier, P. M., Aggregation of squaraine dyes: structure-property relationships and solvent effects. *Canadian Journal of Chemistry* **1995**, 73, (10), 1605-15.
60. Zollinger, H., *Color Chemistry*. 3rd ed.; Verlag Helvetica Chimica Acta: Zuerich, Switzerland, 2003; p 15-16.
61. Law, K. Y., Organic photoconductive materials: recent trends and developments. *Chemical Reviews (Washington, DC, United States)* **1993**, 93, (1), 449-86.
62. Loutfy, R. O.; Hsiao, C. K.; Kazmaier, P. M., Photoconductivity of organic particle dispersions: squaraine dyes. *Photographic Science and Engineering* **1983**, 27, (1), 5-9.
63. Morel, D. L.; Stogryn, E. L.; Ghosh, A. K.; Feng, T.; Purwin, P. E.; Shaw, R. F.; Fishman, C.; Bird, G. R.; Piechowski, A. P., Organic photovoltaic cells. Correlations between cell performance and molecular structure. *Journal of Physical Chemistry* **1984**, 88, (5), 923-33.
64. Piechowski, A. P.; Bird, G. R.; Morel, D. L.; Stogryn, E. L., Desirable properties of photovoltaic dyes. *Journal of Physical Chemistry* **1984**, 88, (5), 934-50.

65. Merritt, V. Y.; Hovel, H. J., Organic solar cells of hydroxy squarylium. *Applied Physics Letters* **1976**, 29, (7), 414-15.
66. Gravesteijn, D. J.; Steenbergen, C.; Van der Veen, J., Single-wavelength optical recording in pure, solvent-coated infrared dye layers. *Proceedings of SPIE-The International Society for Optical Engineering* **1983**, 420, (Opt. Storage Media), 327-31.
67. Mori, T.; Miyachi, K.; Kichimi, T.; Mizutani, T., Electrical and luminescent properties of color-changeable organic electroluminescent diode using squarylium dyes. *Japanese Journal of Applied Physics, Part 1: Regular Papers, Short Notes & Review Papers* **1994**, 33, (12A), 6594-8.
68. Ashwell, G. J., Centrosymmetric molecules for second harmonic generation. *Advanced Materials (Weinheim, Germany)* **1996**, 8, (3), 248-50.
69. Ashwell, G. J.; Jefferies, G.; Hamilton, D. G.; Lynch, D. E.; Roberts, M. P. S.; Bahra, G. S.; Brown, C. R., Strong second-harmonic generation from centrosymmetric dyes. *Nature (London)* **1995**, 375, (6530), 385-8.
70. Chen, C.-T.; Marder, S. R.; Cheng, L.-T., Syntheses and Linear and Nonlinear Optical Properties of Unsymmetrical Squaraines with Extended Conjugation. *Journal of the American Chemical Society* **1994**, 116, (7), 3117-18.
71. Ajayaghosh, A., Chemistry of squaraine-derived materials: Near-IR dyes, low band gap systems, and cation sensors. *Accounts of Chemical Research* **2005**, 38, (6), 449-459.
72. Ajayaghosh, A., Donor-acceptor type low band gap polymers: polysquaraines and related systems. *Chemical Society Reviews* **2003**, 32, (4), 181-191.
73. Volkova, K. D.; Kovalska, V. B.; Tatarets, A. L.; Patsenker, L. D.; Kryvorotenko, D. V.; Yarmoluk, S. M., Spectroscopic study of squaraines as protein-sensitive fluorescent dyes. *Dyes and Pigments* **2006**, 72, (3), 285-292.
74. Basheer, M. C.; Alex, S.; George Thomas, K.; Suresh, C. H.; Das, S., A squaraine-based chemosensor for Hg<sup>2+</sup> and Pb<sup>2+</sup>. *Tetrahedron* **2006**, 62, (4), 605-610.
75. Wallace, K. J.; Gray, M.; Zhong, Z.; Lynch, V. M.; Anslyn, E. V., An artificial siderophore for the detection of iron(III). *Dalton Transactions* **2005**, (14), 2436-2441.
76. Ros-Lis, J. V.; Martinez-Manez, R.; Soto, J., Colorimetric signaling of large aromatic hydrocarbons via the enhancement of aggregation processes. *Organic Letters* **2005**, 7, (12), 2337-2339.

77. Ros-Lis, J. V.; Martinez-Manez, R.; Rurack, K.; Sancenon, F.; Soto, J.; Spieles, M., Highly Selective Chromogenic Signaling of Hg<sup>2+</sup> in Aqueous Media at Nanomolar Levels Employing a Squaraine-Based Reporter. *Inorganic Chemistry* **2004**, 43, (17), 5183-5185.
78. Kim, S.-H.; Han, S.-K.; Park, S.-H.; Yoon, C.-M.; Keum, S.-R., Novel fluorescent chemosensor for Li<sup>+</sup> based on a squarylium dye carrying a monoazacrown moiety. *Dyes and Pigments* **1999**, 43, (1), 21-25.
79. Akkaya, E. U., Squaraine-based long wavelength fluorescent chemosensors for ions. *NATO ASI Series, Series C: Mathematical and Physical Sciences* **1997**, 492, (Chemosensors of Ion and Molecule Recognition), 177-188.
80. Thomas, K. G.; Thomas, K. J.; Das, S.; George, M. V., A squaraine-based near-infrared absorbing sensor for the selective detection of transition and other metal ions in aqueous media. *Chemical Communications (Cambridge)* **1997**, (6), 597-598.
81. Jyothish, K.; Avirah, R. R.; Ramaiah, D., Synthesis of New Cholesterol- and Sugar-Anchored Squaraine Dyes: Further Evidence of How Electronic Factors Influence Dye Formation. *Organic Letters* **2006**, 8, (1), 111-114.
82. Comes, M.; Marcos, M., D; Martinez-Manez, R.; Millian, M. C.; Ros-Lis, J., V; Sancenon, F.; Soto, J.; Villaescusa, L. A., Anchoring Dyes into Multidimensional Large-Pore Zeolites: A Prospective Use as a Chromogenic Sensing Material. *Chemistry--A European Journal* **2006**, 12, 2162-2170.
83. Wallace, K. J.; Jeroni, M.; Lynch, V. M.; Anslyn, E. V., Colorimetric Detection of Chemical Warfare Simulants. *New J. Chem* **2005**, in press.
84. Tatarets, A. L.; Fedyunyaeva, I. A.; Terpetschnig, E.; D, P. L., Synthesis of Novel Squaraine Dyes and their Intermediates. *Dyes and Pigments* **2005**, 64, 125-134.
85. Ros-Lis, J., V; Marcos, M., D; Martinez-Manez, R.; Rurack, K.; Soto, J., A Regenerative Chemodosimeter based on Metal-Induced Dye Formation for the Highly Selective and Sensitive Optical Determination of Hg<sup>2+</sup> ions. *Angew. Chem., Int. Ed* **2005**, 44, 4405-4407.
86. Ramaiah, D.; Arun, K. T., Near-Infrared Fluorescent Probes: Synthesis and Spectroscopic Investigations of a few Amphiphilic Squaraine Dyes. *J. Phys. Chem. A* **2005**, 109, 5571-5578.
87. Nakazumi, H.; Ohta, T.; Etoh, H.; Uno, T.; Colyer, C. L.; Hyodo, Y.; Yagi, S., Near-Infrared Luminescent Bis-Squaraine Dyes Linked by a Thiophene or Pyrene Spacer for Noncovalent Protein Labeling. *Synthetic Metals* **2005**, 153, 33-36.
88. Mohr, G. G., Covalent Bond Formation as an Analytical tool to Optically Detect Neutral and anionic Analytes. *Sensors and Actuators B* **2005**, 107, 2-13.

89. Choa, L.; Wang, W.; Wang, X.; Zhang, B.; Cao, Y., Molecular Design of Squaraine Dyes for Efficient Far-Red and Near-IR Sensitization of Solar Cells. *Chemistry Letters* **2005**, 34, (4), 554-555.
90. Arunkumar, E.; Forbes, C. C.; Noll, F. B.; Smith, B. D., Squaraine-Derived Rotaxanes: Sterically Protected Fluorescent Near-IR Dyes. *J. Chem. Soc., Faraday Trans.* **2005**, 127, 3288-3289.
91. Arunkumar, E.; Ajayoghosh, A.; Daub, J., Selective Calcium Ion Sensing with Bichromophoric Squaraine Foldermer. *J. Am. Chem. Soc.* **2005**, 127, 3156-3164.
92. Arun, K. T.; Ramaiah, D., Near-Infrared Fluorescent Probes: Synthesis and Spectroscopic Investigations of a few Amphiphilic Squaraine Dyes. *J. Phys. Chem.* **2005**, 109, 5571-5578.
93. Alex, S.; Santhosh, U.; Das, S., Dye Sensitization of Nanocrystalline TiO<sub>2</sub>: enhanced efficiency of Unsymmetrical Versus Symmetrical Squaraine Dyes. *Journal of Photochemistry and Photobiology A: Chemistry* **2005**, 172, (63-71).
94. Ajayoghosh, A., Chemistry of Squaraine-Derived Materials: Near-IR Dyes, Low Band Gap Systems, and Cation Sensors. *Acc. Chem. Res* **2005**, 38, 449-459.
95. Ajayoghosh, A.; Arunkumar, E., 1H NMR Spectral Evidence for a Specific Host-Guest Complexation Induced Charge Localization in Squaraine dyes. *Org. Lett.* **2005**, 7, (15), 3135-3138.
96. P.J., V. R. S. N. K. P. L., Palladium Chloride and Tetraphenylphosphonium Bromide Intercalated Clay as a New Catalyst for the Heck Reaction. *Tetrahedron Lett.* **1999**, 40, (11), 2075-2078.
97. W.-J. Liu; Y.-X. Xie; Y. Liang; J.-H. Li, Reusable and Efficient Pd(OAc)<sub>2</sub>/TBAB/PEG-400 System for Suzuki-Miyaura Cross-Coupling Reaction under Ligand-Free Conditions. *Synthesis* **2006**, 860-864.
98. J. Baxter, D. S., M. Palucki, I. W. Davies,, Stereoselective Enol Tosylation: Preparation of Trisubstituted  $\alpha,\beta$ -Unsaturated Esters. *Organic Letters* **2005**, 7, 215-218.
99. Buchwald, S., L ; Mauger, C.; Mignani, G.; Scholze, U., Industrial-Scale Palladium-Catalyzed Coupling of Aryl Halides and Amines – A Personal Account. *Adv. Synth. Catal.* **2006**, 348, 23-39.
100. Riina K. Arvela; Leadbeater, N. E.; Michael J. Collins, J., Automated batch scale-up of microwave-promoted Suzuki and Heck coupling reactions in water using ultra-low metal catalyst concentrations. *Tetrahedron* **2005**, 61, (39), 9349-9355.
101. Wallace, K. J.; Anslyn, E. V., *Unpublished results*.
102. Houk, R. J. T.; Anslyn, E. V., *Unpublished results*.



103. Ros-Lis, J., V; Garcia, B.; Jimeenez, D.; Martinez-Manez, R.; Sancenon, F.; Soto, J.; Gonzalvo, F.; Valldecarbres, M. C., Squaraines as Fluoro-Chromogenic Probes for Thiol-Containing Compounds and their Application to the Detection of Biorelevant Thiols. *J. Chem. Soc., Faraday Trans.* **2004**, 126, 4064-4065.
104. Ros-Lis, J., V ; Martinez-Manez, R.; Rurack, K.; Sancenon, F.; Soto, J.; Spieles, M., Highly Selective Chromogenic Signaling of Hg<sup>2+</sup> in Aqueous Media at Nanomolar Levels Employing a Squaraine-Based Reporter. *Inorg. Chem.* **2004**, 43, (17), 5183-5185.
105. *CRC Handbook of Chemistry and Physics*. 76th ed.; CRC Press: Boca Raton, 1995; p 9-(65-66).
106. Houk, R. J. T.; Anslyn, E. V., Luminescent assays for ketones and aldehydes employing catalytic signal amplification. *New Journal of Chemistry* **2007**, In Press.
107. Wallace, K. J.; Houk, R. J. T.; Anslyn, E. V., *Unpublished results*.
108. Gordon, A. J.; Ford, R. A., *The Chemist's Companion*. John Wiley and Sons Inc.: New York, 1972; p 57-59.
109. Chrisment, J.; Nicole, D.; Delpuech, J. J., Comparative acidities of organic substances in anhydrous dimethyl sulfoxide. *Comptes Rendus des Seances de l'Academie des Sciences, Serie C: Sciences Chimiques* **1978**, 286, (21), 541-4.
110. Lensink, C.; Xi, S. K.; Daniels, L. M.; Verkade, J. G., The unusually robust phosphorus-hydrogen bond in the novel cation [cyclic] HP(NMeCH<sub>2</sub>CH<sub>2</sub>)<sub>3</sub>N<sup>+</sup>. *Journal of the American Chemical Society* **1989**, 111, (9), 3478-9.
111. Laramay, M. A. H.; Verkade, J. G., The \"anomalous\" basicity of P(NHCH<sub>2</sub>CH<sub>2</sub>)<sub>3</sub>N relative to P(NMeCH<sub>2</sub>CH<sub>2</sub>)<sub>3</sub>N and p(NBzCH<sub>2</sub>CH<sub>2</sub>)<sub>3</sub>N: a chemical consequence of orbital charge balance? *Journal of the American Chemical Society* **1990**, 112, (25), 9421-2.
112. Armarego, W. L. F.; Chai, C., *Purification of Laboratory Chemicals*. 5th ed.; Butterworth & Heineman Ltd.: Oxford, UK, 2003.
113. Brown, W. H.; Foote, C. S.; Iverson, B. L., *Organic Chemistry*. 4th ed.; Brooks/Cole: Belmont, CA, 2005; Vol. 1, p 1168.
114. McCleskey, S. C.; Griffin, M. J.; Schneider, S. E.; McDevitt, J. T.; Anslyn, E. V., Differential receptors create patterns diagnostic for ATP and GTP. *Journal of the American Chemical Society* **2003**, 125, (5), 1114-1115.
115. McDevitt, J. T.; Anslyn, E. V.; Shear, J. B.; Neikirk, D. P. Sensor arrays for the measurement and identification of multiple analytes in solutions. 6680206, 2004.
116. Wright, A. T.; Anslyn, E. V., Differential receptor arrays and assays for solution-based molecular recognition. *Chemical Society Reviews* **2006**, 35, (1), 14-28.

117. Wright, A. T.; Anslyn, E. V.; McDevitt, J. T., A Differential Array of Metalated Synthetic Receptors for the Analysis of Tripeptide Mixtures. *Journal of the American Chemical Society* **2005**, 127, (49), 17405-17411.
118. Wright, A. T.; Griffin, M. J.; Zhong, Z.; McCleskey, S. C.; Anslyn, E. V.; McDevitt, J. T., Differential receptors create patterns that distinguish various proteins. *Angewandte Chemie, International Edition* **2005**, 44, (39), 6375-6378.

## Bibliography

- Ajayaghosh, A., Donor-acceptor type low band gap polymers: polysquaraines and related systems. *Chemical Society Reviews* **2003**, 32, (4), 181-191.
- Ajayaghosh, A., Chemistry of squaraine-derived materials: Near-IR dyes, low band gap systems, and cation sensors. *Accounts of Chemical Research* **2005**, 38, (6), 449-459.
- Ajayoghosh, A.; Arunkumar, E., <sup>1</sup>H NMR Spectral Evidence for a Specific Host-Guest Complexation Induced Charge Localization in Squaraine dyes. *Org. Lett.* **2005**, 7, (15), 3135-3138.
- Akkaya, E. U., Squaraine-based long wavelength fluorescent chemosensors for ions. *NATO ASI Series, Series C: Mathematical and Physical Sciences* **1997**, 492, (Chemosensors of Ion and Molecule Recognition), 177-188.
- Albery, W. J.; Knowles, J. R., Evolution of enzyme function and the development of catalytic efficiency. *Biochemistry* **1976**, 15, (25), 5631-40.
- Albery, W. J.; Knowles, J. R., Free-energy profile for the reaction catalyzed by triosephosphate isomerase. *Biochemistry* **1976**, 15, (25), 5627-31.
- Alex, S.; Santhosh, U.; Das, S., Dye Sensitization of Nanocrystalline TiO<sub>2</sub>: enhanced efficiency of Unsymmetrical Versus Symmetrical Squaraine Dyes. *Journal of Photochemistry and Photobiology A: Chemistry* **2005**, 172, (63-71).
- Alter, G. M.; Casazza, J. P.; Zhi, W.; Nemeth, P.; Srere, P. A.; Evans, C. T., Mutation of essential catalytic residues in pig citrate synthase. *Biochemistry* **1990**, 29, (33), 7557-63.
- Alvarez, F. J.; Parekh, N. J.; Matuszewski, B.; Givens, R. S.; Higuchi, T.; Schowen, R. L., Multiple intermediates generate fluorophore-derived light in the oxalate/peroxide chemiluminescence system. *Journal of the American Chemical Society* **1986**, 108, (20), 6435-7.
- Andres, M. A.; Chang, T. C. T.; Cheng, C. W. F.; Kapustay, L. V.; Kelly, K. P.; Zweifel, M. J., Nitration of alkenes by palladium nitro complexes. *Organometallics* **1984**, 3, (10), 1479-84.
- Anslyn, E. V.; Dougherty, D. A., *Modern Physical Organic Chemistry*. 1 ed.; University Science Books: Sausalito, CA, 2006; Vol. 1.

- Antonkina, O. A.; Smirnov, S. K.; Gitel, P. O., Electrochemical behavior of polycyclic arenes - the activators of peroxide-oxalate chemiluminescence. Oxidation potential as a criterion of the activator efficiency in the reaction of bis-(2,4-dichloro-6-carboalkoxyphenyl)-oxalates with hydrogen peroxide. *Elektrokhimiya* **1992**, 28, (9), 1335-43.
- Antonkina, O. A.; Smirnov, S. K.; Gitel, P. O.; Kryukova, E. V.; Tomilov, A. P., Electrochemical behavior of polycyclic arenes - activators of peroxide-oxalate chemiluminescence. The oxidation potential of substituted naphthalenes and anthracenes as their efficiency criterion. *Elektrokhimiya* **1991**, 27, (3), 394-401.
- Arimori, S.; Bosch, L. I.; Ward, C. J.; James, T. D., Fluorescent internal charge transfer (ICT) saccharide sensor. *Tetrahedron Letters* **2001**, 42, (27), 4553-4555.
- Armarego, W. L. F.; Chai, C., *Purification of Laboratory Chemicals*. 5th ed.; Butterworth & Heineman Ltd.: Oxford, UK, 2003.
- Arun, K. T.; Ramaiah, D., Near-Infrared Fluorescent Probes: Synthesis and Spectroscopic Investigations of a few Amphiphilic Squaraine Dyes. *Journal of Physical Chemistry A* **2005**, 109, 5571-5578.
- Arunkumar, E.; Ajayoghosh, A.; Daub, J., Selective Calcium Ion Sensing with Bichromophoric Squaraine Foldermer. *J. Am. Chem. Soc.* **2005**, 127, 3156-3164.
- Arunkumar, E.; Forbes, C. C.; Noll, F. B.; Smith, B. D., Squaraine-Derived Rotaxanes: Sterically Protected Fluorescent Near-IR Dyes. *J. Chem. Soc., Faraday Trans.* **2005**, 127, 3288-3289.
- Ashwell, G. J., Centrosymmetric molecules for second harmonic generation. *Advanced Materials (Weinheim, Germany)* **1996**, 8, (3), 248-50.
- Ashwell, G. J.; Jefferies, G.; Hamilton, D. G.; Lynch, D. E.; Roberts, M. P. S.; Bahra, G. S.; Brown, C. R., Strong second-harmonic generation from centrosymmetric dyes. *Nature (London)* **1995**, 375, (6530), 385-8.
- Baader, W. J.; Silva, S. M.; Oyamaguchi, K. H.; Ciscato, L. F. L. M.; Stevani, C. V., Further studies on the mechanism of the peroxyoxalate reaction. *Chemiluminescence at the Turn of the Millennium* **2001**, 33-38.
- Babbitt, P. C.; Hasson, M. S.; Wedekind, J. E.; Palmer, D. R. J.; Barrett, W. C.; Reed, G. H.; Rayment, I.; Ringe, D.; Kenyon, G. L.; Gerlt, J. A., The enolase superfamily: A general strategy for enzyme-catalyzed abstraction of the  $\alpha$ -protons of carboxylic acids. *Biochemistry* **1996**, 35, (51), 16489-16501.
- Basheer, M. C.; Alex, S.; George Thomas, K.; Suresh, C. H.; Das, S., A squaraine-based chemosensor for  $Hg^{2+}$  and  $Pb^{2+}$ . *Tetrahedron* **2006**, 62, (4), 605-610.
- Bearne, S. L.; Wolfenden, R., Mandelate Racemase in Pieces: Effective Concentrations of Enzyme Functional Groups in the Transition State. *Biochemistry* **1997**, 36, (7), 1646-1656.

- Beer, P. D.; Cadman, J., Electrochemical and optical sensing of anions by transition metal based receptors. *Coordination Chemistry Reviews* **2000**, 205, 131-155.
- Belasco, J. G.; Knowles, J. R., Direct observation of substrate distortion by triosephosphate isomerase using Fourier transform infrared spectroscopy. *Biochemistry* **1980**, 19, (3), 472-7.
- Bell, T. W.; Hext, N. M., Supramolecular optical chemosensors for organic analytes. *Chemical Society Reviews* **2004**, 33, (9), 589-598.
- Bellus, D., Synthesis and reactivity of compounds with cyclobutane ring(s). 11. [2 + 2] Cycloadditions of tetraalkoxyethylenes with ketenes: a general route to 2-substituted 1-hydroxycyclobut-1-ene-3,4-diones. *Journal of the American Chemical Society* **1978**, 100, (25), 8026.
- Bender, M. L.; Turnquest, B. W., The kinetics and oxygen exchange of the cupric ion-catalyzed hydrolysis of  $\alpha$ -amino esters. *Journal of the American Chemical Society* **1957**, 79, 1889-93.
- Benning, M. M.; Taylor, K. L.; Liu, R. Q.; Yang, G.; Xiang, H.; Wesenberg, G.; Dunaway-Mariano, D.; Holden, H. M., Structure of 4-chlorobenzoyl coenzyme A dehalogenase determined to 1.8 Å resolution: an enzyme catalyst generated via adaptive mutation. *Biochemistry* **1996**, 35, (25), 8103-9.
- Bernasconi, C. F., The principles of nonperfect synchronization. *Advances in Physical Organic Chemistry* **1992**, 27, 119-238.
- Bigelow, R. W.; Freund, H. J., An MNDO and CNDO/S(S + DES CI) study on the structural and electronic properties of a model squaraine dye and related cyanine. *Chemical Physics* **1986**, 107, (2-3), 159-74.
- Bollyky, L. J.; Whitman, R. H.; Roberts, B. G.; Rauhut, M. M., Chemiluminescence from reactions of oxalic anhydrides with hydrogen peroxide in the presence of fluorescent compounds. *Journal of the American Chemical Society* **1967**, 89, (25), 6523-6.
- Bordwell, F. G.; Boyle, W. J., Jr., Acidities, Broensted coefficients, and transition state structures for 1-arylnitroalkanes. *Journal of the American Chemical Society* **1972**, 94, (11), 3907-11.
- Bordwell, F. G.; Boyle, W. J., Jr., Kinetic isotope effects for nitroalkanes and their relation to transition-state structure in proton-transfer reactions. *Journal of the American Chemical Society* **1975**, 97, (12), 3447-52.
- Bos, R.; Barnett, N. W.; Dyson, G. A.; Lim, K. F.; Russell, R. A.; Watson, S. P., Studies on the mechanism of the peroxyoxalate chemiluminescence reaction. Part 1. Confirmation of 1,2-dioxetanedione as an intermediate using  $^{13}\text{C}$  nuclear magnetic resonance spectroscopy. *Analytica Chimica Acta* **2004**, 502, (2), 141-147.

- Brown, W. H.; Foote, C. S.; Iverson, B. L., *Organic Chemistry*. 4th ed.; Brooks/Cole: Belmont, CA, 2005; Vol. 1, p 1168.
- Bruice, T. C.; Schmir, G. L., Imidazole catalysis. II. The reaction of substituted imidazoles with phenyl acetates in aqueous solution. *Journal of the American Chemical Society* **1958**, 80, 148-56.
- Buchwald, S., L ; Mauger, C.; Mignani, G.; Scholze, U., Industrial-Scale Palladium-Catalyzed Coupling of Aryl Halides and Amines – A Personal Account. *Adv. Synth. Catal.* **2006**, 348, 23-39.
- Buncel, E.; McKerrow, A. J.; Kazmaier, P. M., Solvent-controlled aggregation of a photoconductive dye. *Journal of the Chemical Society, Chemical Communications* **1992**, (17), 1242-3.
- Cao, D. R.; Schollmeyer, D.; Meier, H., (Phenylethynyl)- and (phenylethenyl)metacyclophanes with p,p interactions. *European Journal of Organic Chemistry* **1999**, (4), 791-795.
- Catherall, C. L. R.; Palmer, T. F.; Cundall, R. B., Chemiluminescence from reactions of bis(pentachlorophenyl) oxalate, hydrogen peroxide, and fluorescent compounds. Role of the fluor and nature of chemielectronic process(es). *Journal of the Chemical Society, Faraday Transactions 2: Molecular and Chemical Physics* **1984**, 80, (7), 837-49.
- Catherall, C. L. R.; Palmer, T. F.; Cundall, R. B., Chemiluminescence from reactions of bis(pentachlorophenyl) oxalate, hydrogen peroxide, and fluorescent compounds: kinetics and mechanism. *Journal of the Chemical Society, Faraday Transactions 2: Molecular and Chemical Physics* **1984**, 80, (7), 823-36.
- Chae, M. Y.; Czarnik, A. W., Fluorometric chemodosimetry. Mercury(II) and silver(I) indication in water via enhanced fluorescence signaling. *Journal of the American Chemical Society* **1992**, 114, (24), 9704-5.
- Chandross, E. A., A new chemiluminescent system. *Tetrahedron Letters* **1963**, 1963, (12), 761-5.
- Chandross, E. A.; Sonntag, F. I., Novel chemiluminescent electron transfer reaction. *Journal of the American Chemical Society* **1964**, 86, (15), 3179-80.
- Chen, C.-T.; Marder, S. R.; Cheng, L.-T., Syntheses and Linear and Nonlinear Optical Properties of Unsymmetrical Squaraines with Extended Conjugation. *Journal of the American Chemical Society* **1994**, 116, (7), 3117-18.
- Chen, H.; Law, K.-Y.; Perlstein, J.; Whitten, D. G., Amphiphilic Squaraine Dye Aggregates: Evidence for a Cyclic Chiral Structure as a General Supramolecular Structure for Aggregates of Dyes and Aromatic Molecules. *Journal of the American Chemical Society* **1995**, 117, (27), 7257-8.

- Chiang, Y.; Kresge, A. J., Enols and other reactive species. *Science (Washington, DC, United States)* **1991**, 253, (5018), 395-400.
- Chiang, Y.; Kresge, A. J.; Pruszynski, P.; Schepp, N. P.; Wirz, J., Mandelic acid enols: determination of the acidity in aqueous solutions and estimation of keto-enol equilibrium constants and CH acidity of mandelic acid. *Angewandte Chemie* **1990**, 102, (7), 810-12.
- Choa, L.; Wang, W.; Wang, X.; Zhang, B.; Cao, Y., Molecular Design of Squaraine Dyes for Efficient Far-Red and Near-IR Sensitization of Solar Cells. *Chemistry Letters* **2005**, 34, (4), 554-555.
- Chow, C.-F.; Chiu, B. K. W.; Lam, M. H. W.; Wong, W.-Y., A trinuclear heterobimetallic Ru(II)/Pt(II) complex as a chemodosimeter. Selective for sulfhydryl-containing amino acids and peptides. *Journal of the American Chemical Society* **2003**, 125, (26), 7802-7803.
- Chow, C.-F.; Lam, M. H. W.; Sui, H.; Wong, W.-Y., Design and synthesis of heterobimetallic donor-acceptor chemodosimetric ensembles for the detection of sulfhydryl-containing amino acids and peptides. *Dalton Transactions* **2005**, (3), 475-484.
- Chow, C.-F.; Lam, M. H. W.; Wong, W.-Y., A Heterobimetallic Ruthenium(II)-Copper(II) Donor-Acceptor Complex as a Chemodosimetric Ensemble for Selective Cyanide Detection. *Inorganic Chemistry* **2004**, 43, (26), 8387-8393.
- Chrismont, J.; Nicole, D.; Delpuech, J. J., Comparative acidities of organic substances in anhydrous dimethyl sulfoxide. *Comptes Rendus des Seances de l'Academie des Sciences, Serie C: Sciences Chimiques* **1978**, 286, (21), 541-4.
- Chung, Y.; Lee, H.; Ahn, K. H., N-Acyl Triazenes as Tunable and Selective Chemodosimeters Toward Cyanide Ion. *Journal of Organic Chemistry* **2006**, 71, (25), 9470-9474.
- Clarkson, J.; Tonge, P. J.; Taylor, K. L.; Dunaway-Mariano, D.; Carey, P. R., Raman Study of the Polarizing Forces Promoting Catalysis in 4-Chlorobenzoate-CoA Dehalogenase. *Biochemistry* **1997**, 36, (33), 10192-10199.
- Cleland, W. W., Low-barrier hydrogen bonds and enzymic catalysis. *Archives of Biochemistry and Biophysics* **2000**, 382, (1), 1-5.
- Cleland, W. W.; Kreevoy, M. M., Low-barrier hydrogen bonds and enzymic catalysis. *Science (Washington, DC, United States)* **1994**, 264, (5167), 1887-90.
- Cohen, A. O.; Marcus, R. A., Slope of free energy plots in chemical kinetics. *Journal of Physical Chemistry* **1968**, 72, (12), 4249-56.

- Comes, M.; Marcos, M., D; Martinez-Manez, R.; Millian, M. C.; Ros-Lis, J., V; Sancenon, F.; Soto, J.; Villaescusa, L. A., Anchoring Dyes into Multidimensional Large-Pore Zeolites: A Prospective Use as a Chromogenic Sensing Material. *Chemistry--A European Journal* **2006**, 12, 2162-2170.
- Costero, A. M.; Peransi, S.; Gil, S., A selective colorimetric chemodosimeter for the naked eye detection of benzoate anion. *Tetrahedron Letters* **2006**, 47, (37), 6561-6564.
- CRC Handbook of Chemistry and Physics*. 76th ed.; CRC Press: Boca Raton, 1995; p 9- (65-66).
- Creighton, T. E., *Proteins: Structures and Molecular Properties*. 2nd ed.; W.H. Freeman and Company: New York, 1993.
- Czarnik, A. W., Fluorescent chemosensors for metal and non-metal ions in aqueous solution based on the CHEF paradigm. *Advances in Supramolecular Chemistry* **1993**, 3, 131-57.
- Das, S.; Thanulingam, T. L.; Thomas, K. G.; Kamat, P. V.; George, M. V., Photochemistry of squaraine dyes. 5. Aggregation of bis(2,4-dihydroxyphenyl)squaraine and bis(2,4,6-trihydroxyphenyl)squaraine and their photodissociation in acetonitrile solutions. *Journal of Physical Chemistry* **1993**, 97, (51), 13620-4.
- Das, S.; Thomas, K. G.; George, M. V., *Photophysical and photochemical properties of squaraines in homogeneous and heterogeneous media*. Marcel Dekker, Inc: New York, 1997; Vol. 1, p 467-517.
- Davenport, R. C.; Bash, P. A.; Seaton, B. A.; Karplus, M.; Petsko, G. A.; Ringe, D., Structure of the triosephosphate isomerase-phosphoglycolohydroxamate complex: an analog of the intermediate on the reaction pathway. *Biochemistry* **1991**, 30, (24), 5821-6.
- De Boer, H. J. R.; De Kanter, F. J. J.; Akkerman, O. S.; Bickelhaupt, F., 1-Bromo-2,6-bis(chloromagnesiomethyl)benzene from the attempted synthesis of a doubly benzylic 1,3,5-tri-Grignard reagent. *Main Group Metal Chemistry* **2001**, 24, (12), 841-844.
- de Silva, A. P.; de Silva, S. A., Fluorescent signaling crown ethers: switching on of fluorescence by alkali metal ion recognition and binding in situ. *Journal of the Chemical Society, Chemical Communications* **1986**, (23), 1709-10.
- Descalzo, A. B.; Jimenez, D.; Haskouri, J. E.; Beltran, D.; Amoros, P.; Marcos, M. D.; Martinez-Manez, R.; Soto, J., A new method for fluoride determination by using fluorophores and dyes anchored onto MCM-41. *Chemical Communications (Cambridge, United Kingdom)* **2002**, (6), 562-563.



- Desvergne, J. P.; Czarnik, A. W.; Editors, *Chemosensors of Ion and Molecule Recognition. (Proceedings of the NATO Advanced Research Workshop, held 31 August-4 September 1996, in Bonas, France.) [In: NATO ASI Ser., Ser. C, 1997; 492].* 1997; p 245 pp.
- Detty, M. R.; Virkler, P. R. Production of dye intermediates and polymethine dyes therefrom. 2001-US19981 2002000642, 20010622., 2002.
- Dirk, C. W.; Herndon, W. C.; Cervantes-Lee, F.; Selnau, H.; Martinez, S.; Kalamegham, P.; Tan, A.; Campos, G.; Velez, M.; et al., Squarylium Dyes: Structural Factors Pertaining to the Negative Third-Order Nonlinear Optical Response. *Journal of the American Chemical Society* **1995**, 117, (8), 2214-25.
- Dix, J. P.; Voegtle, F., Ligand structure and complexation. L. Ion-selective crown ether dyes. *Chemische Berichte* **1980**, 113, (2), 457-70.
- Dix, J. P.; Voegtle, F., New chromoionophores. *Chemische Berichte* **1981**, 114, (2), 638-51.
- Dorland, W. A. N., *Dorland's Illustrated Medical Dictionary*. 31st ed.; W.B. Saunders: Philadelphia, PA, 2007; Vol. 1.
- Du, H.; Fuh, R.-C. A.; Li, J.; Corkan, L. A.; Lindsey, J. S., Photochem CAD: a computer-aided design and research tool in photochemistry. *Photochemistry and Photobiology* **1998**, 68, (2), 141-142.
- Dujols, V.; Ford, F.; Czarnik, A. W., A Long-Wavelength Fluorescent Chemodosimeter Selective for Cu(II) Ion in Water. *Journal of the American Chemical Society* **1997**, 119, (31), 7386-7387.
- Dunleavy, J. K., Sulfur as a catalyst poison. *Platinum Metals Review* **2006**, 50, (2), 110.
- Evans, C. E.; Bohn, P. W., Characterization of an Aggregate-Sensitive Single-Component
- Energy-Transfer System. *Journal of the American Chemical Society* **1993**, 115, 3306-3311.
- Fabbrizzi, L.; Pallavicini, P.; Parodi, L.; Perotti, A.; Taglietti, A., Molecular recognition of the imidazole residue by a dicopper(II) complex with a bisdien macrocycle bearing two pendant arms. *Journal of the Chemical Society, Chemical Communications* **1995**, (23), 2439-40.
- Fee, J. A.; Hegeman, G. D.; Kenyon, G. L., Mandelate racemase from *Pseudomonas putida*. Subunit composition and absolute divalent metal ion requirement. *Biochemistry* **1974**, 13, (12), 2528-32.
- Fisher, L. M.; Albery, W. J.; Knowles, J. R., Energetics of triosephosphate isomerase: the nature of the proton transfer between the catalytic base and solvent water. *Biochemistry* **1976**, 15, (25), 5621-6.

- Fletcher, S. J.; Herlihy, J. M.; Alberty, W. J.; Knowles, J. R., Energetics of triosephosphate isomerase: the appearance of solvent tritium in substrate glyceraldehyde 3-phosphate and in product. *Biochemistry* **1976**, 15, (25), 5612-17.
- Frey, P. A., Low-barrier hydrogen bonds. *Science (Washington, D. C.)* **1995**, 268, (5208), 189.
- Frey, P. A., Isotope effects in the characterization of low barrier hydrogen bonds. *Isotope Effects in Chemistry and Biology* **2006**, 975-993.
- Frey, P. A.; Whitt, S. A.; Tobin, J. B., A low-barrier hydrogen bond in the catalytic triad of serine proteases. *Science (Washington, DC, United States)* **1994**, 264, (5167), 1927-30.
- Fuhrmann, C. N.; Daugherty, M. D.; Agard, D. A., Subangstrom Crystallography Reveals that Short Ionic Hydrogen Bonds, and Not a His-Asp Low-Barrier Hydrogen Bond, Stabilize the Transition State in Serine Protease Catalysis. *Journal of the American Chemical Society* **2006**, 128, (28), 9086-9102.
- Fujihara, H.; Chiu, J. J.; Furukawa, N., Synthesis, conformation, and the stereoselective sulfur extrusion reaction of a new intraannular dibromo-substituted tetrathia[4.4]metacyclopentane. *Chemistry Letters* **1991**, (1), 141-4.
- Gerlt, J. A., Understanding the mechanisms and rates of enzyme-catalyzed proton transfer reactions to and from carbon. *Bioorganic Chemistry: Peptides and Proteins* **1998**, 279-311, 500-501.
- Gerlt, J. A.; Gassman, P. G., Understanding the rates of certain enzyme-catalyzed reactions: Proton abstraction from carbon acids, acyl transfer reactions, and displacement reactions of phosphodiester. *Biochemistry* **1993**, 32, (45), 11943-52.
- Geymayer, P.; Bahr, N.; Reymond, J.-L., A general fluorogenic assay for catalysis using antibody sensors. *Chemistry--A European Journal* **1999**, 5, (3), 1006-1012.
- Gianneschi, N. C.; Nguyen, S. T.; Mirkin, C. A., Signal Amplification and Detection via a Supramolecular Allosteric Catalyst. *Journal of the American Chemical Society* **2005**, 127, (6), 1644-1645.
- Gokel, G. W.; Editor, *Advances in Supramolecular Chemistry, Volume 9*. 2003; p 263 pp.
- Gordon, A. J.; Ford, R. A., *The Chemist's Companion*. John Wiley and Sons Inc.: New York, 1972; p 57-59.
- Graf, N.; Goeritz, M.; Kraemer, R., A metal-ion-releasing probe for DNA detection by catalytic signal amplification. *Angewandte Chemie, International Edition* **2006**, 45, (24), 4013-4015.

- Gravesteijn, D. J.; Steenbergen, C.; Van der Veen, J., Single-wavelength optical recording in pure, solvent-coated infrared dye layers. *Proceedings of SPIE-The International Society for Optical Engineering* **1983**, 420, (Opt. Storage Media), 327-31.
- Gubitz, G.; Van Zoonen, P.; Gooijer, C.; Velthorst, N. H.; Frei, R. W., Immobilized fluorophores in dynamic chemiluminescence detection of hydrogen peroxide. *Analytical Chemistry* **1985**, 57, (11), 2071-4.
- Gunnlaugsson, T.; Davis, A. P.; O'Brien, J. E.; Glynn, M., Fluorescent Sensing of Pyrophosphate and Bis-carboxylates with Charge Neutral PET Chemosensors. *Organic Letters* **2002**, 4, (15), 2449-2452.
- Hang, H. C.; Yu, C.; Pratt, M. R.; Bertozzi, C. R., Probing Glycosyltransferase Activities with the Staudinger Ligation. *Journal of the American Chemical Society* **2004**, 126, (1), 6-7.
- Harris, T. K.; Turner, G. J., Structural basis of perturbed pKa values of catalytic groups in enzyme active sites. *IUBMB Life* **2002**, 53, (2), 85-98.
- Hartwell, E.; Hodgson, D. R. W.; Kirby, A. J., Exploring the Limits of Efficiency of Proton-Transfer Catalysis in Models and Enzymes. *Journal of the American Chemical Society* **2000**, 122, (38), 9326-9327.
- Hegeman, G. D.; Rosenberg, E. Y.; Kenyon, G. L., Mandelic acid racemase from *Pseudomonas putida*. Purification and properties of the enzyme. *Biochemistry* **1970**, 9, (21), 4029-36.
- Heilbron, I. M.; Heaton, J. S., 9,10-Dibromoanthracene. *Organic Syntheses* **1923**, III, 41-3.
- Hennrich, G.; Walther, W.; Resch-Genger, U.; Sonnenschein, H., Cu(II)- and Hg(II)-Induced Modulation of the Fluorescence Behavior of a Redox-Active Sensor Molecule. *Inorganic Chemistry* **2001**, 40, (4), 641-644.
- Hercules, D. M., Chemiluminescence resulting from electrochemically generated species. *Science (Washington, DC, United States)* **1964**, 145, (3634), 808-9.
- Herlihy, J. M.; Maister, S. G.; Albery, W. J.; Knowles, J. R., Energetics of triosephosphate isomerase: the fate of the 1(R)-3H label of tritiated dihydroxyacetone phosphate in the isomerase reaction. *Biochemistry* **1976**, 15, (25), 5601-7.
- Hibbert, F.; Emsley, J., Hydrogen bonding and chemical reactivity. *Advances in Physical Organic Chemistry* **1990**, 26, 255-79.
- Hol, W. G. J., The role of the  $\alpha$ -helix dipole in protein function and structure. *Progress in Biophysics & Molecular Biology* **1985**, 45, (3), 149-95.
- Houk, R. J. T.; Anslyn, E. V., *Unpublished results*.

- Houk, R. J. T.; Anslyn, E. V., Luminescent assays for ketones and aldehydes employing catalytic signal amplification. *New Journal of Chemistry* **2007**, In Press.
- Houk, R. J. T.; Anslyn, E. V.; Stanton, J. F., Carbonyl Coordination Chemistry from a New Angle: A Computational Study of  $\alpha$ -Carbon Acidity Based on Electrophile Coordination Geometry. *Organic Letters* **2006**, 8, (16), 3461-3463.
- Ishida, T., Low-Barrier Hydrogen Bond Hypothesis in the Catalytic Triad Residue of Serine Proteases: Correlation between Structural Rearrangement and Chemical Shifts in the Acylation Process. *Biochemistry* **2006**, 45, (17), 5413-5420.
- J. Baxter, D. S., M. Palucki, I. W. Davies, Stereoselective Enol Tosylation: Preparation of Trisubstituted  $\alpha,\beta$ -Unsaturated Esters. *Organic Letters* **2005**, 7, 215-218.
- Jares-Erijman, E. A.; Jovin, T. M., Imaging molecular interactions in living cells by FRET microscopy. *Current Opinion in Chemical Biology* **2006**, 10, (5), 409-416.
- Jencks, W. P., Binding energy, specificity, and enzymic catalysis: the Circe effect. *Advances in Enzymology and Related Areas of Molecular Biology* **1975**, 43, 219-410.
- Jimenez, D.; Martinez-Manez, R.; Sancenon, F.; Ros-Lis, J. V.; Benito, A.; Soto, J., A New Chromo-chemodosimeter Selective for Sulfide Anion. *Journal of the American Chemical Society* **2003**, 125, (30), 9000-9001.
- Jimenez, D.; Martinez-Manez, R.; Sancenon, F.; Soto, J., Selective fluoride sensing using colorimetric reagents containing anthraquinone and urea or thiourea binding sites. *Tetrahedron Letters* **2002**, 43, (15), 2823-2825.
- Jyothish, K.; Avirah, R. R.; Ramaiah, D., Synthesis of New Cholesterol- and Sugar-Anchored Squaraine Dyes: Further Evidence of How Electronic Factors Influence Dye Formation. *Organic Letters* **2006**, 8, (1), 111-114.
- Kallarakal, A. T.; Mitra, B.; Kozarich, J. W.; Gerlt, J. A.; Clifton, J. R.; Petsko, G. A.; Kenyon, G. L., Mechanism of the Reaction Catalyzed by Mandelate Racemase: Structure and Mechanistic Properties of the K166R Mutant. *Biochemistry* **1995**, 34, (9), 2788-97.
- Kamlet, M. J.; Abboud, J. L.; Taft, R. W., The solvatochromic comparison method. 6. The  $p^*$  scale of solvent polarities. *Journal of the American Chemical Society* **1977**, 99, (18), 6027-38.
- Karpusas, M.; Branchaud, B.; Remington, S. J., Proposed mechanism for the condensation reaction of citrate synthase: 1.9-ANG. structure of the ternary complex with oxaloacetate and carboxymethyl coenzyme A. *Biochemistry* **1990**, 29, (9), 2213-19.
- Karpusas, M.; Holland, D.; Remington, S. J., 1.9-ANG. Structures of ternary complexes of citrate synthase with D- and L-malate: mechanistic implications. *Biochemistry* **1991**, 30, (24), 6024-31.

- Kasha, M.; Rawls, H. R.; El-Bayoumi, M. A., Exciton model in molecular spectroscopy. *Pure and Applied Chemistry* **1965**, 11, (3-4), 371-92.
- Kato, Y.; Toledo, L. M.; Rebek, J., Jr., Energetics of a Low Barrier Hydrogen Bond in Nonpolar Solvents. *Journal of the American Chemical Society* **1996**, 118, (36), 8575-8579.
- Kelly-Rowley, A. M.; Lynch, V. M.; Anslyn, E. V., Molecular Recognition of Enolates of Active Methylene Compounds in Acetonitrile. The Interplay between Complementarity and Basicity and the Use of Hydrogen Bonding to Lower Guest pK<sub>a</sub>s. *Journal of the American Chemical Society* **1995**, 117, (12), 3438-47.
- Kenichiro Nakashima, K. M. S. A. K. I., Evaluation of pyrimido[5,4-*d*]pyrimidine derivatives as peroxyoxalate chemiluminescence reagents using a flow injection system. *Biomedical Chromatography* **1990**, 4, (3), 105-107.
- Kenyon, G. L.; Hegeman, G. D., Mandelate racemase. *Advances in Enzymology and Related Areas of Molecular Biology* **1979**, 50, 325-60.
- Kim, S.-H.; Han, S.-K.; Park, S.-H.; Yoon, C.-M.; Keum, S.-R., Novel fluorescent chemosensor for Li<sup>+</sup> based on a squarylium dye carrying a monoazacrown moiety. *Dyes and Pigments* **1999**, 43, (1), 21-25.
- Kim, T.-H.; Swager, T. M., A fluorescent self-amplifying wavelength-responsive sensory polymer for fluoride ions. *Angewandte Chemie, International Edition* **2003**, 42, (39), 4803-4806.
- Kimura, E.; Kitamura, H.; Koike, T.; Shiro, M., Facile and selective electrostatic stabilization of uracil N(1)- anion by a proximate protonated amine: A chemical implication for why uracil N(1) is chosen for glycosylation site. *Journal of the American Chemical Society* **1997**, 119, (45), 10909-10919.
- King, G.; Lee, F. S.; Warshel, A., Microscopic simulations of macroscopic dielectric constants of solvated proteins. *Journal of Chemical Physics* **1991**, 95, (6), 4366-77.
- Koike, R.; Motoyoshiya, J.; Takaguchi, Y.; Aoyama, H., The key intermediates that interact with the fluorophores in the peroxyoxalate chemiluminescence reaction of 2,4,6-trichlorophenyl N-aryl-N-tosyloxamates. *Chemical Communications (Cambridge, United Kingdom)* **2003**, (6), 794-795.
- Komives, E. A.; Chang, L. C.; Lolis, E.; Tilton, R. F.; Petsko, G. A.; Knowles, J. R., Electrophilic catalysis in triosephosphate isomerase: the role of histidine-95. *Biochemistry* **1991**, 30, (12), 3011-19.
- Konopelski, J. P.; Kotzyba-Hibert, F.; Lehn, J. M.; Desvergne, J. P.; Fages, F.; Castellán, A.; Bouas-Laurent, H., Synthesis, cation binding, and photophysical properties of macrobicyclic anthracenocryptands. *Journal of the Chemical Society, Chemical Communications* **1985**, (7), 433-6.

- Kovacs, J.; Roedler, T.; Mokhir, A., Chemodosimeter for CuII detection based on cyclic peptide nucleic acids. *Angewandte Chemie, International Edition* **2006**, 45, (46), 7815-7817.
- Kresge, A. J., Generation and study of enols and other reactive species. *Pure and Applied Chemistry* **1991**, 63, (2), 213-21.
- Kroll, H., The participation of heavy-metal ions in the hydrolysis of amino acid esters. *Journal of the American Chemical Society* **1952**, 74, 2036-9.
- Kroll, H., Manganous complexes of several amino acids. *Journal of the American Chemical Society* **1952**, 74, 2034-6.
- Kurz, L. C.; Drysdale, G. R., Evidence from Fourier transform infrared spectroscopy for polarization of the carbonyl of oxaloacetate in the active site of citrate synthase. *Biochemistry* **1987**, 26, (9), 2623-7.
- Lancaster, J. S., Chemiluminescence detection in analytical chemistry. *Endeavour* **1992**, 16, (4), 194-200.
- Landro, J. A.; Gerlt, J. A.; Kozarich, J. W.; Koo, C. W.; Shah, V. J.; Kenyon, G. L.; Neidhart, D. J.; Fujita, S.; Petsko, G. A., The role of lysine 166 in the mechanism of mandelate racemase from *Pseudomonas putida*: Mechanistic and crystallographic evidence for stereospecific alkylation by (R)- $\alpha$ -phenylglycidate. *Biochemistry* **1994**, 33, (3), 635-43.
- Laramay, M. A. H.; Verkade, J. G., The "anomalous" basicity of  $P(NHCH_2CH_2)_3N$  relative to  $P(NMeCH_2CH_2)_3N$  and  $p(NBzCH_2CH_2)_3N$ : a chemical consequence of orbital charge balance? *Journal of the American Chemical Society* **1990**, 112, (25), 9421-2.
- Law, K.-Y., *Absorption, fluorescence emission, and photophysics of squaraines*. Marcel Dekker, Inc: New York, 1997; Vol. 1, p 519-584.
- Law, K. Y., Squaraine chemistry: effects of structural changes on the absorption and multiple fluorescence emission of bis[4-(dimethylamino)phenyl]squaraine and its derivatives. *Journal of Physical Chemistry* **1987**, 91, (20), 5184-93.
- Law, K. Y., Organic photoconductive materials: recent trends and developments. *Chemical Reviews (Washington, DC, United States)* **1993**, 93, (1), 449-86.
- Law, K. Y.; Bailey, F. C., Squaraine chemistry. Synthesis of bis[4-(dimethylamino)phenyl]squaraine from dialkyl squarates. Mechanism and scope of the synthesis. *Canadian Journal of Chemistry* **1986**, 64, (12), 2267-73.
- Lechtken, P.; Turro, N. J., Peroxyoxalate chemiluminescence. Chemiexcitation of high-energy excited states in acceptor molecules. *Molecular Photochemistry* **1974**, 6, (1), 95-9.

- Lehn, J. M., Supramolecular chemistry. *Science (Washington, DC, United States)* **1993**, 260, (5115), 1762-3.
- Lensink, C.; Xi, S. K.; Daniels, L. M.; Verkade, J. G., The unusually robust phosphorus-hydrogen bond in the novel cation [cyclic] HP(NMeCH<sub>2</sub>CH<sub>2</sub>)<sub>3</sub>N<sup>+</sup>. *Journal of the American Chemical Society* **1989**, 111, (9), 3478-9.
- Li, I. T.; Pham, E.; Truong, K., Protein biosensors based on the principle of fluorescence resonance energy transfer for monitoring cellular dynamics. *Biotechnology Letters* **2006**, 28, (24), 1971-1982.
- Li, J. J., *Name Reactions*. 2nd ed.; Springer-Verlag: Berlin, Germany, 2003; Vol. 1, p 465.
- Liang, J.-G.; Ai, X.-P.; He, Z.-K.; Pang, D.-W., Functionalized CdSe quantum dots as selective silver ion chemodosimeter. *Analyst (Cambridge, United Kingdom)* **2004**, 129, (7), 619-622.
- Liu, B.; Tian, H., A selective fluorescent ratiometric chemodosimeter for mercury ion. *Chemical Communications (Cambridge, United Kingdom)* **2005**, (25), 3156-3158.
- Liu, L.; Zhang, Y.; Xin, B., Synthesis of Biaryls and Polyaryls by Ligand-Free Suzuki Reaction in Aqueous Phase. *Journal of Organic Chemistry* **2006**, 71, (10), 3994-3997.
- Lodi, P. J.; Knowles, J. R., Neutral imidazole is the electrophile in the reaction catalyzed by triosephosphate isomerase: structural origins and catalytic implications. *Biochemistry* **1991**, 30, (28), 6948-56.
- Loehr, H. G.; Voegtle, F., Chromo- and fluoroionophores. A new class of dye reagents. *Accounts of Chemical Research* **1985**, 18, (3), 65-72.
- Los, M., Virus detection today. *Modern Bacteriophage Biology and Biotechnology* **2006**, 131-152.
- Loutfy, R. O.; Hsiao, C. K.; Kazmaier, P. M., Photoconductivity of organic particle dispersions: squaraine dyes. *Photographic Science and Engineering* **1983**, 27, (1), 5-9.
- MacBeath, G.; Hilvert, D., Monitoring Catalytic Activity by Immunoassay: Implications for Screening. *Journal of the American Chemical Society* **1994**, 116, (14), 6101-6.
- Maister, S. G.; Pett, C. P.; Albery, W. J.; Knowles, J. R., Energetics of triosephosphate isomerase: the appearance of solvent tritium in substrate dihydroxyacetone phosphate and in product. *Biochemistry* **1976**, 15, (25), 5607-12.
- Man, W. J.; Li, Y.; O'Connor, C. D.; Wilton, D. C., Conversion of citrate synthase into citryl-CoA lyase as a result of mutation of the active-site aspartic acid residue to glutamic acid. *Biochemical Journal* **1991**, 280, (2), 521-6.

- Marcus, R. A., Unusual slopes of free energy plots in kinetics. *Journal of the American Chemical Society* **1969**, 91, (26), 7224-5.
- Martinez-Manez, R.; Sancenon, F., Fluorogenic and Chromogenic Chemosensors and Reagents for Anions. *Chemical Reviews (Washington, DC, United States)* **2003**, 103, (11), 4419-4476.
- Martinez-Manez, R.; Sancenon, F., New advances in fluorogenic anion chemosensors. *Journal of Fluorescence* **2005**, 15, (3), 267-285.
- McCleskey, S. C.; Griffin, M. J.; Schneider, S. E.; McDevitt, J. T.; Anslyn, E. V., Differential receptors create patterns diagnostic for ATP and GTP. *Journal of the American Chemical Society* **2003**, 125, (5), 1114-1115.
- McDevitt, J. T.; Anslyn, E. V.; Shear, J. B.; Neikirk, D. P. Sensor arrays for the measurement and identification of multiple analytes in solutions. 6680206, 2004.
- McKerrow, A. J.; Buncel, E.; Kazmaier, P. M., Aggregation of squaraine dyes: structure-property relationships and solvent effects. *Canadian Journal of Chemistry* **1995**, 73, (10), 1605-15.
- Merritt, V. Y.; Hovel, H. J., Organic solar cells of hydroxy squarylium. *Applied Physics Letters* **1976**, 29, (7), 414-15.
- Mitra, B.; Kallarakal, A. T.; Kozarich, J. W.; Gerlt, J. A.; Clifton, J. R.; Petsko, G. A.; Kenyon, G. L., Mechanism of the Reaction Catalyzed by Mandelate Racemase: Importance of Electrophilic Catalysis by Glutamic Acid 317. *Biochemistry* **1995**, 34, (9), 2777-87.
- Mohr, G. G., Covalent Bond Formation as an Analytical tool to Optically Detect Neutral and anionic Analytes. *Sensors and Actuators B* **2005**, 107, 2-13.
- Mohr, G. J., Chromo- and fluororeactands: indicators for detection of neutral analytes by using reversible covalent-bond chemistry. *Chemistry--A European Journal* **2004**, 10, (5), 1082-1090.
- Morel, D. L.; Stogryn, E. L.; Ghosh, A. K.; Feng, T.; Purwin, P. E.; Shaw, R. F.; Fishman, C.; Bird, G. R.; Piechowski, A. P., Organic photovoltaic cells. Correlations between cell performance and molecular structure. *Journal of Physical Chemistry* **1984**, 88, (5), 923-33.
- Mori, T.; Miyachi, K.; Kichimi, T.; Mizutani, T., Electrical and luminescent properties of color-changeable organic electroluminescent diode using squarylium dyes. *Japanese Journal of Applied Physics, Part 1: Regular Papers, Short Notes & Review Papers* **1994**, 33, (12A), 6594-8.
- Nakazumi, H.; Ohta, T.; Etoh, H.; Uno, T.; Colyer, C. L.; Hyodo, Y.; Yagi, S., Near-Infrared Luminescent Bis-Squaraine Dyes Linked by a Thiophene or Pyrene Spacer for Noncovalent Protein Labeling. *Synthetic Metals* **2005**, 153, 33-36.



- Nickbarg, E. B.; Davenport, R. C.; Petsko, G. A.; Knowles, J. R., Triosephosphate isomerase: removal of a putatively electrophilic histidine residue results in a subtle change in catalytic mechanism. *Biochemistry* **1988**, 27, (16), 5948-60.
- Nishizawa, S.; Kato, Y.; Teramae, N., Fluorescence Sensing of Anions via Intramolecular Excimer Formation in a Pyrophosphate-Induced Self-Assembly of a Pyrene-Functionalized Guanidinium Receptor. *Journal of the American Chemical Society* **1999**, 121, (40), 9463-9464.
- Oguri, H.; Hiram, M.; Tsumuraya, T.; Fujii, I.; Maruyama, M.; Uehara, H.; Nagumo, Y., Synthesis-Based Approach toward Direct Sandwich Immunoassay for Ciguatoxin CTX3C. *Journal of the American Chemical Society* **2003**, 125, (25), 7608-7612.
- Orlovic, M.; Schowen, R. L.; Givens, R. S.; Alvarez, F.; Matuszewski, B.; Parekh, N., A simplified model for the dynamics of chemiluminescence in the oxalate-hydrogen peroxide system: toward a reaction mechanism. *Journal of Organic Chemistry* **1989**, 54, (15), 3606-10.
- Pasqualato, S.; Cherfils, J., Crystallographic Evidence for Substrate-Assisted GTP Hydrolysis by a Small GTP Binding Protein. *Structure (Cambridge, MA, United States)* **2005**, 13, (4), 533-540.
- Piechowski, A. P.; Bird, G. R.; Morel, D. L.; Stogryn, E. L., Desirable properties of photovoltaic dyes. *Journal of Physical Chemistry* **1984**, 88, (5), 934-50.
- Powers, V. M.; Koo, C. W.; Kenyon, G. L.; Gerlt, J. A.; Kozarich, J. W., Mechanism of the reaction catalyzed by mandelate racemase. 1. Chemical and kinetic evidence for a two-base mechanism. *Biochemistry* **1991**, 30, (38), 9255-63.
- Prados, P.; Higashidate, S.; Imai, K., A fully automated HPLC method for the determination of catecholamines in biological samples utilizing ethylenediamine condensation and peroxyoxalate chemiluminescence detection. *Biomedical Chromatography* **1994**, 8, (1), 1-8.
- Prodi, L., Luminescent chemosensors: from molecules to nanoparticles. *New Journal of Chemistry* **2005**, 29, (1), 20-31.
- Qi, X.; Jun, E. J.; Xu, L.; Kim, S.-J.; Hong, J. S. J.; Yoon, Y. J.; Yoon, J., New BODIPY Derivatives as OFF-ON Fluorescent Chemosensor and Fluorescent Chemodosimeter for Cu<sup>2+</sup>: Cooperative Selectivity Enhancement toward Cu<sup>2+</sup>. *Journal of Organic Chemistry* **2006**, 71, (7), 2881-2884.

- Rauhut, M. M.; Bollyky, L. J.; Roberts, B. G.; Loy, M.; Whitman, R. H.; Iannotta, A. V.; Semsel, A. M.; Clarke, R. A., Chemiluminescence from reactions of electronegatively substituted aryl oxalates with hydrogen peroxide and fluorescent compounds. *Journal of the American Chemical Society* **1967**, 89, (25), 6515-22.
- Remington, S.; Wiegand, G.; Huber, R., Crystallographic refinement and atomic models of two different forms of citrate synthase at 2.7 and 1.7 Å resolution. *Journal of Molecular Biology* **1982**, 158, (1), 111-52.
- Remington, S. J., Mechanisms of citrate synthase and related enzymes (triose phosphate isomerase and mandelate racemase). *Current Opinion in Structural Biology* **1992**, 2, (5), 730-5.
- Ren, J.; Cramer, C. J.; Squires, R. R., Superacidity and Superelectrophilicity of BF<sub>3</sub>-Carbonyl Complexes. *Journal of the American Chemical Society* **1999**, 121, (11), 2633-2634.
- Richardson, W. H.; Montgomery, F. C.; Yelvington, M. B.; O'Neal, H. E., Kinetics of the thermal decomposition of 3,3-diphenyl- and 3,3-dibenzyl-1,2-dioxetane. Consideration of stepwise and concerted mechanisms. *Journal of the American Chemical Society* **1974**, 96, (24), 7525-32.
- Richarz, R.; Wuethrich, K., Carbon-13 NMR chemical shifts of the common amino acid residues measured in aqueous solutions of the linear tetrapeptides H-Gly-Gly-X-L-Ala-OH. *Biopolymers* **1978**, 17, (9), 2133-41.
- Rieder, S. V.; Rose, I. A., Mechanism of the triose phosphate isomerase reaction. *Journal of Biological Chemistry* **1959**, 234, 1007-10.
- Riina K. Arvela; Leadbeater, N. E.; Michael J. Collins, J., Automated batch scale-up of microwave-promoted Suzuki and Heck coupling reactions in water using ultra-low metal catalyst concentrations. *Tetrahedron* **2005**, 61, (39), 9349-9355.
- Roeschlaub, C. A.; Maidwell, N. L.; Reza Rezai, M.; Sammes, P. G., A fluorescent probe for the detection of NAD(P)H. *Chemical Communications (Cambridge)* **1999**, (17), 1637-1638.
- Ros-Lis, J. V.; Garcia, B.; Jimenez, D.; Martinez-Manez, R.; Sancenon, F.; Soto, J.; Gonzalvo, F.; Valldecabres, M. C., Squaraines as fluoro-chromogenic probes for thiol-containing compounds and their application to the detection of biorelevant thiols. *Journal of the American Chemical Society* **2004**, 126, (13), 4064-4065.
- Ros-Lis, J. V.; Marcos, M. D.; Martinez-Manez, R.; Rurack, K.; Soto, J., A regenerative chemodosimeter based on metal-induced dye formation for the highly selective and sensitive optical determination of Hg<sup>2+</sup> ions. *Angewandte Chemie, International Edition* **2005**, 44, (28), 4405-4407.

- Ros-Lis, J. V.; Martinez-Manez, R.; Rurack, K.; Sancenon, F.; Soto, J.; Spieles, M., Highly Selective Chromogenic Signaling of Hg<sup>2+</sup> in Aqueous Media at Nanomolar Levels Employing a Squaraine-Based Reporter. *Inorganic Chemistry* **2004**, 43, (17), 5183-5185.
- Ros-Lis, J. V.; Martinez-Manez, R.; Soto, J., A selective chromogenic reagent for cyanide determination. *Chemical Communications (Cambridge, United Kingdom)* **2002**, (19), 2248-2249.
- Ros-Lis, J. V.; Martinez-Manez, R.; Soto, J., Colorimetric signaling of large aromatic hydrocarbons via the enhancement of aggregation processes. *Organic Letters* **2005**, 7, (12), 2337-2339.
- Rostovtsev, V. V.; Green, L. G.; Fokin, V. V.; Sharpless, K. B., A stepwise Huisgen cycloaddition process: copper(I)-catalyzed regioselective "ligation" of azides and terminal alkynes. *Angewandte Chemie, International Edition* **2002**, 41, (14), 2596-2599.
- Saghatelian, A.; Guckian, K. M.; Thayer, D. A.; Ghadiri, M. R., DNA Detection and Signal Amplification via an Engineered Allosteric Enzyme. *Journal of the American Chemical Society* **2003**, 125, (2), 344-345.
- Sancenon, F.; Descalzo, A. B.; Martinez-Manez, R.; Miranda, M. A.; Soto, J., A colorimetric ATP sensor based on 1,3,5-triaryl-pent-2-en-1,5-diones. *Angewandte Chemie, International Edition* **2001**, 40, (14), 2640-2643.
- Sancenon, F.; Martinez-Manez, R.; Miranda, M. A.; Segui, M.-J.; Soto, J., Towards the development of colorimetric probes to discriminate between isomeric dicarboxylates. *Angewandte Chemie, International Edition* **2003**, 42, (6), 647-650.
- Santhanam, K. S. V.; Bard, A. J., Chemiluminescence of electrogenerated 9,10-diphenylanthracene anion radical. *Journal of the American Chemical Society* **1965**, 87, (1), 139-40.
- Schmidt, A. H., *Oxocarbons*. Academic Press: New York, 1980; p 185-231.
- Schuster, G. B., Chemiluminescence of organic peroxides. Conversion of ground-state reactants to excited-state products by the chemically initiated electron-exchange luminescence mechanism. *Accounts of Chemical Research* **1979**, 12, (10), 366-73.
- Scott, G. W.; Tran, K., Squaraine Photophysics in Polymer Films. *Journal of Physical Chemistry* **1994**, 98, (44), 11563-9.
- Seebach, D.; Kolb, M., Umpolung (dipole inversion) of carbonyl reactivity. *Chemistry & Industry (London, United Kingdom)* **1974**, (17), 687-92.
- Sekar, N., Rhodamine fluorophores - functional applications. *Colourage* **2001**, 48, (7), 50-52.

- Sessler, J. L.; Weghorn, S. J., *Expanded, Contracted and Isomeric Porphyrins*. 1 ed.; Pergamon: Oxford, UK; New York, NY, 1997; Vol. 1.
- Sheehan, J. C.; Coderre, R. A.; Cruickshank, P. A., The formation of five- and six-membered rings by the acyloin condensation. IV. The natural estrogenic steroids. *Journal of the American Chemical Society* **1953**, 75, 6231-33.
- Shinde, P. D.; Borate, H. B.; Wakharkar, R. D., Thioacetalization of the carbonyl function, transthioacetalization of acetals, ketals, oximes and hydrazones catalyzed by aqueous hydrobromic acid. *ARKIVOC (Gainesville, FL, United States)* **2004**, (14), 110-117.
- Sigvardson, K. W.; Birks, J. W., Peroxyoxalate chemiluminescence detection of polycyclic aromatic hydrocarbons in liquid chromatography. *Analytical Chemistry* **1983**, 55, (3), 432-5.
- Sigvardson, K. W.; Birks, J. W., Detection of nitro-polycyclic aromatic hydrocarbons in liquid chromatography by zinc reduction and peroxyoxalate chemiluminescence. *Journal of Chromatography* **1984**, 316, 507-18.
- Sigvardson, K. W.; Kennish, J. M.; Birks, J. W., Peroxyoxalate chemiluminescence detection of polycyclic aromatic amines in liquid chromatography. *Analytical Chemistry* **1984**, 56, (7), 1096-102.
- Silva, S. M.; Casallanovo, F., Jr.; Oyamaguchi, K. H.; Ciscato, L. F. L. M.; Stevani, C. V.; Baader, W. J., Kinetic studies on the peroxyoxalate chemiluminescence reaction: determination of the cyclization rate constant. *Luminescence* **2002**, 17, (5), 313-320.
- Silva, S. M.; Wagner, K.; Weiss, D.; Beckert, R.; Stevani, C. V.; Baader, W. J., Studies on the chemiexcitation step in peroxyoxalate chemiluminescence using steroid-substituted activators. *Luminescence* **2002**, 17, (6), 362-369.
- Snowden, T. S.; Bisson, A. P.; Anslyn, E. V., A Comparison of NH- $\pi$  versus Lone Pair Hydrogen Bonding Effects on Carbon Acid pKa Shifts. *Journal of the American Chemical Society* **1999**, 121, (26), 6324-6325.
- Snowden, T. S.; Bisson, A. P.; Anslyn, E. V., Artificial receptors involved in enolization and pKa shifts. *Bioorganic & Medicinal Chemistry* **2001**, 9, (9), 2467-2478.
- Song, K. C.; Kim, J. S.; Park, S. M.; Chung, K.-C.; Ahn, S.; Chang, S.-K., Fluorogenic Hg<sup>2+</sup>-Selective Chemodosimeter Derived from 8-Hydroxyquinoline. *Organic Letters* **2006**, 8, (16), 3413-3416.
- Sprenger, H. E.; Ziegenbein, W., Cyclobutenediylum cation, a novel chromophore from squaric acid. *Angewandte Chemie, International Edition in English* **1967**, 6, (6), 553-4.
- St. Maurice, M.; Bearne, S. L., Kinetics and Thermodynamics of Mandelate Racemase Catalysis. *Biochemistry* **2002**, 41, (12), 4048-4058.

- Stahl, N.; Jencks, W. P., Hydrogen bonding between solutes in aqueous solution. *Journal of the American Chemical Society* **1986**, 108, (14), 4196-205.
- Stanton, J. F.; Gauss, J.; Watts, J. D.; Lauderdale, W. J.; Bartlett, R. J., The ACES II program system. *International Journal of Quantum Chemistry, Quantum Chemistry Symposium* **1992**, 26, (Proc. Int. Symp. At., Mol., Condens. Matter Theory Comput. Methods, 1992), 879-94.
- Staunton, J., *Pyrylium salts*. Pergamon: Oxford, UK, 1979; Vol. 4, p 607-27.
- Steed, J. W.; Atwood, J. L., *Supramolecular Chemistry: A Concise Introduction*. 2000; p 400 pp.
- Stevani, C. V.; Baader, W. J., Kinetic studies on the chemiluminescent decomposition of an isolated intermediate in the peroxyoxalate reaction. *Journal of Physical Organic Chemistry* **1997**, 10, (8), 593-599.
- Stevani, C. V.; Da Silva, S. M.; Baader, W. J., Studies on the involvement of the CIEEL sequence in the peroxyoxalate reaction. *Bioluminescence and Chemiluminescence: Perspectives for the 21st Century, Proceedings of the International Symposium on Bioluminescence and Chemiluminescence, 10th, Bologna, Sept. 4-8, 1998* **1999**, 53-56.
- Stevani, C. V.; Silva, S. M.; Baader, W. J., Studies on the mechanism of the excitation step in peroxyoxalate chemiluminescence. *European Journal of Organic Chemistry* **2000**, (24), 4037-4046.
- Stigbrand, M.; Ponten, E.; Irgum, K., 1,1'-Oxalyldiimidazole as Chemiluminescence Reagent in the Determination of Low Hydrogen Peroxide Concentrations by Flow Injection Analysis. *Analytical Chemistry* **1994**, 66, (10), 1766-70.
- Sutherland, I. O., Crown compounds. Molecule and cation recognition by synthetic host molecules. *Crown Compd.* **1992**, 235-60.
- Swager, T. M.; Gil, C. J.; Wrighton, M. S., Fluorescence Studies of Poly(p-phenyleneethynylene)s: The Effect of Anthracene Substitution. *Journal of Physical Chemistry* **1995**, 99, (14), 4886-93.
- Taran, F.; Gauchet, C.; Mohar, B.; Meunier, S.; Valleix, A.; Renard, P. Y.; Creminon, C.; Grassi, J.; Wagner, A.; Mioskowski, C., Communications: High-throughput screening of enantioselective catalysts by immunoassay. *Angewandte Chemie, International Edition* **2002**, 41, (1), 124-127.
- Tatarets, A. L.; Fedyunyaeva, I. A.; Terpetschnig, E.; D, P. L., Synthesis of Novel Squaraine Dyes and their Intermediates. *Dyes and Pigments* **2004**, 64, 125-134.
- Thomas, K. G.; Thomas, K. J.; Das, S.; George, M. V., A squaraine-based near-infrared absorbing sensor for the selective detection of transition and other metal ions in aqueous media. *Chemical Communications (Cambridge)* **1997**, (6), 597-598.

- Tian, M.; Furuki, M.; Iwasa, I.; Sato, Y.; Pu, L. S.; Tatsuura, S., Search for Squaraine Derivatives That Can Be Sublimed without Thermal Decomposition. *Journal of Physical Chemistry B* **2002**, 106, (17), 4370-4376.
- Tornøe, C. W.; Christensen, C.; Meldal, M., Peptidotriazoles on Solid Phase: [1,2,3]-Triazoles by Regiospecific Copper(I)-Catalyzed 1,3-Dipolar Cycloadditions of Terminal Alkynes to Azides. *Journal of Organic Chemistry* **2002**, 67, (9), 3057-3064.
- Treibs, A.; Jacob, K., Cyclotrimethine dyes derived from quadratic acid [1,2-dihydroxycyclobutenedione]. *Angew. Chem.* **1965**, 77, (15), 680-1.
- Tsunoda, M.; Imai, K., Analytical applications of peroxyoxalate chemiluminescence. *Analytica Chimica Acta* **2005**, 541, (1-2), 13-23.
- Ueda, H.; Tsumoto, K.; Kobota, K.; Suzuki, E.; Nagamune, T.; Nishimura, H.; Schueler, P. A.; Winter, G.; Kumagai, I.; Mahoney, W. C., Open sandwich ELISA: a novel immunoassay based on the interchain interaction of antibody variable region. *Nature Biotechnology* **1996**, 14, (13), 1714-1718.
- Van Zoonen, P.; Kamminga, D. A.; Gooijer, C.; Velthorst, N. H.; Frei, R. W.; Gubitz, G., A solid-state chemiluminescence detector for hydrogen peroxide based on an immobilized luminophore. Application to rain water. *Analytica Chimica Acta* **1985**, 174, 151-61.
- Varma, R. S.; Naicker, K. P.; Liesen, P. J., Palladium chloride and tetraphenylphosphonium bromide intercalated clay as a new catalyst for the Heck reaction. *Tetrahedron Letters* **1999**, 40, (11), 2075-2078.
- Vock, P.; Engst, S.; Eder, M.; Ghisla, S., Substrate Activation by Acyl-Coenzyme A Dehydrogenases: Transition-State Stabilization and pKs of Involved Functional Groups. *Biochemistry* **1998**, 37, (7), 1848-1860.
- Voet, D.; Voet, J. G., *Biochemistry*. 3rd ed.; John Wiley & Sons Inc.: Hoboken, NJ, 2004.
- Volkova, K. D.; Kovalska, V. B.; Tatarets, A. L.; Patsenker, L. D.; Kryvorotenko, D. V.; Yarmoluk, S. M., Spectroscopic study of squaraines as protein-sensitive fluorescent dyes. *Dyes and Pigments* **2006**, 72, (3), 285-292.
- W.-J. Liu; Y.-X. Xie; Y. Liang; J.-H. Li, Reusable and Efficient Pd(OAc)<sub>2</sub>/TBAB/PEG-400 System for Suzuki-Miyaura Cross-Coupling Reaction under Ligand-Free Conditions. *Synthesis* **2006**, 860-864.
- Wallace, K. J.; Anslyn, E. V., *Unpublished results*.
- Wallace, K. J.; Gray, M.; Zhong, Z.; Lynch, V. M.; Anslyn, E. V., An artificial siderophore for the detection of iron(III). *Dalton Transactions* **2005**, (14), 2436-2441.
- Wallace, K. J.; Houk, R. J. T.; Anslyn, E. V., *Unpublished results*.

- Wallace, K. J.; Morey, J.; Lynch, V. M.; Anslyn, E. V., Colorimetric detection of chemical warfare simulants. *New Journal of Chemistry* **2005**, 29, (11), 1469-1474.
- Wang, W.; Gao, X.; Wang, B., Boronic acid-based sensors. *Current Organic Chemistry* **2002**, 6, (14), 1285-1317.
- Ward, C. J.; Patel, P.; James, T. D., A molecular colour sensor for fluoride. *Chemistry Letters* **2001**, (5), 406-407.
- Warshel, A., Calculations of enzymatic reactions: calculations of pKa, proton transfer reactions, and general acid catalysis reactions in enzymes. *Biochemistry* **1981**, 20, (11), 3167-77.
- Warshel, A.; Aqvist, J., Electrostatic energy and macromolecular function. *Annual Review of Biophysics and Biophysical Chemistry* **1991**, 20, 267-98.
- Warshel, A.; Levitt, M., Theoretical studies of enzymic reactions: dielectric, electrostatic and steric stabilization of the carbonium ion in the reaction of lysozyme. *Journal of Molecular Biology* **1976**, 103, (2), 227-49.
- Warshel, A.; Papazyan, A., Energy considerations show that low-barrier hydrogen bonds to not offer a catalytic advantage over ordinary hydrogen bonds. *Proceedings of the National Academy of Sciences of the United States of America* **1996**, 93, (24), 13665-13670.
- Warshel, A.; Papazyan, A.; Kollman, P. A., On low-barrier hydrogen bonds and enzyme catalysis. *Science (New York, N.Y.)* **1995**, 269, (5220), 102-6.
- Weizmann, Y.; Patolsky, F.; Katz, E.; Willner, I., Amplified DNA sensing and immunosensing by the rotation of functional magnetic particles. *Journal of the American Chemical Society* **2003**, 125, (12), 3452-3454.
- Wendling, L. A.; Koster, S. K.; Murray, J. E.; West, R., Syntheses and properties of 1,2- and 1,3-diquinocyclobutanediones. *Journal of Organic Chemistry* **1977**, 42, (7), 1126-30.
- Williams, D. C., III; Huff, G. F.; Seitz, W. R., Evaluation of peroxyoxalate chemiluminescence for determination of enzyme generated peroxide. *Analytical Chemistry* **1976**, 48, (7), 1003-6.
- Williams, D. C., III; Seitz, W. R., Automated chemiluminescence method for determining the reduced form of nicotinamide adenine dinucleotide coupled to the measurement of lactate dehydrogenase activity. *Analytical Chemistry* **1976**, 48, (11), 1478-81.
- Wright, A. T.; Anslyn, E. V., Differential receptor arrays and assays for solution-based molecular recognition. *Chemical Society Reviews* **2006**, 35, (1), 14-28.

- Wright, A. T.; Anslyn, E. V.; McDevitt, J. T., A Differential Array of Metalated Synthetic Receptors for the Analysis of Tripeptide Mixtures. *Journal of the American Chemical Society* **2005**, 127, (49), 17405-17411.
- Wright, A. T.; Griffin, M. J.; Zhong, Z.; McCleskey, S. C.; Anslyn, E. V.; McDevitt, J. T., Differential receptors create patterns that distinguish various proteins. *Angewandte Chemie, International Edition* **2005**, 44, (39), 6375-6378.
- Wu, J.-S.; Hwang, I.-C.; Kim, K. S.; Kim, J. S., Rhodamine-Based Hg<sup>2+</sup>-Selective Chemodosimeter in Aqueous Solution: Fluorescent OFF-ON. *Organic Letters* **2007**, 9, (5), 907-910.
- Wu, Q.; Anslyn, E. V., Catalytic Signal Amplification Using a Heck Reaction. An Example in the Fluorescence Sensing of Cu(II). *Journal of the American Chemical Society* **2004**, 126, (45), 14682-14683.
- Wu, Q.; Anslyn, E. V., Heavy metal analysis using a Heck-catalyzed cyclization to create coumarin. *Journal of Materials Chemistry* **2005**, 15, (27-28), 2815-2819.
- Xu, S.; Chen, K.; Tian, H., A colorimetric and fluorescent chemodosimeter: fluoride ion sensing by an axial-substituted subphthalocyanine. *Journal of Materials Chemistry* **2005**, 15, (27-28), 2676-2680.
- Yamaguchi, S.; Akiyama, S.; Tamao, K., Synthesis, Structures, Photophysical Properties, and Dynamic Stereochemistry of Tri-9-anthrylsilane Derivatives. *Organometallics* **1998**, 17, (20), 4347-4352.
- Yamaguchi, S.; Akiyama, S.; Tamao, K., Photophysical Properties Changes Caused by Hypercoordination of Organosilicon Compounds: From Trianthrylfluorosilane to Trianthryldifluorosilicate. *Journal of the American Chemical Society* **2000**, 122, (28), 6793-6794.
- Yamaguchi, S.; Akiyama, S.; Tamao, K., Colorimetric fluoride ion sensing by boron-containing pi-electron systems. *Journal of the American Chemical Society* **2001**, 123, (46), 11372-5.
- Yang, W.; Drueckhammer, D. G., Computational Study of the Citrate Synthase Catalyzed Deprotonation of Acetyl-Coenzyme A and Fluoroacetyl-Coenzyme A: Demonstration of a Layered Quantum Mechanical Approach. *Journal of Physical Chemistry B* **2003**, 107, (24), 5986-5994.
- Yang, X.-F.; Li, Y.; Bai, Q., A highly selective and sensitive fluorescein-based chemodosimeter for Hg<sup>2+</sup> ions in aqueous media. *Analytica Chimica Acta* **2007**, 584, (1), 95-100.
- Yang, Y.-K.; Tae, J., Acridinium salt based fluorescent and colorimetric chemosensor for the detection of cyanide in water. *Organic Letters* **2006**, 8, (25), 5721-3.



- Yang, Y.-K.; Yook, K.-J.; Tae, J., A Rhodamine-Based Fluorescent and Colorimetric Chemodosimeter for the Rapid Detection of Hg<sup>2+</sup> Ions in Aqueous Media. *Journal of the American Chemical Society* **2005**, 127, (48), 16760-16761.
- Zhang, G.; Zhang, D.; Yin, S.; Yang, X.; Shuai, Z.; Zhu, D., 1,3-Dithiole-2-thione derivatives featuring an anthracene unit: new selective chemodosimeters for Hg(II) ion. *Chemical Communications (Cambridge, United Kingdom)* **2005**, (16), 2161-2163.
- Zhang, X. M.; Bordwell, F. G.; Bares, J. E.; Cheng, J. P.; Petrie, B. C., Homolytic bond dissociation energies of the acidic carbon-hydrogen bonds in  $\alpha$ -substituted and 10-substituted 9-methylanthracenes and their related radical anions. *Journal of Organic Chemistry* **1993**, 58, (11), 3051-9.
- Zhang, Z.; Zhang, S.; Zhang, X., Recent developments and applications of chemiluminescence sensors. *Analytica Chimica Acta* **2005**, 541, (1-2), 37-46.
- Zhi, W.; Srere, P. A.; Evans, C. T., Conformational stability of pig citrate synthase and some active-site mutants. *Biochemistry* **1991**, 30, (38), 9281-6.
- Zhong, Z.; Postnikova, B. J.; Hanes, R. E.; Lynch, V. M.; Anslyn, E. V., Large pK<sub>a</sub> shifts of  $\alpha$ -carbon acids induced by copper(II) complexes. *Chemistry--A European Journal* **2005**, 11, (8), 2385-2394.
- Zhong, Z.; Snowden, T. S.; Best, M. D.; Anslyn, E. V., Rate of Enolate Formation Is Not Very Sensitive to the Hydrogen Bonding Ability of Donors to Carboxyl Oxygen Lone Pair Acceptors; A Ramification of the Principle of Non-Perfect Synchronization for General-Base-Catalyzed Enolate Formation. *Journal of the American Chemical Society* **2004**, 126, (11), 3488-3495.
- Zhu, L.; Lynch, V. M.; Anslyn, E. V., FRET induced by an allosteric cycloaddition reaction regulated with exogenous inhibitor and effectors. *Tetrahedron* **2004**, 60, (34), 7267-7275.
- Zhu, X.-J.; Fu, S.-T.; Wong, W.-K.; Guo, J.-P.; Wong, W.-Y., A near-infrared-fluorescent chemodosimeter for mercuric ion based on an expanded porphyrin. *Angewandte Chemie, International Edition* **2006**, 45, (19), 3150-3154.
- Zollinger, H., *Color Chemistry*. 3rd ed.; Verlag Helvetica Chimica Acta: Zuerich, Switzerland, 2003; p 15-16.
- Zou, X.; Jin, G., Synthesis of pyridazinone-substituted 1,3,4-thiadiazoles, -1,3,4-oxadiazoles and -1,2,4-triazoles. *Journal of Heterocyclic Chemistry* **2001**, 38, (4), 993-996.

## **Vita**

Ronald James Travis Houk was born in Oxford, OH on September 29<sup>th</sup>, 1979 to Mary Sue and T. William Houk. He graduated from St. Xavier High School in Cincinnati, OH in 1997 in the top 5% of his class. He then matriculated at the College of William & Mary in Williamsburg, VA in the fall of 1998. He conducted undergraduate chemistry research under Dr. Christopher J. Abelt on the mechanism of the sodium perborate promoted azo-coupling of substituted anilines, which earned him High Honors in Chemistry. Ron graduated from the College of William & Mary in May of 2001 with an American Chemical Society Accredited Bachelor of Science degree in Chemistry. He then began his graduate degree at the University of Texas in July of 2001.

Permanent address: 6 Bull Run Dr., Oxford, OH, 45056

This dissertation was typed by Ronald James Travis Houk